

# Advanced fatigue theory and structural response monitoring for safety verification of existing RC slabs subject to railway traffic

THÈSE N° 6847 (2015)

PRÉSENTÉE LE 22 DÉCEMBRE 2015

À LA FACULTÉ DE L'ENVIRONNEMENT NATUREL, ARCHITECTURAL ET CONSTRUIT  
LABORATOIRE DE MAINTENANCE, CONSTRUCTION ET SÉCURITÉ DES OUVRAGES  
PROGRAMME DOCTORAL EN GÉNIE CIVIL ET ENVIRONNEMENT

ÉCOLE POLYTECHNIQUE FÉDÉRALE DE LAUSANNE

POUR L'OBTENTION DU GRADE DE DOCTEUR ÈS SCIENCES

PAR

Vasileios GRIGORIOU

acceptée sur proposition du jury:

Prof. A.-G. Dumont, président du jury  
Prof. E. Brühwiler, directeur de thèse  
Prof. K. Thoma, rapporteur  
Prof. J. R. Casas Rius, rapporteur  
Prof. J.-F. Molinari, rapporteur



ÉCOLE POLYTECHNIQUE  
FÉDÉRALE DE LAUSANNE

Suisse  
2015



*στη Δήμητρα.*



# Table of contents

<b>List of figures</b>	ix
<b>List of tables</b>	xi
<b>Abstract</b>	xiii
<b>Résumé</b>	xv
<b>Foreword</b>	xvii
<b>Acknowledgements</b>	xix
<b>0. INTRODUCTION</b>	<b>1</b>
<b>0.1. Context and motivation</b>	<b>3</b>
<b>0.2. Definition of the engineering problem</b>	<b>3</b>
<b>0.3. Current approach and shortcomings</b>	<b>4</b>
<b>0.4. Objectives of thesis</b>	<b>6</b>
0.4.1. Resistance side	6
0.4.2. Action effect side	6
0.4.3. Reliability calculation	6
<b>0.5. Scope of thesis</b>	<b>7</b>
0.5.1. Fatigue crack initiation theory	7
0.5.2. Action effect determination by SRM	7
<b>0.6. Structure of thesis</b>	<b>7</b>
<b>0.7. References</b>	<b>8</b>
<b>1. PROBABILITY OF OBSERVABLE FLAW INITIATION AT HIGH CYCLE FATIGUE</b>	<b>9</b>
<b>1.1. Introduction</b>	<b>11</b>
<b>1.2. Theory</b>	<b>12</b>
1.2.1. Basic notions	12
1.2.2. Idealization of the RVE	13
1.2.2.1. <i>Absolutely simple RVE</i>	14
1.2.2.2. <i>Asymptotically simple RVE</i>	14
1.2.2.3. <i>Apparently simple RVE</i>	14
1.2.3. Energy balance of the RVE	14
1.2.3.1. <i>Absolutely simple RVE</i>	15
1.2.3.2. <i>Asymptotically simple RVE</i>	15
1.2.3.3. <i>Apparently simple RVE</i>	15
1.2.4. Limit state of ultimate failure	16
1.2.4.1. <i>Asymptotically simple RVE</i>	16
1.2.4.2. <i>Apparently simple RVE</i>	16
1.2.5. Partition of inelastic work into irreversible heat and intrinsic dissipation	18
<b>1.3. Calculations</b>	<b>18</b>
1.3.1. Elastic strain energy that can possibly be released in case of ultimate failure of a RVE	19
1.3.2. Inelastic work history of a RVE	19
1.3.2.1. <i>Definition of stimulus and response</i>	20

1.3.2.2.	<i>Distribution of stimulus over the microsystem population – The hypothesis of strain energy density equivalence</i>	20
1.3.2.3.	<i>Behavior of a single microsystem</i>	21
1.3.2.4.	<i>Statistical description of the behavior of a microsystem population</i>	21
1.3.2.5.	<i>Statistical simulation of the behavior of a microsystem population</i>	23
1.3.3.	RVEs modeled with a mixture of microsystem populations	24
1.3.3.1.	<i>Contribution of inelastic work to the critical amount of intrinsic dissipation energy</i>	24
1.2.4.	Algorithm	25
<b>1.4.</b>	<b>Scope and limitations of the model</b>	<b>25</b>
<b>1.5.</b>	<b>Calibration and validation using experimental S-N data</b>	<b>26</b>
1.5.1.	Experimental data	26
1.5.2.	Model input	27
1.5.3.	Calculation of the number of cycles to failure for a given failure probability	28
1.5.4.	Calibration	28
1.5.5.	Validation	30
1.6.	<b>Conclusions</b>	<b>30</b>
1.7.	<b>References</b>	<b>32</b>
	<b>Annex:</b> Algorithm for the implementation of the proposed model	<b>35</b>
<b>2.</b>	<b>MONITORING OF STRAIN PROFILE VARIATIONS IN THE RC SLAB OF A SHORT-SPAN RAILWAY UNDERPASS</b>	<b>37</b>
<b>2.1.</b>	<b>Introduction</b>	<b>39</b>
<b>2.2.</b>	<b>Monitoring scheme</b>	<b>40</b>
2.2.1.	Device for measuring strain profile variations	40
2.2.2.	Installation of monitoring devices on the structure	40
2.2.3.	Signal acquisition	41
2.2.4.	Signal post-processing	41
<b>2.3.</b>	<b>Results and discussion</b>	<b>46</b>
2.3.1.	Evaluation of the monitoring scheme	46
2.3.2.	Comparison with results from structural analysis	50
<b>2.4.</b>	<b>Conclusions</b>	<b>50</b>
<b>2.5.</b>	<b>References</b>	<b>52</b>
<b>3.</b>	<b>MONITORING-BASED SAFETY VERIFICATIONS AT THE ULTIMATE LIMIT STATE OF FRACTURE OF THE RC SLAB OF A SHORT-SPAN RAILWAY UNDERPASS</b>	<b>53</b>
<b>3.1.</b>	<b>Introduction</b>	<b>55</b>
<b>3.2.</b>	<b>Action incident – Action incident effect</b>	<b>55</b>
3.2.1.	Action incident	55
3.2.2.	Action incident effect	56
3.2.3.	Leading and accompanying action incident effects	56
3.2.4.	Action incident effect for verification of RC sections in bending failure	56
<b>3.3.</b>	<b>The sample of the representative action-incident effect</b>	<b>55</b>
3.3.1.	Records included in the sample	57
3.3.2.	Macroscopic distinction of incident types	57

3.3.3.	Indirect effect of seasonal and daily temperature variations – Representativeness of the sampling period	57
3.3.4.	Week-day variations in the traffic mixture	58
<b>3.4.</b>	<b>Probabilistic modeling of the representative action-incident effect</b>	<b>58</b>
3.4.1.	Determinant distribution	59
3.4.2.	Identification of the determinant instances and modeling of the determinant distribution– Explicit approach	60
3.4.3.	Identification of the determinant instances and modeling of the determinant distribution– Implicit approach	61
<b>3.5.</b>	<b>Safety verification format</b>	<b>64</b>
3.5.1.	Safety requirement in terms of examination values	64
3.5.2.	Distinction of uncertainty sources	64
3.5.3.	Treatment of the uncertainty in the measurements and primary-data post-processing	65
3.5.4.	Treatment of the uncertainty in the leading action incident effect extreme value and its probabilistic modeling	65
3.5.5.	Examination value of resistance and accompanying action incident effects	66
3.5.6.	Application of the safety verification format in the present case	67
<b>3.6.</b>	<b>Efficiency of the proposed format in a Bayesian probability context</b>	<b>68</b>
3.6.1.	Including the random statistical error in the probability of exceedance	68
3.6.2.	Including the systematic estimation error in the probability of exceedance	69
<b>3.7.</b>	<b>Conclusions</b>	<b>69</b>
<b>3.8.</b>	<b>References</b>	<b>70</b>
<b>4.</b>	<b>RELIABILITY OF THE STEEL REINFORCEMENT OF EXISTING RC SLABS SUBJECT TO RAILWAY TRAFFIC USING ADVANCED FATIGUE THEORY AND STRUCTURAL RESPONSE MONITORING</b>	<b>71</b>
<b>4.1.</b>	<b>Introduction</b>	<b>73</b>
<b>4.2.</b>	<b>Construction of case specific S-N curves for ribbed steel reinforcement bars</b>	<b>73</b>
4.2.1.	Characterization of the fatigue properties of the material at the surface of the bar using hardness	73
4.2.2.	Characterization of the loading conditions in the vicinity of the rib root	74
4.2.3.	Validation of the crack initiation S-N curve prediction method	78
4.2.4.	Crack propagation phase – Constant amplitude limit of fatigue	80
<b>4.3.</b>	<b>Probabilistic size effect in fatigue crack initiation life</b>	<b>81</b>
4.3.1.	Fundamental relation between damage factor and reliability	81
4.3.2.	Effect of the number of potential crack initiation locations – probabilistic size effect	82
4.3.3.	Size effect transform of the constant amplitude fatigue crack initiation life	84
4.3.4.	Number of potential crack initiation locations for test specimens and structural components	84
<b>4.4.</b>	<b>Damage factor increase rate</b>	<b>85</b>
4.4.1.	Calculation of damage factor increase	85
4.4.1.1.	<i>Palmgren-Miner rule</i>	86
4.4.1.2.	<i>Advanced theories for accounting for load sequence effects</i>	86
4.4.1.3.	<i>Proposed microplasticity theory</i>	86
4.4.1.4.	<i>Relation between damage factors as calculated by Miner's theory and the microplasticity theory</i>	86
4.4.2.	Material properties	87
4.4.3.	Input load history	88

4.4.3.1.	<i>Artificial action effect histories</i>	88
4.4.3.2.	<i>Action effect histories obtained from structural response monitoring</i>	88
4.4.3.3.	<i>Calculation of nominal stress histories</i>	89
4.4.3.4.	<i>Calculation of local work density histories for use with the proposed microplasticity theory</i>	91
4.4.4.	Results and discussion	91
<b>4.5.</b>	<b>Reliability of a single bar</b>	<b>93</b>
4.5.1.	Reliability with respect to formation of the first initial crack	93
4.5.2.	Reliability with respect to failure taking into account the CAFL	95
<b>4.6.</b>	<b>Conclusions</b>	<b>97</b>
<b>4.7.</b>	<b>References</b>	<b>97</b>
<b>5.</b>	<b>CONCLUSIONS AND OUTLOOK</b>	<b>99</b>
<b>5.1.</b>	<b>Main contributions and findings</b>	<b>101</b>
5.1.1.	Resistance side	101
5.1.2.	Action effect side	101
5.1.3.	Reliability calculation	102
<b>5.2.</b>	<b>Outlook</b>	<b>102</b>
<b>5.3.</b>	<b>Future work</b>	<b>103</b>
	<b>Epilogue</b>	<b>105</b>
	<b>ANNEX: Drawings of the monitoring device</b>	<b>107</b>
	<b>Curriculum Vitae</b>	<b>135</b>



# List of figures

<b>Fig. 0.1:</b>	Fatigue of RC structures as a problem of crack initiation at the root of the ribs of the steel reinforcement bars	3
<b>Fig. 0.2:</b>	Illustration of the Palmgren-Miner theory	5
<b>Fig. 1.1:</b>	A RVE at the moment of its ultimate failure.	12
<b>Fig. 1.2:</b>	Illustration of the quantities involved in Eq. (1.8). $\int_{t_0}^t \dot{\phi} dt$ is actually only a part of the indicated inelastic work .	17
<b>Fig. 1.3:</b>	The RVE (outer box) as a population of microsystems (small cycles) organized in collectivities (inner boxes); microsystems may respond in elastic (blank cycles) or in plastic mode (solid cycles) or may have attained ultimate failure (dashed cycles).	19
<b>Fig. 1.4:</b>	Illustration of the relation between: (a) strain energy $a$ , relative strain energy $a$ and strain energy at the point of latest reversal $\hat{a}$ , (b) inelastic work $w^{in}$ , relative inelastic work $w^{in}$ yield energy $a^y$ and relative yiled energy $a^y$ , for an elastic perfectly plastic system. The current state of the system is denoted by point C. In (b) inelastic work is performed between points B and C.	20
<b>Fig. 1.5:</b>	A mixed (discrete-gamma) probability distribution used for the statistical modeling of microsystem collectivities.	23
<b>Fig. 1.6:</b>	Two equally critical elements connected in series with a third noncritical one.	25
<b>Fig. 1.7:</b>	Experimetal data used for the calibration of the proposed model (after Pereira et al. [49], notched specimens and de Jesus et al. [50], smooth specimens). Blank signs imply run-outs	27
<b>Fig. 1.8:</b>	Geometry of the specimens used in the fatigue tests: (a) notched (replotted from Pereira et al. [49]), (b) smooth (replotted from de Jesus et al. [50]). Dimensions in mm.	27
<b>Fig. 1.9:</b>	The proposed model fitted to the experimental results of Pereira et al. [49] and De Jesus et al. [50]. Blank squares imply run-outs.	29
<b>Fig. 1.10:</b>	The proposed model fitted to the cyclic inelastic work calculated by the stress-strain curve of the material (idealized using Ramberg-Osgood relations and Masing hypothesis) .	30
<b>Fig. 1.11</b>	Block types used for validation of the model (Perreira [53])	31
<b>Fig. 1.12</b>	Comparaision of model prediction to experimetal results (Perreira [53]) for variable amplitude loading.	32
<b>Fig. 2.1:</b>	(a) Principle of mesurment of strain profile variations. (b) The device during testing and calibration in the laboratory. (c) Bottom view and (d) elevetions of the strain profile monitoring device. (e) Longitudinal section and (f) cross-section of the underpass with the installed device.	42
<b>Fig. 2.2:</b>	(a) A segment of signal of strain recorded on one of the bands between the passage of two trains. The two train passages can barely be ditinguished around second 10 and second 550. (b) FFT of the signal; the effect of IMI is clearly manifeted in the peaks regularly spaced at 33.4 Hz.	43
<b>Fig. 2.3</b>	FFT spectra of strain variation in the longitudinal (principal) reinforcement from train types passing on track 1 (over the monitoring point). (a-c) in order of appearance: a passenger train with a four axle locomotive, the same type of passenger train with two defective wheels, a freight train with a six axles locomotive. Black line: direct signal; red line: indirect signal. (d) Comparison of the direct signal FFT spectra for the passenger trains with and without defective wheel; black line: without defective wheel; red line: with defective wheels.	44
<b>Fig. 2.4</b>	Variation of strain in the longitudinal (principal) reinforcement from trains passing on track 1. Black line: band-stop filtered signal for elimination of EMI above 83.5 Hz; red line: 75 Hz low-pass filtered signal.	45
<b>Fig. 2.5</b>	Variation of strain in the longitudinal (principal) reinforcement from trains passing on track 1. 75 Hz low-pass filtered signal; red line: 20 Hz low-pass filtered signal.	46
<b>Fig. 2.6:</b>	Variation of strain in the longitudinal (principal) reinforcement. Black line: direct method; red line: indirect method. (a-f) Tains passing on track 1 (over the monitoring point): (in order of appearence) a suburban train unit, an intercity train unit, a passenger train with a four axle locomotive, the same type of passenger train with two defective wheels (indicated by the arrows), a freight train with a six axles locomotive, a special convoi. (g, h) Trains passing on track 2: a freight train with a six axles locomotive, a passenger train with a four axle locomotive.	47
<b>Fig. 2.7:</b>	Variation of strain in the transvers (secondary) reinforcement. Black line: direct method; red line: indirect method. (a-f) Trains passing on track 1 (over the monitoring point): (in order of appearance) a suburban train unit, an intercity train unit, a passenger train with a four axle locomotive, the same type of passenger train with one defective wheel (indicated by the arrow), a freight train with a six axles locomotive, a special convoi. (g, h) Trains passing on track 2: a freight train with a six axles locomotive, a passenger train with a four axle locomotive.	48

<b>Fig. 2.8:</b>	Distribution of the difference (a) and ratio (b) between the incident maxima of strain at the level of the longitudinal (principal) reinforcement as obtained by the indirect and the direct method. Gray solid bars: distribution in the entire population of traffic incidents; Red outlined bars: distribution in the heavy freight train subpopulation.	49
<b>Fig. 2.9:</b>	Comparison of recorded strain histories with calculated histories. Black line: recorded signal; red line: calculated history (indirect method). (a-b) signal on the longitudinal (principal) reinforcement for an intercity train unit (a) and a freight train (b), (c-d) signal on the transvers (secondary) reinforcement for an intercity train unit (c) and a freight train (d) (not the same incidents as in (a) and (b)), (e-f) the load patterns used in the calculation (dimensions in m).	51
<b>Fig. 2.10:</b>	Distribution of a unit axle load on the nodes of the finite element model (dimensions in m).	51
<b>Fig. 3.1:</b>	(a) The sample of $F$ instances with the corresponding ambient temperature. (b) the histogram of $F$ instances (c) zoom on the extrem value region (d) histogram of the subset of type-1 instances	58
<b>Fig. 3.2:</b>	(a) The sample of $M$ instances (b) the histogram of $M$ instances	58
<b>Fig. 3.3:</b>	(a) Comparison of empirical (dots) and fitted (continuous curve) GEV distribution for type-1 incidents and graphical detection of the threshold as the knee point of a bilinear approximation (dashed lines) using the type-1 sample. (b) Graphical detection of the threshold using the original sample. (c) Comparison of empirical and fitted shifted exponential distribution for type-1 incidents and graphical detection of the threshold as the knee point of a bilinear approximation using the type-1 sample. (d) Same as in (c) but for the original sample.	62
<b>Fig. 4.1:</b>	(a) Axisymmetric FE model used for the calculations of stress distribution at the root of the rib. (b) Axial stress in the direction of the axis of the bar (vertical direction on the figure). (c) Von Miseses equivalent stress. (d) Axial stress in the direction of the radius of the bar (horizontal direction on the figure). (e) Shear stress.	75
<b>Fig. 4.2:</b>	(a) Normalized stress distributions behind the root of a rib as calculated by FE models for various rib geometries (gray lines) and according to the approximation of Eq. (4.13) (black line). (b) Illustration of the distribution of stress behind the root of a rib.	77
<b>Fig. 4.3:</b>	Predicted median (0.5 fractile) crack initiation S-N curves (continuous lines) and constant amplitude fatigue limits (dashed lines) compared to the experimental results of Zheng and Abel [26] for a set of 7 reinforcement bars of different diameter (Australian made TEMPCOR 400Y).	79
<b>Fig. 4.4:</b>	Comparison between predicted and experimentally observed fatigue limit for a set of 8 reinforcement bars of different diameter.	81
<b>Fig. 4.5:</b>	(a) CDF and (b) PDF of damage factor at formation of the initial crack – a standard Fréchet distribution.	83
<b>Fig. 4.6:</b>	(a) PDFs of the damage factor at the first initial crack formation for various value of the number of potential crack initiation locations $M$ . (b) Median and “dispersion” (75% fractile – 25% fractile) of the above distributions as functions of $M$ .	83
<b>Fig. 4.7:</b>	Comparison of the constructed S-N curves (continuous lines) with the S-N curves obtained by the microplasticity model (dashed lines) after its calibration to the constructed S-N curves.	88
<b>Fig. 4.8:</b>	Damage factor evolution calculated by the microplasticity theory for 10 successive stress history blocks acquired by different methods and assumptions. Blocks are defined by vertical gridlines. Note that for monitoring histories each block corresponds to the monitoring period of 156 days while for artificial histories each block correspond to 1 day.	93
<b>Fig. 4.9:</b>	Damage factor increase rate vs dynamic amplification factor for $\rho = 0.536\%$ with concrete crack closure effect, predicted after various calculations methods and assumptions.	94
<b>Fig. 4.10:</b>	PDF of the time to formation of the initial crack for $\rho = 0.536\%$ with concrete crack closure effect and with all trains included in the history.	96

## List of tables

<b>Table 1.1:</b>	Model parameters after calibration with the experimental results of [21].	30
<b>Table 1.2:</b>	Experimental results (Pereira [53]) and model prediction for variable amplitude loading.	32
<b>Table 3.1:</b>	Average number of loaded freight trains on track 1 (type-1 incidents).	59
<b>Table 3.2:</b>	Statistical properties of the extreme value distribution of $F$ .	64
<b>Table 3.3:</b>	FORM sensitivity factors according to the semi-probabilistic method.	66
<b>Table 3.4:</b>	Prescribed values of the various reliability parameters.	68
<b>Table 3.5:</b>	Calculation of the examination values of action effect and resistance.	68
<b>Table 4.1:</b>	Rebar data [25] and intermediate calculation results.	78
<b>Table 4.2:</b>	Rebar characteristics considered in the present application.	87
<b>Table 4.3:</b>	Microplastic model material parameters obtained by model calibration to the constructed S-N curves.	86
<b>Table 4.4:</b>	Traffic mix used in the calculations.	89
<b>Table 4.5:</b>	Concrete crack closure variables.	91
<b>Table 4.6:</b>	Damage factor increment rate according to the various calculations methods and assumptions.	92
<b>Table 4.7:</b>	Safe service life for $\rho = 0.536\%$ predicted after various calculations methods and assumptions.	96



## Abstract

Experience has shown that when the models and methods that have been developed for the design of new structures are “blindly” used for the examination of existing structures, the management of civil infrastructure lacks substantially in financial efficiency and social sustainability. It seems that in these cases the above models and methods are unduly conservative. This is not surprising since the design of new structures is performed under conditions of larger uncertainty and lower risk-reduction-cost comparing to the conditions under which the examination of an existing structure is usually carried out.

Motivated by these observations this work develops around the specific problem of safety verification of existing reinforced concrete slabs (and more precisely of their bending steel reinforcement) subject to railway traffic action. The problem is tackled from both (a) a resistance standpoint (through the development of advanced fatigue-resistance / damage-accumulation models) and (b) an action-effect standpoint (through the development of suitable structural response monitoring schemes). The two approaches are combined in the development of safety verification methods for the ultimate limit states of: (a) excessive deformation (or fracture) and (b) fatigue failure. Accordingly, the work is organized in four chapters.

Chapter 1 deals with the development of a mesoscopic model of resistance to fatigue flaw initiation in the vicinity of a stress concentration (as observed in the case of ribbed reinforcement bars, on the surface of which, fatigue flaws always initiate near the root of the ribs). Fatigue evolution during the flaw initiation phase is described at the level of the representative volume element by the probability that this element fails in a given period of time under given stimulus. This probability is calculated as a function of the accumulated inelastic work density. For the calculation of small amounts of inelastic work in the quasi-elastic domain of materials, a microplasticity model is developed using the hypothesis of strain energy density equivalence and a statistical distribution of power density within the representative volume element. The model is validated and calibrated by comparison to experimental results taken from the literature and derived from constant and variable amplitude fatigue tests on notched steel components.

Chapter 2 presents a novel monitoring scheme oriented towards the structural examination of reinforced concrete slabs subject to railway traffic action. Monitoring is based on the measurement of the mean axial strain profile variation in the slab. The strain profile is reconstructed by measuring the variation of two distances between two pairs of points materialized at two different levels under the slab on rigid attachments fixed on the slab. The distance variations are measured by means of strain gages measuring the strain on two very thin strips connecting the two attachments. The technical aspects of the implementation of the above scheme on a short span railway underpass for a period of seven months and the processing of the acquired signals are presented in detail. Some interesting monitoring records are provided over which the efficiency of the proposed scheme is discussed.

Chapter 3 proposes a monitoring based safety verification format for the ultimate limit state of excessive deformation (or fracture). This format provides the examination value of the critical traffic action effect directly from monitoring data (without resorting to action models and structural analysis) and is characterized by: (a) the use of the notion of action incident (which is particularly well suited for the case of railway traffic where an incident can be identified as the passage of a train over the structure), the distinction of incident types and the isolation of the determinant incidents (those on which the examination value actually depends); (b) the use of the extreme value theory within a semi-probabilistic framework. The development of the verification format is based on the data obtained from the monitoring campaign described in Chapter 2.

Chapter 4 focuses on the fatigue verification of the reinforcement bars which are practically always the critical component of a RC element with respect to fatigue failure. In particular, the following questions are addressed: (a) construction of case specific S-N curves for the steel reinforcement bars embedded in an existing structural element taking into account their surface hardness and the geometry of their ribs; (b) investigation of the load sequence effect using the fatigue resistance model developed in Chapter 1 and nominal stress histories obtained from structural response monitoring; (c) calculation of fatigue reliability taking into account the existence of a constant amplitude fatigue limit.

*Keywords:* crack initiation; strain energy density equivalence; statistical microplasticity; structural response monitoring; strain gages; short span bridges; extreme value theory; steel reinforcement fatigue; S-N curves; damage accumulation; load sequence effects.

---



## Résumé

L'expérience a démontré que lorsque les modèles et les méthodes développées pour la conception de nouvelles structures sont « aveuglement » utilisées pour l'examen des structures existantes, la gestion des infrastructures est loin d'être optimale au niveau de l'économie et du développement durable. Cela n'est pas étonnant étant donné que la conception de nouvelles structures est en général effectuée dans des conditions d'incertitude plus élevées et des coûts plus bas pour la réduction des risques en comparaison avec les conditions habituelles sous lesquelles l'examen des structures existantes est réalisé.

Motivé par ces observations, ce travail se développe autour du problème spécifique de la vérification de la sécurité structurale des dalles existantes en béton armé (et plus précisément de leurs armatures de flexion) soumises à l'action du trafic ferroviaire. Le problème est abordé : (a) du côté de la résistance (à travers le développement de modèles avancés de résistance à la fatigue et d'accumulation de dommage) et aussi (b) du côté de l'effet des actions (à travers le développement d'une méthode de monitoring). Les deux approches sont combinées dans le développement des méthodes de vérification de la sécurité structurale à l'état limite ultime (a) de rupture et (b) de fatigue.

Le chapitre 1 traite le développement d'un modèle méso-scopique de résistance à l'amorçage d'une fissure de fatigue dans le voisinage d'une concentration de contraintes tel qu'observé dans le cas des barres d'armature nervurées où les fissures de fatigue sont toujours amorcées proche de la racine des nervures. L'évolution de la fatigue durant la période d'amorçage est décrite au niveau de l'élément de volume représentatif comme la probabilité que cet élément rompe dans une période de temps donnée et sous une sollicitation donnée. Cette probabilité est calculée comme une fonction de la densité du travail inélastique accumulé. Pour le calcul de petites quantités de travail inélastique, dans le domaine quasi-élastique des matériaux, un modèle de micro-plasticité est développé en utilisant l'hypothèse de l'équivalence de la densité d'énergie de déformation avec une description statistique de la distribution de la densité de puissance à l'intérieur de l'élément de volume représentatif. Le modèle est validé et calibré par comparaison avec des résultats expérimentaux tirés de la littérature et obtenus par des essais de fatigue à amplitude constante et variable effectués sur des éléments entaillés en acier.

Le chapitre 2 présente une nouvelle méthode de monitoring orientée vers l'examen de la sécurité structurale des dalles en béton armé sous sollicitation de trafic ferroviaire. Le monitoring est basé sur la mesure de la variation du profil des déformations de la section de la dalle. Le profil des déformations est reconstruit en mesurant la variation de longueur entre deux paires de points situés sur des attaches rigides à deux niveaux différents sous la dalle. La variation de longueur est mesurée par des jauges d'extensiométrie qui mesurent la déformation sur deux très fines bandes en acier qui relient les deux attaches. Les aspects techniques de l'application de cette méthode sur un pont ferroviaire de courte portée pour des mesures sur une période de sept mois sont présentés en détail ainsi que le traitement des signaux qui en sont acquis. Des résultats intéressants sont également fournis. Avec ces résultats, l'efficacité de la méthode proposée est discutée.

Le chapitre 3 propose une méthode de vérification de la sécurité structurale à l'état limite ultime de rupture. Cette méthode, basée sur des données de monitoring, fournit la valeur d'examen de l'effet de l'action du trafic sans l'utilisation de modèles de charge ni d'analyse structurale. Elle est d'ailleurs caractérisée par : (a) la notion de l'incidence de l'action (qui convient très bien dans le cas du trafic ferroviaire où une incidence peut être définie comme le passage d'un train sur l'ouvrage), la distinction des types d'incidences et l'isolement des incidences déterminantes (celles desquelles la valeur d'examen dépend vraiment) ; (b) l'utilisation de la théorie des valeurs extrêmes dans un cadre semi-probabiliste. Le développement de la méthode de vérification est basé sur les données obtenues par la campagne de monitoring décrite au chapitre 2.

Le chapitre 4 se concentre sur la vérification à la fatigue des barres d'armature, soit la composante critique d'un élément en béton armé vis-à-vis de la fatigue. Plus particulièrement les points suivants sont abordés : (a) construction de courbes S-N pour des barres d'armature incluses dans un élément de béton existant en tenant compte de la géométrie des nervures et de la dureté de surface ; (b) investigation de l'effet de la séquence des sollicitations en utilisant le modèle d'accumulation de dommage développé au Chapitre 1 et les historiques des contraintes obtenus par monitoring ; (c) calcul de la fiabilité à la fatigue en tenant compte de l'existence d'un limite de fatigue à amplitude constante.

*Mots-clés* : amorce d'une fissure ; équivalence de la densité d'énergie de déformation ; micro-plasticité statistique ; monitoring de la réponse structural ; jauges d'extensiométrie ; ponts de courte portée ; théorie des valeurs extrêmes ; fatigue des barres d'armature en acier ; courbes S-N ; accumulation de dommage ; effet de la séquence des sollicitations.



## Foreword

Safety verification of existing bridges is currently still based on the methodology used for the design of new structures. This often leads to the unsatisfactory situation that the safety of existing bridges cannot be verified. The use of over-conservative traffic load models, coupled with excessive dynamic amplification factors, can result in costly unnecessary interventions for strengthening and rehabilitation. Although existing bridges are today often subjected to higher traffic loads than what was assumed when they were built, they usually behave well and show no sign of distress due to traffic loads. Consequently, there is an obvious need to develop engineering methods to adequately address the issues specific to existing structures.

In his doctoral thesis, Vasileios Grigoriou investigates this “dilemma” with the objective to use data from structural response monitoring for the safety verification of slab-like reinforced concrete railway bridges. Techniques for the monitoring of structural response are nowadays readily available, reliable and cost-effective because of important recent progress in measurement and information technologies. The basic approach of the thesis relies on the monitored traffic action effects due to real traffic loading, thus, omitting uncertainties and conservatism in traffic load models. The focus is on “what arrives in the structural member”.

The present doctoral thesis is a step towards this novel methodology as it provides new knowledge towards more accurate examination of bridges. The way how we structural engineers deal with existing structures has a significant socio-economic impact because of the high monetary value of the built infrastructure. Engineers thus need to devise novel ways how to “get more out of existing structures”. This thesis contributes to this ambitious goal.

With his doctoral thesis, Vasileios Grigoriou provides the proof of his capabilities to conduct a significant scientific study and to solve complex scientific questions. The thesis delivers significant findings that are useful and applicable for the examination of bridges.

In the name of the whole MCS Team, I thank him for his constant and thorough investment to the thesis topic as well as for his professional skills and personal qualities.

Lausanne, December 2015

Professor Eugen Brühwiler



## Acknowledgments

First and foremost, I would like to thank Prof. Eugen Brühwiler for giving me the opportunity to conduct my doctoral research at the EPFL, for ensuring optimal work conditions throughout the duration of the project and for his continuous support in my work. I would also like to thank him for introducing me into the concepts of sustainable development of civil infrastructure.

My sincere thanks go also to the members of the jury: Prof. Jean-François Molinari of EPFL, Prof. Karel Thoma of Hochschule Luzern and Prof. Joan Ramon Casas Rius of Universitat Politècnica de Catalunya, who carefully examined the manuscript of the thesis and came up with very interesting comments and insightful suggestions for future work. I would also like to thank Prof. André-Gilles Dumont for kindly accepting to chair the examination session.

I am grateful to Prof. Stefanos Tsinopoulos for his sincere interest in my work, for the many long and constructive discussions we had on the first chapter of the thesis and – the most important – for his precious friendship and his continuous encouragement. The contribution of the anonymous reviewers who reviewed the papers on which this thesis is based is also acknowledged.

I would also like to sincerely thank Mr. Gilles Guignet, engineer in the structures laboratory, for his valuable contribution in the development of the monitoring system, for the ingenious programming of the signal acquisition system and for his assistance in the installation and calibration of the monitoring system in situ. Sincere thanks go also to the skillful technicians of the structures laboratory: Armin Krićić who fabricated the monitoring device and Gérald Rouge who gave us a great help in the installation of the monitoring system on the bridge.

I would like to thank Ms. Christine Benoit, secretary of MCS, for her valuable support in all kinds of administrative issues during the first years of my studies in EPFL. Special thanks go also to Ms. Florence Grandjean for her assistance, her friendship and her precious moral support during the later years of my studies.

Financial support from VALE international SA, CH-1162 Saint-Prex, under grant No 520.222 is acknowledged. The CFF is thanked for allowing us to monitor one of its structures.

The support of Dr. Emmanuel Denarié of MCS, especially in the preparation of the oral examination and defense, is highly acknowledged. Sincere thanks also to my fellow doctoral students in MCS for the useful discussions we had and for their support through the different phases of my studies: Dr. Alexis Kalogeropoulos, Dr. Talayeh Nosiravani, Dr. Tohru Makita, Dr. Hadi Kazemi Kamyab, Dr. Mark Treacy, Dr. Marina Rocha, Mr. Christophe Loraux and especially Dr. Maléna Bastien Masse for her encouragement at the end of the thesis was very important.

Finally, I would like to express my deepest gratitude to my parents, Panagioti and Maria, who have always supported my decisions and efforts in any possible way.

This work belongs to Dimitra whose love warms my heart and keeps me going.



- „6.5 Zu einer Antwort, die man nicht aussprechen kann, kann man auch die Frage nicht aussprechen. Das Rätsel gibt es nicht. Wenn sich eine Frage überhaupt stellen lässt, so kann sie auch beantwortet werden.
- „6.51 Skeptizismus ist nicht unwiderleglich, sondern offenbar unsinnig, wenn er bezweifeln will, wo nicht gefragt werden kann. Denn Zweifel kann nur bestehen, wo eine Frage besteht; eine Frage nur, wo eine Antwort besteht, und diese nur, wo etwas gesagt werden kann.
- „6.52 Wir fühlen, dass, selbst wenn alle möglichen wissenschaftlichen Fragen beantwortet sind, unsere Lebensprobleme noch gar nicht berührt sind. Freilich bleibt dann eben keine Frage mehr; und eben dies ist die Antwort.
- „6.521 Die Lösung des Problems des Lebens merkt man am Verschwinden dieses Problems. (Ist nicht dies der Grund, warum Menschen, denen der Sinn des Lebens nach langen Zweifeln klar wurde, warum diese dann nicht sagen konnten, worin dieser Sinn bestand?)
- „6.522 Es gibt allerdings Unaussprechliches. Dies zeigt sich, es ist das Mystische.
- „6.53 Die richtige Methode der Philosophie wäre eigentlich die: Nichts zu sagen, als was sich sagen lässt, also Sätze der Naturwissenschaft—also etwas, was mit Philosophie nichts zu tun hat—, und dann immer, wenn ein anderer etwas Metaphysisches sagen wollte, ihm nachzuweisen, dass er gewissen Zeichen in seinen Sätzen keine Bedeutung gegeben hat. Diese Methode wäre für den anderen unbefriedigend—er hätte nicht das Gefühl, dass wir ihn Philosophie lehrten—aber sie wäre die einzig streng richtige.
- „6.54 Meine Sätze erläutern dadurch, dass sie der, welcher mich versteht, am Ende als unsinnig erkennt, wenn er durch sie—auf ihnen—über sie hinausgestiegen ist. (Er muss sozusagen die Leiter wegwerfen, nachdem er auf ihr hinauf gestiegen ist.) Er muss diese Sätze überwinden, dann sieht er die Welt richtig.
- „7 Wovon man nicht sprechen kann, darüber muss man schweigen.“
- “6.5 When the answer cannot be put into words neither can the question be put into words. The riddle does not exist. If a question can be framed at all, it is also possible to answer it.
- “6.51 Scepticism is not irrefutable, but obviously nonsensical, when it tries to raise doubts where no questions can be asked. For doubt can exist only where a question exists, a question only where an answer exists, and an answer only where something can be said.
- “6.52 We feel that even when all possible scientific questions have been answered, the problems of life remain completely untouched. Of course there are then no questions left, and this itself is the answer.
- “6.521 The solution of the problem of life is seen in the vanishing of the problem. (Is not this the reason why those who have found after a long period of doubt that the sense of life became clear to them have then been unable to say what constituted that sense?)
- “6.522 There are, indeed, things that cannot be put into words. They make themselves manifest. They are what is mystical.
- “6.53 The correct method in philosophy would really be the following: to say nothing except what can be said, i.e. propositions of natural science—i.e. something that has nothing to do with philosophy—and then, whenever someone else wanted to say something metaphysical, to demonstrate to him that he had failed to give a meaning to certain signs in his propositions. Although it would not be satisfying to the other person—he would not have the feeling that we were teaching him philosophy—this method would be the only strictly correct one.
- “6.54 My propositions serve as elucidations in the following way: anyone who understands me eventually recognizes them as nonsensical, when he has used them—as steps—to climb up beyond them. (He must, so to speak, throw away the ladder after he has climbed up it.) He must transcend these propositions, and then he will see the world aright.
- “7 What we cannot speak about we must pass over in silence.”

Ludwig Wittgenstein  
Logisch-Philosophische Abhandlung

Ludwig Wittgenstein  
Tractatus Logico-Philosophicus  
transl. by David Pears and Brian McGuinness



# **Introduction**

## **Nomenclature**

$D_M$  Miner's damage factor  
 $\tilde{D}$  Damage variable  
 $\tilde{D}_f$  Damage variable at failure  
 $N$  Number of load variations  
 $N_f$  Number of load variations to failure  
CAFL Constant Amplitude Fatigue Limit

CDF Cumulative Distribution Function  
PDF Probability Density Function  
RC Reinforced Concrete  
RVE Representative Volume Element  
SRM Structural Response Monitoring  
SLS Serviceability Limit State  
ULS Ultimate Limit State



## 0.1. Context and motivation

A number of reinforced concrete (RC) railway bridges are operated today (or will have to be operated in the near future) under traffic conditions which are substantially less favorable than those that have been foreseen in the design stage (higher axle loads, increased traffic volume etc.). This fact, raises doubts among transport agents worldwide on whether the safety level actually provided by these bridges meets modern requirements. Fatigue safety, in particular, is of major concern since in general fatigue failures involve, at the stage of final fracture, less energy consumption than failures under a single overload and may lead for that reason to increased failure consequences. Additionally, fatigue failures may occur under normal service loads and are not always related to abnormal or accidental overloads; so that increased control of the axle loads that pass on the bridge may prove insufficient to prevent such failures.

In general, reinforced concrete (RC) bridges are not deemed vulnerable to fatigue. Notwithstanding, their long term behavior under fluctuating traffic load remains today unclear to a considerable degree. In part, this is due to the relatively young age of the majority of these structures (in 2004, only 20% of the European concrete railway bridges were more than 50 years old while 55% were between 25 and 50 years old and the rest were younger [1]). This implies that potential fatigue failures which would have improve our insight to the phenomenon have yet to be observed. Besides that, a far more urgent problem of RC deterioration, that of reinforcement corrosion, has been until recently the main focus of attention of the respective engineering community and has also led to premature deterioration of these structures. The rather incomplete knowledge on the long term fatigue behavior of RC element in conjunction with the low cost of safety measures in construction stage, has led the engineering community towards conservative methods for the fatigue design of new structures which have also been codified in the relevant design standards.

Applied for the examination of existing structures these methods lead often to the conclusion that structural interventions are needed in order ensure the expected level of safety. On the other hand, modern railway network operation requirements increase dramatically the complexity, the execution time and the cost of interventions on operating lines. Hence, in order to achieve sustainable operation and development of the existing railway infrastructure, structural safety with respect to fatigue failure has to be guaranteed with minimal, or even without, intervention on the structures. This social requirement should direct the engineering community towards the development of advanced safety verifications methods based on realistic resistance and action effect models and free from unnecessary conservatism.

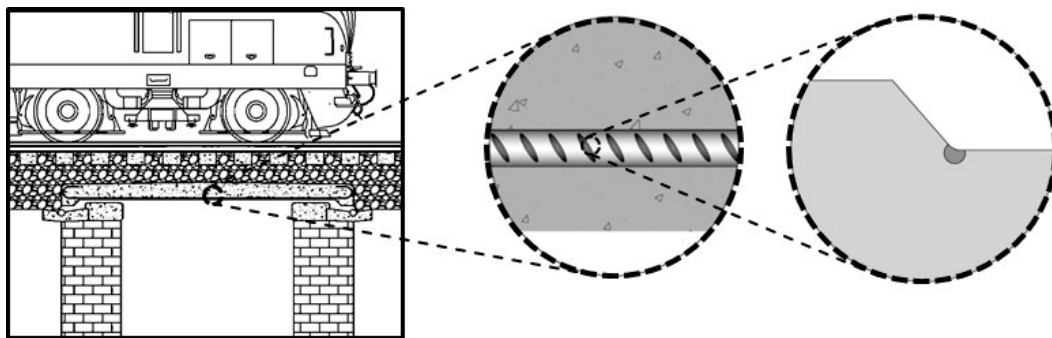


Fig. 0.1: Fatigue of RC structures as a problem of crack initiation at the root of the ribs of the steel reinforcement bars.

## 0.2. Definition of the engineering problem

Motivated by the above considerations, and aiming in a global approach of the above issue, the investigation in this work extends over the domains of fatigue crack initiation theory, action effect determination by Structural Response Monitoring (SRM), and structural safety. Within the above domains the scope of the thesis is defined in relation to the practical problem of *fatigue safety verification of the bending steel*

reinforcement embedded in existing RC slabs subject to railway traffic action. Indeed, it has been shown [2, 3] that in all practical cases, steel reinforcement is the critical components in fatigue failure of RC elements. In particular we consider the case of ribbed bars (ribs ensure proper bond between reinforcement bars and surrounding concrete) in which fatigue is macroscopically manifested by the formation of cracks near the root of the ribs (where geometric stress concentrations occur) and the propagation of these cracks till ultimate failure of the bar [3, 4]. An illustration of the engineering problem is given in **Fig. 0.1**.

### 0.3. Current approach and shortcomings

The major steps of the current engineering practice [5] in fatigue safety verification of reinforcement bars are briefly presented below with the aim to reveal the areas of potential improvement in the applied methods.

- The actual traffic action is modeled as a sequence of traffic load models belonging to a prescribed train type mix. This load model sequence is then applied on a global structural model of the bridge, in order to calculate sectional (or element) force and moment histories (1st level action effect) which are in turn applied on a section (or element) model in order to calculate nominal stress histories in the reinforcement (2<sup>nd</sup> level action effect). Hence, in general, safety verifications involve a three level modeling (without including the statistical modeling which is also necessary in the case where extreme values are of interest). With each modeling level additional uncertainties are introduced in the verification [6].
- Despite the fact that reinforcement bars are in fact structural components with significant variation in their geometrical characteristics and fabrication processes, they are treated in terms of their fatigue resistance as a single material. Most design standards [7, 8] specify only one or two S-N curves for practically all the types of reinforcement bars, distinction being usually made only between small and large diameters. The prescribed S-N curves correspond to a certain (usually the 5%) fractile value of the experimentally observed number of cycles to failure in a sample of bars with very different characteristics [5]. Hence, the uncertainty included in this fractile is to a large extent uncertainty that could be reduced by detailed examination and consideration of the specific characteristics of the bar in the construction of case specific S-N curves. Additionally, some design standards [8] specify, in the same uniform manner, a Constant Amplitude Fatigue Limit (CALF) which, however, is defined somewhat arbitrarily as the value of the S-N curve corresponding to a certain number of cycles (usually between 2 and 10 million cycles).
- Quite often a first level of fatigue safety verification is attempted by comparing the maximum stress range induced in the nominal stress histories calculated in the previous step to the specified CALF [8]. However the only conclusion that can be drawn from this simple comparison is whether the fatigue life of the reinforcement can be assumed infinite or not. If this verification fails then a calculation of accumulated damage is performed in which the existence of the CALF is generally ignored. However, a combined consideration of the accumulated damage and the CALF is possible within a probabilistic safety verification framework and can lead to substantial reduction of conservatism as it has been demonstrated in [9] for the case of welded steel connections.
- Palmgren-Miner theory is used in order to calculate the damage factor for a given history of nominal stress. The application of the Palmgren-Miner theory for a general load history requires that the load history be transformed into an equivalent spectrum of load variations. This spectrum can be given either in the form of a discrete histogram that gives the frequency of load variations within each specified interval of load variation magnitudes or in the form of a continuous density function that gives the load variation frequency density at any load variation magnitude. Usually the rainflow cycle-counting method is employed because it implicitly takes into account the hysteresis loops experienced by the material (either at macroscopic or microscopic level) during its loading history.

After the transformation of the loading history to a load spectrum, the Palmgren-Miner rule suggests that a damage factor  $D_M$  can be calculated from the spectrum as

$$D_M = \sum_i \frac{N_i}{N_f(\Delta s_i)} \quad (0.1a) \text{ for a discrete histogram}$$

$$D_M = \int \frac{N_{\text{tot}} f(\Delta s)}{N_f(\Delta s)} d(\Delta s) \quad (0.1b) \text{ for a continuous density function}$$

where  $\Delta s_i$  is the mid-value of the  $i^{\text{th}}$  load variation magnitude interval,  $N_i$  is the frequency of load variations within the  $i^{\text{th}}$  interval,  $N_f(\Delta s_i)$  is the number of cycle to failure under load variations of constant magnitude  $\Delta s_i$ ,  $N_{\text{tot}}$  is the total number of load variations in the history and  $f(\Delta s)$  is the load range frequency density function. The calculated value of damage factor depends, therefore, to the mathematical method that is used for transforming the load history to the equivalent spectrum. In any case an amount of information is lost in the transformation so that load sequence effects are neglected to a lesser or greater extend. According to the theory an element fails in fatigue when the damage factor reaches the value of one.

The Palmgren miner's theory as described above relies on four hypotheses:

- A certain damage variable  $\tilde{D}$  exists and its value increases monotonically during a load history (however this variable does not have to be explicitly defined).
- The damage resulting from a loading history depends only on the corresponding load spectrum or in other words all the loading histories having the same spectrum result to the same value of damage.
- All load variations with the same magnitude have equal contribution to the value of damage.
- The value of damage variable at failure  $\tilde{D}_f$  is a material property, i.e. independent from the loading history (the combination of hypotheses (c) and (d) this has as direct consequence that the value of the damage factor at failure is one).

All the above hypothesis do not have universal validity and their suitability for the solution of each particular type of fatigue problems needs to be evaluated separately using damage accumulation models of physical origin.

- Palmgren Miners' theory, as presented above, gives merely a deterministic description of damage accumulation. This deterministic description (which is due to the fourth hypothesis stated above) is in strong contrast with the inherently random nature of fatigue failure (which goes beyond the statistical variation of materials properties) and also with the probabilistic approaches which are increasingly used in structural safety verifications. The state of the art in probabilistic fatigue safety verifications consists in a semi-empirical consideration of the relation between damage factor and reliability by assuming (on the basis of experimental results) a probability distribution for the number of load variations to failure at each load variation magnitude [10]. This approach does not allow for a separate treatment of the inherent randomness of the damage accumulation process and the statistical variation of material properties. In that sense it does not also allow for a proper consideration of the statistical "size dependence" of the fatigue resistance of structural components.

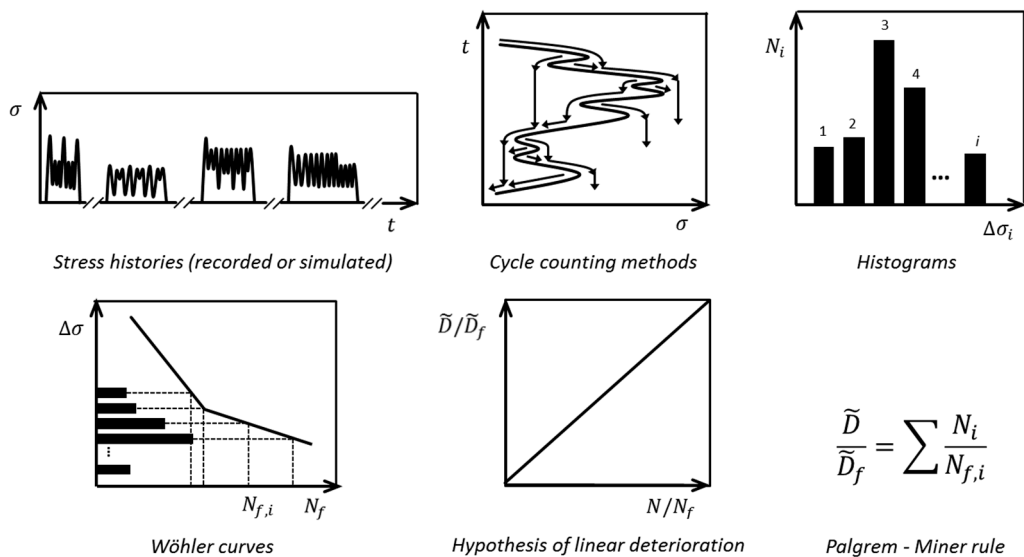


Fig. 0.2: Illustration of the Palmgren-Miner theory.

#### 0.4. Objectives of thesis

The above outlined limitations define the objectives of the thesis which are listed below in three classes depending on whether they refer to modeling and quantification of fatigue deterioration (resistance side), monitoring and modeling of traffic action effects (action effect side) or calculation of reliability.

##### 0.4.1. Resistance side

1. Set a theoretical basis for the macroscopic description of fatigue during the crack initiation phase by defining a physical quantity that meaningfully describes fatigue deterioration<sup>1</sup>.
2. Formulate the fundamental relation between the calculated<sup>2</sup> value of damage and reliability, i.e. the probability that an initial crack will have been formed before damage reaches a given value, or, in other words, the CDF of the calculated value of damage at the moment of initial crack formation<sup>3</sup>.
3. Develop an energy model in order to calculate the evolution of the deterioration measure under any given action effect history for the case of metal components with geometric stress raisers.
4. Present a method for constructing case specific constant amplitude S-N curves taking into account the actual material and rib geometry of the reinforcement bars of a specific structure and use these curves for calibration of the energy model which can subsequently be used with any general action effect history.
5. Calculate the (generally favorable) statistical “size dependence” of the fatigue resistance of steel reinforcement bars embedded in concrete

##### 0.4.2. Action effect side

6. Develop a Structural Response Monitoring (SRM) scheme adapted to existing reinforced concrete slabs.
7. Develop a framework for probabilistic action effect modeling on the basis of long term monitoring records and calculate examination<sup>4</sup> action effect values using extreme value theory.

##### 0.4.3. Reliability calculation

8. Investigate the reliability consequences of neglecting (under Palmgren-Miner theory) the load sequence effects in the case of RC slabs subject to railway traffic actions, using as reference the damage accumulation model developed for Objective 2 and the railway traffic action effect histories recorded under Objective 4
9. Evaluate the evolution of reliability at the level of a single reinforcement bar taking into account the existence of a constant amplitude fatigue limit.

---

<sup>1</sup> Such a physical quantity describing material deterioration (in this work, for example, microstructurally blocked free energy) is referred here as damage variable or simply damage, while a dimensionless deterioration measure obtained by normalizing such a quantity by its ultimate value at the moment of initial crack formation is referred as damage factor.

<sup>2</sup> We make a distinction between the actual (unobservable) value of damage which is a random variable and the calculated (observable) value which is deterministic (for a given deterministic action effect history). The actual and the calculated value of damage factors can be distinguished respectively. The actual damage factor value at the moment of initial crack formation is always equal to 1, the calculated value, however, can take any value in  $[0, \infty)$ . This issue is discussed in Section 1.2.4. In the engineering practice only the calculated values of damage and damage factor can be used. Hence, when no specific indication is given the calculated values are implied.

<sup>3</sup> The “calculated value of damage (or damage factor) at the instant of initial crack formation” is most often encountered in the literature as “critical damage (or damage factor)”. However since it is the actual value of damage that is really critical for crack initiation, we will retain the former slightly longer but more descriptive term throughout this work. It should also be emphasized that the calculated value of damage (or damage factor) at the instant of initial crack formation is an inherently random variable and should not be interpreted as an unknown material property. Its randomness originates from the macroscopic description of the fatigue.

<sup>4</sup> The term “examination value”, as introduced in the Swiss code for existing structures [11], is adopted here. This term corresponds to the term “design value” used for new structures.

## 0.5. Scope of thesis

With respect to the above stated objectives, the scope of investigation is formally delimited by the following postulates which refer exclusively to the work presented in this thesis and should not be considered as general statements:

### 0.5.1. Fatigue crack initiation theory

- *Fatigue cracks initiate in the vicinity of geometric stress concentrations.* This is true for all structural components featuring geometric stress raisers and implies that the exact location of crack initiation or at least a finite number of possible locations can be a priori determined. The adoption of this postulate in this work excludes the investigation of the fatigue of smooth components.
- *Structural components are subject to nominal stress histories which do not induce generalized yield of the component except in very rare accidental incidents.* This means that the investigation here is limited to what is commonly referred as high cycle fatigue – although general loading histories are considered here rather than cyclic loads.
- *Crack initiation phase constitutes the major part of the total fatigue life of a structural component.* This is true for components which at the beginning of their service life may reasonably be assumed as free from initial macroscopic defects and other sharp geometric features. For ribbed reinforcement bars embedded in concrete there is substantial experimental evidence in support of this postulate [4].
- *Macroscopic approach.* Although, understanding of microstructural processes is a step of paramount importance in the formulation of meaningful macroscopic theories, an exact microstructural description of the crack initiation phenomenon is not feasible in most practical cases. It has to be accepted that the microscopic state of a RVE remains unobservable and appropriate probabilistic methods have to be adopted in order to compensate for this ignorance in a consistent way. In other words, adoption of a macroscopic approach obliges us to treat fatigue resistance as an inherently random phenomenon. Besides that, a macroscopic approach imposes the distinction between crack initiation and crack propagation phase.

### 0.5.2. Action effect determination by Structural Response Monitoring

- *The objective of SRM is to provide data for Ultimate Limit State (ULS) verifications under the current traffic conditions.* Other uses of monitoring, such as damage detection, evaluation of dynamic amplification factors for use in ULS verifications under future traffic conditions or determination of the train-track-structure dynamic interaction characteristics for use in Serviceability Limit State (SLS) verifications, are not investigated here.
- *Structural element with short influence lines (<10m) are in general more susceptible to fatigue deterioration.* In this type of elements, the passage of each axle creates a distinct action effect cycle so that the total number of cycles experienced by these elements over their service life is much larger than the number of cycles experienced by elements with longer influence lines in the case of which one cycle corresponds to the passage of a wagon or of an entire train. Additionally, the relatively low permanent action effects on these elements result in that the action effect variations due to traffic action make for a larger fraction of the resistance of the element. The SRM results used in this work have been obtained from a monitoring campaign conducted on the RC slab of a short span rail way underpass.
- *Railway actions and action effects are characterized by stationarity over very long periods.* This means that action effect history records of longue but finite duration (in the order of 6 to 24 months) can be used in order to verify structural safety for much longer periods (in the order of several decades). Estimation of past and prediction of future traffic conditions remain outside the scope of this work.

Within the scope outlined above, considerable effort has also been put in that individual concepts and methods presented in this thesis be formulated with the highest possible degree of generality.

## 0.6. Structure of thesis

Besides this introduction, this thesis comprises four chapters and a conclusion section. For dissemination purposes the chapters of this thesis have been written as individual stand-alone texts, each one dealing with one or two of the particular objective stated above. Notwithstanding, special attention has been paid

in avoiding unnecessary repetition and in the use of uniform and consistent notation so that the compilation of the four texts result in a coherent final document.

Chapter 1 constitutes the theoretical basis for fatigue resistance calculation and responds to Objectives 1, 2 and 3 stated above. The content of this chapter (with the exception of the final validation sub-section) has been published in Engineering Fracture Mechanics journal.

Chapter 2 is largely an experimental contribution which describes the monitoring scheme that has been developed and evaluates its performance by analyzing and commenting on some interesting monitoring results; it responds to Objective 6 stated above. The content of this chapter has been accepted for publication in the Journal of Civil Structural Health Monitoring.

Chapter 3 provides the theoretical basis for monitoring-based structural ULS safety verifications and responds to Objective 7. The content of this chapter has been submitted for publication in the Structural Safety journal.

Chapter 4 provides concrete engineering methods for advanced fatigue safety verification and responds to Objectives 4-5 and 8-9. The content of this chapter will soon be submitted for publication for publication in an internationally peer-reviewed civil engineering journal.

Finally, in the Conclusion section the most important conclusions of the four chapters are summarized along with an outlook and a critique on the entire research work performed for this thesis.

## 0.7. References

- [1] WP1, Bell B, Network rail. European railway bridge demography – sustainable bridges deliverable D1.2. European commission – 6<sup>th</sup> Framework programme; 2004.
- [2] Schläfli M. E. Ermüdung von Brückenfahrbahnplatten aus Stahlbeton [dissertation]. Lausanne: Ecole Polytechnique Fédérale de Lausanne; 1999.
- [3] Herwig A. Reinforced concrete bridges under increased railway traffic loads – Fatigue behavior and safety measures [dissertation]. Lausanne: Ecole Polytechnique Fédérale de Lausanne; 2008.
- [4] Rocha M. Fatigue Behaviour of Steel Reinforcement Bars at Very High Number of Cycles [dissertation]. Lausanne: Ecole Polytechnique Fédérale de Lausanne; 2014.
- [5] CEB, Comité euro-international du béton. Fatigue of concrete structures - state of the art report, bulletin d'information No 188. Lausanne; 1988.
- [6] Treacy MA. The use of monitored data in the verification of structural and fatigue safety of existing post-tensioned concrete highway bridges [dissertation]. Lausanne: Ecole Polytechnique Fédérale de Lausanne; 2014.
- [7] CEN. EN 1992-1-1: Eurocode 2 – Design of concrete structures – Part 1-1: General rules and rules for buildings. Brussels: European Committee of Standardisation; 2004.
- [8] SIA. SN 505 262: Concrete structures. Zurich: Swiss Society of Engineers and Architects; 2003.
- [9] D'Angelo L, Nussbaumer A. Reliability based fatigue assessment of existing motorway bridge. Structural Safety. 2015;57:35-42.
- [10] Rodrigues JFS, Casas JR, Almeida PAO. Fatigue-safety assessment of reinforced concrete (RC) bridges: application to the Brazilian highway network. Structure and Infrastructure Engineering. 2011;9(6) 601-616.
- [11] SIA. SN 505 269/1: Existing structures – Actions. Zurich: Swiss Society of Engineers and Architects; 2011.

# Chapter I: Probability of observable flaw initiation at high cycle fatigue

With the exception of Section 1.5.5, the content of this chapter has already been published in the following paper: Grigoriou V, Brühwiler E. Probability of observable flaw initiation at high cycle fatigue. Eng Fract Mech. 2015; 145:p.161-180.

## Abstract

Fatigue evolution during the flaw initiation phase and under high cycle fatigue conditions is described at the level of the representative volume element by the probability that this element fails in a given period of time under given stimulus. This probability is calculated as a function of the accumulated inelastic work density. For the calculation of small amounts of inelastic work in the quasi-elastic domain of materials, a microplasticity model is developed using the hypothesis of strain energy density equivalence and a statistical distribution of work concentration within the RVE. The model is calibrated and validated using experimental data.

*Keywords:* fatigue flaw initiation; representative volume element (RVE); ultimate failure probability; statistical microplasticity; strain energy density equivalence.

## Nomenclature

RVE	Representative Volume Element	$\dot{w}_\mu$	+1: if micros. $\mu$ is being loaded; -1 if it is being unloaded after the latest reversal of loading
$a_b$	blocked strain energy density	$\mathcal{D}, D$	damage factor (unobservable and observable value)
$a_e$	elastic strain energy density	$D_{\text{ini}}$	observable value of damage factor at the onset of observable flaw
$a_e^{\text{rel}}$	elastic strain energy density released at failure	$E$	modulus of elasticity
$a_\mu^d$	distortional (elastic) strain energy density of microsystem $\mu$	$G$	shear modulus
$\dot{a}_\mu^d$	distortional (elastic) strain energy density of microsystem $\mu$ at the point of the latest reversal of loading	$K_t$	elastic stress concentration factor
$a_\mu^v$	volumetric (elastic) strain energy density of microsystem $\mu$	$\dot{K}$	Ramberg-Osgood parameter for cyclic loading
$a_\mu^y$	yield distortional strain energy density of microsystem $\mu$	$R$	load ratio
$a_\mu^d$	relative (elastic) strain energy density of microsystem $\mu$	$T$	temperature (absolute)
$a_\mu^y$	relative yield distortional strain energy density of micros. $\mu$	$\alpha_{\text{my}}$	microsystem yield strain energy (mat. prop.)
$a_\mu$	sign of elastic strain energy of microsystem $\mu$	$\alpha_u$	ultimate strain energy (material property)
$\dot{a}_\mu$	sign of elastic strain energy of microsystem $\mu$ at the point of the latest reversal of loading	$\beta$	ratio of intrinsic dissipation to inelastic work
$k_\mu$	partial power conc. factor of $\mu$ within its collectivity	$\gamma$	percentage of a component in a RVE
$\dot{n}$	Ramberg-Osgood parameter for cyclic loading	$\boldsymbol{\varepsilon}_e$	elastic strain (tensor)
$p_i, p_j$	weight factor of collectivity class $i$ or micros. class $j$ .	$\zeta$	factor of reliability relation between components (material property)
$q$	heat per volume	$\eta$	internal friction coefficient (material property)
$q_{\text{ir}}$	irreversible heat per volume	$\eta_m$	microsystem internal friction coefficient (mat. prop.)
$u$	internal energy density	$\lambda_C, \lambda_M$	parameter of the gamma distribution of power concentration factor at the collectivity and microsystem level.
$s$	entropy density	$\mu_C, \mu_M$	percentage of the inhomogeneous subpopulation at the collectivity and microsystem level.
$r_{\text{FO}}$	resolution of fictitious observation	$\xi_t$	theoretical heterogeneity of the RVE
$v_{\text{RVE}}$	volume of the RVE	$\xi_{\text{FO}}$	fictitiously observable heterogeneity of the RVE
$v_{\text{FO}}$	sub-volume of a fictitious observation	$\boldsymbol{\sigma}$	stress (tensor)
$w$	work per volume	$\sigma$	local stress
$w^d$	distortional work per volume	$\bar{\sigma}$	remote stress
$w_{\text{in}}$	inelastic work per volume	$\phi$	intrinsic dissipation per volume
$w_\mu^{\text{in}}$	inelastic work per volume on microsystem $\mu$	$\chi$	any variable
$w_\mu^{\text{in}}$	relative inelastic work per volume on microsystem $\mu$		
$w_\mu$	+1: if micros. $\mu$ is being loaded; -1 if it is being unloaded		

### Note

The index  $\mu$  may be substituted with  $c$  to refer to a microsystem collectivity, or with  $i$  to refer to a class of collectivities, or with  $ij$  to refer to a class of microsystems. In the absence of these indices the quantity refers to the RVE.



## 1.1. Introduction

Fatigue is often described as the phenomenon of initiation and propagation of flaws in a material as a consequence of a history of external stimulus. However, a formal distinction between initiation and propagation cannot be made without reference to the indivisible unit element which is used for the geometric description<sup>1</sup> of the system and its flaws. In the context of solid continuum mechanics, the smallest unit element, which can be used in a meaningful way, is by definition the Representative Volume Element (RVE). Hence, in that context, the flaw “initiation phase” is simply defined as the period during which the flaw, assuming that it exists, is so small that it escapes geometric description by means of RVEs [1, 2] or, in other words, it is indescribable by a meaningful use of continuum mechanics. It seems that the most meaningful way of describing fatigue during the initiation phase is by using, as a measure of its evolution, the probability of ultimate failure of a critical RVE in a given period of time and under stated conditions of external stimulus. In fact, the ultimate failure of a RVE marks either the onset of a describable flaw either the propagation, by one unit element, of an already existing (describable) flaw. It is indeed possible to describe flaw propagation as a succession of initiations as it has been done by Pecker [3] and more recently in the UniGrow model of Noroozi et al. [4, 5]. However, flaw propagation, a phenomenon that depends on much more factors than initiation, remains outside the scope of this work.

The design of structural components against onset of describable flaw is traditionally performed by means of empirically derived expressions relating the intensity and the duration of a history of external stimulus to a certain probability of onset of describable flaw (e.g. S-N-P curves). In principle, the validity of each set of such expressions is limited to materials and histories of stimulus very similar to those for which the expressions have been derived. Because of this limitation considerable research effort has been devoted to the development of theoretical methods for predicting flaw initiation under a more or less general history of stimulus and using only a limited set of experimentally derived material properties. This is the objective towards which the present work contributes.

These efforts follow, in general, two main approaches: Microstructural approaches attempt to explain the ultimate failure of a RVE by using appropriate theories which make possible the description and investigation of the propagation of imperfections already existing at a structural level lower than the level of the RVE (e.g. crystal, atomic level etc.). Macroscopic (or meso-scopic<sup>2</sup>) approaches treat the RVE using the principles of statistical mechanics and attempt to explain flaw initiation by investigating energy balances.

While microstructural investigations provide valuable insight into the mechanisms that lead to the onset of a describable flaw, macroscopic approaches are usually simpler and more flexible in application and for this reason they are more likely to find their way in engineering practice. In this work a macroscopic approach is followed.

Among the first to associate energy of hysteresis to fatigue is Hanstock [6], who also suggested that there is a part of hysteresis that “does not contribute to fatigue failure”. Feltner and Morrow [7] attribute this “nondamaging” part of hysteresis to anelastic mechanisms and they associate fatigue damage to plastic strain energy. Kaleta et al [8] suggest that the nondamaging part is the part of hysteresis that is dissipated as heat while the remaining part is stored in the system as energy blocked in the generation of *new* internal structures. Considerable research work has been devoted in establishing the corresponding energy balance by performing self-heating measurements during fatigue tests [9-11]. Amiri, Naderi and Khonsari [12, 13] associate fatigue to the amount of *generated* entropy, which they also measure by means of self-heating fatigue tests.

Onset of describable flaw is a phenomenon characterized by uncertainty, at least when examined macroscopically. Esin [14], among the first to introduce the concept of statistical microplasticity, associates flaw initiation, especially at high number of cycles, with the statistically calculated amount of microplastic strain energy. More recently, Doudard, Poncolet, Munier and others [15-18] develop a two scale model in which they consider a population of microplastic sites distributed within an elastic matrix and activated following a poison process. Bathe, Chan and others [19, 20] use the principle of maximum information entropy in order to derive a probabilistic criterion for fatigue fracture formulated in terms of generated

---

<sup>1</sup> The terms “description” and “observation”, which appears later in the text, are deemed in this work as essentially equivalent.

<sup>2</sup> The term “meso” is used by some authors when the term “macro” is reserved for the scales of structural components.

entropy. Castillo, Fernandez-Canteli and others [21-23] propose and use a statistical fatigue model based on the Weibull distribution as the only model satisfying a number of reasonable physical and statistical requirements.

Building on many of the concepts presented on the above contributions, the present work aims in the first place to clarify the notions and establish the principles which are necessary for the description of fatigue during the flaw-initiation phase. In the second place a material model is developed for the prediction of the time to onset of describable flaw by failure of a RVE. The model is shown to be capable of representing and predicting in a rather meaningful way the resistance to fatigue crack initiation of steel notched components, as experimentally observed in a series of tests reported in the literature.

## 1.2. Theory

### 1.2.1. Basic notions

In the context of structural integrity engineering, fatigue could be defined as a decrease of the reliability of a system, i.e. as an increase of the probability of *ultimate* failure of the system under a given history of external stimulus and for a specified period of time.

Ultimate failure is the result of an unstable and irreversible process and is identified by a fundamental transformation of the nature of the system. At the end of that process the system does not any more exist as the originally conceived entity, but it has been transformed to a different type of entity. (Hence, ultimate failure is not a failure of the system to perform in a certain way but the loss of its ability to perform in any way characteristic of the originally conceived entity).

These definitions are consistent with the empirical fact that fatigue results in a reduction of the expected remaining life-time of a system when the history of external stimulus can be approximated by an ergodic process.

Consider now a system consisting of a certain amount of solid mater occupying a *connected* volume. The description of the system directly suggests that it is possible to conceive its ultimate failure as the fact that it does not occupy a cohesive volume any more i.e. that it is fragmented in two or more volumes, separated by boundary surfaces on which interactions between the matter of adjacent volumes may take place. **Fig. 1.1** provides a fictitious illustration of how such a system may look like at the moment of its ultimate failure. Particular ultimate failure criteria may be formulated depending on how one conceives and describes the nature of the boundary surfaces (e.g. as Euclidian planes [Griffith's theory], as fractal surfaces [24, 25] or as surfaces dotted with a certain thickness [26]), the possible interactions on the surfaces (e.g. possibility of transferring tensile forces [27]) and the configuration of the surfaces (e.g. just one surface that separates the initial volume in two, or many intersecting surfaces resulting in more volumes).



**Fig. 1.1:** A RVE at the moment of its ultimate failure.

A novel idealization of ultimate failure of the above considered system consists in assuming a fragmentation of the system to an infinite number of infinitesimal fragments interacting by friction or, in other

words, a transformation of the solid material to a cohesionless one. It is reminded that a cohesionless material is a mathematical idealization of granular materials, like dry sand, in which the only mechanism of resistance to shear is friction between the grains.

Of course, none of the possible mathematical descriptions of ultimate failure does fully correspond to the facts, and the proposed one makes no exception to that. It has, however, the advantage of completely bypassing the problem of the description of internal boundary surfaces. This particularity makes the proposed idealization compatible with the notion of the RVE, which is by definition the smallest material system that can be meaningfully described geometrically and for which the possibility of explicitly describing internal (smaller) geometric structures is a priori ruled out.

As a final note to this subsection, it is pointed out that the ultimate failure of a RVE is merely a conventional and *instantaneous* time threshold (transformations remain indescribable until the *entire* element fails, *thereof* they are partially describable). In order for the time to ultimate failure of a RVE to say something meaningful about the evolution of the unobservable internal processes and to lead to predictions in acceptable accordance with the experimental facts, ultimate failure has to take place *almost simultaneously* over the *entire* volume of the element. This “almost” obtains its meaning only within the context of a specific fatigue case and in comparison with the time scale of the fatigue life. Hence, the term “representative” should be interpreted here in the sense that the RVE *is representative of itself* with respect to the *time to ultimate failure*. To ensure this representativeness the size of the RVE needs to be appropriately selected. The question of prescribing the size of the RVE in the context of fatigue flaw initiation has been extensively and efficiently treated for the case of notched components by Lazzarin, Susmel, Taylor and others [28-32].

### 1.2.2. Idealization of the RVE

Let us consider a RVE occupying a certain volume  $v_{\text{RVE}}$ . Let us also consider a certain variable  $\chi$  defined at every point of the RVE. It is assumed that the actual, although non-describable, distribution of  $\chi$  over the volume of the RVE identifies fully the microscopic state of the RVE, while the average value of  $\chi$  over the volume of the RVE

$$\bar{\chi}_{\text{RVE}} = \frac{\int_{v_{\text{RVE}}} \chi \, dv}{v_{\text{RVE}}}$$

identifies fully the macroscopic state of the RVE.

The theoretical heterogeneity  $\xi_t$  of variable  $\chi$  in the RVE is the heterogeneity that would be observed if it was possible to observe the value of  $\chi$  at infinite resolution. It could, in that case, be calculated as

$$\xi_t = \sqrt{\frac{1}{v_{\text{RVE}}} \int_{v_{\text{RVE}}} (\chi - \bar{\chi}_{\text{RVE}})^2 \, dv}$$

On the other hand, a fictitious observation (FO) of the value of  $\chi$  in the vicinity of a certain point at a finite resolution consists in selecting an observation region of volume  $v_{\text{FO}}$  around the point and then using a certain experimental or theoretical method in order to evaluate the average value of  $\chi$  in  $v_{\text{FO}}$ . The ratio  $r_{\text{FO}} = v_{\text{RVE}}/v_{\text{FO}}$  is the resolution of the fictitious observation.

The *observable heterogeneity*  $\xi_{\text{FO}}$  of the RVE at a fictitious resolution  $r_{\text{FO}}$ , could be theoretically evaluated by performing a very large number  $N$  of random samplings of volume  $v_{\text{FO}}$  from volume  $v_{\text{RVE}}$  and then approximating the limit

$$\xi_{\text{FO}}|_{v_{\text{FO}}} = \lim_{N \rightarrow \infty} \sqrt{\frac{1}{N-1} \sum_{i=1}^N (\bar{\chi}_{\text{FO},i} - \bar{\chi}_{\text{RVE}})^2}$$

It follows directly from the definitions that a RVE demonstrates zero observable heterogeneity at fictitious resolution equal to 1. On the contrary nothing can be said *a priori* about its observable heterogeneity at any fictitious resolution smaller than 1, nor for its theoretical heterogeneity. It is, so to speak, a system

for which an *a priori* ignorance with respect to its internal structure has been imposed or accepted. Eventually, this ignorance has to be compensated with appropriate hypotheses, i.e. hypotheses which lead to predictions which are in acceptable agreement to the experimental facts.

#### 1.2.2.1. Absolutely simple RVE

The simplest of the possible hypothesis regarding the internal structure of the observation element is that there is no internal structure or in other words that the theoretical heterogeneity is zero. This means that the observable heterogeneity remains zero at any finite fictitious resolution and also at infinite resolution (i.e.  $\xi_o|_{v_o} = 0$  for every  $v_o \in v_{RVE}$ ). This is the fundamental hypothesis of classical continuum mechanics (visco-elastic perfectly plastic material) and provided that the size of the observation element has been appropriately selected, it is an appropriate hypothesis for many practical purposes such as calculating stress distributions and predicting fracture loads for structural components. However, the assumption of an absolutely simple RVE is obviously not an appropriate idealization for calculating the evolution of fatigue during the initiation phase since it makes impossible any description of an internal process.

#### 1.2.2.1. Asymptotically simple RVE

In order to overcome the above theoretical obstacle, a certain intellectual devise is often proposed. It consists in considering a heterogeneity pattern so fine that remains unobservable even when the fictitious resolution tends to infinity. According to this concept the RVE is conceived as a system characterized by observable heterogeneity equal to zero for any finite fictitious resolution and at the same time of theoretical heterogeneity greater than zero (i.e.  $\xi_o|_{v_o} = 0$  for every  $(v_o \neq 0) \in v_{RVE}$ ,  $\xi_o|_{v_o=0} \equiv \xi_t \neq 0$ ). Of course, this is an essentially absurd concept – since it is equivalent to the concept of homogenous heterogeneity

However, the idealization of the RVE as an asymptotically simple system is a very useful assumption and constitutes the fundamental hypothesis of continuum damage mechanics (and in general of continuum mechanics with internal variables). Note also that the idealization of ultimate failure proposed in the previous Section 1.2.1 implies actually the hypothesis of an asymptotically simple RVE.

#### 1.2.2.2. Apparently simple RVE

A third possible approach is to accept ignorance as to the actual value of  $\bar{\chi}_{RVE}$  and admit that the value that can possibly be calculated, by examining energy balances, under the assumption of an asymptotically simple element, is at best (i.e. provided that the size of the RVE has been appropriately selected) equal to the expectation  $\langle \bar{\chi}_{RVE} \rangle$ . Given the expectation and making appropriate assumptions about the probability distribution of  $\bar{\chi}_{RVE}$ , it is possible to calculate the probability that the observation element has reached a limit state of ultimate failure. This hypothesis of an apparently simple RVE (further discussed in the following subsection) is proposed in this work for the first time, although a similar argument has already been put forward in the work of Bhate et al. and Chan et al [19, 20].

To summarize, the hypothesis of an absolutely simple RVE makes theoretically impossible any description of a fatigue process during the initiation phase, the assumption of an asymptotically simple RVE permits a deterministic description of such a process, while the hypothesis of an apparently simple RVE (which is the only of the three that is both theoretically and empirically substantiated) imposes a probabilistic description of the process.

### 1.2.3. Energy balance of the RVE

Let us now consider a process during which a RVE possibly develops heterogeneity. Let us consider in addition that the RVE does not exchange matter with its environment and maintains constant density so that thermodynamic relations can be formulated per volume, i.e. in terms of densities of energy, entropy, work, heat etc. (Slightly abusing the standard notation these densities are denoted by lower case letters which are normally used to denote specific quantities.) In fact all the quantities appearing in the following balances should be interpreted as averages over the volume or the boundary of the RVE. However, in order to keep the notation simple only the symbol of the quantity  $\chi$  is used instead of  $\bar{\chi}_{RVE}$ .

When a small amount of work  $\delta w$  is performed on the RVE, part of this work is dissipated as heat  $\delta q$  and another part is transformed into internal energy  $du$

$$\delta w - \delta q = du$$

The exact description of the internal energy variation  $du$  depends on the assumptions made for the RVE. Assuming that neither chemical reactions nor phase transitions take place, the energy balance is written as

$$\delta w - \delta q = Tds + \sigma d\epsilon_e + \delta\phi \quad (1.1)$$

where  $\delta\phi$  represents the intrinsic dissipation, i.e. an *apparent* deficit in the observable energy balance. By defining inelastic work as  $\delta w_{in} = \delta w - \sigma d\epsilon_e$  and irreversible heat as  $\delta q_{ir} = \delta q + Tds$ , Eq. (1.1) becomes

$$\delta w_{in} = \delta q_{ir} + \delta\phi \quad (1.2)$$

This equation expresses the well-known partition of inelastic work into thermal and intrinsic dissipation.

In this work it is proposed that intrinsic dissipation  $\delta\phi$  should be associated to an amount of strain energy blocked in internal structures  $da_b$ .

In that sense, three cases can be distinguished depending on the assumption for the nature of the RVE:

### 1.2.3.1. Absolutely simple RVE

This is the trivial case. It seems logical to conclude that if heterogeneity of internal state remains zero it is impossible that any amount of strain energy be blocked in internal structures of the system since in that case such structures simply should not exist. Hence, under the hypothesis of an absolutely simple RVE, it is not possible to describe fatigue evolution in the initiation phase. In that case

$$d\phi \equiv 0$$

$$\delta w_{in} = \delta q_{ir}.$$

This equation describes an elastic – perfectly plastic element in which all the inelastic work is transformed irreversibly to heat.

### 1.2.3.2. Asymptotically simple RVE

In such a RVE it may be considered that free energy can be blocked in an infinitely fine microstructure. Under this interpretation one can write

$$d\phi \equiv da_b \quad (1.3a)$$

$$da_b = \delta w_{in} - \delta q_{ir} \quad (1.3b)$$

### 1.2.3.3. Apparently simple RVE

Following the discussion made in the Section 1.2.2, a reasonable assumption for the relation of the apparent intrinsic dissipation and the blocked strain energy would be

$$\delta\phi \equiv \langle da_b \rangle \quad (1.4a)$$

$$\langle da_b \rangle = \delta w_{in} - \delta q_{ir} \quad (1.4b)$$

This assumption is motivated but not rigorously derived by the theorems presented in [33] and [34].

Hence,  $da_b$  is considered as a stochastic variable of which only the expected value is observable (calculable)<sup>3</sup>. By integrating both parts of the identity of Eq. (1.4a) between  $t_0$  and  $t$  and by assuming that at  $t_0$ ,  $\langle a_b \rangle = 0$  one obtains

$$\langle a_b \rangle = \int_{t_0}^t \phi dt \quad (1.5)$$

Eq. (1.5) provides a link that makes it possible to use the specific hypothesis of an asymptotically simple RVE (in the right hand of the equation) in order to estimate the state of the RVE under the much more general (and theoretically legitimate) hypotheses of an apparently simple element. It is evident that the cost of simplification is uncertainty.

---

<sup>3</sup> This interpretation is consistent with the Bayesian interpretation of probability.

#### 1.2.4. Limit state of ultimate failure

A fundamental hypothesis, proposed in this work, is that ultimate failure occurs when the sum of the blocked strain energy density and the part of the elastic strain energy density that can possibly be released in case of ultimate failure  $a_e^{\text{rel}}$ , reaches an ultimate value  $\alpha_u$  which is considered a property of the material. The possibility of defining such a property depends on the “representativeness” of the RVE as discussed at the end of Section 1.2.1. The above hypothesis is formulated in the following expression

$$a_b + a_e^{\text{rel}} < \alpha_u \quad (1.6)$$

Excluding the trivial hypothesis of  $a_b \equiv 0$ , which makes impossible the description of any fatigue process, there are at least two possible ways to proceed from this point.

##### 1.2.4.1 Asymptotically simple RVE

In this case  $a_b$  is a deterministic quantity and can be calculated by integrating the energy balance of Eq. (1.3). It can, furthermore, be expressed as a fraction of the fracture energy:  $a_b = \mathfrak{D}\alpha_u$ . Damage factor  $\mathfrak{D}$  is, accordingly, defined as

$$\mathfrak{D} = \frac{a_b}{\alpha_u}$$

Hence, the fracture criterion of Eq. (1.6) becomes:

$$\frac{a_e^{\text{rel}}}{1 - \mathfrak{D}} < \alpha_u$$

If one considers a fictitious RVE, resulting from the actual element after completely removing heterogeneity, then the quantity of the left-hand side of the above inequality can be interpreted as the effective elastic strain energy density that results in ultimate failure of the fictitious RVE. Thus, the hypothesis of an asymptotically simple RVE, combined with the proposed criterion of ultimate failure, leads naturally to the formulation of the strain energy equivalence concept of damage mechanics [35].

##### 1.2.4.2. Apparently simple RVE

In this case, blocked energy density  $a_b$  is treated as random variable for which we assume no information other than: (a) it has a non-negative value and (b) its expected value is given by Eq. (1.5). It is however desired to describe this variable by a probability distribution. The selection of the most appropriate distribution is based on the Principle of Maximum Entropy. Originally proposed by Jaynes in 1957 [36] as a generalization of Laplace’s Principle of Insufficient Reason, this principle states that of all the distributions that are consistent with some known constrains (information), the one with the largest entropy should be chosen<sup>4</sup> [37]. Although this principle has been subject to criticism mainly on philosophical-epistemological grounds [38], it has been applied to many scientific and engineering problems giving useful and consistent results [37]. Hence, it can be said that its use is empirically substantiated.

In the present case, the maximum entropy probability distribution, given constrains (a) and (b) of the previous paragraph, is the exponential distribution with parameter  $\lambda = (\int_{t_0}^t \dot{\phi} dt)^{-1}$  (inverse of mean value) [54]. Thus

$$P(a_b < x) = \begin{cases} 1 - \exp\left(-\frac{x}{\int_{t_0}^t \dot{\phi} dt}\right), & x \geq 0 \\ 0, & x < 0 \end{cases} \quad (1.7)$$

Or in terms of damage factor  $\mathfrak{D}$

$$P(\mathfrak{D} < x) = \begin{cases} 1 - \exp\left(-\frac{x}{\langle \mathfrak{D} \rangle}\right), & x \geq 0 \\ 0, & x < 0 \end{cases}$$

---

<sup>4</sup> Here also a Bayesian interpretation is implied.

where  $\langle \mathfrak{D} \rangle = \langle a_b \rangle / \alpha_u = \int_{t_0}^t \dot{\phi} dt / \alpha_u$  (from Eq. (1.5))

By rearranging terms the fracture criterion of Eq. (1.6) becomes

$$a_b < \alpha_u - a_e^{\text{rel}}$$

The right hand part of the above inequality has a deterministic value. Then, the probability of ultimate failure of the RVE  $P_f$  is derived from Eq. (1.7) as  $P_f = P(a_b \geq \alpha_u - a_e^{\text{rel}}) = 1 - P(a_b < \alpha_u - a_e^{\text{rel}})$ . Hence,

$$P_f = \begin{cases} \exp\left(-\frac{\alpha_u - a_e^{\text{rel}}}{\int_{t_0}^t \dot{\phi} dt}\right), & a_e^{\text{rel}} < \alpha_u \\ 1, & a_e^{\text{rel}} \geq \alpha_u \end{cases} \quad (1.8)$$

The use of Eq. (1.8) is illustrated in **Fig. 1.2** for the simple case of uniaxial tensile loading. Assume a virgin RVE which is subjected to the following two stage test: First, a given history of stimulus between points A and B is imposed to the RVE. *A priori* it is not known whether the RVE survives this first stage or not, what is assumed *a priori* known, however, is the total amount of intrinsic hysteresis  $\int_{t_0}^t \dot{\phi} dt$  produced by the RVE during this history, if it survives. Then, at the end of this history the RVE, provided that it survives, is loaded to a proof load (point C) characterized by a given  $a_e^{\text{rel}}$ . (Point C does not necessarily lie above B.) The *a priori* probability (before the execution of the two stage test) that the RVE survives the test is given Eq. (1.8) by using the quantities of energy as illustrated in **Fig. 1.2** and the fracture energy  $\alpha_u$ .

An alternative definition of the damage factor is also possible as

$$D = \frac{\langle a_b \rangle}{\alpha_u} = \frac{\int_{t_0}^t \dot{\phi} dt}{\alpha_u}$$

This is in fact the observable (calculated) value of the damage factor. Following this definition and assuming, as it is most often the case, that  $\alpha_u \gg a_e^{\text{rel}}$ , Eq. (1.8) can be written in terms of damage factor  $D$  as

$$P(D_{\text{ini}} < D) = \exp[-(D)^{-1}]$$

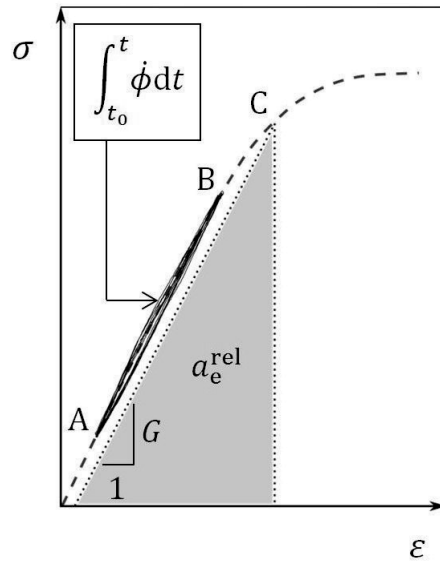


**Fig. 1.2:** Illustration of the quantities involved in Eq. (1.8).  $\int_{t_0}^t \dot{\phi} dt$  is actually only a part of the indicated inelastic work. In the above relation  $D_{\text{ini}}$  is the observable (calculated) value of damage factor at the onset of initial flaw.

There is an ontological difference between damage factor as defined in Section 1.2.4.1 and damage factor as defined above. Damage  $\mathfrak{D}$  is a random variable (following according to the present theory an

exponential distribution) with a deterministic critical value equal to  $1 - a_e^{\text{el}}/\alpha_u \cong 1$ , while damage factor  $D$  is a deterministic variable with a random value  $D_{\text{ini}}$ . This observable value of damage factor at the onset of initial flaw follows a Fréchet distribution with shape parameter equal to 1 and location and scale parameters equal to 0 and 1 respectively. It has to be noted that the neither the expectation nor the variance nor any higher moment of the above distribution has a finite value.

### 1.2.5. Partition of inelastic work into irreversible heat and intrinsic dissipation

The partition of inelastic work into irreversible heat and intrinsic dissipation, as suggested by Eq. (1.2), cannot be formally calculated at a macroscopic level without resorting to the use of internal variables for which appropriate evolution laws have to be specified on the base of experimental results (as it is done, for instance, by Rosakis et al. in [39]).

However, in the case where the temperature difference between the RVE and its surroundings remains almost zero throughout the stimulus history, it can be argued that the production of irreversible heat remains minimal and that the ratio  $\beta$  of intrinsic dissipation rate to inelastic work rate ( $\dot{\phi} = \beta \dot{w}_{\text{in}}$ ) can be assumed constant and equal to a value close to 1.

The assumption that the temperature of the RVE (relative to the temperature of its surroundings) does not increase during the fatigue process can be theoretically justified by considering a limited number of heat sources emerged in a thermal reservoir. The role of heat sources is assumed by the overstimulated energy dissipating regions of microplasticity inside the RVE. The role of the thermal reservoir is assumed by the rest of the volume of the RVE, which is supposed to be much less stimulated. Under this consideration, it is can be assumed that the heat produced by the over stimulated regions is dispersed over the RVE without affecting its temperature. Obviously, however, the heat capacity of the RVE is finite; thus additional conditions, related to the duration and intensity of the blocks of stimulus, have to be fulfilled in order for the assumption of the heat bath to be reasonable.

For example, in the case where the stimulation is interrupted in regular intervals the (relative) temperature increase should remain indeed insignificant. This is suggested by the work of Vincent [42] who performs a series of microthermomechanical simulations using various microplasticity constitutive laws in order to predict the evolution of temperature and of the energy storage ratio. He compares the evolution of temperature predictions from the simulations with experimental results. He concludes that the plasticity models that best reproduce the experimentally observed long term evolution of temperature also predict a ratio of energy storage of the order of 0.8-0.9 for the first one hundred loading cycles while this ratio decreases progressively to reach a stabilized value of around 0.7 at the steady state temperature. Interrupted stimulus histories are very often encountered in the context of civil infrastructure fatigue; for example, in the case of fatigue induced by railway traffic. In this particular case stimulus is applied in discrete blocks of relative short duration, corresponding to passages of trains, separated by time intervals of several minutes or even hours.

On the other hand, this is not what usually happens in the context of experimental investigations of fatigue or of fatigue problems induced by the continuous operations of machines. In these cases a more reasonable assumption is that after a limited number of stimulus cycles the RVE reach a steady state (relative) temperature. Kaleta [40] was able to experimentally establish an energy balance at the steady state temperature for the case of ferritic-perlitic steel specimens stimulated cyclically at various load levels corresponding to a range of fatigue life going from  $10^5$  to  $5 \times 10^6$  cycles. He establishes the relation  $\beta = 0.0598(N_f)^{0.15}$  between  $\beta$  and the number of cycles to failure  $N_f$ . This leads, for example, to a value of 0.67 for  $10^7$  cycles. Berthel [41] has also arrived to similar results using a completely different experimental method. At the opposite site of the spectrum an energy storage ratio of 0.2 is traditionally adopted in the case of monotonic plastic loading at high plastic deformation [39]

### 1.3. Calculations

In this section the quantities required for the use of Eq. (1.8) are calculated. These quantities are  $a_e^{\text{el}}$  and  $\int_{t_0}^t \dot{\phi} dt$ . Following the discussion in Section 1.2.5,  $\dot{\phi}$  is expressed as

$$\dot{\phi} = \beta \dot{w}_{\text{in}} \quad (1.9)$$



with  $\beta$  assumed a known constant. By this approximation, the thermomechanical problem of calculating  $\int_{t_0}^t \phi dt$  is reduced to the mechanical problem of calculating  $\int_{t_0}^t w_{in} dt$ .

### 1.3.1. Elastic strain energy that can possibly be released in case of ultimate failure of a RVE

The objective here is to calculate which part of the total elastic strain energy stored in a RVE at a given moment would be released if ultimate failure occurred at this moment.

For this calculation, the elastic strain energy density is decomposed into a volumetric part  $a_e^v = I_1^2/(6B)$  and a distortional part  $a_e^d = J_2/(2G)$ , where  $I_1$  and  $J_2$  are the first invariant of the Cauchy stress tensor and the second invariant of the stress deviator tensor respectively, while  $B$  and  $G$  are the bulk and the shear moduli of the material respectively. (This is an approach that has been followed many several researchers for the formulation of fatigue failure criteria; see [43] for a review). The volumetric part is stored either in tension (denoted as  $a_e^{v+}$ ) either in compression (denoted as  $a_e^{v-}$ ). The resistance of the RVE to shear deformation is assumed to rely on the combined action of two mechanisms: cohesion and friction. Following the definition of ultimate failure as the event of the RVE becoming cohesionless, it is assumed that the elastic strain energy released in case of ultimate failure equals the total elastic strain energy (stored in the RVE at any given moment) minus the part of it that is associated with stresses that can develop under the sole action of the friction mechanism.

Precisely, the following assumptions are made: In presence of  $a_e^{v+}$ , the totality of the elastic strain energy stored in the system is released at ultimate failure. On the other hand,  $a_e^{v-}$  is not released at ultimate failure. Additionally, in the presence of  $a_e^{v-}$ , a certain part of  $a_e^d$ , proportional to  $a_e^{v-}$ , is also not released at ultimate failure. Under these assumptions the elastic strain energy released at fracture is calculated as

$$a_e^{rel} = \max[a_e - a_e^{v-}(1 + \eta), 0] \quad (1.10)$$

$\eta$  is a material parameter corresponding to internal friction.

### 1.3.2. Inelastic work history of a RVE

In order to calculate the history of inelastic work, required for the use of Eq. (1.8), the RVE is considered here as an asymptotically simple element consisting of an *infinite* number of absolutely simple microsystems of infinitesimal volume. A hierarchical organization of the microsystems is also considered as it will be explained in detailed in the following. An illustration of a microsystem population of a RVE is provided in **Fig. 1.3**.

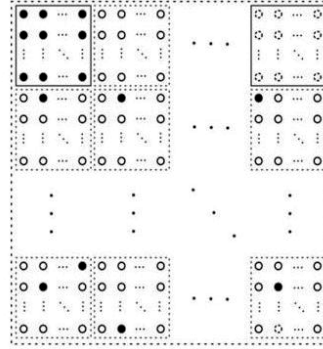


**Fig. 1.3:** The RVE (outer box) as a population of microsystems (small cycles) organized in collectivities (inner boxes); microsystems may respond in elastic (blank cycles) or in plastic mode (solid cycles) or may have attained ultimate failure (dashed cycles).

The properties of the microsystems are assumed to be material dependent constants common for all the members of a given population. Depending on the nature of the material it is possible to consider the RVE as consisting of either a single population or a mixture of two or more populations roughly corresponding to the various phases present in the RVE. On the other hand, the stimulus of the microsystems at any given moment is assumed to vary among the members of the population with the average stimulus remaining

equal to the stimulus of the RVE. The evolution of the inelastic work in the RVE is calculated as the evolution of the average inelastic work in the population of microsystems by means of a statistical simulation of the response of the population under a given history of external stimulus.

### 1.3.2.1. Definition of stimulus and response

Before proceeding to further describing the mathematical model, it is important to define the notion of stimulus of a system as used in this work. This is done in the way suggested by Buczynski and Glinka [44]. Stimulus is considered as an attempt to increase the elastic strain energy of the system by providing to the system an equal amount of work per volume  $\delta w$  during an elementary time interval  $dt$ . Stimulus is, therefore, described in terms of power density. Accordingly, the response of the system is defined as the actual increase of the elastic strain energy density at the end of the time interval and is described in terms of elastic strain energy density rate.

### 1.3.2.2. Distribution of stimulus over the microsystem population – The hypothesis of strain energy density equivalence

The power density in each microsystem at any given moment can be expressed as the given stimulus of the RVE times a power concentration factor. At any given moment the average of the power concentration factor in the population equals to 1. However, power concentration factors cannot a priori be assumed constant in the course of the history of stimulus. Indeed, because of the interactions between the microsystems, the stimulus of any given microsystem depends, in principle, on the response of all the other microsystems in the population, so that strictly speaking a full simulation of the interactions between the microsystems is required by which the response and stimuli of the microsystems are calculated simultaneously. In order to avoid such an explicit simulation the hypothesis of strain energy density equivalence is introduced. It states that the work density provided to a subsystem by the much larger system in which the subsystem belongs, does not depend on the response of the subsystem but only on the work density provided to it by the larger system and on the *form* of the interactions between the subsystems (i.e. the structure of the larger system). This hypothesis has been proposed and found to be acceptably accurate for the calculation of inelastic stresses and strains at the tip of notches of metal components provided that the plastified volume is small with respect to the size of the component [44-48]. The use of this hypothesis in the modeling of the RVE is justified by the fact that in high cycle fatigue, plastification can be assumed to be limited to a small number of microsystems while the bulk of the material remains elastic. Under this hypothesis, the distribution of power concentration factor over the population depends only on the microstructure of the RVE.

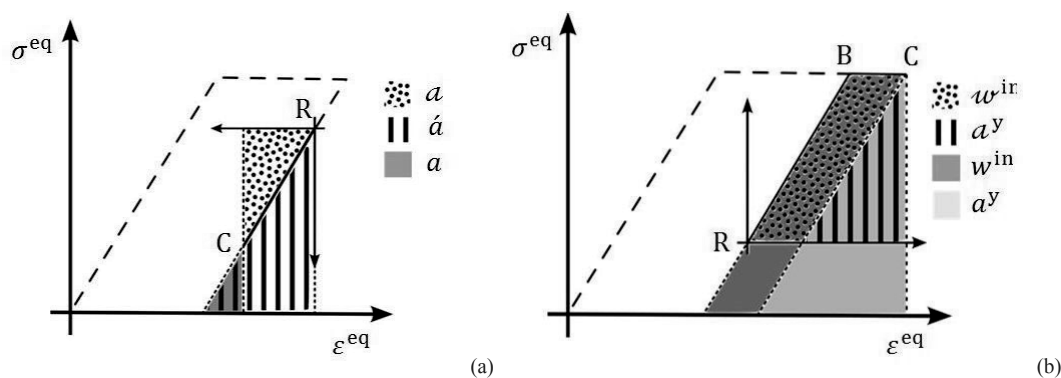


**Fig. 1.4:** Illustration of the relation between: (a) strain energy  $a$ , relative strain energy  $\hat{a}$  and strain energy at the point of latest reversal  $\hat{a}$ , (b) inelastic work  $w^{in}$ , relative inelastic work  $\hat{w}^{in}$ , yield energy  $a^y$  and relative yield energy  $\hat{a}^y$ , for an elastic perfectly plastic system. The current state of the system is denoted by point C. In (b) inelastic work is performed between points B and C.

It is further assumed that this distribution can be modeled analytically by means of appropriate statistical distributions as it will be explained in detail in the following.

Special care needs to be given so that the origin for the calculation of the work increments is set at each time at the point of the last loading reversal (proportional loading is implied here so that loading reversals can be uniquely defined). In order to emphasize that provided work and elastic strain energy at each time

refer in general to different origins we shall call those relative work density and relative elastic strain energy density and denote them with calligraphic letters ( $a$ ,  $w$ ). An illustration of how this assumption applies in the case of an elastic perfectly plastic onedimensional system is given in **Fig. 1.4**.

### 1.3.2.3. Behavior of a single microsystem

At this point, it is reminded that absolutely simple systems in general, and microsystems in particular, have only three possible modes of response: elastic, perfectly plastic and ultimate failure, while any given simple system has only two of them: elastic and either perfectly plastic either ultimate failure; this is a direct consequence of the definition of a simple system. In this work only elastic perfectly plastic microsystems are considered and for their modeling the Drucker-Prager yield criterion is adopted in the form

$$\sqrt{a_\mu^d} < \sqrt{a_\mu^y} \quad ; \quad a_\mu^y = (\sqrt{\alpha_{my}} - \eta_m^a \sqrt{a_\mu^v})^2$$

In the above expression  $a_\mu^d$  and  $a_\mu^v$  are the distortional and the volumetric part of the elastic strain energy of a particular microsystem “ $\mu$ ” (the subscript “e” standing for elastic is dropped for simplicity when reference is made to a microsystem which by definition can only store strain energy elastically).  $a$  takes the value -1 if  $a_\mu^v$  is in compression and +1 if it is in tension. Also,  $\eta_m$  and  $\alpha_{my}$  are microscopic material properties; they correspond to internal friction and yield energy at the level of microsystems and they are not directly associated with the respective macroscopic properties; provided that the RVE includes only one component, these properties are common for the entire population of microsystems in the RVE.

### 1.3.2.4. Statistical description of the behavior of a microsystem population

It is considered that the population of microsystems is hierarchically organized in *collectivities*. At the higher level lays the RVE itself; this is subdivided into an *infinite* number of collectivities laying at the immediately lower level and this hierarchical subdivision could theoretically continue ad infinitum; at the lower level the microsystems themselves are found. In the following, only three levels are considered, namely the RVE level, the collectivity level and the microsystem level.

A *microsystem collectivity* is conceived as a group of microsystems constituted as a mixture of a subpopulation with homogeneously distributed power concentration (i.e. all the microsystems of this subpopulation have the same power concentration) and an inhomogeneous subpopulation (in which power concentration varies over the microsystems according to a given statistical distribution). The percentage of the inhomogeneous subpopulation in a collectivity is denoted as  $\mu_M$  and is considered as a material property, while the percentage of the homogeneous subpopulation is  $(1 - \mu_M)$ . This concept is extended to the RVE level (the collectivity of collectivities): It is assumed that the RVE consists from two subpopulations of collectivities, one in which power concentration is homogeneously distributed over its collectivities and one in which power concentration is distributed to the collectivities following a given statistical distribution. The percentage of the inhomogeneous subpopulation in a RVE is denoted as  $\mu_C$  and is considered also as a material property, while the percentage of the homogeneous subpopulation is  $(1 - \mu_C)$ .

Let us present this concept in more detail. Similarly to the elastic strain energy density, work density can also be decomposed to a distortional and a volumetric component, both at the RVE level ( $\delta w^d$ ,  $\delta w^v$ ) and the microsystem level ( $\delta w_m^d$ ,  $\delta w_m^v$ ). A calligraphic  $w$  is used to refer to relative work density as explained above. For simplicity it is assumed that for a particular microsystem “ $\mu$ ” the power concentration factor is common for both the distortional and the volumetric component. In a first step, power concentration is assumed to be distributed over the collectivities of the inhomogeneous subpopulation of the RVE with a factor  $k_c$  following a gamma distribution with mean equal to 1 and a given variance  $(1/\lambda_c)$  considered as a property of the RVE microstructure. On the other hand, power concentration is distributed to all the collectivities of the homogeneous subpopulation of the RVE with factor  $k_c = 1$ . Hence, the power concentration distribution from the RVE to the entire population of its collectivities is described by a factor which follows in fact a mixed (discrete-gamma) distribution as illustrated in **Fig. 1.5**. In a second step, the power concentration previously distributed to the collectivities is further distributed to the microsystems of the inhomogeneous subpopulation of each collectivity with a factor  $k_\mu$  following again a gamma distribution with mean equal to 1 and variance  $1/\lambda_M$  also considered as a property of the RVE microstructure. The microsystems of the homogeneous subpopulation in a collectivity all have the same power concentration

equal to the mean power concentration of the collectivity ( $k_\mu = 1$ ). Hence the power concentration distribution from the collectivity to the entire population of its microsystems is also given by a mixed (discrete-gamma) distribution as illustrated in **Fig. 1.5**. According to the above it possible to write

$$\delta w_\mu^d = k_c k_\mu \delta w^d \quad (1.11a)$$

$$\delta w_\mu^v = k_c k_\mu \delta w^v \quad (1.11b)$$

$$k_c \sim \{\text{Gamma}(\lambda_C, 1/\lambda_C), \mu_C\} \quad (1.11c)$$

$$k_\mu \sim \{\text{Gamma}(\lambda_M, 1/\lambda_M), \mu_M\} \quad (1.11d)$$

The right hand part of expressions (1.11c,d) implies the mixed distribution of **Fig. 1.5**. Eventually, the statistical distributions change during the process as new internal structures are developed resulting in entropy generation. The parameters of the statistical distributions could therefore be considered as functions of the blocked free energy or equivalently of a certain damage variable (for instance as defined in Section 1.2.4). Although this dependence may be important, its investigation is not included in this work. It is, thus, assumed that for the largest part of the lifetime of the RVE the effect of damage on intrinsic dissipation remains small.

The use of the Drucker-Prager yield criterion implies the assumption that only distortional work provided to a microsystem can possibly be dissipated as inelastic work. This has already been suggested in [43].

The above stated assumptions on the behavior of a population of microsystem allow the formulation of the following expressions

$$\delta w_\mu^{\text{in}} = \begin{cases} 0, & \sqrt{a_\mu^d} < \sqrt{a_\mu^y} \\ k_c k_\mu \delta w^d, & \text{otherwise} \end{cases} \quad (1.12a)$$

In the above expression  $\delta w_\mu^{\text{in}}$  is the relative (with reference to the latest reversal point) inelastic work density. Since at any given moment the relative inelastic work density is calculated with a reference reversal point which is in general different of each microsystem, these relative work densities need to be expressed with reference to the common datum of zero absolute elastic strain energy before the calculation of their average. This is done with the following expression which is graphically demonstrated in **Fig. 1.4(b)**.

$$\delta w_\mu^{\text{in}} = \delta w_\mu^{\text{in}} \sqrt{a_\mu^y / a_\mu^y} \quad (1.12b)$$

In the above expression  $a_\mu^y$  is the distortional strain energy corresponding to yielding of the microsystem and  $a_\mu^y$  is its relative value with respect to the latest point of reversal. (For the exact calculation of these quantities see the algorithm presented in Annex). Finally the inelastic work density of the RVE is calculated as the mean inelastic work density of all the microsystems:

$$\delta w_{\text{in}} = \overline{[\delta w_\mu^{\text{in}}]_{\text{RVE}}} \quad (1.12c)$$

The originality of the proposed model with respect to other models based on the concept of statistical microplasticity that have already been presented in the literature [14-18] lies mainly on the way in which the stimulus of the microsystems is described (i.e. in terms of work density increments) and on the fact that statistical variation is attributed to the stimulus and not to the properties of microsystems.

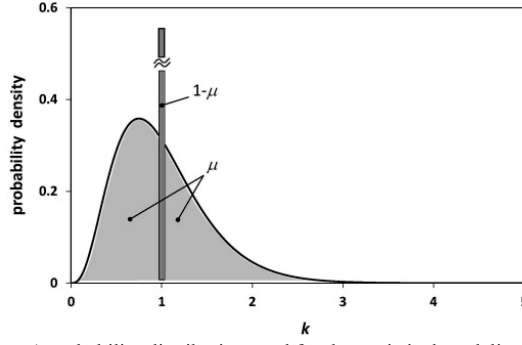


Fig. 1.5: A mixed (discrete-gamma) probability distribution used for the statistical modeling of microsystem collectivities.

At this point it needs to be emphasized that although a statistical description of the microsystem population is used, the calculation of inelastic work is absolutely deterministic since an infinite number of microsystems is considered. It is reminded that uncertainty at the level of RVE is considered by the fundamental Eq. (1.8).

### 1.3.2.5. Statistical simulation of the behavior of a microsystem population

The statistical simulation is based on the distribution of the collectivities and the microsystems of a RVE in classes according to their power concentration factor. More precisely, collectivities of the inhomogeneous subpopulation are distributed into  $n_C$  classes according to their  $k_c$ . These classes are referred to as C-classes and are numbered by  $i = 1 \dots n_C$ . The homogeneous subpopulation is considered as an additional C-class with  $i = 0$  and  $k_{i=0} = 1$ . The microsystems of the inhomogeneous subpopulation within each collectivity are also distributed into  $n_M$  classes according their  $k_\mu$  (referred to as M-classes and numbered by  $j = 1 \dots n_M$ ). The homogeneous subpopulation is considered as an additional M-class with  $j = 0$  and  $k_{j=0} = 1$ . C-classes ( $i \geq 1$ ) are defined by subdividing the range  $[0, 1 + 10 (\text{Var}[k_c])^{1/2}]$  (i.e. the range from 0 to the mean plus 10 standard deviations of  $k_c$ ) into  $n_C$  equal segments  $\Delta k_c$ . Similarly, M-classes ( $j \geq 1$ ) are defined by subdividing the range  $[0, 1 + 10 (\text{Var}[k_\mu])^{1/2}]$  into  $n_M$  equal segments  $\Delta k_\mu$ . In this way, the entire population of microsystems is distributed into a total of  $(n_C + 1) \cdot (n_M + 1)$  classes, named CM-classes, numbered by  $ij$  and characterized by the product  $k_i k_j$ , where  $k_i$  is the central value of  $k_c$  for the  $i^{\text{th}}$  C-class and  $k_j$  is the central value of  $k_\mu$  for the  $j^{\text{th}}$  M-class. Thus,  $k_i$ ,  $k_j$ ,  $\Delta k_c$  and  $\Delta k_\mu$  are calculated as

$$k_i = (i + 1/2)\Delta k_c \quad \Delta k_c = (1 + 10/\sqrt{\lambda_C})/N, \quad i = 1 \dots n_C$$

$$k_j = (j + 1/2)\Delta k_\mu \quad \Delta k_\mu = (1 + 10/\sqrt{\lambda_M})/M, \quad j = 1 \dots n_M$$

$$k_{i=0} = k_{j=0} = 1.$$

To each of the CM-classes a weight factor is assigned. These weight factors are equal to the relative frequency of the class in the population and are expressed as the product of two partial factors  $p_i$  and  $p_j$ . These partial factors are equal to the relative frequency of C-classes and M-classes respectively and are calculated as

$$p_i = f_{k_c}(k_i)\Delta k_c = \mu_C \left[ \frac{(\lambda_C)^{\lambda_C}}{\Gamma(\lambda_C)} (k_i)^{(\lambda_C-1)} e^{-\lambda_C k_i} \right] \Delta k_c, \quad i = 1 \dots n_C \quad (1.13a)$$

$$p_j = f_{k_\mu}(k_j)\Delta k_\mu = \mu_M \left[ \frac{(\lambda_M)^{\lambda_M}}{\Gamma(\lambda_M)} (k_j)^{(\lambda_M-1)} e^{-\lambda_M k_j} \right] \Delta k_\mu, \quad j = 1 \dots n_M \quad (1.13b)$$

$$p_i = 1 - \mu_C, \quad i = 0 \quad (1.13c)$$

$$p_j = 1 - \mu_M, \quad j = 0 \quad (1.13d)$$

In the above equations,  $f_X(x)$  denotes the probability density function of the corresponding variable and  $\Gamma(x)$  denotes the gamma function.

Finally, the calculation of the inelastic work density history of the RVE, for a given history of stimulus expressed in terms of work density increments, is performed by calculating step by step the inelastic work history of each of the CM-classes. For this calculation Eq. (1.12abc) are reformulated in terms of classes and relative frequencies as follows

$$\delta w_{ij}^{\text{in}} = \begin{cases} 0, & \sqrt{a_{ij}^{\text{d}}} < \sqrt{a_{ij}^{\text{y}}} \\ p_i p_j k_i k_j \delta w^{\text{d}}, & \text{otherwise} \end{cases} \quad (1.14a)$$

$$\delta w_{ij}^{\text{in}} = \delta w_{ij}^{\text{d}} \sqrt{a_{ij}^{\text{y}}/a_{ij}^{\text{d}}} \quad (1.14b)$$

$$\delta w_{\text{in}} = \sum_i \sum_j \delta w_{ij}^{\text{in}} \quad (1.14c-i)$$

### 1.3.3. RVEs modeled with a mixture of microsystem populations

In the analysis so far, it has implicitly be assumed that the RVE consists of (or can be modeled with) a single component (with unobservable heterogeneity due to its microstructure). It seems, however, that quite often the RVE behavior is described better by using a mixture of two or more populations with different properties ( $\alpha_{\text{my}}, \eta_{\text{m}}, \lambda_{\text{M}}, \lambda_{\text{C}}, \mu_{\text{M}}, \mu_{\text{C}}$ ). With a certain degree of abstraction, it can be said that these populations correspond to the various components of the material; however an explicit correspondence between populations and actual material phases need not necessarily be established. When more than one populations are used in the description, the above properties need to be defined for each of the populations. In that case, Eq. (1.14) should be rewritten with all the population depending quantities featuring an additional subscript  $I$  enumerating the populations from 1 to  $N_{\text{comp}}$ . Additionally, the proportions of the different populations in the mixture (more accurately, the partition of power between the populations) needs to be defined. This is done by multiplying  $\delta w^{\text{d}}$  by a factor  $\gamma_I$  such that  $\sum_I \gamma_I = 1$ . Eq. (1.14c-i) then becomes

$$\delta w_{\text{in}} = \sum_I \gamma_I \sum_i \sum_j \delta w_{ij,I}^{\text{in}} \quad (1.14c-ii)$$

#### 1.3.3.1. Contribution of inelastic work to the critical amount of intrinsic dissipation energy

When just one component is considered, the increment of intrinsic dissipation is simply calculated according to Eq. (1.9) as

$$\delta \phi = \beta \delta w_{\text{in}} \quad (1.14d-i)$$

On the other hand, when a multi-component material (in the above sense) is considered, the question rises whether the ultimate failure of a component implies also the ultimate failure of the RVE or not. In other words the question is whether, in terms of reliability, the components are connected in parallel or in series. This is taken into account here with a factor  $\zeta_I$ . If the components are connected in series  $\zeta_I$  takes the value 1 for the critical component and zero for all the others while if the case of parallel connection  $\zeta_I$  takes the value 1 for all the components. Other cases can also be envisaged like the one illustrated in **Fig. 1.6** in which two components connected in parallel are assumed equally critical and are assigned  $\zeta_1 = \zeta_2 = 1$  while a third component connected in series to the first two is assumed non-critical and is assigned  $\zeta_3 = 0$ . Intermediate values of  $\zeta_I$  and in particular transitions from 1 to 0 might be a way to describe the effect of damage accumulation in one of the components but this possibility is not further investigated here. After the above discussion Eq. (1.14d-i) takes the form

$$\delta \phi = \beta \sum_I \zeta_I \gamma_I \sum_i \sum_j \delta w_{ij,I}^{\text{in}} \quad (1.14d-ii)$$

It has to be noted that the introduction of the factor  $\zeta_I$  is not strictly required for the efficiency of the model from the point of view of purely fatigue calculations. Indeed the components with  $\zeta_I = 0$  could simply be excluded from the model. The benefit from the use of this factor is of rather theoretical nature since it provides a way to explain (by means of the consideration of an additional component) the discrepancy between the microyielding energy that has to be specified for modeling the macroscopic yield behavior

of the material on one hand and the fatigue resistance on the other. This is further discussed in the following example.

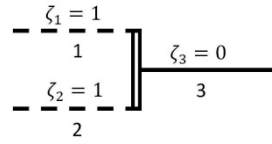


**Fig. 1.6:** Two equally critical elements connected in series with a third noncritical one.

#### 1.3.4. Algorithm

For the step by step calculation of the quantities involved in the above equations the algorithm presented in the Annex is developed. The algorithm implements Eq. (1.12-1.14) and is based on the classic concept of elastic prediction – plastic correction and is characterized by three original features: (a) It is exclusively formulated in terms of signed energy and work. (b) The points of reversal of stimulus are tracked separately for each CM-class. (c) Work and energy are expressed relatively to the point of the latest reversal of stimulus.

#### 1.4. Scope and limitations of the model

While individual parts of the proposed theory maintain great deal of generality, the approach as a whole is oriented towards cases of blunt notched components with the local stress at the tip of the notch remaining mainly below the yield limit of the material and a stress history that induces minimal raise of temperature at the notch tip. Four aspects of the model with their corresponding consequences on its application are highlighted.

(a) The model applies at the level of RVE. In that sense it is a macroscopic (or mesoscopic) material model. In this work the development is mainly oriented towards the simplest case in which it is assumed that a critical RVE, from which a flaw initiates, can be identified (or in other words the case in which the location of flaw initiation can be predicted). This is mainly the case of notched components where by high probability the flaw initiates from the tip of the notch.

(b) The purpose of the model is to calculate inelastic work due to microplasticity, i.e. the inelastic work due to slightly non-linear stress-strain response occurring at stress levels generally below and occasionally around the generalized yield stress as illustrated in **Fig. 1.2**. This is the domain which one might call quasi-elastic domain and in which fatigue phenomena at medium to high number of cycles take place.

The model is formulated in terms of *applied* and *dissipated* power instead of stress and strain. Hence, the application of the model requires as input the power history applied to this RVE. In the “standard” approach, the history of power at a local level is calculated from the local stress-strain history which in turn is calculated from the remote load history by means of analytical or numerical methods and by using a nonlinear material model formulated in terms of stress and strain. In addition time or history dependent behavior needs to be modeled.

This is not just a complicated procedure but it also appears to render worthless a power-formulated material model. However, there is a range of cases in which the local power history can be approximated using only linear elasticity independently of the occurrence of local non-linear behavior. Most notched component cases fall precisely in this range. In these cases, it can be assumed that nonlinear and history-dependent behavior is limited to the neighborhood of the tip of the notch while the behavior of the rest of the component remains linear and history-independent during the loading history. The hypothesis of strain energy equivalence asserts, in this case, that the local power history is efficiently approximated by the theoretical power history calculate assuming linear behavior also in the region of the tip of the notch.

Under the above conditions the use of a power-formulated model is of great advantage since it completely bypasses the need to calculate nonlinear stress and strains. In other words it is an approach oriented towards applications where the loading of the critical RVE is power controlled rather than stress or strain controlled.

It is noted however that since the proposed model is formulated in terms of energy, it is generally not suitable for describing fatigue under non-proportional loading.

(c) When we refer to the input power history applied to the critical RVE we actually refer to some kind of average power over the volume of the RVE. Taylor [32] proposes several methods for defining and calculating an average stress from a stress field in the region of the critical RVE calculated using linear elasticity. From this average stress the equivalent average linear elastic power history can be calculated.

In the case of blunt notches, i.e. when the radius of curvature at the tip of the notch is several times larger than the characteristic length of the RVE, the average power history can be approximated by the power history calculated using the maximum stress at the tip of the notch instead of the average stress. The maximum elastic stress at the tip of the notch is often expressed in term of the remote or nominal stress of the component by means of the elastic stress concentration factor  $K$ . These aspects are discussed in much detail in several publications including [28-32]. It has to be emphasized that the assumption of blunt notch is not essential for the development or application of the model. It is just an assumption that defines a subset of cases in which the calculation of the input required by the model is significantly simplified.

(d) As a final point here it is reminded that the assumption of minimal increase of the temperature of the RVE was introduced in Section 1.2.5. It has also been suggested there that this assumption becomes increasingly accurate as the intensity of the stimulus diminish or if the stimulus is regularly interrupted. In these cases a factor  $\beta$  close to unity can be adopted (with unity representing the most unfavorable case). Another possible assumption is the assumption of an ergodic and uninterrupted loading history leading to steady state temperature. In these case  $\beta$  has been found to depend on the loading frequency and can be specified experimentally as, for instance, in [41].

## 1.5. Calibration and validation using experimental S-N data

### 1.5.1. Experimental data

In this section the above developed model is fitted to experimental data reported in the work of Pereira et al. [49] and de Jesus et al. [50]. The data used for the calibration of the model refer to constant amplitude fatigue tests on P3355NL1 steel specimens and include results from remote stress controlled tests on (i) notched plate specimens at load ratios of  $R = 0.0$ ,  $R = 0.15$  and  $R = 0.30$  and (ii) smooth specimens at load ratio of  $R = -1$ . For the reader's convenience, these data are re-plotted from the original papers in **Fig. 1.7**. The geometry of the specimens is also re-plotted from the original papers in **Fig. 1.8**. The notched specimen test data are presented in terms of the local (at the tip of the notch) equivalent elastic stress range  $\Delta\sigma_{\text{eq}}$  calculated by simply multiplying the remote (controlled) stress range  $\Delta\tilde{\sigma}$  by the analytical elastic stress concentration factor  $K$  (for the present case  $K_t = 2.17$ ).

$$\Delta\sigma_{\text{eq}} = K_t\Delta\tilde{\sigma} \quad (1.15)$$

For consistency the data from the smooth specimen tests are also presented in terms of an equivalent elastic stress range calculated using the elastic strain energy equivalence principle and the Ramberg-Osgood material model. The following equation is employed:

$$\frac{(\Delta\sigma_{\text{eq}})^2}{E} = \frac{(\Delta\tilde{\sigma})^2}{E} + 2\Delta\tilde{\sigma} \left(\frac{\Delta\tilde{\sigma}}{2\hat{K}}\right)^{1/\hat{n}} \quad (1.16)$$

where the Ramberg-Osgood parameters ( $\hat{K} = 777$  MPa,  $\hat{n} = 0.11$ ) for cyclic loading and the elasticity parameters ( $E = 205.2$  GPa,  $\nu = 0.28$ ) are obtained from [51]. It is noted that the assumption of a Ramberg-Osgood material is not involved in the proposed model. This assumption is used in the present example with reference to a specific material (for which it happens to be a reasonable idealization) in order to consistently express all the experimental data in terms of an equivalent elastic stress range.



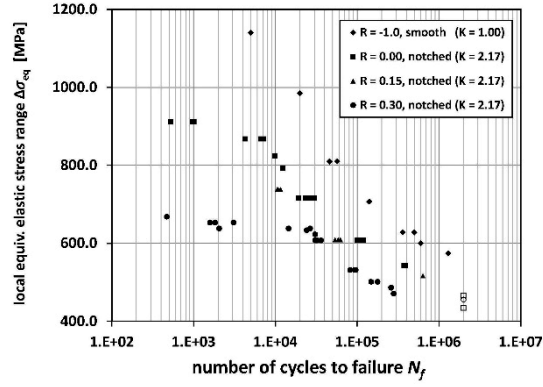


Fig. 1.7: Experimental data used for the calibration of the proposed model (after Pereira et al. [49], notched specimens and de Jesus et al. [50], smooth specimens). Blank signs imply run-outs.

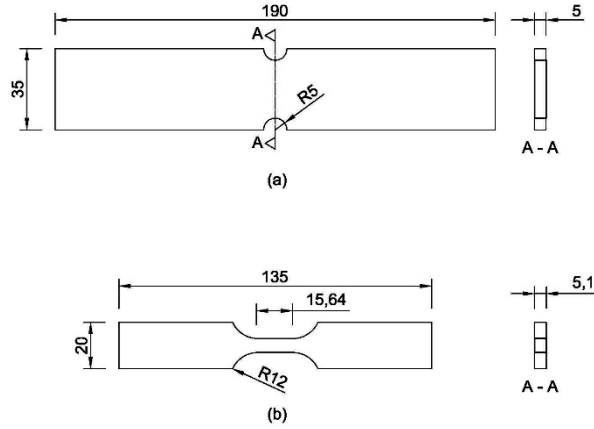


Fig. 1.8: Geometry of the specimens used in the fatigue tests: (a) notched (replotted from Pereira et al. [49]), (b) smooth (replotted from de Jesus et al. [50]). Dimensions in mm.

### 1.5.2. Model input

The input for the proposed model in terms of increments of the applied local distortional and hydrostatic work density is calculated assuming uniaxial stress conditions.

$$(\delta w^d)_n = (\sigma_{eq,n}^2 - \sigma_{eq,n-1}^2)/(6G) \quad (1.17a)$$

$$(\delta w^h)_n = (\sigma_{eq,n}^2 - \sigma_{eq,n-1}^2)/(6B) \quad (1.17b)$$

$$\sigma_{eq} = K_t \tilde{\sigma} \quad (1.17c)$$

where  $n$  refers to the calculation step and  $G$  and  $B$  are the shear and bulk modulus respectively. For each step it is additionally required as input the sign (+1 or -1) of the equivalent local elastic strain energy  $a_n$ . This sign is conventionally taken equal to the sign of the local hydrostatic stress; for the present example as the sign of  $\sigma_{eq,n}$ . The corresponding relative values of work increments  $(\delta w^d)_n$  (required as input in Eq. (1.14a)) are calculated step by step from  $(\delta w^d)_n$  and  $a_n$  according to the algorithm in Annex.

For the present example the initial value of  $s$  is assumed equal to 0. Then a first step is considered during which  $\tilde{\sigma}$  goes to its maximum value and then two loading cycles are applied between the maximum and minimum value of  $\tilde{\sigma}$ . For the present example each cycle is divided in 64 steps and a sinusoidal variation

of  $s$  is assumed. While Eq. (1.17) are used for this simple example, the history of  $\delta w^d$  may, in general, be calculated by any appropriate analytical or numerical method of elastic analysis.

According to [29], the use of the elastic strain energy density at the tip of the notch (calculated using the analytical stress concentration factor) instead of the average strain energy over the volume of the RVE (which could be calculated by means of an empirical fatigue stress concentration factor) is, in this case, an accurate approximation, given that the radius of the tip of the notch (5mm) is quite larger than the size of the RVE for this type of steel ( $\cong 0.03$ mm, as calculated for instance in [23]).

### 1.5.3. Calculation of the number of cycles to failure for a given failure probability

Following the algorithm presented in Annex and Eq. (1.14d-ii), intrinsic dissipation is calculated step by step. The total amount of intrinsic dissipation energy  $\Delta\phi$  produced during the second cycle of the calculated history is recorded. In fact, the amount of intrinsic dissipation predicted by the model per cycle remains constant after the second cycle. Eq. (1.8) then becomes

$$P_f = \exp\left[-\frac{\alpha_u - a_{e,\max}^{\text{rel}}}{N\Delta\phi}\right]$$

The history of  $a_e^{\text{rel}}$  and thus also its maximum value  $a_{e,\max}^{\text{rel}}$  are also calculated during the loading cycle. However, given the large value of  $\alpha_u$ , the influence of  $a_{e,\max}^{\text{rel}}$  in the above equation is, in general, minimal.

$$P(N_f < N) = \exp[-(\alpha_u/\Delta\phi)N^{-1}]$$

The number of cycles corresponding to a probability of crack initiation  $P_f$  are calculated from Eq. (1.8) as

$$N_f = \frac{\alpha_u - a_{e,\max}^{\text{rel}}}{\Delta\phi \ln(P_f)}$$

### 1.5.4. Calibration

In **Fig. 1.9** the fatigue resistance curves (for  $P_f$  equal to 0.5, 0.1 and 0.9) obtained from the calibration of the proposed model to the experimental data are superimposed to these data. The results are presented in terms of the applied range of local distortional work density  $\Delta w^d$  (relative values are used in order to have the same datum independently of the load ratio  $R$ ). For the experimental data,  $\Delta w^d$  is calculated from the local equivalent elastic stress range  $\Delta\sigma_{\text{eq}}$  as

$$\Delta w^d = (\Delta\sigma_{\text{eq}})^2 / (6G) \quad (1.18)$$

The number of cycles to failure is used instead of the number of cycles to crack initiation. This is based on the assumption that most of the fatigue life of the specimen corresponds to the initiation phase. This assumption has been verified in [52] where it is shown that fatigue initiation corresponds to approximately 90% of the total fatigue life. The curves presented in **Fig. 1.9** are derived using the parameters listed in **Table 1.1**. The complexity of the model can be increased or decreased in a systematic way either by considering more or fewer hierarchy levels or by adding or removing components. The number of parameters required by the model is given by  $2 + I[4 + 2(J - 1)]$ , ( $I$ : number of components,  $J$ : number of hierarchy levels). For the present example three hierarchy levels and three components are considered which result in a total of 26 parameters.

This is admittedly a large number of parameters. However, for the description of the fatigue behavior of the component at medium to high number of cycles, consideration of just the first component would be sufficient. The introduction of the second component makes possible to capture the plateau of the fatigue resistance observed at low number of cycles. The use of these two components, with their parameters (mainly the microsystem yield strain energy) calibrated on the base of the fatigue curves, results in amounts of inelastic work per cycle which are significantly lower than those calculated from the actual cyclic stress-strain relation of the material (idealized again, for this example, as a Ramberg-Osgood material with the above specified parameters  $K'$  and  $n'$ ). In order to eliminate this discrepancy (which in any case has no

significant influence on the calculated fatigue resistance), the third (noncritical for fatigue failure) component is introduced. In **Fig. 1.10**, the inelastic work density per cycle  $\Delta w_{in}$  versus  $\Delta \omega^d$  level as calculated from the material cyclic stress-strain curve (idealized using Ramberg-Osgood relations and Masing hypothesis) is compared to that given from the proposed model calibrated to this curve. The above suggest that although 3 material components (leading to 26 parameters) have to be considered in order to capture the full plastic behavior of the material at all stress levels, the modeling of the plastic behavior at the low stress levels corresponding to high cycle fatigue can be done using only one component (and reducing the amount of parameters to 10)

The model parameters are evaluated in this work by curve fitting. Further research is required in order to investigate which is the smallest number of required parameters for modeling the fatigue behavior of specific materials and how these parameters could be evaluated in a systematic and rigorous way on the basis of standard tests.

Generally speaking, the most promising way to achieve this goal is by combining top-down approaches, like the one presented here, with bottom-up approaches in the way that it is suggested by a number of researchers including W. Curtin, J.-F. Molinari and N. Marzari of EPFL. In these bottom-up approaches the objective is to calculate the macroscopic engineering material properties starting from the first principles and using explicit numerical simulation of microstructural transformations in the domains of quantum mechanics, molecular dynamics statistical mechanics dislocation theory, single crystal plasticity and multigrain modeling [55].

Notwithstanding, the results presented in **Fig. 1.9** and **Fig. 1.10** suggest that the proposed model is capable to represent very accurately the fatigue resistance of the tested components for a large range of stress ratios and stress amplitudes and also the cyclic production of inelastic work. The discrepancy that can be observed in the low to medium number of cycles for  $R = -1$  is attributed to the fact that the corresponding experimental data were obtained under “local” stress control conditions (use of smooth specimens) and not under local power control conditions as assumed by the proposed model. Given these results, it can be reasonably hoped that, once calibrated on the basis of constant amplitude test results, the model can be used for the prediction of crack initiation under a general loading history.

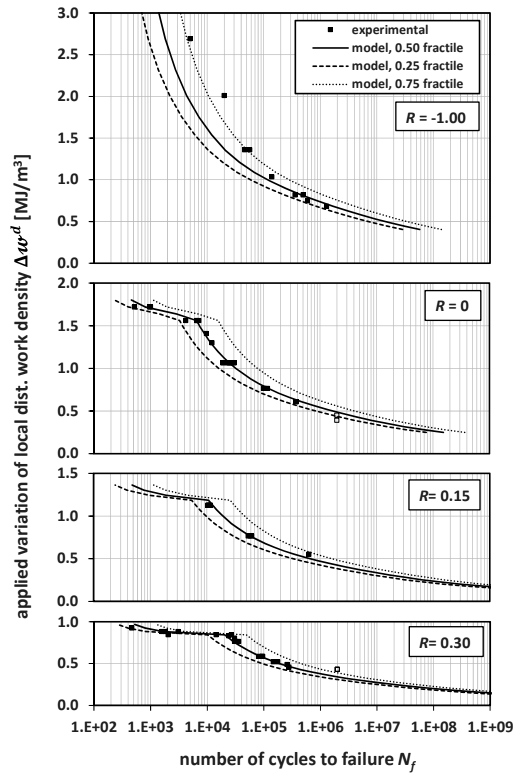


**Fig. 1.9:** The proposed model fitted to the experimental results of Pereira et al. [49] and De Jesus et al. [50].

**Table 1.1:** Model parameters after calibration with the experimental results of [49, 50].

$\alpha_u$ [MJ/m <sup>3</sup> ]	$\beta$		$\alpha_{my}$ [MJ/m <sup>3</sup> ]	$\gamma_I$	$\zeta_I$	$\eta_{m,I}$	$\lambda_{M,I}$	$\lambda_{C,I}$	$\mu_{M,I}$	$\mu_{C,I}$
10.0	0.50	component								
		1	0.620	0.0075	1	0.3	4	3	1.00	0.10
		2	1.400	0.1425	1	1.2	4	4	0.01	0.01
		3	0.275	0.8500	0	0.4	6	5	1.00	1.00

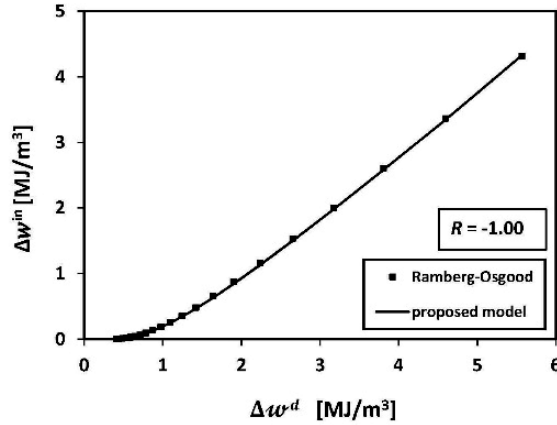


**Fig. 1.10:** The proposed model fitted to the cyclic inelastic work calculated by the stress-strain curve of the material (idealized using Ramberg-Osgood relations and Masing hypothesis).

### 1.5.5. Validation

For evaluating the predictive capacity of the model for a general loading history, additional experimental data provided by Pereira [53] are used. In the corresponding variable amplitude fatigue tests the same geometry of notched specimen as depicted in **Fig. 1.8(a)** was used. Ten types of loading history are considered and for each type three specimens are tested. Each loading history type consists of a loading block of 100 or 200 cycles which is repeated until failure. The blocks are depicted in **Fig. 1.11**. The results, in terms of number of cycles to failure, are reproduced in **Table 1.2** for convenience. For the above loading histories the number of cycles corresponding to a failure probability of 0.50 is calculated by the proposed model using the parameters that have been determined in Section 1.5.1.2. Predictions are compared to the experimental results in **Fig. 1.12** in which the predicted mean number of cycles to failure is plotted versus the observed number of cycles for test considered here. In the same figure three auxiliary lines are also plotted. These lines show the number of cycles that, given a certain value for the predicted mean, have a probability of 0.3, 0.5 and 0.7 not be reached in a particular test according to the model. The PDF of the theoretical distribution of the number of cycles to failure are also plotted indicatively for two mean values. Although the number of data points is limited, it can be seen that the distribution of the number of cycles to failure calculated by the proposed model are in good agreement with the experimental results.

## 1.6. Conclusions

- The probability of ultimate failure of a critical RVE is a physically meaningful measure of the evolution of fatigue during the initiation phase and can be calculated as a function of the cumulative intrinsic dissipation energy density during the history of stimulus.

- The cumulative intrinsic dissipation energy density can be calculated by means of a statistical simulation of a hierarchically organized population of elastic – perfectly plastic microsystems.
- The proposed model is capable of representing the experimentally observed resistance of notched steel components at various stress ratios. However, further investigation is needed in order to find out whether the parameters of the model or at least some of them can be related to classic mechanical properties of materials.

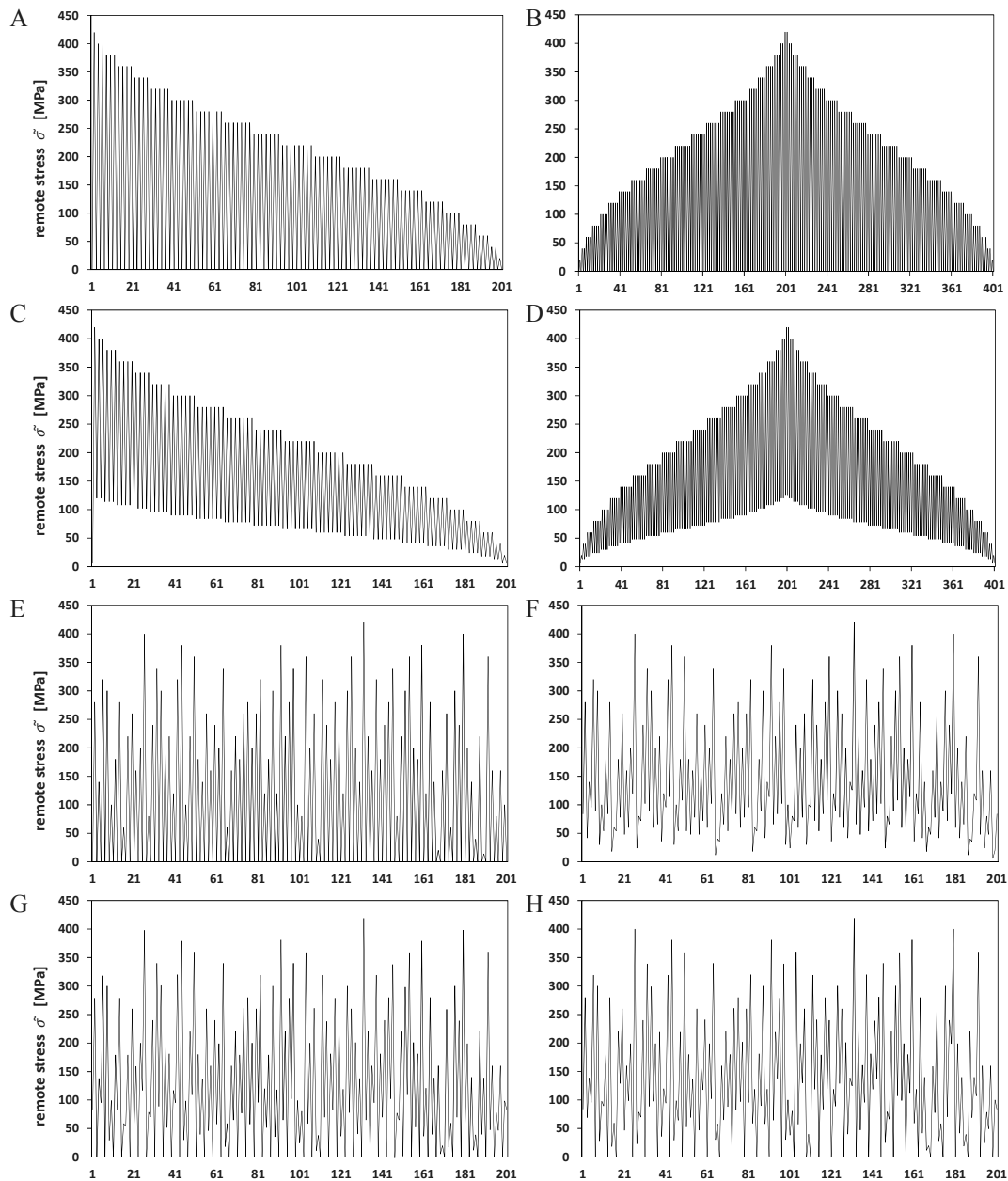


Fig. 1.11: Block types used for validation of the model (Perreira [53]).

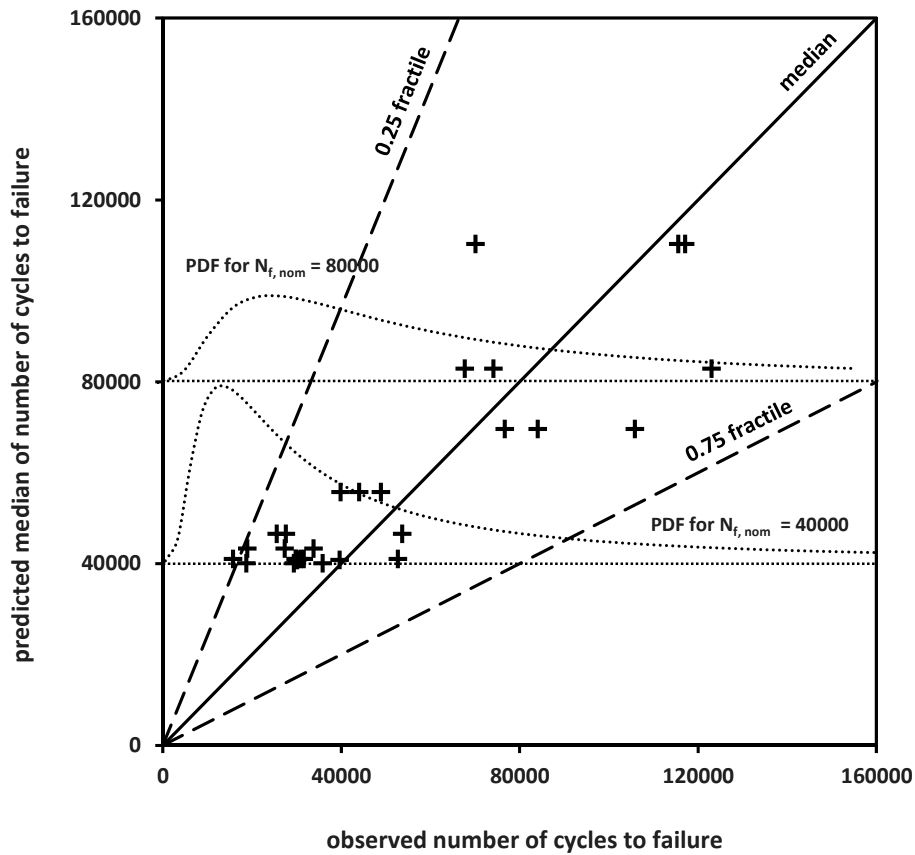


Fig. 1.12: Comparison of model prediction to experimental results (Perreira [53]) for variable amplitude loading.

Table 1.2: Experimental results (Perreira [53]) and model prediction for variable amplitude loading

Block type	Specimen 1	Specimen 2	Specimen 3	Predicted median
A (H-L)	39600	30002	30115	40874
A (L-H)	29788	31600	15773	41059
B	52704	30900	29909	41059
A (H-L)	74100	123000	67700	82932
A (L-H)	84000	105800	76600	69691
D	70100	115530	117100	110353
E	29366	18668	35791	40120
F	39868	43996	48832	55815
G	53679	25568	27591	46620
H	18919	27319	33814	43387

## 1.7. References

- [1] Chaboche J-L. Continuous damage mechanics – A tool to describe phenomena before crack initiation. Nucl Eng Design. 1981;64(2):233-47.
- [2] Lemaitre J. How to use damage mechanics. Nucl Engng Design. 1984;80(2):233-45.
- [3] Peeker E. Extended numerical modeling of fatigue behavior [dissertation]. Lausanne(CH): Ecole Polytechnique Fédérale de Lausanne; 1997.
- [4] Noroozi AH, Glinka G, Lambert S. A two parameter driving force for fatigue crack growth analysis. Int J Fatigue. 2005;27(10-12):1277-96.
- [5] Noroozi AH, Glinka S, Lambert S. A study of the stress ratio effects on fatigue crack growth using the unified two-parameter fatigue crack growth driving force. Int J Fatigue. 2007;29(9-11):1616-33.

- [6] Hanstock RF. Damping capacity, strain hardening and fatigue. *Proc Phys Society*. 1947;9(2):275-87
- [7] Feltner CE, Morrow JD. Microplastic strain hysteresis energy as a criterion for fatigue fracture. *J Fluids Engng*. 1961;83(1):15-22.
- [8] Kaleta J, Blotny R, Harig H. Energy stored in a specimen under fatigue limit loading conditions. *J Test Eval*. 1990;19(4):326-33.
- [9] Boulanger T, Chrysochoos A, Mabru C, Galtier A. Calorimetric analysis of dissipative and thermoelastic effects associated with the fatigue behavior of steels. *Int J Fatigue*. 2004;26(3):221-9.
- [10] Berthel B, Wattrisse B, Chrysochoos A, Galtier A. Thermographic analysis of fatigue dissipation properties of steel sheets. *Strain*. 2007;43(3):273-9.
- [11] Chrysochoos A, Blanche A, Berthel B, Wattrisse B. Energy balance properties of steels subjected to high cycle fatigue. In: Proulx T, editor. *Thermomechanics and infra-red imaging – Volume 7*. New York: Springer; 2011. p. 39-49.
- [12] Naderi M, Khonsari MM. A thermodynamic approach to fatigue damage accumulation under variable loading. *Mater Sci Engng A*. 2010;527(23):6133-9.
- [13] Amiri M, Naderi M, Khonsari MM. An experimental approach to evaluate the critical damage. *Int J Damage Mech*. 2011;20(1):89-112.
- [14] Esin A. The microplastic strain energy criterion applied to fatigue. *J Fluids Engng*. 1968;90(1): 8-36.
- [15] Doudard C, Calloch S, Cugy P, Galtier A, Hild F. A probabilistic two-scale model for high-cycle fatigue life predictions. *Fatigue Fract Engng Mater Struct*. 2005;28(3):279-88.
- [16] Doudard C, Hild F, Calloch S. A probabilistic model for multiaxial high cycle fatigue. *Fatigue Fract Engng Mater Struct*. 2007;30(2):107-14.
- [17] Poncelet M, Doudard C, Calloch S, Weber B, Hild F. Probabilistic multiscale models and measurements of self-heating under multiaxial high cycle fatigue. *J Mech Phys Solids*. 2010;58(4):578-93.
- [18] Munier R, Doudard C, Calloch S, Weber B. Determination of high cycle fatigue properties of a wide range of steel sheet grades from self-heating measurements. *Int J Fatigue*. 2014;63(0):46-61.
- [19] Bhate D, Mysore K, Subbarayan G. An information theoretic argument on the form of damage accumulation in solids. *Mech Adv Mater Struct*. 2012;19(1-3): 184-95.
- [20] Chan D, Subbarayan G, Nguyen L. Maximum-entropy principle for modeling damage and fracture in solder joints. *J Electron Mater*. 2012;41(2):398-411.
- [21] Castillo E, Fernández-Canteli A. A general regression model for lifetime evaluation and prediction. *Int J Fracture*. 2001;107(2):117-37.
- [22] Castillo E, Fernández-Canteli A, Ruiz-Ripoll ML. A general model for fatigue damage due to any stress history. *Int J Fatigue*. 2008;30(1):150-64.
- [23] Correia JAFO, De Jesus AMP, Fernández-Canteli A. Local unified probabilistic model for fatigue crack initiation and propagation: Application to a notched geometry. *Eng Struct*. 2013;52(0):394-407.
- [24] Saouma V, Fava G. On fractals and size effects. *Int J Fract*. 2006;137(1):231-49.
- [25] Carpinteri A, Paggi M. Dimensional analysis and fractal modeling of fatigue crack growth. *J ASTM Int*. 2011;8(10).
- [26] Bazant ZP. Size effect in blunt fracture: concrete, rock, metal. *J Eng Mech*. 1984;110(4):518-35.
- [27] Hillerborg A. Analysis of one single crack. *Dev Civ Engng*. 1983;223-49.
- [28] Lazzarin P, Berto F. Some expressions for the strain energy in a finite volume surrounding the root of blunt V-notches. *Int J Fracture*. 2005;135(1-4):161-85.
- [29] Lazzarin P, Tovo R, Meneghetti G. Fatigue crack initiation and propagation phases near notches in metals with low notch sensitivity. *Int J Fatigue*. 1997;19(8-9):647-57.
- [30] Lazzarin P, Zambardi R. A finite volume energy based approach to predict the static and fatigue behavior of components with sharp V-shaped notches. *Int J Fracture*. 2001;112(3):275-98.
- [31] Susmel L. The theory of critical distances: a review of its applications in fatigue. *Eng Fract Mech*. 2008;75(7):1706-24.
- [32] Taylor D. Geometrical effects in fatigue: a unifying theoretical model. *Int J Fatigue*. 1999;21(5):413-20.
- [33] Crooks GE. Entropy production fluctuation theorem and the non-equilibrium work relation for free energy differences. *Phys Rev E*. 1999;60(3):2721-26.
- [34] Jarzynski C. Equalities and inequalities: irreversibility and the second law of thermodynamics at the nanoscale. In: Duplantier B, editor. *Time*. Basel: Springer; 2013. p. 145-172.
- [35] Voyiadjis GZ, Taqieddin ZN, Kattan PI. Theoretical formulation of a coupled elastic-plastic anisotropic damage model for concrete using the strain energy equivalence concept. *Int J Damage Mech*. 2009;18(7):603-38.
- [36] Jaynes ET. Information theory and statistical mechanics I. *Phys Rev*. 1957;106:620-30
- [37] Shore J, Johnson R. Axiomatic derivation of the principle of maximum entropy and the principle of minimum cross-entropy. *IEEE Trans Inf Theory*. 1980;26(1):26-37.
- [38] Uffink J. Can the maximum entropy principle be explained as a consistency requirement? *Stud Hist Philos Mod Phys*. 1995;26(3):223-61.
- [39] Rosakis P, Rosakis AJ, Ravichandran G, Hodowany J. A thermodynamic internal variable model for the partition of plastic work into heat and stored energy in metals. *J Mech Phys Solids*. 2000;48(3):581-607.
- [40] Kaleta J. Determination of cold work energy in LCF/HCF region. In: Rie KT, Portella PD, editors. *Proceedings of 4th International Conf. on LCF and Elasto-Plastic Behaviour of Materials*; 1998; Garmisch-Partenkirchen. Elsevier Science Ltd. p.93-95.
- [41] Berthel B. Mesures thermographiques de champs de dissipation accompagnant la fatigue à grand nombre de cycles des aciers [dissertation], Montpellier(FR) : Université Montpellier II Sciences et Techniques du Languedoc; 2007.
- [42] Vincent L. On the ability of some cyclic plasticity models to predict the evolution of stored energy in a type 304L stainless steel submitted to high cycle fatigue. *Eur J Mech-A/Solids*. 2008;27(2):161-180.
- [43] Qilafku G, Kadi N, Dobranski J, Azari Z, Gjonaj M, Pluvinaige G. Fatigue of specimens subjected to combined loading – Role of hydrostatic pressure. *Int J Fatigue*. 2001;23(8):689-701.

- [44] Buczynski A, Glinka G. An analysis of elasto-plastic strains and stresses in notched bodies subjected to cyclic non-proportional loading paths. In: Carpinteri A, de Freitas M, Spagnoli A, editors. *Biaxial/Multi-axial Fatigue and Fracture: Proceedings of the 6<sup>th</sup> International Conference on Biaxial /Multi-axial Fatigue and Fracture*; 2003 Jun 28-28; Lisbon, Portugal. Elsevier; 2003. p. 265-83.
- [45] Molski K, Glinka G. A method of elastic-plastic stress and strain calculation at a notch root. *Mat Sci Eng*, 1981. 50(1): p. 93-100.
- [46] Glinka G. Energy density approach to calculation of inelastic strain-stress near notches and cracks. *Eng Fract Mech*. 1985;22(3):485-508.
- [47] Glinka G. Calculation of inelastic notch-tip strain-stress histories under cyclic loading. *Eng Fract Mech*. 1985;22(5):839-54.
- [48] Berto F, Lazzarin P. A review of the volume-based strain energy density approach applied to V-notches and welded structures. *Theor Appl Fract Mech*. 2009;52(3):183-94.
- [49] Pereira HFSG, De Jesus AMP, Ribeiro AS, Fernandes AA. Fatigue damage behavior of a structural component made of P355NL1 steel under block loading. *J Pressure Vessel Technol*. 2009;131(2):021407-1 – 9.
- [50] De Jesus AMP, Ribeiro AS, Fernandes AA. Finite element modeling of fatigue damage using a continuum damage mechanics approach. *J Pressure Vessel Technol*. 2005;127(2):157-164.
- [51] De Jesus AMP, Ruiz Ripoll ML, Fernández-Canteli A, Castillo E, Pereira HFSG. Probabilistic Fatigue Assessment of a Notched Detail Taking Into Account Mean Stress Effects. *J Pressure Vessel Technol*. 2012;134(2):021203-1 – 9.
- [52] Pereira HFSG, de Jesus, AMP, Ribeiro AS, Fernandes AA. Fatigue Modeling of a Notched Flat Plate Under Variable Amplitude Loading Supported by Elastoplastic Finite Element Method Analyses. *J Pressure Vessel Technol.*, 2011;133(6): 061207-1 – 061207-10.
- [53] Pereira HFSG. Fatigue behavior of structural components under variable amplitude loading [MSc dissertation], Porto (P): University of Porto; 2006 (in Portuguese).
- [54] Park SY, Bera AK. Maximum entropy autoregressive conditional heteroskedasticity model. *J Econometrics*. 2009;150(2):219-230.
- [55] Krajewski PE et al. Atoms to autos: A multi-scale approach to modeling aluminum deformation. *JOM*. 2011; 63(11): p. 24-32.



## Annex: Algorithm for the implementation of the proposed model

```

start
do  $i = 1 \dots N$  ; do  $j = 1 \dots M$  ; read  $p_i$   $p_j$   $k_i$   $k_j$  enddo ; enddo
 $\mathfrak{a}_0 = \mathbf{0}$  ;  $\mathfrak{s}_0 = \mathbf{0}$ 
do  $n = 1 \dots L$ 
  read  $\delta w_n^d$   $\delta w_n^d$   $\mathfrak{a}_n$ 

  “Calculation of relative work increment at RVE level”
  if  $\mathfrak{a}_n \mathfrak{a}_{n-1} \geq \mathbf{0}$  then  $\mathfrak{s}_n = \mathfrak{a}_n \text{sign}(\delta w^d)$  ; else if  $\mathfrak{a}_n > \mathbf{0}$  then  $\mathfrak{s}_n = \mathbf{1}$  ; else  $\mathfrak{s}_n = -\mathbf{1}$ 
  if  $\mathfrak{s}_n \mathfrak{s}_{n-1} \leq \mathbf{0}$  then  $\hat{\mathbf{a}}^d = \mathbf{a}_{n-1}^d$ ,  $\hat{\mathfrak{a}} = \mathfrak{a}_{n-1}$ 
  if  $(\mathfrak{a}_n (\mathbf{a}_n^d)^{1/2} + \mathfrak{a}_{n-1} (\mathbf{a}_{n-1}^d)^{1/2}) / 2 \neq \mathbf{0}$  then  $\delta w^d = (1 - 2\hat{\mathfrak{a}} (\hat{\mathbf{a}}^d)^{1/2} / (\mathfrak{a}_n (\mathbf{a}_n^d)^{1/2} + \mathfrak{a}_{n-1} (\mathbf{a}_{n-1}^d)^{1/2}) / 2) \delta w^d$ 
    else  $\delta w^d = 4(\mathbf{a}_{n-1}^d)^{1/2} (\hat{\mathbf{a}}^d)^{1/2}$  ; endif

  “Initial microsystem values”
  if  $n = 1$ 
  do  $i = 1 \dots N$  ; do  $j = 1 \dots M$  ;  $\hat{w}_{ij} = \mathbf{1}$  ;  $\mathfrak{a}_{ij,n} = \hat{\mathfrak{a}}_{ij} = \mathfrak{a}_n$  ;  $\mathbf{a}_{ij,0}^d = \mathbf{0}$  ;  $\hat{\mathbf{a}}_{ij}^d = \mathbf{0}$  ;  $\mathbf{a}_{ij,0}^d = \mathbf{0}$  ;  $\mathbf{a}_{ij,0}^v = \mathbf{0}$  ; enddo ; enddo
  endif

  “Shift of the microsystem datum to the latest reversal point”
  if  $\mathfrak{s}_n \mathfrak{s}_{n-1} < \mathbf{0}$  then  $\hat{\mathbf{a}}_{ij}^d = \mathbf{0}$  ;  $\hat{\mathbf{a}}_{ij}^d = \mathbf{a}_{ij,n-1}^d$  ;  $\hat{\mathfrak{a}}_{ij} = \mathfrak{a}_{ij,n-1}$  ;  $\hat{w}_{ij} = \mathfrak{s}_n \hat{\mathfrak{a}}_{ij}$  ; endif

  “Elastic prediction”
  do  $i = 1 \dots N$  ; do  $j = 1 \dots M$ 
   $\mathbf{a}_{ij}^{d,tr} = \mathbf{a}_{ij,n-1}^d + p_i p_j k_i k_j \delta w_n^d$  ;  $\mathbf{a}_{ij}^{d,tr} = ((\hat{\mathbf{a}}_{ij}^d)^{1/2} + \hat{w}_{ij} (\mathbf{a}_{ij}^{d,tr})^{1/2})^2$  ;  $\mathbf{a}_{ij,n}^v = \mathbf{a}_{ij,n-1}^v + p_i p_j k_i k_j \delta w_n^v$ 
  if  $\hat{\mathbf{a}}_{ij}^d + \hat{w}_{ij} \mathbf{a}_{ij}^{d,tr} < \mathbf{0}$  then  $\mathfrak{a}_{ij}^{tr} = -\hat{\mathfrak{a}}_{ij}$  ; else;  $\mathfrak{a}_{ij}^{tr} = \hat{\mathfrak{a}}_{ij}$  ; endif
   $\mathbf{a}_{ij}^y = ((p_i p_j \alpha_{my})^{1/2} - \eta_\mu \mathfrak{a}_n (\mathbf{a}_{ij,n}^v)^{1/2})^2$  ;  $\mathbf{a}_{ij}^y = ((\mathbf{a}_{ij}^v)^{1/2} - \hat{w}_{ij} (\hat{\mathbf{a}}_{ij}^d)^{1/2})^2$ 
  end do ; end do

  “Plastic correction”
  do  $i = 1 \dots N$ , do  $j = 1 \dots M$ 
  if  $\mathbf{a}_{ij}^{tr} \geq \mathbf{a}_{ij}^y$  then
     $\delta w_{ij,n}^{in} = (\mathbf{a}_{ij}^{tr} - \mathbf{a}_{ij}^y)$  ;  $\delta w_{ij,n}^{in} = \delta w_{ij,n}^{in} (\mathbf{a}_{ij}^y / \mathbf{a}_{ij}^{tr})^{1/2}$  ;  $\mathbf{a}_{ij,n}^d = \mathbf{a}_{ij}^y$  ;  $\mathfrak{a}_{ij,n} = \mathfrak{a}_{ij}^{tr}$  ;  $\mathbf{a}_{ij,n}^d = \mathbf{a}_{ij}^y$ 
  else
     $\delta w_{ij,n}^{in} = \delta w_{ij,n}^{in} = \mathbf{0}$  ;  $\mathbf{a}_{ij,n}^d = \mathbf{a}_{ij}^{d,tr}$  ;  $\mathbf{a}_{ij,n}^d = \mathbf{a}_{ij}^{d,tr}$  ;  $\mathfrak{a}_{ij,n} = \mathfrak{a}_{ij}^{tr}$ 
  end if
  enddo, enddo
   $\delta w_n^{in} = \sum_j \sum_j \delta w_{ij,n}^{in}$ 
enddo
end

```



## **Chapter II: Monitoring of strain profile variations in the RC slab of a short span railway bridge**

The content of this chapter has been submitted for publication in the Journal of Civil Structural Health Monitoring in the form of the following paper: Grigoriou V, Brühwiler E. Monitoring of strain profile variations in the RC slab of a short span railway bridge.

### **Abstract**

A novel monitoring scheme oriented towards the structural examination of reinforced concrete slabs subject to railway traffic action is presented. Monitoring is based on the measurement of the mean axial strain profile variation in the slab. The strain profile is reconstructed under the assumption of plane sections by measuring the variation of two distances between two pairs of points that are materialized at two different levels under the slab on rigid attachments fixed on the slab. The distance variations are measured by means of strain gages measuring the deformation of two very thin strips connecting the two attachments. The technical aspects of the implementation of the above scheme on a short span railway bridge for a period of seven months and of the processing of the acquired signals are presented in detail. Some interesting monitoring records are provided over which the efficiency of the proposed scheme is discussed.

*Keywords:* structural response monitoring; strain profile; strain gages; signal processing; railway traffic action; RC slabs

## Nomenclature

$\varepsilon$	Strain
$\varepsilon_{\text{train max,d}}$	Maximum strain recorded on a reinforcement bar during the passage of a train according to the direct method.
$\varepsilon_{\text{train max,ind}}$	Maximum strain at the level of the reinforcement during the passage of a train according to the indirect method
FBG	Fiber Bragg Grating (sensors)
RC	Reinforced Concrete
SRM	Structural response monitoring
ULS	Ultimate Limit State.

## 2.1. Introduction

In recent decades Structural Response Monitoring (SRM) has been applied efficiently in several cases of examination of existing structures as a mean to obtain accurate estimations of the structural demand on a particular structural element [1-6]. The advantage of Structural Response Monitoring (i.e. action effect monitoring) over load (i.e. action) monitoring is that it reduces considerably the amount of structural modeling that is needed in order to obtain the action effects which are actually involved in the formulation of safety requirements. The objective of this work is to develop a SRM scheme, oriented towards existing Reinforced Concrete (RC) elements, which could provide data that can be used for safety verifications without resorting to structural modeling.

SRM is mainly based on the measurement of stains and displacements. In the case of RC elements such measurements present particular difficulties due to the composite character of the material (concrete and steel), the inhomogeneity of concrete itself and the possible existence of cracks.

The most important problem lays in the fact that the strain which is critical in most Ultimate Limit States (ULS), i.e. the strain in the reinforcement at the location of cracks, cannot be measured except under very specific circumstances. The most efficient method for performing such measurements is by means of Fiber Bragg Grating (FBG) sensors. This type of sensors can be epoxy-glued on a reinforcement bar, which is subsequently embedded in the concrete element (before casting), and can give a quasi-continuous strain profile along the bar capturing efficiently the strain peaks at the crack locations [7]. Such sensors have been embedded in a number of RC bridges showing very good behavior and durability [8-9]. However, the instrumentation of existing RC structures with such sensors is not possible. In these cases the usual practice is to remove locally the concrete cover and to install sensors, usually strain gages, directly on a reinforcement bar. But neither with this method the measurement of reinforcement strains at the location of cracks is reliable since, even if the concrete cover is removed around the location of a crack, the resulting disturbance of the concrete-reinforcement bond may affects the measurement [7]. It seems therefore that in the case of existing cracked RC elements the direct measurement of the critical strain in the reinforcement is not practically possible.

In the case of uncracked sections, on the other hand, direct measurements on the bar, after local removal of the concrete cover, represent rather accurately the strain in the reinforcement under Stage-I<sup>1</sup> conditions; these data, however, cannot be used for statistical extrapolation to the strain levels at the ULS of fracture since at this ULS the element is by definition in Stage-II<sup>2</sup>.

In view of the above limitations the approach that is proposed in this work is to perform measurements at a section level rather than a fiber level. This approach does not actually solve the above problems but it rather proposes an alternative way to work around them. In the proposed monitoring method the focus is placed on the measurement of variations of curvature and variations of the axial strain at the centroid of the section. The measured quantities are in fact the mean curvature and axial strain variations along a certain length (0.5 m in this case) in the vicinity of maximum moment location on the element. From these two quantities, the moment and axial force in the section can be calculated if the mean bending and axial stiffness of the section are also known. Then, the critical stress in the reinforcement under Stage-II conditions can be calculated using concrete section analysis. Hence, the need for structural analysis is eliminated but there is still need for section modeling and analysis. In the above approach the only difference between monitoring on an uncracked and a cracked element (and this is an important difference) is that in the former case the bending and axial stiffness of the section can be easily determined from the geometry of the section, the reinforcement ratio and the modulus of elasticity of the concrete (which can be measured by a Schmidt hammer), while in the latter case this determination is considerably more complicated and less precise since

---

<sup>1</sup> A RC section in bending is said to be in “stage-I” when the tensile strain of concrete  $\varepsilon_{ct}$  remains below the strain  $\varepsilon_{ctu}$  corresponding to its tensile strength  $f_{ct}$ , in “stage II” when  $\varepsilon_{ct} > \varepsilon_{ctu}$  but the stress in the reinforcement  $\sigma_s$  remains below its yield strength  $f_y$  and in “stage-III” when both  $\varepsilon_{ct} > \varepsilon_{ctu}$  and  $\sigma_s > f_y$ .

<sup>2</sup> It is implied here that the ultimate moment is determined by the yielding of the reinforcement. This is a simplification since the moment sustained by the section can still increase after steel yielding and strictly speaking the ultimate moment is determined by the ultimate strain of concrete.

tension stiffening and the contribution of concrete softening<sup>3</sup> have to be taken into account. In this work only the case of monitoring on uncracked element is treated in detail. However, the use of the above method can still prove useful for cracked elements since it eliminates at least the need for overall structural analysis (although the need to model cracked section stiffness remains).

The main difficulty in monitoring curvature variations in reinforced concrete slabs is the fact that under service conditions it is very often only one of the slab surfaces that is accessible for measurements; while strain measurements at, at least, two levels on a certain section are required to reconstruct the strain profile over that section.

The first part of this article presents the technical aspects of the development of a measurement scheme for the monitoring of strain profile variations and of its application in the case of a short span railway underpass. To the knowledge of the authors this type of measurements is presented here for the first time. In the second part some interesting monitoring results are presented and discussed.

## 2.2. Monitoring scheme

### 2.2.1. Device for measuring strain profile variations

The measuring principle of the proposed monitoring device is illustrated in **Fig. 2.1(a)**. The mean axial strain profile variation along a given straight line segment in a given direction is reconstructed by monitoring the variation of two distances between two pairs of points that are materialized at two different levels outside the slab on “rigid” attachments fixed on the slab. The distance variations are monitored by measuring the deformation of very thin strips connecting the two attachments. The monitoring is performed in two directions (perpendicular among them and parallel to the sides of the slab) by means of two devices in a cruciform configuration as shown in **Fig. 2.1(c, d)**.

The rigid attachments are made from aluminum and are fixed on the slab by means of anchors and bolts. The flexible strips are made of stainless steel. At the middle of each strip two strain gages connected in a half bridge configuration are glued. The first one measures the axial strain of the strip while the other one, aligned at a right angle to the first, measures the transverse strain induced by the Poisson effect. Since the Poisson ratio of the strip material is known this half bridge configuration can be used in order to systematically remove the thermal strain variations from the signal. The strips are fixed on the attachments by specially designed connectors. By means of these connectors a pretension is applied on the strips in order to provide them a bending rigidity. Through the same connectors it is also possible to adjust the ends of the strips around a horizontal and a vertical axis before fixing them at their final position. In this way small misalignments of the installed attachments can be accommodated without inducing non-axial deformation in the strips. This is important because such residual deformation may affect the measured strain variations. The dimensions of the strain gages are approximately  $\frac{1}{4}$  of the width of the strips and are placed exactly in the center of the strips in order to avoid the border effect on the strain measurements.

Before installation on the slab the devices were tested and calibrated in the laboratory using a statically loaded steel beam (**Fig. 2.1(b)**). Calibration consists in calculating appropriate correction factors applied on the measured deformation of each strip in order to compensate the small elastic deformation of the theoretically rigid attachments.

### 2.2.2. Installation of monitoring devices on the structure

The elevation and cross section of the monitored structure are depicted in **Fig. 2.1(e, f)**. It is a short single span railway underpass carrying two tracks and consisting of a reinforced concrete slab simply supported on masonry abutments. This structure has mainly been selected because of its structural simplicity (which facilitates the interpretation of the monitoring results), its accessibility and the fact that it is located on a rather busy branch of the railway network. Additionally the selection of a short span structure offers potentially an interesting case for the study of fatigue at a relatively high number of cycles since the passage of each axle over the slab corresponds approximately to a fatigue loading cycle.

---

<sup>3</sup> Under service conditions the crack opening displacement  $w$  is limited by the reinforcement and does not exceed, in general, the opening  $w_{\max}$  which corresponds to the formation of a true crack (for common structural concrete  $w_{\max}$  is about 0.25 to 0.30 mm). This means that these cracks remain, in fact, virtual cracks (Hillerborg [10]) through which concrete can still transfer tensile stress.

An examination of the bottom surface of the slab revealed that there are no cracks in the transverse direction (perpendicular to the principal reinforcement), while in the longitudinal direction (perpendicular to the secondary reinforcement) there are fine cracks (with opening in the order of 0.1mm) spaced at approximately 250 mm. These cracks are attributed to deformations restrained at the supports of the slab during early shrinkage.

Instrumentation is placed at the bottom surface of the slab and is limited to one of the two locations of maximum bending moments. These locations have been calculated numerically, using a detailed finite element model of the slab and a detailed distribution of axle loads through the rails, sleepers and ballast. The calculations verified what was already expected, i.e. that bending moments obtain their maximum value at the middle of the span and under the *axes* of the two tracks (the track over the point of measurements is referred to as track 1).

Besides the strain profile monitoring device, strain gages are also glued directly on one longitudinal and one transverse reinforcement bar in the bottom of the slab (for that the concrete cover had to be removed locally over an area of approximately 100 mm by 100 mm). These measurements are used for the evaluation of the monitoring scheme. It has to be noted that this local removal of the concrete cover does not constitute a crack in the section but rather a local weakening of the section which has a negligible influence on the mean stiffness of the section (and consequently on the strain measurements on the device) over the measuring length of 0.5 m and the width of the slab.

### 2.2.3. Signal acquisition

Signal collection and transmission scheme is adapted from Treacy [11]. Signal is collected only when a train is passing on the bridge. The acquisition system is triggered by the signal of an accelerometer fixed on the slab. The system is programmed to keep constantly in its memory the measurements of the last two seconds. Hence, the record which is finally acquired for each passage includes also the two seconds before the triggering so that the strain just before and during the beginning of the event is not lost. Signal is collected at a frequency of 600Hz and is stored as is with no filter applied to it at this stage. Just one measurement of temperature is stored per train passage.

One disadvantage of the proposed strain profile monitoring device is that it cannot be used for monitoring of the temperature action effect. This is because of the fact that the device and the slab have different response time to the changes of the ambient temperature and as a consequence the strips and the slab do not have in general the same temperature. The above phenomenon is independent of the fact that the thermal strain of the strips is automatically compensated by the half bridge configuration of the strain gages. In any case, it is reasonable to assume that during the few seconds that each train passage lasts, the temperature variations are negligible. For each train passage the base line of the signal (strain corresponding to the unloaded slab) is set to zero by subtracting from the signal the average of the first 600 points (1s) of the record during which the slab is indeed completely unloaded. Thus, the signals that are finally used do not include any effect induced by thermal strain.

### 2.2.4. Signal post-processing

Most of the time, but not constantly, electromagnetic interference (EMI) noise has been interfering in the signals of all the strain gages. This noise, when present, was persisting with apparently unaltered characteristics and intensity also between the crossings of the trains. However the intensity of the noise was in general different for the various strain gages and was also varying during the day. It was, in general during night time that the noise was becoming weaker or was even disappearing. At the end of the monitoring period, the cable of one of the strain gages was replaced by a cable with double shielding. It seems that this measure solves the problem. It has to be noted that the problem of EMI can be entirely avoided by using fiber optic sensors on the strips instead of strain gages. This is a possible improvement to the above method that has to be investigated in the future.

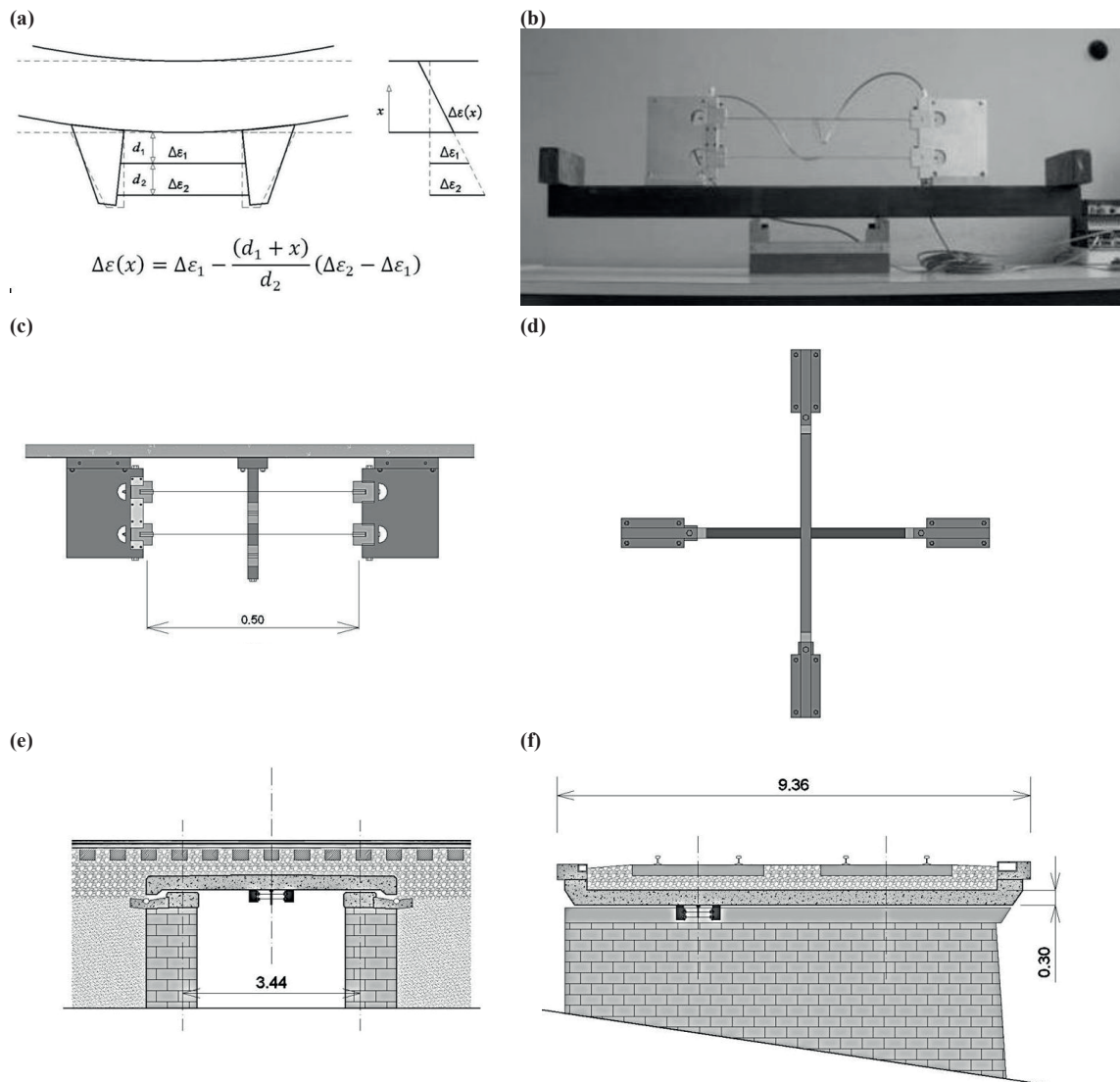


**Fig. 2.1:** (a) Principle of measurement of strain profile variations. (b) The device during testing and calibration in the laboratory. (c) Bottom view and (d) elevations of the strain profile monitoring device. (e) Longitudinal section and (f) cross-section of the underpass with the installed device.

It is believed that this EMI is caused by electric currents traveling in the rails. It seems that the mere movement of a train on the track several kilometers away from monitoring system may result in significant EMI as explained in [12]. A similar type of EMI in the function of an automated railway traffic regulator is reported in [13]. On the other hand EMI is not reported in recent works dealing with monitoring of electrified railway bridges using strain gages [2, 4]; this may be due to the fact that these two bridges were large steel structures that somehow acted as Faraday cages for the monitoring system.

A signal recorded during and between two successive train passages during a rather noisy period is shown in **Fig. 2.2(a)**. It is interesting to observe the characteristic beat form of this noise and how it remains unaffected by the crossing of the trains. A fast Fourier transform (**Fig. 2.2(b)**) of the above signal reveals that this noise has a very distinct nature and consists of a superposition of harmonics spaced at approximately 33.4 Hz, exactly two times the frequency of the electric current used by the Swiss Federal Railways (16.7 Hz). It is interesting to observe that it is the higher harmonics ( $\geq 83.5\text{Hz}$ ) which mainly contribute to the noise while the lower ones, although observable in this particular graph, are very often hidden among the contribution of other frequencies.



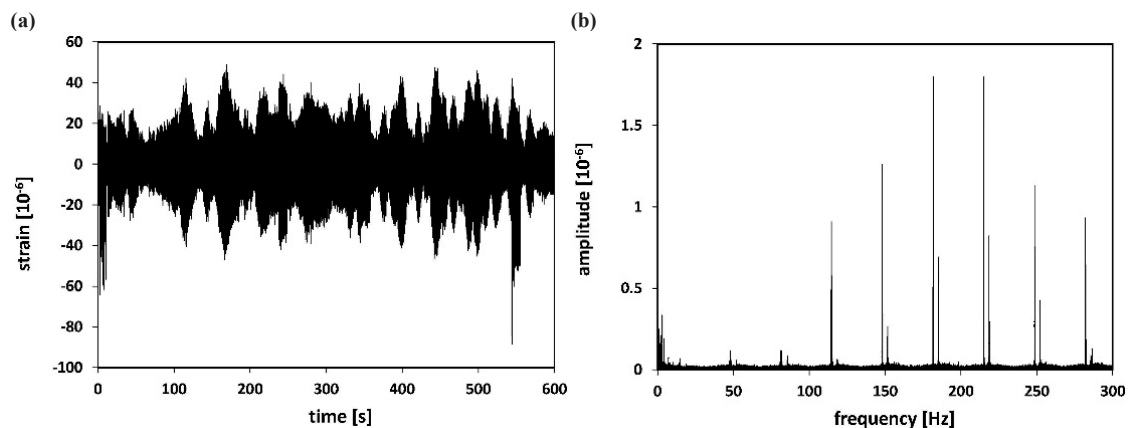


**Fig. 2.2:** (a) A segment of signal of strain recorded on one of the bands between the passage of two trains. The two train passages can barely be distinguished around second 10 and second 550. (b) FFT of the signal; the effect of IMI is clearly manifested in the peaks regularly spaced at 33.4 Hz.

In order to remove much of the EMI noise without accidentally suppressing any significant feature of the signal originating from a real mechanical vibration of the structure, a step by step procedure is followed.

First, the specific frequencies of the EMI equal or above 83.5Hz are filtered out one by one by a successive application of band stop filters and using a small width of frequency bands just around each specific EMI frequency. This procedure is performed for both the strains measured directly on the bar (direct signals) and those calculated from the apparatus measurements (indirect signals). After this operation the characteristic beat noise disappears but still considerable perturbation persists. This can be seen in the FFT spectra of the band stop filtered signals which are plotted in **Fig. 2.3**<sup>4</sup>.

In this figure observe that for frequencies above approximately 75 Hz the FFT spectra remain quasi constant (with the exception of the frequency bands that have been removed) and that the spectrum tails for the indirect signals are much thicker than for the direct ones, suggesting a higher level of noise. This higher level of noise can be attributed, in one part, to undesired vibrations of the steel strips which amplify the effect of very small (insignificant) high frequency vibrations in the slab and, in another part, to error amplification in the process of indirect calculation of the signal. Observe also the enhancement of the frequency content around 50 Hz which is due to EMI that has not yet been removed since in this frequency domain important frequencies might also exist. It is also interesting to observe that the natural frequencies of the slab (the two first of which are expected to lay somewhere between 20 and 40Hz) are not manifested at all in the FFT spectra. It seems therefore that there is no significant dynamic train-structure interaction. In fact, the slab acts as a rigid support for the vibrating track-train system and receives the reactions from this vibrating system as quasi-static loads.

In any case, these FFT spectra suggest that an additional low pass filtering at 75Hz preserves all the significant features of the EMI-filtered signals. This has been confirmed by an extensive comparison between the signals filtered only for removal of the EMI and those resulting from an additional low pass filtering at 75Hz. The comparison included a careful visual examination of all the available records. In these records, not a single case was found where the low pass filtering suppressed (qualitatively) a significant feature of the EMI-filtered signal. Such comparisons are presented in **Fig. 2.4** for a passenger and a freight train and for both the direct and indirect signals. In this figure it can be seen that for the direct measurements the low pass filtering at 75 Hz results in a fairly clear signal. For the indirect measurements, on the other hand, the higher levels of noise observed above in the FFT plots (**Fig. 2.3**) are also evident here, while it can also be seen that considerable level of noise persists even after the low pass filtering at 75 Hz.

It is therefore accepted that the 75Hz low-pass filtered direct signals represent adequately the real strain history of the bars including any possible dynamic amplification effect. On the other hand the use of 75Hz low-pass filtered indirect signals for the calculation of extreme values would lead to unduly conservative

<sup>4</sup> This figure is better viewed on screen using the digital version of this document.

results because of the presence of noise. It is therefore examined in the following whether further filtering can be justified for the indirect signals.

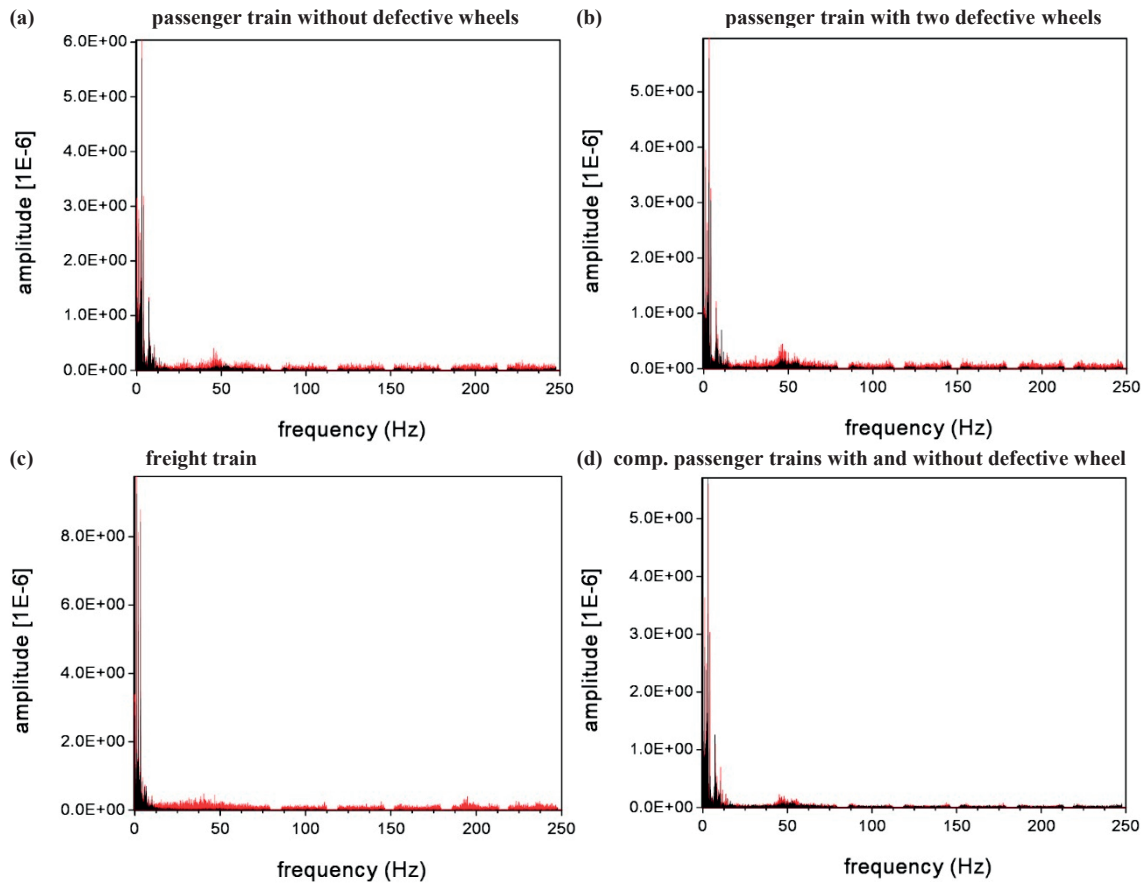


**Fig. 2.3:** FFT spectra of strain variation in the longitudinal (principal) reinforcement from train types passing on track 1 (over the monitoring point). (a-c) in order of appearance: a passenger train with a four axle locomotive, the same type of passenger train with two defective wheels, a freight train with a six axles locomotive. Black line: direct signal; red line: indirect signal. (d) Comparison of the direct signal FFT spectra for the passenger trains with and without defective wheel; black line: without defective wheel; red line: with defective wheels.

The vibrations of the trains are in the range of frequencies between 0 and 10Hz. On the other hand, vibrations of the track in the range of 20 to approximately 75Hz are mainly due to the successive passage of the wheels over the sleepers, and occasionally by the periodic impact of a defective wheel on the rail [14]. The local perturbations indicated by arrows in **Fig. 2.4** and **2.5** are probably due to the passage of defective wheels. If this is true, cars with defective wheels can easily be identified by a careful macroscopic examination of the 75Hz-low-pass-filtered signals (either direct or indirect). These defective wheel induced vibrations are the only track vibrations that have been observed to have a significant impact on the peak values of the reinforcement strain. This means that an additional low-pass filtering down to 20Hz does not significantly affect the peak values of the signal except in the cases of a flat wheel. In **Fig. 2.3(d)** the FFTs of a train signal without flat wheels and a train of the same time with two flat wheel are compared. It can be seen that the presence of the defective wheels results in an enhancement of the frequency content in the region around 50 Hz. It is probably by coincidence that the frequencies resulting from the wheel out of roundness coincide with the band of EMI-induced frequencies in that region. It is also interesting to mention that flat wheel effect is in general less pronounced during the crossings of the heavier trains.

It is therefore suggested that the signals obtained by the device be filtered with a low pass filter at 20Hz before used for structural examination purposes. The effect that this further filtering has on the accuracy and precision of the monitoring scheme is discussed in detail in Section 2.3.1.

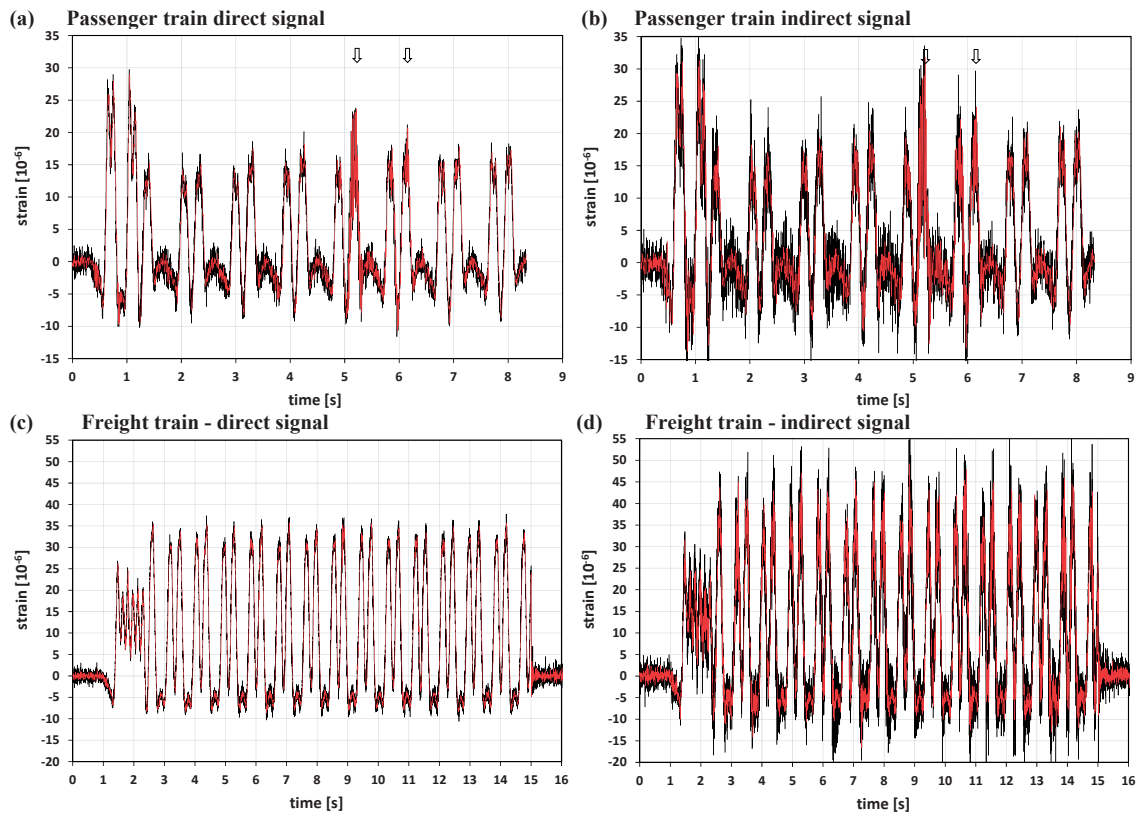


Fig. 2.4: Variation of strain in the longitudinal (principal) reinforcement from trains passing on track 1. Black line: band-stop filtered signal for elimination of EMI above 83.5 Hz; red line: 75 Hz low-pass filtered signal.

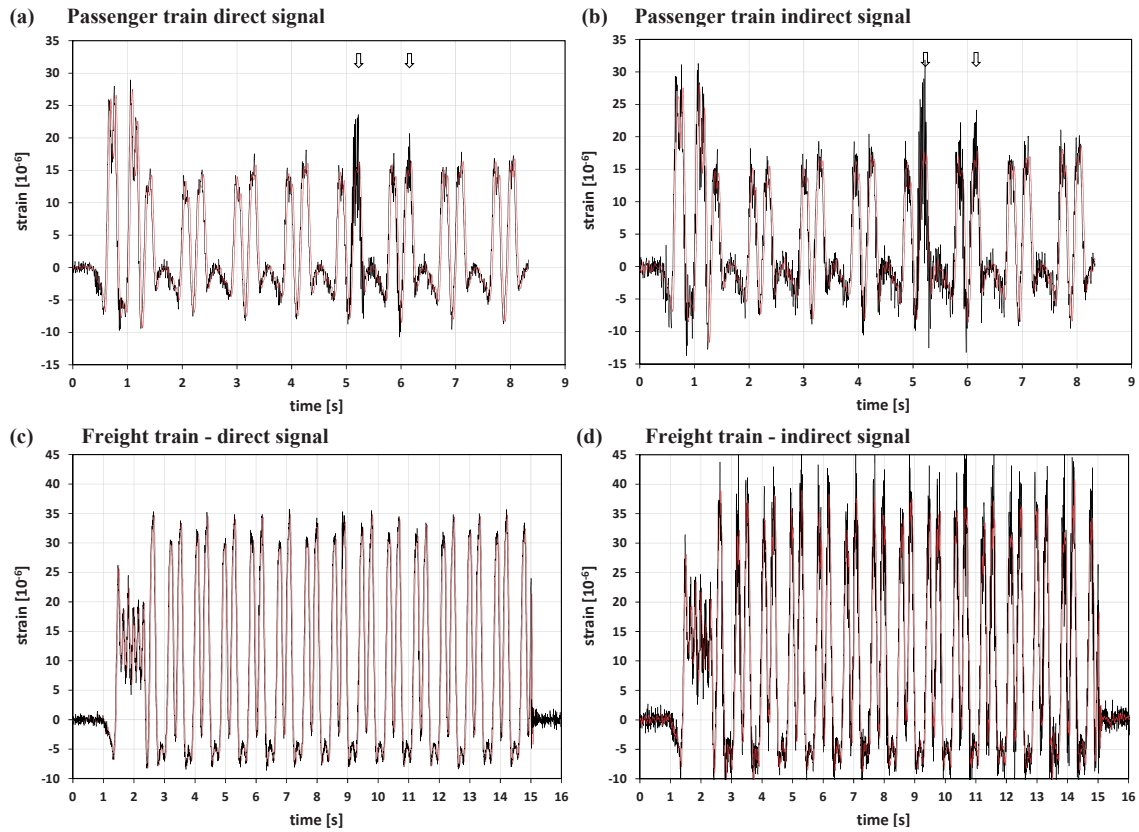
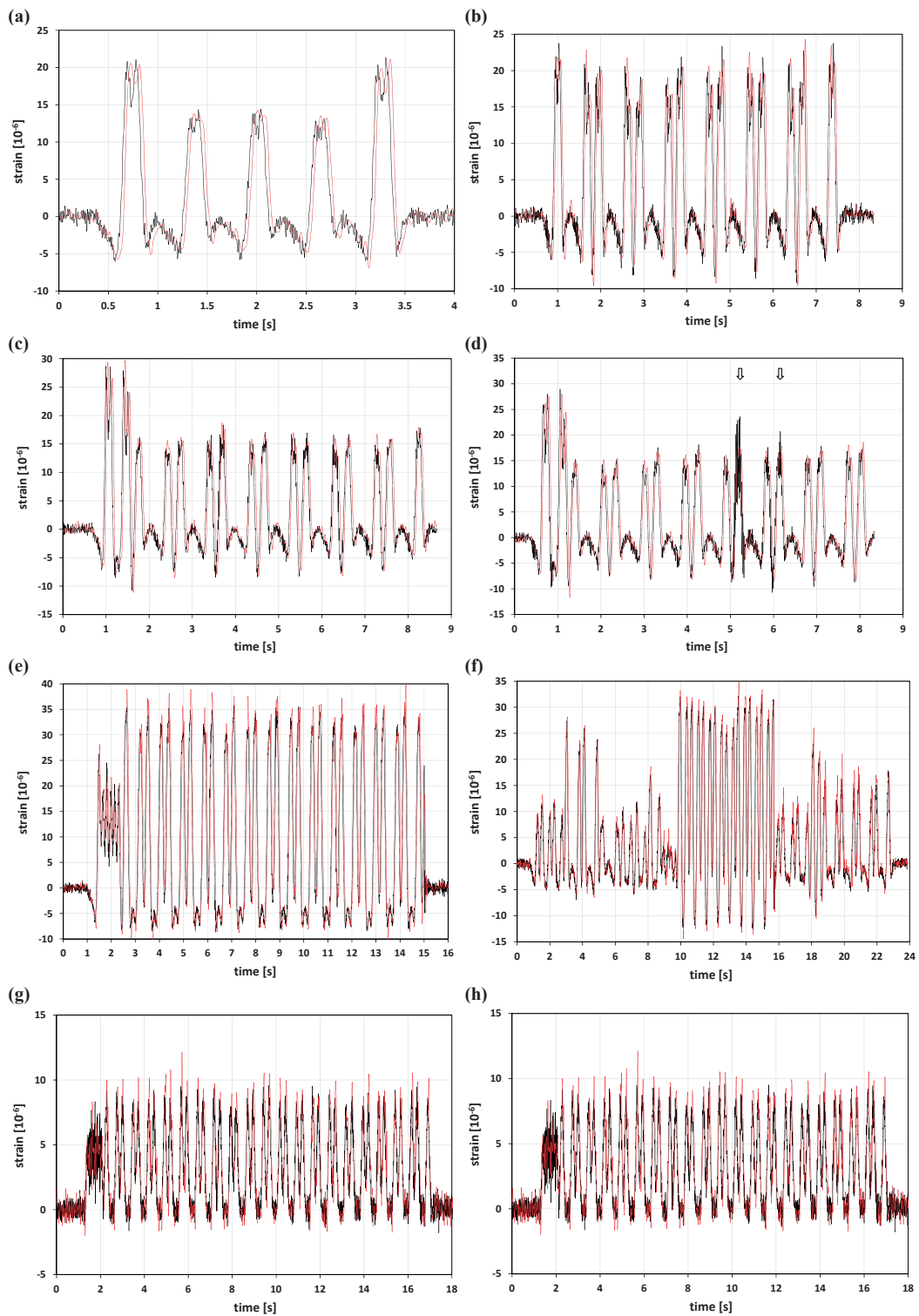


Fig. 2.5: Variation of strain in the longitudinal (principal) reinforcement from trains passing on track 1. 75 Hz low-pass filtered signal; red line: 20 Hz low-pass filtered signal.

## 2.3. Results and discussion

### 2.3.1. Evaluation of the monitoring scheme

In Fig. 2.6 and Fig. 2.7 the signals recorded directly on the bars and filtered with a low pass at 75 Hz—the “direct method”—are compared to the signals of the strain at the level of the bars as calculated from the measurements on the device and filtered with a low pass filter at 20 Hz—the “indirect method”. Fig. 2.6 refers to the longitudinal (principal) reinforcement, while Fig. 2.7 refers to the transvers reinforcement. The signals correspond to the most common types of trains passing either on track 1 (over the point of measurements) or on track 2—in the following each train passage is referred to as “traffic incident”. It can be observed that for all the types of traffic incidents, the two signals follow closely each other. The only exception is in the case of flat wheels (Fig. 2.6(d) and Fig. 2.7(d)).



**Fig. 2.6:** Variation of strain in the longitudinal (principal) reinforcement. Black line: direct method; red line: indirect method. (a-f) Trains passing on track 1 (over the monitoring point): (in order of appearance) a suburban train unit, an intercity train unit, a passenger train with a four axle locomotive, the same type of passenger train with two defective wheels (indicated by the arrows), a freight train with a six axles locomotive, a special convoi. (g, h) Trains passing on track 2: a freight train with a six axles locomotive, a passenger train with a four axle locomotive.

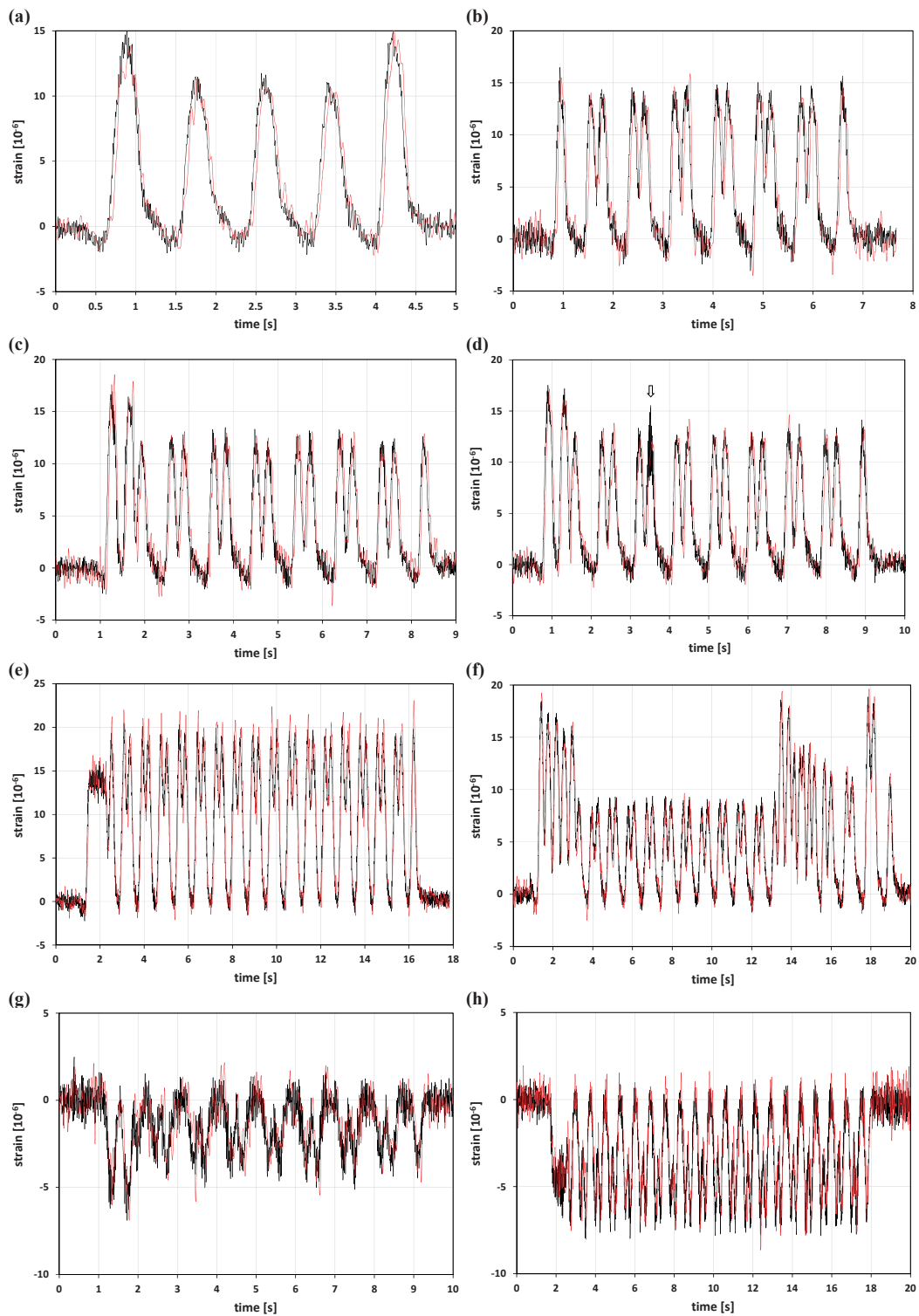


**Fig. 2.7:** Variation of strain in the transversers (secondary) reinforcement. Black line: direct method; red line: indirect method. (a-f) Trains passing on track 1 (over the monitoring point): (in order of appearance) a suburban train unit, an intercity train unit, a passenger train with a four axle locomotive, the same type of passenger train with one defective wheel (indicated by the arrow), a freight train with a six axles locomotive, a special convoi. (g, h) Trains passing on track 2: a freight train with a six axles locomotive, a passenger train with a four axle locomotive.

**Fig. 2.8(a, b)** present the distribution of the difference and the ratio respectively of the maximum strain per incident—the incident maximum—obtained by the direct and the indirect measurement method for the principal reinforcement (the incident maximum is not necessarily recorded at the same time by the two methods). The mean and standard deviation of the distributions are also indicated in the figures. Two distributions are presented: one referring to the total population of recorded traffic incidents and one corresponding to the sub-population of incidents giving a maximum strain higher than  $30 \cdot 10^{-6}$ . The later sub-population represents quite accurately the freight train incidents which are practically the type of incidents that needs to be considered in safety verifications at the ultimate limit state of fracture and fatigue. It can be observed that over the entire population the indirect measurement tends to give slightly larger incident maxima than the direct method by 3% ( $0.5 \mu\text{m/m}$ ) on average. This tendency is more pronounced in the subpopulation of freight trains for which the indirect method gives on average values larger by 8% ( $3 \mu\text{m/m}$ ). Similar characteristics are observed for the transverse reinforcement.

The origins of this discrepancy observed in the higher loads could not be identified and is neither clear whether one of these methods is substantially more accurate than the other so that it can be used as a reference. At least a part of this discrepancy is due to the higher noise of the indirect signals which remains present in frequencies below 20 Hz. In any case these differences are barely larger than the precession of the strain gages which is in the order of  $1 \mu\text{m/m}$ .

Since it is the subpopulation of freight train incidents that is critical for structural verifications (at both the ULS of fracture and the ULS of fatigue), the precision of the proposed monitoring scheme, with respect to the incident maximum of strain in the reinforcement, can be taken, in the context of a probabilistic monitoring based verification procedure, as  $\pm 10\%$ . This value is obtained as  $\pm 1.65$  times the standard deviation of the ratio of incident maxima for the freight train subpopulation (**Fig. 2.8(b)**) and corresponds to the 90% of measurements. This value is in any case an upper bound of the real precision since it is assumed that the statistical variation is entirely due to random error of the proposed scheme (i.e. that the measurements directly on the bar are absolutely correct). Besides that, the precision with respect to incident maxima of curvature is expected to be lower because the effect of the factors that influence in the same way the measurements on both strips is mutually compensated (the measurements on the two strips are subtracted for the calculation of curvature).

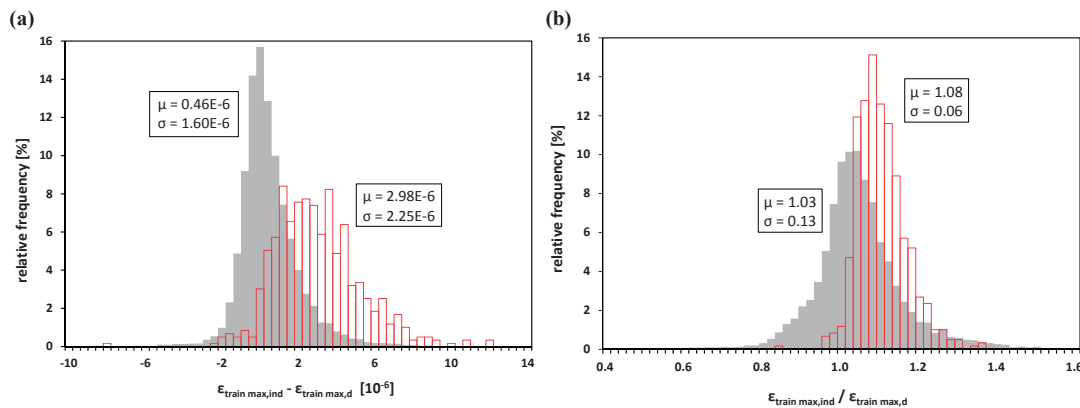


**Fig. 2.8:** Distribution of the difference (a) and ratio (b) between the incident maxima of strain at the level of the longitudinal (principal) reinforcement as obtained by the indirect and the direct method. Gray solid bars: distribution in the entire population of traffic incidents; Red outlined bars: distribution in the heavy freight train subpopulation.

To conclude this section, it can be said that the developed monitoring provides a rather accurate picture of the structural response with respect to both the action effect incident maxima—relevant to verifications at the ULS of fracture—and the number and amplitude of cycles, relevant to damage accumulation verification. However, since signal fluttering constitutes a potential source of inaccuracy, in a future application of this scheme additional measures have to be taken in order to: (a) reduce electromagnetic interference and (b) stiffen the strips of the device. These measures will enable to reduce noise and undesired amplifications and eliminated or reduced the need for filtering the signals.

### 2.3.2. Comparison with results from structural analysis

The objective of this small section is not to examine in depth the mechanisms behind the various phenomena observed in the behavior of the slab but rather to show that this behavior is affected significantly by a number of factors which is difficult to identify, model and eventually consider in structural analysis. In that sense verification methods based on structural response monitoring represent an important advancement with respect to traditional methods based on traffic load models and structural analysis.

In **Fig. 2.9** the monitoring records for two types of incidents and for both the principal and secondary reinforcement are compared to those obtained from an elastic static structural analysis using the known patterns of axle loads (also displayed in the figure). For the analysis a finite element model of the slab is used and the axle loads are distributed on the slab taking into account load distribution through rails, sleepers and ballast. The cross-section is considered un-cracked and the contribution of the reinforcement to the section moment of inertia is taken into account. The modulus of elasticity of the concrete is determined using results of Schmidt rebound hammer measurements. No dynamic amplification or impact factor is applied on the axle loads.

The finite element model requires also the determination of a number of parameters that cannot be obtained by measurements on the structure but whose value has significant influence on the analysis results. It has been found, for example, that the exact pattern of the axle load distribution on the slab through rails, sleepers and ballast (mainly in the transverse direction), affects significantly the maximum values of the calculated strain histories in the transverse direction. The vertical stiffness of the neoprene strip that serves as bearing at the one of the two supports of the slab has also an equally significant effect, on the strain histories in the transverse direction. Notwithstanding, a parametric analysis of these effects lays outside the scope of this work. For the results shown in **Fig. 2.9** the load distribution pattern shown in **Fig. 2.10** has been used and a value of 20MN/m/m has been admitted for the vertical stiffness of the neoprene bearing band (calculated after the dimensions of the band and assuming a value of 6.5 MPa for the shear modulus of neoprene).

The calculated histories show in general a good agreement with the recorded signals. However a number of discrepancies are observed. For example the effect of the locomotive loads is overestimated on the longitudinal reinforcement and underestimated on the transverse reinforcement. The effect of the intercity train on the transverse reinforcement is also underestimated. Of course the assumptions used in the model could be adjusted in order to achieve better overall agreement between calculated and recorded histories. The finite element model itself could be also refined by explicitly including the stiffness of rails, track, ballast and other non-structural elements. Then of course the material laws and properties for these elements should be determined, increasing, in that way, the number of the model parameters that have to be calibrated. It has to be noted that in any case calibration of model parameters by curve fitting presents several theoretical and practical problems. A rigorous approach to this problem of structural identification is given in [15] and falls outside the scope of this work.

## 2.4. Conclusions

A novel monitoring scheme oriented towards RC slabs is developed. Compared to direct measurement of strain variation on the reinforcement bars, this scheme results in a more complete representation of the strain profile at the section level and to an easier interpretation of the results in the context of safety verifications at ULS.

The proposed monitoring scheme gives results of good accuracy and precision but there is still room for improvement in that domain, mainly by providing more rigid strips and double shield cables in order to reduce undesired vibrations and electromagnetic interference.

The monitoring results show that even for the simple case of a simply supported slab subject to very well defined loads, detailed structural analysis fails to represent accurately the behavior of the slab. This observation demonstrates the importance of structural response monitoring for a realistic determination of structural demand at an element level, especially in the cases where considerable interaction between structural and non-structural elements exists.



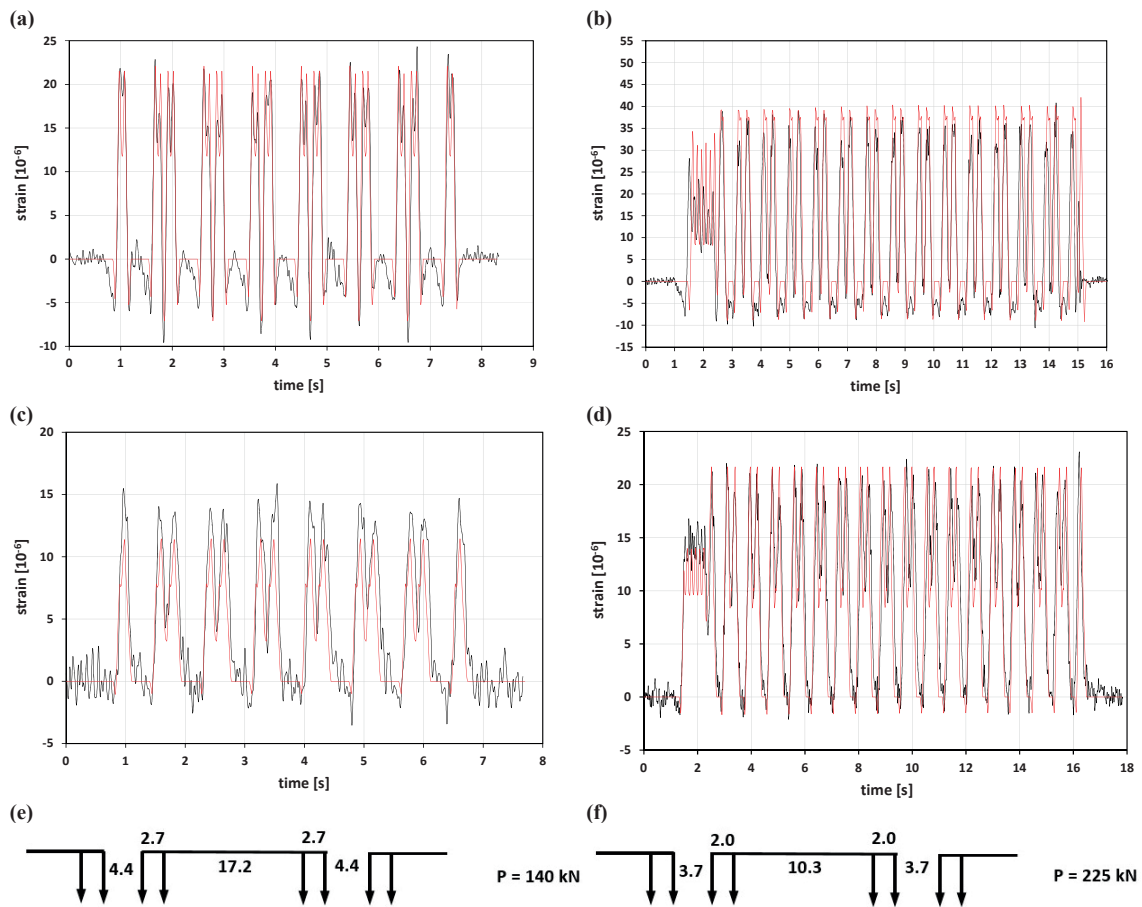


**Fig. 2.9:** Comparison of recorded strain histories with calculated histories. Black line: recorded signal; red line: calculated history (indirect method). (a-b) signal on the longitudinal (principal) reinforcement for an intercity train unit (a) and a freight train (b), (c-d) signal on the transvers (secondary) reinforcement for an intercity train unit (c) and a freight train (d) (not the same incidents as in (a) and (b)), (e-f) the load patterns used in the calculation (dimensions in m).

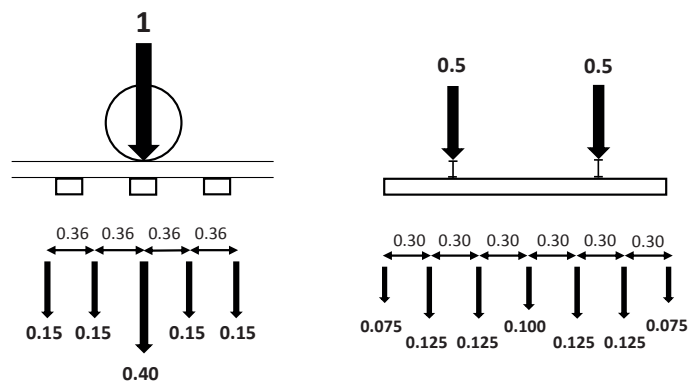


**Fig. 2.10:** Distribution of a unit axle load on the nodes of the finite element model (dimensions in m).

## 2.5 References

- [1] Treacy MA, Brühwiler, Action effects in post-tensioned concrete box-girder bridges obtained from high-frequency monitoring. *J Civil Struct Health Monitoring*. 2015;5(1):11-28.
- [2] Brühwiler E, Bosshard M, Steck P, Meyer C, Tschumi M, Haldimann S. Fatigue safety examination of a riveted railway bridge using data from long term monitoring. In: *IABSE Symposium Report*; 2013; 99(25): p.477-484.
- [3] Rodrigues JFS, Casas JR, Almeida PAO. Fatigue-safety assessment of reinforced concrete (RC) bridges: application to the Brazilian highway network. *Struct Infrastructure Engng*. 2011;9(6):601-616.
- [4]. Leander J, Andersson A, Karoumi R. Monitoring and enhanced fatigue evaluation of a steel railway bridge. *Eng Struct*. 2010;32(3):854-863.
- [5] Catbas FN, Susoy M, Frangopol DM. Structural health monitoring and reliability estimation: Long span truss bridge application with environmental monitoring data. *Engng Struct*. 2008;30(12):2347-2359.
- [6] Frangopol DM, Strauss A, Kim S. Bridge reliability assessment based on monitoring. 2008;13:258-270.
- [7] Kenel A, Nellen P, Frank A, Marti P. Reinforcing Steel Strains Measured by Bragg Grating Sensors. *J Mat Civil Eng*; 2005;17(4):p.423-431.
- [8] Casas JR, Cruz P, Fiber Optic Sensors for Bridge Monitoring. *J Bridge Engng*;2003;8(6):p.362-373.
- [9] Li HN, Li DS, Song GB. Recent applications of fiber optic sensors to health monitoring in civil engineering. *Eng Struct*. 2004;26(11):p.1647-1657.
- [10] Hilleerborg A. Analysis of a single crack. In: Wittmann FH, editor. *Fracture mechanics of Concrete* Amsterdam: Elsevier; 1983. p. 223-249.
- [11] Treacy MA. The use of monitored data in the verification of structural and fatigue safety of existing post-tensioned concrete highway bridges [dissertation]. Lausanne: Ecole Polytechnique Fédérale de Lausanne; 2014.
- [12] Morant A, Wisten A, Galar D, Kumar U, Niska S. Railway EMI impact on train operation and environment. In: *Proceedings of the 2012 International Symposium on Electromagnetic Compatibility (EMC EUROPE)*; 2012 Sept 17-21; Rome, Italy.
- [13] Niska S. Measurements and Analysis of Electromagnetic Interferences in the Swedish Railway Systems [dissertation]. Luleå: Luleå University of Technology; 2008.
- [14] Connolly DP, Kouroussis G, Laghrouche O, Ho CL, Forde MC. Benchmarking railway vibrations – Track, vehicle, ground and building effects. *Construction and Building Materials*. 2015;92:64-81
- [15] Pasquier R. Performance assessment and prognosis for civil infrastructure based on model falsification reasoning [dissertation]. Lausanne: Ecole Polytechnique Fédérale de Lausanne; 2015.

## **Chapter III: Monitoring-based safety verification at the ultimate limit state of fracture of the RC Slab of a short-span railway underpass**

The content of this chapter has been submitted for publication in Structural Safety journal in the form of the following paper: Grigoriou V, Brühwiler E. Monitoring-based Safety Verification at the Ultimate Limit State of Fracture of the RC Slab of a Short Span Railway Underpass.

### **Abstract**

A safety verification method that provides the examination value of the railway traffic action effect directly from monitoring data (without resorting to action models and structural analysis) is developed. The development is based on data obtained from a monitoring campaign conducted on the RC slab of a short span railway underpass. Extreme value theory is used within a semi-probabilistic framework. Simplicity and efficiency in the formulation is achieved by the use of the notion of action incident (which is particularly well suited for the case of railway traffic where an incident can be identified as the passage of a train over the structure), the distinction of incident types and the isolation of the determinant incidents (those on which the examination value actually depends). The determinant instances of the action incident effect are shown to follow excellently a shifted exponential distribution. The duration of the monitoring period, in terms of the number of recorded determinant incidents, is formally taken into account into the examination value of the action effect by means of a confidence upper bound.

*Keywords:* structural response monitoring; safety verification railway infrastructure; action incident effect; semi-probabilistic method.

## Nomenclature

$a$	complement of a confidence level ( $1 - a$ )
$A_s$	area of steel reinforcement
$c$	characteristic fractile for a resistance property
$d$	distance of the centroid of the tensile reinforcement from the top surface of the slab
$d_1$	distance of the centroid of the tensile reinforcement from the bottom surface of the slab
$E$	action incident effect in general
$E$	an empirical CDF in general
$f_{pt1}$	estimated level of $F$ with probability of exceedance $p_{t1}$
$a_{\hat{f}_{pt1}}$	upper confidence bound at $(1 - a)$ confidence level
$f_{ym}$	mean value of steel yield stress
$f_{yk}$	characteristic value of steel yield stress
$F, f$	incident maximum of the force per slab width in the tensile reinforcement under stage-II conditions (random variable, a particular instance)
$\mathcal{F}$	incident time history of the force per slab width in the tensile reinforcement under stage-II conditions
$G$	a CDF in general
$h$	depth of the slab
$M, m$	incident maximum of bending moment (per slab width) (random variable, a particular instance)
$\mathcal{M}$	incident time history of bending moment (per slab width)
$n$	number of observed incidents
$N$	number of incidents in the service life
$\mathcal{N}$	incident time history of axial force (per slab width)
$p$	probability of exceedance in a single incident
$\rho$	probability of exceedance including statistical sampling error
$\mathbb{P}$	probability of exceedance including statistical sampling error and epistemic uncertainty
$p_N, p_{SL}$	target probability of exceedance in $N$ incidents or in service life
$R$	resistance in general
$x$	a variable in general
$\alpha_E, \alpha_R$	FORM sensitivity factor for the leading action effect and the resistance
$\beta$	reliability index
$\gamma_{MON}$	ignorance factor for the monitoring method
$\gamma_{PR}$	ignorance factor for probabilistic modeling

$\gamma_{STR}$	ignorance factor for structural modeling
$\varepsilon$	strain
$\zeta_{t1}$	ratio of number of type-1 incidents over all incidents and its statistically estimated value
$\kappa_a$	confidence level fractile value $\Phi^{-1}(1 - a)$
$\kappa_c$	resistance characteristic fractile $\Phi^{-1}(1 - c)$
$\lambda$	threshold parameter of the generalized Parreto distribution
$\mu$	location parameter of the GEV distribution and its statistically estimated value
$\xi$	shape parameter of the GEV distribution and its statistically estimated value
$\rho$	$1/\tau$ – Alternative scale parameter of the generalized Parreto distribution
$\sigma$	scale parameter of the GEV distribution and its statistically estimated value
$\tau$	scale parameter of the generalized Parreto distribution and its estimated value
$\Phi$	CDF of the standard normal distribution
CDF	Cumulative Distribution Function
FORM	First Order Reliability Analysis
GEV	Generalized Extreme Value (distribution)
PDF	Probability Density Function
SRM	Structural Response Monitoring

### Notes:

- A hat “ $\hat{x}$ ”, a star “ $x^*$ ”, a tilt “ $\tilde{x}$ ” and “ $\bar{x}$ ” denote respectively: a statistically estimated value, a target value, an approximated value and mean value of variable/parameter  $x$ .
- The subscripts “Q1”, “Qi”, “G”, “E” and “R” imply that the corresponding variable refers respectively to: the leading variable action, an accompanying variables action, an accompanying permanent action an action effect or action incident effect in general and a resistance.
- The subscript “e” denotes the examination value of the corresponding variable.
- The subscripts “all”, “t1” and “th” imply that the corresponding variable refers respectively to: all types of incidents, type-1 incidents and incidents exceeding a threshold.
- Indices  $i, j$  and  $k$  count respectively: all types of incidents, type-1 incidents and incidents exceeding a threshold

### 3.1. Introduction

In the context of the design of new and examination of existing structures, safety verifications with respect to the Ultimate Limit State of fracture or excessive deformation (ULS-STR<sup>1</sup>) need to be performed. Most often this ULS is defined at a local level (element or cross-section level) and with respect to a specified ultimate failure mode so that the corresponding safety requirement is formulated in terms of the corresponding action-effect and the local resistance. This type of formulation lies on the simplifying approximation that by keeping the risk related to each ultimate failure mode of each single element or cross-section under an acceptable level, it is implicitly guaranteed that the risk from ultimate failure of larger parts of the structure or the entire structure is also kept under an acceptable level. This assumption makes it possible to develop action and resistance models which are, to a large extent, independent of the particular form of the structure.

For the design of new structures, action-effects have to be calculated from action models by means of appropriate structural models. However, for the examination of existing structures the need of action models and structural models—with all the conservatism that these models involve—can be partially eliminated by using Structural Response Monitoring (SRM) data in order to develop case-specific probabilistic action effect models suitable for safety verifications.

This concept has already been introduced and investigated by a number of researchers including Frangopol et al [1, 2], Strauss et al. [3], Catbas et al. [4], Rodrigues et al. [5], and Treacy et al. [6,7]. In this paper, the above presented concept is further investigated through an application in the case of a short span railway bridge for which a monitoring campaign has been designed and conducted (see Chapter 2). It has to be noted that this bridge shows no signs of deterioration and there were no particular doubts on its safety. Its monitoring has been performed as part of an applied research program whose objective is to investigate in praxis both theoretical and practical aspects of the use of monitoring data in the examination of existing RC structures.

Through this practical application a general procedure for the development of case specific action effect models and their implementation in safety verifications is outlined. The results of this investigation can be used in cases where the safety of a structural element under the *current* traffic regime is in question (for instance a structural element for which a preliminary analysis using standard load models would suggest a limited (<25%) lack of resistance). When safety doubts refer to a *future* increase of traffic load, monitoring is (by its nature) less efficient as examination tool and such possible uses of it are not covered in this work.

### 3.2. Action incident – Action incident effect

#### 3.2.1. Action incident

For the probabilistic modeling of monitoring results it is useful to introduce the notion of *action incident* that is defined as an extract of the evolution of an action contained within specified temporal (and if appropriate also spatial) limits. As long as they are unambiguously defined, these limits may be fixed (e.g. predefined periods of one hour, day, year etc.) or dependent on the evolution of a more global phenomenon involving the action (e.g. the duration of a social event defines a loading incident for the floor of a concert hall) or, finally, dependent on the evolution of the action itself or of an action effect (e.g. the time during which action exceeds a predefined threshold). In any case, the action incident is considered as an elementary random experiment that needs to be probabilistically modeled. In that sense, it is also important that the above limits be defined in such a way that the resulting action incidents can be considered mutually independent.

In this work, it is the duration of the passage of a train on the underpass (on either track) that defines a traffic action incident.

---

<sup>1</sup>According to the nomenclature of EN1990 [15].

### 3.2.2. Action incident effect

For the purpose of safety verification with respect to a certain failure mode at the ULS-STR, the manifestation of an action is considered sufficiently described by the history of the variation that the action induces in a representative component of the structural response. This variation history is the action effect. Accordingly, the outcome of an action incident is considered sufficiently described by the maximum value of the representative action-effect during the action incident. This value is the *action incident effect* and is modeled by a random variable. The instances of the action incident effect occurring within the monitoring period constitute the sample from which the probability distribution of the corresponding random variable is inferred.

### 3.2.3. Leading and accompanying action incident effects

In most cases the representative component of structural response depends on more than one actions acting coincidentally on a structure. However, depending on the monitoring scheme, the measured variations are due to only some, or just one, of these actions. In the domain of railway infrastructure for instance, the contribution of permanent actions cannot, in general be measured, while stress or force variations due to constrained thermal deformations may or may not be included in the measurements. Even if the contributions of all the acting variable actions are included in the measurements, it is useful, for ULS-STR verifications, to separate the contribution of each action from the combined signal in order to model each contribution separately and according to its specific stochastic characteristics. This is in general possible when the variations of each contribution are manifested in very distinct frequency ranges as it is, for instance, the case with the contributions of temperature and traffic actions [8]. Obviously, such a separation is in principle meaningful when the structural response remains or is assumed to remain essentially linear.

In the above case, action incident and the action incident effect, as defined above, should refer to the leading action only (the action at an extreme realization of which failure will occur [9]) and, depending on the context will be also referred as the leading incident effect. The effect of an accompanying action (either variable or permanent) is represented in the verification by an accompanying incident effect which is defined as the value of the accompanying action effect that coincides with the maximum of the leading action effect per incident.

### 3.2.4. Action incident effect for verification of RC sections in bending failure

In this sub-section the discussion is limited to the safety verification with respect to the ULS-STR in longitudinal bending at the mid-span of the slab. It is assumed, in addition, that the critical failure mode for the above ULS is characterized by fully developed cracks in the concrete tension zone and yielding of the tensile longitudinal reinforcement accompanied by plastification of the concrete compression zone. For the above stated ultimate failure mode, the critical component of structural response is defined as the force per “unit width” in the tensile longitudinal reinforcement under stage II conditions. For the action of traffic, in particular, the history of the variation of this force  $\mathcal{F}_Q$  is approximated as

$$\mathcal{F}_Q = \left( \mathcal{M}_Q - \mathcal{N}_Q(h/2 - d_1) \right) / (0.9d) + \mathcal{N}_Q \quad (3.1)$$

where,  $\mathcal{M}_Q$  and  $\mathcal{N}_Q$  are the variation histories of the moment and the axial force, respectively, applied at the cross section due to traffic action,  $h$  is the depth of the slab,  $d$  is the effective depth of the slab (distance of the centroid of the tensile reinforcement from the top surface of the slab) and  $d_1$  is the distance of the centroid of the tensile reinforcement from the bottom surface of the slab. Eventually, the action incident effect  $F_Q$  is defined as the maximum of  $\mathcal{F}_Q$  per incident.

It should be emphasized that  $\mathcal{F}_Q$  is not an action effect that is necessarily manifested during the monitoring period or even during the entire life of the structure. In fact the major assumption implied in its definition, the assumption of stage II conditions, is not the case for most reinforced concrete elements during their service life (including the examined slab on the bottom surface of which no cracks due to longitudinal bending can be observed). However, stage II conditions *will*, by definition, be the case at the ULS-STR and at that time  $\mathcal{F}_Q$  *will* be manifested. Hence, the fact that this action effect is not manifested does

not mean that it does not exist as a notional quantity on the value of which the safety of a reinforced concrete element depends.

### 3.3. The sample of the representative action-incident effect

The sample of  $F_Q$ -instances obtained from the above described monitoring campaign is discussed in the following<sup>2</sup>. This sample  $\{f_i, i = 1, \dots, n_{\text{all}}\}$  of  $n_{\text{all}} = 31635$  instances, for brevity  $\{f_i, \text{all}\}$ , is plotted in **Fig. 3.1(a)**. The corresponding sample  $\{m_i, \text{all}\}$  of the principal bending moment action-incident maximum  $M$  is also plotted in **Fig. 3.2(a)** for comparison. Relative frequency histograms of the above samples are plotted in **Fig. 3.1(b)** and **Fig. 3.2(b)** respectively. The index “all” implies that instances from all traffic incident types are included in the sample.

#### 3.3.1. Records included in the sample

These samples were recorded between February the 15<sup>th</sup>, 2013 (day index 1) and September the 12<sup>th</sup>, 2014 (day index 156). During this period, however, there were interruptions of the monitoring which lasted from a few hours to several days. All the instances which occurred on a date of interrupted monitoring are excluded from the sample. This prevents the introduction of bias in the representation of the various traffic incident types within the sample. Such bias could, otherwise, be introduced because of the significant variation through the day of the mean frequency with which each type of traffic incident tends to occur. Day indices, wherever indicated, refer to dates of uninterrupted monitoring.

#### 3.3.2. Macroscopic distinction of incident types

Instances  $f_i$  and  $m_i$  tend to form clusters which in **Fig. 3.1(a)** and **Fig. 3.2(a)** are reflected as zones of instance concentration while in **Fig. 3.1(b)** and **Fig. 3.2(b)** as distinct modes of the histograms. These clusters, which are approximately indicated in both figures by capital letters A to F (either at the end of the zones or on top of the modes), echo approximately the major types of traffic incident: (1) loaded freight trains passing on track 1 (the one under which the measurements are taken), (2a) standard passenger trains on track 1, (2b) lighter suburban trains on track 1, (3) empty freight trains on track 1, (4) loaded freight trains on track 2, (5a) passenger trains on track 2, (5b) lighter suburban trains on track 2 and (6) empty freight trains on track 2.

It is interesting to observe that the above traffic incident types are reflected more distinctively in  $\{m_i, \text{all}\}$  (**Fig. 3.2**) than in  $\{f_i, \text{all}\}$  (**Fig. 3.1**). This may be attributed to the fact that the axial force  $N$ , which contributes to the calculation of  $F$ , according Eq. (3.1), is much more sensitive to variations in the track-structure interaction effect than the bending moment  $M$  and is also affected by small accelerations and decelerations of the vehicles.

#### 3.3.3. Indirect effect of seasonal and daily temperature variations – Representativeness of the sampling period

**Fig. 3.1(a)** and **Fig. 3.2(a)** show also significant variations through time in the statistical characteristics of  $F$  and  $M$ . During the monitoring period, daily average has a generally ascending trend for  $F$  and a less pronounced generally descending trend for  $M$ . These variations may be attributed to variations in the degree of track-structure interaction which, in turn, may be affected by variations of the ambient temperature. In **Fig. 3.1(a)** the values of ambient temperature  $T_i$  recorded at the beginning of each traffic incident are also plotted. The comparison between  $T$  and  $F$  trends provides some support to the above claim or at least does not contradict it. However, the mechanism by which temperature may affect traffic action effects will not be investigated in this work.

The above observations and speculations suggest that the representative action effect does not depend solely on traffic action but also on an *indirect* thermal action. It may, therefore, be considered as the combined output of a primary traffic action process, for which stationarity may be admitted, and of a secondary

---

<sup>2</sup> In the following the subscript Q will be omitted for simplicity.

thermal action process expected to demonstrate daily and seasonal variations (similar observation were made by Treacy for highway bridges [6]).

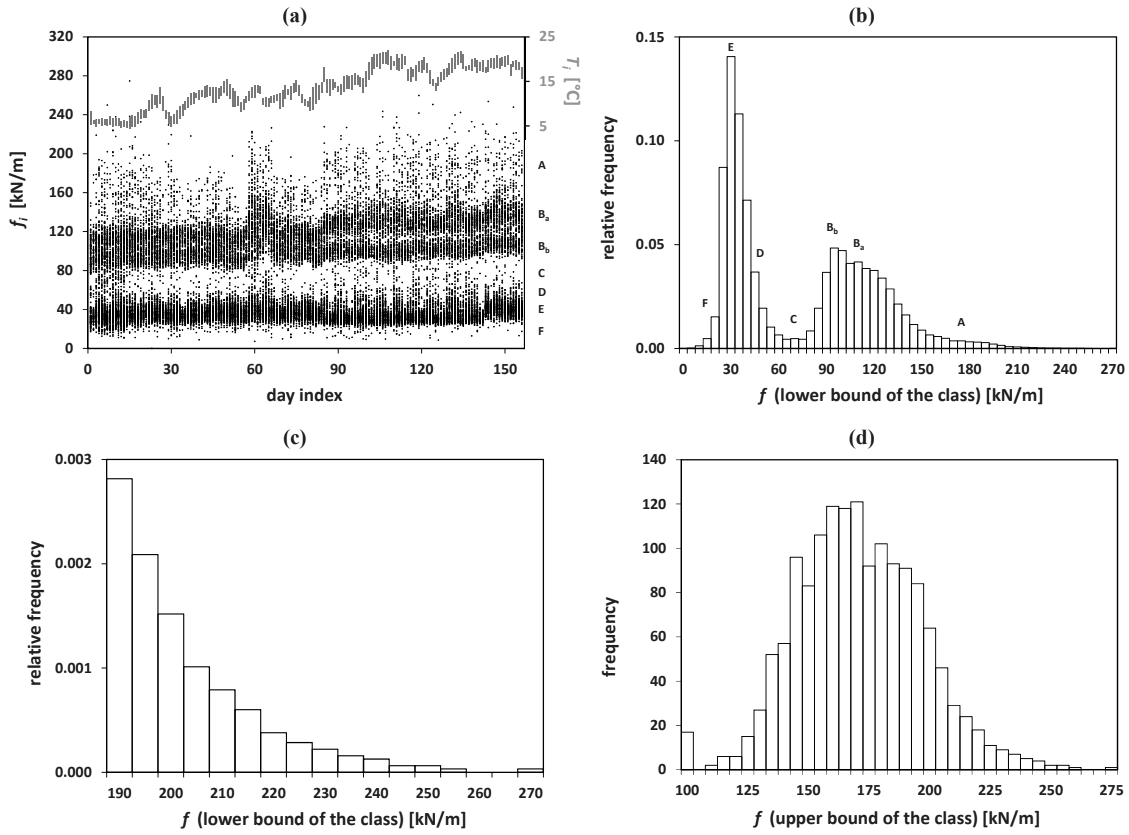


Fig. 3.1: (a) The sample of  $F$  instances with the corresponding ambient temperature. (b) the histogram of  $F$  instances (c) zoom on the extreme value region (d) histogram of the subset of type-1 instances.

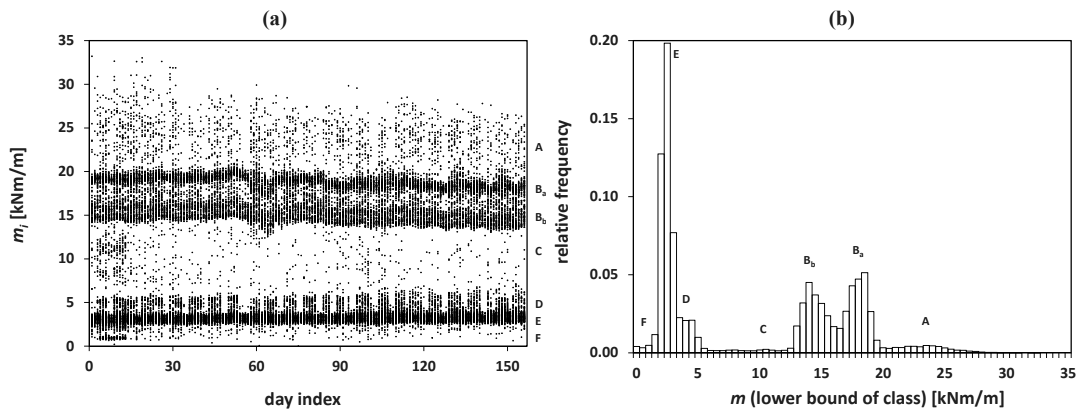


Fig. 3.2: (a) The sample of  $M$  instances (b) the histogram of  $M$  instances.

Each of these cyclic variations has a deterministic and a random component; these components may introduce considerable systematic and random error, respectively, in the statistical estimation of the long-term stochastic characteristics of  $F$ . The way to take into account the effect of each component is discussed in the following:



- Provided that the daily schedule of the various traffic incident types does not *systematically* change in the long term and that the sample is obtained from *full* days of monitoring only, the systematic estimation error due to the deterministic component of the daily temperature variation can be neglected.
- The effect of the random daily temperature variation cannot be separated from the random primary traffic action effect. The combined random estimation error due to these two random components is evaluated statically in Section 4.
- The deterministic component of the seasonal temperature variation requires special considerations in order to ensure that the selection of a particular monitoring period does lead to systematic error of estimation. In particular monitoring periods should be chosen as integer multiples of 1 year. Alternatively, ½ year multiples can be adopted if a symmetry argument is adopted and if the start and end of the period are selected so that warm and cold seasons are equally represented in the monitoring period. In the above sense, the presented samples are expected to be slightly biased since the warm season is somewhat overrepresented. However, since this bias is to the “safe” side, the entire sample will be used for the example application.
- The random error due to the random seasonal variation of the temperature is the most difficult to treat. Its statistical evaluation requires monitoring over several years. Alternatively, engineering judgment seems a more cost-efficient way for taking this error into account in the context of safety verification as discussed in Section 6.

### 3.3.4. Week-day variations in the traffic mixture

As a last note on the qualitative characteristics of the sample it is reported that the vast majority of action incidents related to the passage of loaded freight trains (types 1 and 4) occur during weekdays. This is again more evident in **Fig. 3.2(a)** and especially for freight trains on track 2 (type-4) incidents. By assuming that type-1 incidents can approximately be identified as those resulting to an incident moment greater than 21 kNm (observe the corresponding mode A in **Fig. 3.2(b)**), the estimated average number of loaded freight trains on track 1 per week and per day of the week is presented in **Table 3.1**. Provided that the necessary precautions for avoiding bias in the sample are taken, as already discussed, the above difference between weekdays and weekends does not have any influence on the probabilistic modeling, performed hereafter, since all probabilities are expressed as “per incident” rather than “per day” probabilities. However, for the subsequent safety verification the number of incidents in larger periods of time (e.g. one year) needs to be specified. For that, in the present application, the number of incidents per week presented in **Table 3.1** is used as a basis.

**Table 3.1:** Average number of loaded freight trains on track 1 (type-1 incidents).

Mon	Tue	Wed	Thu	Fri	Sat	Sun	weekly	yearly
10.1	12.8	12.1	11.7	11.9	4.3	1.6	<b>64.5</b>	<b>3363</b>

## 3.4. Probabilistic modeling of the representative action-incident effect

### 3.4.1. Determinant distribution

As suggested by **Fig. 3.1(b)** and **Fig. 3.2(b)**, the traffic action incident effect follows a multimodal distributions that could, in principle, be expressed as a mixture of simple distributions; each simple distribution in a mixture corresponding to a different type of incident. It should be noted that the major types of incidents that are described above (type 1 to 6) are not necessarily the only ones that can, at least in principle, be described; other types, of equal or lower hierarchical order, may be hidden among or within the major types.

Notwithstanding, for the calculation of the very small probabilities of exceedance which are usually required for ULS-STR safety verifications it is only the distribution of the extreme instances of the action incident effect that needs to be modeled (the tail of the full distribution). Probabilistic modeling of action effect extreme values is also required for fatigue verifications when the constant amplitude fatigue limit is taken into account (As it will be shown in the next chapter fatigue limit exceedances are rather rare events and this fact has a beneficial effect on the calculated fatigue reliability). It might be the case that these

extreme instances are the outcome of a single *simple* type of incident, the *determinant* incident type, and that they can consequently be modeled by a single simple distribution of the action incident effect, the *determinant* distribution. This is very desirable since, by reducing the number of parameters that need to be estimated, more accurate extreme instance predictions can be obtained.

The first and most important step in modeling the determinant distribution is the identification and isolation from the original sample of the determinant subset of instances corresponding to the determinant distribution. The method for performing this task depends largely on the characteristics of the original sample. However, two different approaches can be outlined; both of them require some engineering judgment.

### 3.4.2. Identification of the determinant instances and modeling of the determinant distribution—Explicit approach

The explicit approach begins by postulating that the determinant subset coincides with the subset of the sample instances which are the outcome of an *a priori explicitly specified* type of incident; in the present application, for example, incident type-1 as specified above. The formulation of such a postulate requires, of course, some insight into the general phenomenon in which the action belongs, so that types of action incidents can be specified unambiguously. In the present application, for example, some knowledge of the characteristics of the traffic regime, particularly on the typology of the rolling stock is needed. Eventually, the pertinence of the postulate needs to be evaluated and the postulate itself may have to be refined or abandoned.

The identification and isolation of the determinant subset is, in principle, not possible unless additional information is used. For example, instances corresponding to a particular type of train passage may usually be identified by examining the complete signal of each incident which reveals, through its qualitative characteristics, the type of the train and the track on which it moves. This is however a very time consuming task involving a great deal of human judgment. Alternatively, if the extreme (rightmost) mode of the histogram of an action incident effect is sufficiently distinct and can be associated, using engineering judgment, to a specific type of incident, it may be possible to identify these instances approximately (i.e. with a certain number of false positive and false negative identifications) as those exceeding the value corresponding to the lowest point of the histogram valley that separates the rightmost mode from the one at its left. If this is *not* the case for the histogram of the representative action incident effect, as it is *not* for  $F$ , it might be possible to use the histogram of another action effect with more distinct modes. In the present application, for example, it may be argued, by reference to the histogram of bending moment (**Fig. 3.2(b)**), that type-1 incidents can be approximately identified as those resulting in a bending moment larger than 21 kNm/m. The  $F$ -instances corresponding to type-1 incidents can then be easily isolated as a subset  $\{f_j, j = 1, \dots, \tilde{n}_{t1}\}$ , for brevity  $\{\widehat{f}_j, t1\}$ , with  $\tilde{n}_{t1} = 1510$  being the approximate number of these instances in the original sample<sup>3</sup>. The frequency histogram of  $\{f_j, t1\}$ , is presented in **Fig. 3.1(d)** and shows that, in this case, the above used approximate identification method preforms rather well. The small number of instances below 100 kN/m in **Fig. 3.1(d)** is clearly due to false positive identifications.

It is now examined whether, in the present application, the initial postulate is correct, that is whether the distribution of  $\{f_j, t1\}$  can be modeled by a single simple distribution of  $F$ . If this is the case, it is expected that this simple distribution will belong to the family of the Generalized Extreme Value (GEV) distribution; its CDF will be given by ([10])

$$G(f; \mu, \sigma, \xi) = \exp \left[ - \left[ 1 + \xi \left( \frac{f - \mu}{\sigma} \right) \right]^{-\frac{1}{\xi}} \right], \quad \xi \neq 0 \quad (3.2a)$$

$$G(f; \mu, \sigma, 0) = \exp \left[ - \exp \left[ - \left( \frac{f - \mu}{\sigma} \right) \right] \right], \quad \xi = 0 \quad (3.2b)$$

with  $\mu$ ,  $\sigma$  and  $\xi$  being the parameters of the distribution.

---

<sup>3</sup> The tilt, which implies *approximation* of the subset, is omitted in the following for simplicity and generality.

The estimated parameters of this distribution are calculated from the sample  $\{f_j, t1\}$  by means of the maximum likelihood method [10] ( $\hat{\mu} = 158.46 \text{ kN}$ ,  $\hat{\sigma} = 26.18 \text{ kN}$ ,  $\hat{\xi} = -0.21$ ). Accordingly, the theoretically estimated value  $\hat{f}_{p_{t1}}$  of the  $F$ -level which is exceeded with probability  $p_{t1}$ , conditional on the occurrence of a type-1 incident, is calculated as

$$\hat{f}_{p_{t1}} = G^{-1}\left((1 - p_{t1}); \hat{\mu}, \hat{\sigma}, \hat{\xi}\right) \quad (3.3)$$

On the other hand, the empirical CDF of  $F$  as observed in  $\{f_j, t1\}$  is expressed as

$$E(f_j) = 1 - p_{t1,j} = j/(n_{t1} + 1) \quad (3.4)$$

where  $j$  is the rank of the instance when  $f_j$  are sorted in ascending order. Hence the empirical equivalent of Eq. (3.3) is symbolically expressed as

$$f_j = E^{-1}(1 - p_{t1,j}) \quad (3.5)$$

The estimated theoretical distribution and the empirical distribution, as expressed by Eq. (3.3) and Eq. (3.5) respectively, are compared in **Fig. 3.3(a)**, where the double negative logarithm:  $-\ln(-\ln(1 - p_{t1}))$ , is plotted on the horizontal axis instead of  $p_{t1}$  itself. This scaling has the advantage to reveal qualitatively the value of  $\xi$  and accordingly the particular sub-family of the GEV distribution. Hence, on such a graph Gumbel distributions with  $\xi = 0$  are plotted as straight lines while Fréchet and Weibull distributions with  $\xi > 0$  and  $\xi < 0$  are plotted as convex and concave curves respectively [10]. The comparison shows that the assumption of a single distribution for the entire population of  $\{f_j, t1\}$  leads to unsatisfactory modeling of the extreme instances of  $F$ . Hence, the postulate that  $\{f_j, t1\}$  is the determinant subset is not accurate.

In fact, a closer examination of **Fig. 3.3(a)** shows that a bilinear curve fits better the points of the empirical distribution. This suggests that  $\{f_j, t1\}$  could probably be modeled more realistically as a mixture of two Gumbel distributions, each of them corresponding to a subtype of type-1 incidents. This claim is also supported by a closer examination of the histogram in **Fig. 3.1(d)** where two modes might be distinguished.

Pursuing with the explicit approach would, therefore, require a more precise specification of the determinant type of action incident, using additional insight into the rolling stock typology, followed by an identification of the critical instances, for which the above used approximate method would not be applicable any more. These difficulties lead us to the implicit approach.

#### 3.4.3. Identification of the determinant instances and modeling of the determinant distribution—Implicit approach

In the implicit approach it is accepted that the critical type of incident cannot be specified. Hence, it is attempted to detect a threshold such that the distribution of the sample instances exceeding the threshold can be *practically* modeled by a single simple distribution. In this case the determinant distribution is necessarily a threshold exceedance distribution and the determinant subset is simply defined as the subset of the threshold exceeding instances in the original sample, without any assumption on their origin being involved in the definition.

However, for the detection of the threshold, a guess on the family of the determinant distribution is required. As in the explicit approach, it is expected that the instances produced by the (not any more explicitly specified) critical incident follow a GEV distribution. Hence, the plot of  $F$ -instances versus scaled empirical probability of exceedance  $-\ln(-\ln(1 - p))$  can be used again as a tool for the detection of an appropriate threshold. This plot has been done already in **Fig. 3.3(a)** for  $\{f_j, t1\}$  (which is not any more assumed to coincide with the determinant subset) and is also done in **Fig. 3.3(b)** for the original sample  $\{f_i, \text{all}\}$ . For the later plot the empirical CDF of  $F$  is given by  $E(f_i) = i/(n_{\text{all}} + 1)$ , resulting in  $f_i = E^{-1}(1 - p_{\text{all},i})$ , where  $p_{\text{all}}$  is conditional to the occurrence of an incident of any type. On both graphs a straight line fits very well the points greater than 190kN while for points lower than 190 kN the plot tends

to deviate from this straight line. A threshold of 190 kN can then be defined on both graphs. The determinant subset is expressed as  $\{f_k, k = 1, \dots, n_{th}\}$ , for brevity  $\{f_k, th\}$ , with  $n_{th}$  being the number of threshold exceedances in either  $\{f_j, t1\}$  or  $\{f_i, all\}$  ( $n_{th} = 307$  or  $322$  respectively). Of course, the detection of the threshold requires some engineering judgment and is much more evident in the case of a Gumbel distribution.

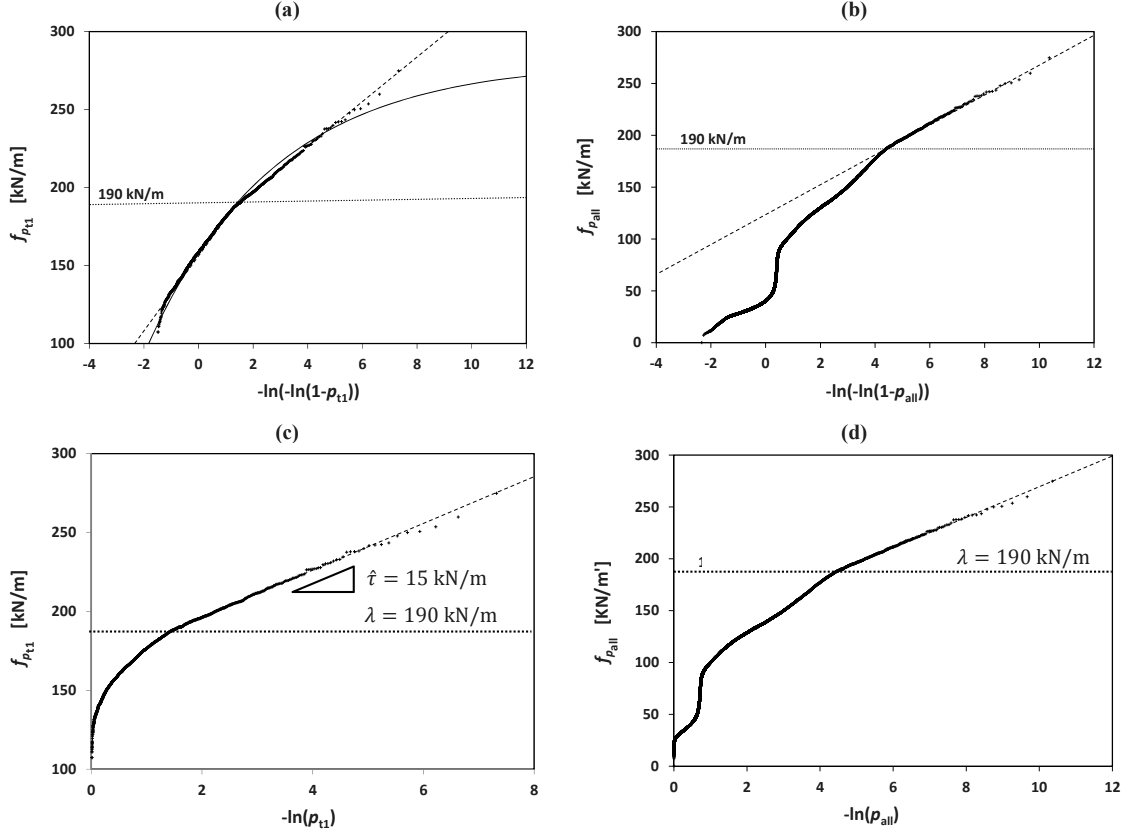


**Fig. 3.3:** (a) Comparison of empirical (dots) and fitted (continuous curve) GEV distribution for type-1 incidents and graphical detection of the threshold as the knee point of a bilinear approximation (dashed lines) using the type-1 sample. (b) Graphical detection of the threshold using the original sample. (c) Comparison of empirical and fitted shifted exponential distribution for type-1 incidents and graphical detection of the threshold as the knee point of a bilinear approximation using the type-1 sample. (d) Same as in (c) but for the original sample.

In fact, the implicit approach can be pursued either from the beginning or from the point where the explicit approach is abandoned; i.e. it can be applied either using the original sample or on the subset identified through the explicit approach, assuming that the later contains the determinant instances. Theoretically, the specified threshold and the number of identified exceedances will also be the same in both cases independently of the total number of instances in the original sample. The only thing that changes is the type of incident conditional on the occurrence of which the probability of exceedance is expressed.

The threshold exceedances of a variable that follows a GVE follow a Generalized Pareto (GP) distribution the CDF of which is given by ([10])

$$G(x; \lambda, \tau, \xi) = 1 - \left[ 1 + \xi \left( \frac{x-\lambda}{\tau} \right) \right]^{-\frac{1}{\xi}} ; \quad \xi \neq 0 \quad (3.6a)$$

$$G(x; \lambda, \tau, 0) = 1 - \exp \left[ - \left( \frac{x-\lambda}{\tau} \right) \right] ; \quad \xi = 0 \quad (3.6b)$$

The second case coincides, in fact, with a shifted exponential distribution. The parameters of a GP distribution are related to those of its parent GEV distribution by [10]

$$\xi = (\tau - \sigma)/(\lambda - \mu) \quad ; \quad \xi \neq 0$$

$$\tau = \sigma \quad ; \quad \xi = 0$$

An estimation of the  $F$ -level  $\hat{f}_{p_{th}} > \lambda$  with exceedance probability  $p_{th}$ , conditional on the occurrence of an incident resulting in  $f > \lambda$ , is calculated as

$$\hat{f}_{p_{th}} = G^{-1}\left((1 - p_{th}); \lambda, \hat{\tau}, \hat{\xi}\right) \quad (3.7)$$

which in the case of  $\xi = 0$  takes the form

$$\hat{f}_{p_{th}} = \lambda + \hat{\tau} \ln(1/p_{th}) \quad (3.8)$$

For the present application, the *combined* use of the explicit and implicit approach seems more appropriate since it provides the maximum amount of information that can be extracted from the monitoring data. It is, therefore, more meaningful to express Eq. (3.8) using a probability  $p_{t1}$ , expressed per incident of type-1. In order to do this one more parameter  $\zeta$  is introduced in the distribution which expresses the probability of a threshold exceedance given the occurrence of a type-1 incident. This parameter can be estimated as  $\hat{\zeta}_{t1} = n_{th}/n_{t1}$ . Thus, Eq. (3.8) can be expressed in the following alternative formulation

$$\hat{f}_{p_{t1}} = \lambda + \hat{\tau} \ln(\hat{\zeta}_{t1}/p_{t1}) \quad (3.9)$$

By using again the method of maximum likelihood the estimated parameter  $\hat{\tau}$  of the shifted exponential distribution of Eq. (3.9) is calculated as

$$\hat{\tau} = \left[ \sum_{k=1}^{n_{th}} (f_k - \lambda) \right] / n_{th} \quad (3.10)$$

The comparison of the theoretical distribution to the obtained monitoring data is shown in **Fig. 3.3(c, d)**. The exponential distribution is often parametrized using  $\rho = 1/\tau$ , in which case  $\hat{\rho} = 1/\hat{\tau}$ . The estimated parameters are summarized in **Table 3.2**.

Additionally, it might be desired to calculate an upper confidence bound  ${}^a\hat{f}_{p_{t1}}$  such that, at confidence level  $(1 - a)$ ,  $\hat{f}_{p_{t1}}$  is less than  ${}^a\hat{f}_{p_{t1}}$ . This confidence bound can be approximated as [10]

$${}^a\hat{f}_{p_{t1}} \approx \hat{f}_{p_{t1}} + \kappa_a \sqrt{\text{Var}(\hat{f}_{p_{t1}})} \quad (3.11)$$

where

$$\kappa_a = \Phi^{-1}(1 - a) \quad (3.12)$$

$\Phi^{-1}$  is the inverse of the CDF of the standard normal distribution and  $\text{Var}(\hat{f}_{p_{t1}})$  is calculated using the  $\Delta$ -method [10] as

$$\text{Var}(\hat{f}_{p_{t1}}) = \frac{\hat{\tau}^2}{n_{th}} \left( \left( \ln(\hat{\zeta}_{t1}/p_{t1}) \right)^2 + (1 - \hat{\zeta}_{t1}) \right) \quad (3.13)$$

For large values of  $\hat{\zeta}_{t1}/p_{t1}$ , ( $>100$ ), as it is usually the case, Eq. (3.13) can be further simplified by neglecting the term  $(1 - \hat{\zeta}_{t1})$  and Eq. (3.11) becomes

$${}^a\hat{f}_{p_{t1}} \approx \lambda + (1 + \kappa_a/\sqrt{n_{th}})\hat{\tau} \ln(\hat{\zeta}_{t1}/p_{t1}) \quad (3.14)$$

**Table 3.2:** Statistical properties of the extreme value distribution of  $F$ .

$n_{th}$	$\lambda$	$\hat{\zeta}_{t1}$	$\hat{\tau}$
307	190.0 kN	0.20	15.0 kN

### 3.5. Safety verification format

#### 3.5.1. Safety requirement in terms of examination<sup>4</sup> values

The implementation of monitoring based action effect probabilistic models in ULS-STR safety verifications requires the development of an appropriate safety verification format. The format proposed in this work is based on the concepts of EN1990 Annex C [11] and uses the semi-probabilistic (Level I) reliability method. The classical statistical approach is adopted mainly because it leads to a more straightforward examination procedure. In Section 7 the question of validation and calibration of the format within the context of Bayesian statistics is addressed

The objective here is to calculate an examination value of the total incident effect  $E_e$  and to compare it with the corresponding examination value of the resistance  $R_e$  in order to ensure that

$$E_e < R_e \quad (3.15)$$

Since the combination is performed at the action effect-level,  $E_e$  can be expressed as the sum of the partial examination values of the leading (Q1) and the accompanying variable (Qi) and permanent (G) action incident effects.

$$E_{Q1,e} + E_{Qi,e} + E_{G,e} < R_e \quad (3.16)$$

This separation of examination values is not in accordance with EN1990 where in principle a single design value of the action effect is assumed. However, in the case of monitoring-based verifications, this separation is in generally necessary since most often the monitoring data correspond only to the effect of a single action (in the present application, for instance, the effect of the permanent load and of the direct temperature actions is not included in the data). In this paper it is assumed that at least the examination value of the leading incident effect is calculated semi-probabilistically using monitoring data. The examination value of the resistance should also be calculated semi-probabilistically while the examination values of the accompanying action effects can be calculated using the partial factor method.

#### 3.5.2. Distinction of uncertainty sources

As a first step in the development of a monitoring-based safety verification format, the various origins of uncertainty related to the acquisition and the statistical interpretation of monitoring data should be identified. It is pertinent to distinguish between:

a) an aleatoric uncertainty originating from: (i) the inherent imprecision of the monitoring method (including signal processing) and (ii) the inherent randomness of the action effect extreme values, modeled by a certain probability distribution  
and

b) an epistemic uncertainty (systematic and random error) originating from: (i) eventual imperfections in the implementation of the monitoring scheme (systematic error of measurements), (ii) idealizations and simplifications in structural and cross-section models used for the calculation of the representative action effect from the measured deformations/displacements, e.g. plane section hypothesis, assumptions involved in Eq. (3.1) etc. (systematic error in structural modeling), (iii) limited number of sample instances (random sampling error), (iv) incomplete phenomenological knowledge for the formulation or the selection of a probability distribution family suitable for extrapolation (systematic error in probabilistic modeling).

In the following step, the risk corresponding to each of the above identified, origins of uncertainty should be either accepted or controlled or mitigated by appropriate provisions in the safety verification format.

<sup>4</sup> The term “examination value”, as introduced in the Swiss standard for existing structures [12], is adopted here. This term corresponds to the term “design value” used for new structures.

### 3.5.3. Treatment of the uncertainty in the measurements and primary-data post-processing

For the inherent imprecision of the monitoring method (a.i) no specific measures are foreseen in the safety format. The corresponding risk is accepted. As a matter of fact these imprecisions cannot be separated from the inherent randomness of the action incident effect. Eventually, it has to be accepted that, excluding systematic error, the obtained signal (after possible processing) reflects the transient realization of a random phenomenon.

On the other hand, the risk related to imperfections in the application of the monitoring method (b.i) should be mitigated by applying an ignorance factor  $\gamma_{\text{MON}}$  on the values of the sample. This factor depends on the monitoring scheme and should be defined on the basis of previous experience and engineering judgment. More specifically, in the case of the proposed monitoring scheme, the data set may be systematically affected by: (i) inaccuracies in the positioning of the measuring devices on the critical point of the structure, (ii) imperfect calibration of the measuring devices on the field and (iii) systematically ignoring the effect of higher frequencies as a result of the applied signal acquisition and processing procedure.

Additionally, an ignorance factor  $\gamma_{\text{STR}}$  should also be applied on values of the original sample in order to cover uncertainty related to the used structural and cross-section models (b.ii) (Very often a cross-section model, e.g. Eq. (3.1), is considered as a resistance model. In this work, however, a cross-section model is used in order to calculate what has been defined as the representative action effect, i.e. the force in the tensile reinforcement, so it should naturally be considered as an action effect model).

It should be noted that the above ignorance factors are not correction factors in the strict sense, i.e. they do not reflect an *expected* deviation of the sample values from the reality. Correction factors are *known deterministic* (albeit *ad hoc*) parameters which are constituent part of a measurement method or a structural model. Hence, any such correction should already be included in the sample values. The above ignorance factors cover the error in the estimation of the required correction, i.e. the ratio between the applied (expected) correction and the actually required correction. In the classical statistical approach, this ratio has a *deterministic* but *unknown* value (this is why the term “ignorance” is used). Hence, for the moment, these factors should be defined deterministically by using engineering judgment.

In many cases, as a matter of fact, it can be assumed that the above error can be largely compensated at the ULS-STR by the redundancy that the structural elements usually dispose [14]. In these cases, admitting  $\gamma_{\text{MON}} = \gamma_{\text{STR}} = 1$  is an acceptable decision. This is definitely true for the present application.

### 3.5.4. Treatment of the uncertainty in the leading action incident effect extreme value and its probabilistic modeling

The uncertainty related to the inherent randomness of the action incident effect (a.ii) should be controlled by considering the action-incident effect level with probability of being exceeded during the remaining service life of the structure equal to a target probability  $p_{\text{SL}}^*$ . It is noted that this probability does not include any epistemic uncertainty (which in the classical statistical approach cannot be described by probability). It is in fact a probability “given” that the monitoring data are accurate, free from sampling error and absolutely representative of the traffic loading conditions during the future service life of the structure. This approach deviates somehow from the standard approach of JCSS Probabilistic Model Code [15] in which an exclusive Bayesian interpretation of probability is adopted.

In the present application, knowing that the determinant incident type is a subtype of incident type-1, makes it possible to formulate future traffic scenarios solely on the basis of the total number of loaded freight trains  $N_{\text{t1}}$  expected to pass on the structure during its remaining service life. The target probability of exceedance of a given  $F$ -level in a single type-1 incident,  $p_{\text{t1}}^*$ , given the target probability of exceedance of this level in  $N_{\text{t1}}$  incidents is calculated as<sup>5</sup>

$$p^* = 1 - (1 - p_{\text{N}}^*)^{(1/N)} \quad (3.17)$$

Obviously  $p_{\text{N}}^*$  is equal to  $p_{\text{SL}}^*$  and can be calculated from a target reliability index  $\beta^*$  as

---

<sup>5</sup> From Eq. (3.17) till the end of the section the index “t1” is omitted for convenience and generality.

$$p_N^* = p_{SL}^* = \Phi(\alpha_E \beta^*) \quad (3.18)$$

where  $\Phi$  is the CDF of the standard normal distribution and  $\alpha_E$  is the value of the First Order Reliability Method (FORM) sensitivity factor for the leading action incident effect Q1. In the context of the semi-probabilistic method,  $\alpha_E$  takes predetermined “conservative” values which depend only “qualitatively” on the probability distributions of the resistance. In fact, the value of  $\alpha_E$  depends only on the ratio between the standard deviation of the action effect  $\sigma_E$  and that of the resistance  $\sigma_R$  as summarized in **Table 3.3**.

**Table 3.3.** FORM sensitivity factors according to the semi-probabilistic method.

$\sigma_E/\sigma_R$	<0.16	0.16 – 7.6	>7.6
$\alpha_E$	-0.4	-0.7	-1.0
$\alpha_R$	1.0	0.8	0.4

This approach simplifies the formulation of the safety format since the examination value of each action-effect can be expressed independently from the examination value of the resistance. However, a “qualitative” dependence remains in the selection among the predetermined values of  $\alpha_E$  and the adoption of the values of the middle column of **Table 3.3** are a safe option in practically all cases.

In symbolic form, this action-incident effect level corresponding to  $p^*$  can be expressed as

$$\hat{E}_{Q1,p^*} = \hat{G}_{Q1}^{-1} \left( (1 - p^*); \{ \gamma_{MON,Q1} \gamma_{STR,Q1} e_i \} \right) \quad (3.19)$$

Where  $\hat{G}_{Q1}^{-1}$  is the inverse CDF of the leading incident effect Q1 and  $\{ \gamma_{MON,Q1} \gamma_{STR,Q1} e_i \}$  is the factored sample of  $E$ -instances and is included as a parameter in the above expression in order to emphasize that the parameters of  $\hat{G}_{Q1}^{-1}$  depend on this sample.

The risk originating from random sampling error (b.iii) is mitigated by prescribing a confidence level  $(1 - a)$  and considering the upper bound  ${}^a \hat{E}_{\bar{p}_{inc}}$  of the corresponding one sided confidence interval. This can be approximated as [10]

$${}^a \hat{E}_{Q1,p^*} \approx \hat{E}_{Q1,p^*} + \kappa_a \sqrt{\text{Var}(\hat{E}_{Q1,p^*})} \quad (3.20)$$

Finally, in order to control the uncertainty due to systematic error in probabilistic modeling, an ignorance safety factor  $\gamma_{PR,Q1}$  is introduced. This factor covers also the error due to the indirect effect of climatic temperature variation and should be specified on the basis of engineering judgment. Thus the examination value of the action incident effect is finally expressed as

$$E_{Q1,e} = \gamma_{PR,Q1} {}^a \hat{E}_{Q1,p^*} \quad (3.21)$$

In this format, which follows the classical statistical approach, three different types of reliability requirement are prescribed corresponding to the three types of uncertainty: A target failure probability (in the form of a target reliability index) is prescribed for controlling the risk due to the inherent randomness of the action incident effect, a confidence level is prescribed for mitigating the risk due to random sampling error and deterministic ignorance factors are prescribed for mitigating the risk from systematic error of all kinds.

### 3.5.5. Examination value of resistance and accompanying action incident effects

As it is discussed in Section 3.7 the examination values of the resistance and accompanying action effects can in most cases be calculated by the partial factor method. A semi-probabilistic calculation is however always possible. For example, following again the principles of [11] the examination value of resistance can be calculated as



$$R_e = G_R^{-1}(\Phi(\alpha_R \beta_{inc}); X_i, d_i) / (\gamma_{STR,R} \gamma_{PR,R}) \quad (3.22)$$

Where  $\gamma_{STR,R}$  and  $\gamma_{PR,R}$  are ignorance factors covering epistemic uncertainty in the resistance mechanical model (if such model is used) and geometric data and the resistance probability distribution respectively,  $G_R^{-1}$  is the inverse CDF of resistance,  $\alpha_R$  is the value of the First Order Reliability Method (FORM) sensitivity factor for resistance and finally  $X_i$  and  $d_i$  are the parameters of  $G_R$  which are related to material properties and geometric data respectively. These parameters are assumed to have known deterministic values.

### 3.5.6. Application of the safety verification format in the present case

The first step in calculating the examination values of the leading action incident effect and the resistance is the calculation of the ratio of the standard deviations of the leading action incident effect and the resistance  $\sigma_E/\sigma_R$  so that the appropriate sensitivity factors can be selected from **Table 3.3**. Since the threshold exceedances of the action incident have been shown to follow a GP distribution the underlying distribution is a Gumbel distribution with  $\sigma = \tau$ . Hence the standard deviation of the leading action incident effect can be calculated as [16]

$$\sigma_E = \tau(\pi/\sqrt{6}) \quad (3.23)$$

The statistical variability of the yield strength of steel reinforcement is usually described in standards by its mean yield stress  $f_{ym}$  defined as the value corresponding to a certain fractile  $c$ . Assuming that the yield stress follows a normal distribution and that the variation of its cross sectional area  $A_s$  is negligible, it is possible to calculate the standard deviation of the yield force as

$$\sigma_R = A_s(f_{ym} - f_{yk})/\kappa_c \quad (3.24)$$

where

$$\kappa_c = \Phi^{-1}(1 - c) \quad (3.25)$$

For the present application, the values  $f_{ym} = 550$  kPa and  $f_{yk} = 450$  kPa (corresponding to a fractile value  $c = 5\%$ ) are obtained from Swiss standard for the examination of existing R/C structures [13] for the steel class prescribed on the construction documents (class III used in Switzerland around year 1975, time of the construction of the underpass).

In the particular case where the tail of the distribution can be described with a shifted exponential distribution, Eq. (3.21) takes the following specific form

$$F_{Q1,e} \cong \gamma_{IGN} \left( \lambda + \hat{\tau} \ln(\hat{\xi}_{t1}/p^*) (1 + \kappa_a/\sqrt{n_{th}}) \right) \quad (3.26)$$

where Eq. (3.14) has been used, while  $\hat{\tau}$  is calculated from Eq. (3.10),  $p^*$  from Eq. (3.17, 3.18),  $\kappa_a$  from Eq. (3.12) and  $\gamma_{IGN} = \gamma_{STR,Q1} \gamma_{PR,Q1} \gamma_{MON}$  is a global ignorance factor. The adopted values for the reliability parameters involved in Eq. (3.26) are summarized in **Table 3.4**. At this stage, the confidence interval and the partial factors are chosen on the basis of engineering judgment. In Section 7 the suitability of the adopted values for the present case is investigated in the context of a Bayesian interpretation of probability.

For the normally distributed resistance, Eq. (3.21) takes the following specific form

$$F_{R,e} = A_s(f_{ym} - \beta(f_{ym} - f_{yk})/\kappa_c) / (\gamma_{STR,R} \gamma_{PR,R}) \quad (3.27)$$

The only accompanying incident effect that is considered is the permanent effect of self-weight. Its examination value is calculated by using a partial factor equal to 1.2 [16]. The effect of other variable actions is considered insignificant (in particular, for the case of thermally imposed strains this is true because the structure is, theoretically statically determined).

The calculations of Eq. (3.26, 3.27) and the selected values of the FORM sensitivity factors are summarized in line 1 of **Table 3.5** where  $F_{Q1,e}$  is calculated equal to 467 kN. Note, however, that for the steel

class considered here the calculated standard deviation of steel resistance seems to be excessive by modern standards. If, for instance, a modern steel class is considered (B500) (Table 3.5 – line 2) the calculated examination value is 520 kN. (The increased examination value for the action effect is of course compensated by a decreased examination value for the resistance.) For comparison, the examination value is also calculated using: (a) the axle load model prescribed by the Swiss standards [12] for the *observed* conditions of exploitation of this particular line segment (line class D4: 2\*225 kN augmented by 10% to account for inappropriate loading and spaced at 1.80 m) (b) a dynamic amplification factor equal 1.49, corresponding according to [12] to the maximum observed speed of the freight trains on the bridge (80km/h), (c) a partial factor equal to 1.45 for the train load as the leading action and (d) a finite element model with detailed distribution of the load through rail, sleepers and ballast. This calculation results in  $F_{Q1,e}=498$  kN. This value is very close (within 5%) to the value calculated above from monitoring data.

The above example reveals also that in the context of the safety verification of existing structures the partial factor method should be used with much more caution than in the case of design of new structures. Indeed, in the process of updating the characteristic values of either the leading action effect or the resistance, the various *case specific* methods that are employed for this purpose (e.g. monitoring for the action effect, investigation of the literature or testing for the resistance) may involve uncertainties (standard deviations), accompanying the specified characteristic values, which differ substantially from the “standard” uncertainties that have been considered for the calibration of the partial factors. Additionally, the ratio of the standard deviations of the leading action effect and the resistance may also fall outside its normally assumed range, leading, in the context of FORM calculation, to sensitivity factors that are not covered by the partial factors. These differences may in some cases lead to overestimation of the reliability. Given the above considerations it is suggested that, in the context of monitoring based verifications at least the examination value of the leading action-incident effect *and* of the resistance be calculated using the semi-probabilistic method.

Table 3.4. Prescribed values of the various reliability parameters.

$\beta$	$N_{t1}$	$\alpha$	$\gamma_{MON}$	$\gamma_{STR,Q1}$	$\gamma_{PR,Q1}$	$\gamma_{STR,R}$	$\gamma_{PR,R}$
3.8	336300	0.01	1.00	1.00	1.10	1.00	1.00

Table 3.5. Calculation of the examination values of action effect and resistance.

	$f_{ym}$ [MPa]	$f_{yk}$	$A_s$ [mm <sup>2</sup> ]	$\tau$	$\sigma_E$ [MPa]	$\sigma_R$ [MPa]	$\frac{\sigma_E}{\sigma_R}$	$\alpha_E$	$\alpha_R$	$F_{Q1,d}$ [kN]	$F_{G,d}$ [kN]	$F_{R,d}$ [kN]
1	550	450	3171	15	19	192	0.10	-0.4	1.0	467	104	841
2	550	500	3171	15	19	98	0.20	-0.7	0.8	520	109	1382

### 3.6. Efficiency of the proposed format in a Bayesian probability context

The weakness of the classical statistical approach is that it does not allow for a consistent prescription of the required level of confidence and of the ignorance factors. This problem is bypassed within the Bayesian approach, at the cost of additional mathematical complexity, by considering the parameters of the probability distribution and the ignorance factors as random variables.

#### 3.6.1. Including the random statistical error in the probability of exceedance

In a first step, the uncertainty from the inherent variability of the action incident effect can be combined to the random statistical error resulting in a “combined” probability of exceedance [16]

$$p(E) = 1 - \int_{\Theta} G_E(E|\theta)g_{\theta}(\theta) d\theta \quad (3.28)$$

where  $G_E(E|\theta)$  is the CDF of E, now explicitly stated as conditional to the values of the vector of its parameters  $\theta \in \Theta$  and  $g_{\theta}(\theta)$  is the PDF of  $\theta$ .

Ideally, for the  ${}^a\hat{E}_{Q1,p^*}$  calculated by Eq. (3.20) for the prescribed confidence level,  $p({}^a\hat{E}_{Q1,p^*})$  has to be lower but as close as possible to  $p^*$ . Hence Eq. (3.28) provides a way for calibrating the confidence level requirement over a number of cases.

In particular, for the case where the extreme value distribution of  $F$  can be expressed as a (shifted) exponential distribution and using for mathematical convenience the parametrization  $\rho = 1/\tau$  with the additional assumption that  $\rho$  has a gamma distribution with  $E(\rho) = \hat{\rho} = 1/\hat{\tau}$  and  $\text{Var}(\rho) = \hat{\rho}^2/n_{\text{th}}$ , Eq. (3.28) takes, after some manipulation, the following simple form

$$p(E) = \left(1 + (E - \lambda)/(n_{\text{th}}\hat{\tau})\right)^{-n_{\text{th}}} \quad (3.29)$$

In the present case, considering the actually placed steel class III (**Table 3.5** – line 1), the target probability according to Eq. (3.17, 3.18) is  $p^* = 1 - (1 - \Phi(-0.4\beta))^{1/N} = 1.97 * 10^{-7}$ , while  $p({}^a\hat{E}_{Q1,p^*}) = p(467/1.1\text{kN}) = 2.38 * 10^{-7}$  which is only slightly larger than the target probability. Similarly, for the case of steel class B500 (**Table 3.5** – line 2),  $p^* = 1 - (1 - \Phi(-0.7\beta))^{1/N} = 1.16 * 10^{-8}$ , while  $p({}^a\hat{E}_{Q1,p^*}) = p(520/1.1\text{kN}) = 1.14 * 10^{-9}$  which is slightly less than the target probability.

These results suggest that the adoption of a confidence level  $(1 - \alpha) = 99\%$  is reasonable with respect to the target reliability within the Bayesian context.

### 3.6.2. Including the systematic estimation error in the probability of exceedance

In a second step, a probability of exceedance  $\mathbb{p}$  including also the uncertainty covered by the factors  $\gamma_{\text{STR},Q1}\gamma_{\text{PR},Q1}\gamma_{\text{MON}}$  can also be defined by assuming appropriate probability distributions for these factors. One possibility is to assume uniform distributions centered on unity and with a certain range selected by engineering judgment. For the present application only the variability of  $\gamma_{\text{PR},Q1}$  is considered. In particular  $\gamma_{\text{PR},Q1}$  is assumed to follow a uniform distribution  $U(\gamma^-, \gamma^+) = U(0.85, 1.15)$ . The probability of exceedance per incident combining inherent uncertainty as well as random and systematic estimation error is calculated as<sup>6</sup>

$$\mathbb{p}(E) = \frac{1}{\gamma^+ - \gamma^-} \int_{\gamma^-}^{\gamma^+} \left(1 + \hat{\rho} \frac{(E/\gamma - \hat{\lambda})}{n_{\text{th}}}\right)^{-n_{\text{th}}} d\gamma \quad (3.30)$$

Again, a successful selection of  $\gamma_{\text{PR},Q1}$  for use in Eq. (3.21) would lead to the calculation of a  $E_{Q1,e}$  that when substituted in the place of  $E$  in Eq. (3.30) gives a combined exceedance probability that is smaller but close to  $p^*$ .

For the same two cases considered above:  $\mathbb{p}(E_{Q1,e}) = \mathbb{p}(467\text{kN}) = 1.06 * 10^{-7} < p^* = 1.97 * 10^{-7}$  and  $\mathbb{p}(E_{Q1,e}) = \mathbb{p}(520\text{kN}) = 0.52 * 10^{-8} < p^* = 1.16 * 10^{-8}$ . Both these values are less than but quite close to  $p^*$  which suggests that the adoption of a factor  $\gamma_{\text{PR},Q1} = 1.1$  is also a rational choice in the present case. Of course, engineering judgment is again involved in the selection of the boundaries  $\gamma^+$  and  $\gamma^-$ ; however this is done here in a lesser degree than for the direct selection of the ignorance factor value.

## 3.7. Conclusions

- Simplicity and efficiency in the monitoring based probabilistic modeling of railway traffic action-effects can be achieved if: (a) the entire history of the action effect variations is subdivided into traffic action incidents (train passages) and the statistical sample of action effect instances is composed as a set of incident maxima (as opposed, for instance, to daily maxima or peaks over threshold samples) and (b) modeling is based only on the determinant incidents and the corresponding subset of action incident effect instances which have to be identified and isolated from the original sample beforehand.
- In the particular case examined here, the distribution of the determinant action incident effect instances can be modeled excellently by a shifted exponential distribution—this is indeed one of the simplest analytical distributions that exist.
- The duration of the monitoring period, in terms of the number of recorded determinant incidents, can be formally taken into account into the examination value of the action effect by means of a confidence upper bound.

<sup>6</sup> Calculations performed with the aid of Wolfram *Mathematica*.

- On the other hand the annual variation of temperature has a significant indirect effect on the traffic action effect. It is therefore recommended that the minimum duration of monitoring should be taken equal to 1 year (or 6 months equally distributed between cold and warm seasons), independently of the number of recorded determinant incidents, so as to avoid bias in the sample.

### 3.8. References

- [1] Frangopol DM, Strauss A, Kim S. Bridge reliability assessment based on monitoring. 2008;13:258-270.
- [2] Frangopol DM, Strauss A, Kim S. Use of monitoring extreme data for the performance prediction of structures: General approach. Eng Struct. 2008;30(12):3644-3653.
- [3] Strauss A., Frangopol DM, Kim S. Use of monitoring extreme data for the performance prediction of structures: Bayesian updating. Eng Struct. 2008;30(12):3654-3666.
- [4] Catbas FN, Susoy M, Frangopol DM. Structural health monitoring and reliability estimation: Long span truss bridge application with environmental monitoring data. Engng Struct. 2008;30(12):2347-2359.
- [5] Rodrigues JFS, Casas JR, Almeida PAO. Fatigue-safety assessment of reinforced concrete (RC) bridges: application to the Brazilian highway network. Struct Infrastructure Eng. 2011;9(6):601-616.
- [6] Treacy MA. The use of monitored data in the verification of structural and fatigue safety of existing post-tensioned concrete highway bridges [dissertation]. Lausanne: Ecole Polytechnique Fédérale de Lausanne; 2014.
- [7] Treacy MA, Brühwiler E, Caprani CC. Monitoring of traffic action local effects in highway bridge deck slabs and the influence of measurement duration on extreme value estimates. Struct Infrastructure Eng. 2013;10(12):1555-1572.
- [8] Treacy MA, Brühwiler. Action effects in post-tensioned concrete box-girder bridges obtained from high-frequency monitoring. J Civil Struct Health Monitoring. 2015;5(1):11-28.
- [9] Turkstra CJ. Theory of Structural Design Decisions, Study No 2. Waterloo, Ontario, Canada: Solid Mechanics Division, University of Waterloo; 1972.
- [10] Coles S. An introduction to statistical modeling of extreme values. London: Springer-Verlag; 2001
- [11] CEN. EN 1990:2002: Eurocode – Basis of structural design. Brussels: European Committee of Standardisation; 2002.
- [12] SIA. SN 505 269/1: Existing structures – Actions. Zurich: Swiss Society of Engineers and Architects; 2011.
- [13] SIA. SN 505 269/2: Existing structures – Concrete structures. Zurich: Swiss Society of Engineers and Architects; 2011.
- [14] Herwig A. Reinforced concrete bridges under increased railway traffic loads – Fatigue behavior and safety measures [dissertation]. Lausanne: Ecole Polytechnique Fédérale de Lausanne; 2008.
- [15] Joint Committee on Structural Safety. Probabilistic model code – 12<sup>th</sup> draft. 2001.
- [16] Ang AH, Tang WH. Probability Concepts in Engineering Planning and Design – Volume I. New York: John Wiley & Sons; 1984.

## **Chapter 4: Reliability of the steel reinforcement of existing RC slabs subject to railway traffic using advanced fatigue theory and structural response monitoring**

### **Abstract**

A number of refinements in the state of the art on fatigue safety verification of RC elements is proposed: (a) construction of case specific S-N curves for the reinforcement bars using surface hardness and rib geometry as input, (b) consideration of the beneficial probabilistic “size effect” for bars embedded in concrete, (c) use of structural monitoring data, (d) consideration of the concrete crack closure effect on the reinforcement nominal stress range and (e) incorporation of the CAFL in the calculation of reliability. Additionally, the validity of Palmgren-Miner rule is investigated by comparing its predictions to those of an advanced method for calculating damage accumulation based on statistical microplasticity. It is shown that for the case of a short span RC slab subject railway traffic, the application of these refinement leads to important increase of the calculated safe service life. Palmgren-Miners rule is shown to give results which are in generally good agreement with those of the advanced method provided that the S-N curve that is used is obtained for a load ratio  $R$  which is representative of the actual loading history.

*Keywords:* fatigue; reinforced concrete; steel reinforcement bars; S-N curves; notched components; size effect; structural response monitoring; damage accumulation; reliability.

## Nomenclature

$a$	complement of a confidence level ( $1 - a$ )	$\Delta K_{th}$	threshold value of stress intensity factor range
$a$	crack size (length)	$M$	moment
$a_0$	size of initial crack	$M_{exp}$	number of potential crack initiation locations the test specimens
$a_b$	blocked strain energy density	$M_{str}$	number of potential crack initiation locations on the structural component
$b$	measure of Burgers vector	$N$	axial force
$b$	fatigue stress exponent	$N_{ini}$	number of cycles to formation of initial crack
$c$	fatigue strain exponent	$\dot{N}$	cycle number increase rate
$c$	crack width	$P$	probability
$d$	static depth of concrete cross-section	$R$	local stress ratio
$d_1$	concrete cover thickness of tensile reinforcement	$\bar{R}$	nominal stress ratio
$f_t$	tensile strength of concrete	$Y$	correction factor for stress intensity factor
$g_{t_f}$	PDF of $t_f$	$Y_{3D}$	the above correction factor for a 3D crack
$g_{t_{ini}}$	PDF of $t_{ini}$	$Y_{2D}$	the above cor. factor for the corresponding 2D crack
$g_{\Delta\bar{\sigma}_0}$	PDF of $\Delta\bar{\sigma}_0$	$\alpha_u$	ultimate strain energy (material property)
$h$	depth of concrete cross section	$\gamma_{IGN}$	ignorance factor
$k$	stress concentration factor	$\Delta\varepsilon$	local strain range
$k_f$	fatigue stress concentration factor	$\Delta\bar{\varepsilon}$	nominal strain range
$k_t$	theoretical stress concentration factor	$\varepsilon_f$	fatigue ductility coefficient
$l_m$	material characteristic length	$\zeta_{t1}$	ratio of number of type-1 incidents over all incidents and its statistically estimated value
$l_{eq}$	equivalent rebar free length close to a concrete crack	$\kappa_a$	confidence level fractile value $\Phi^{-1}(1 - a)$
$n$	Ramberg-Osgood exponent	$\lambda$	threshold parameter of the general. Parreto distrib.
$n$	ratio of steel to concrete modulus of elasticity	$\rho$	reinforcement ratio
$n_{th}$	number of observed incidents exceeding threshold $\lambda$	$\rho_{eff}$	effective reinforcement ratio
$p$	probability	$\Delta\sigma$	local stress range
$r$	radius at the root of the rib	$\Delta\sigma_0$	material Constant Amplitude Fatigue Limit (CAFL)
$t$	time	$\Delta\bar{\sigma}$	nominal stress range
$t$	time as an integration variable	$\Delta\bar{\sigma}_0$	nominal constant amplitude fatigue limit (CAFL)
$t_{ini}$	time at formation of initial crack	$\bar{\sigma}_{min}$	minimum nominal stress in stress cycle
$w^d$	distortional work per volume	$\bar{\sigma}_{max}$	maximum nominal stress in stress cycle
$w^v$	volumetric work per volume	$\bar{\sigma}_{cl}$	nom. stress in reinforcement at concrete crack closure
$w_{res}$	residual concrete crack opening displacement	$\sigma_f$	fatigue strength coefficient
$A_s$	area of steel reinforcement	$\bar{\sigma}_{in}$	nom. stress in reinforcement assuming no concrete crack closure
$B$	bulk modulus	$\sigma_u$	tensile strength
$D$	damage factor	$\hat{t}$	Scale parameter of the generalized Parreto distribution and its estimated value
$\dot{D}$	damage factor increase rate	$\phi$	intrinsic dissipation per volume
$D_f$	damage factor at formation of the initial crack	$\phi$	reinforcement bar diameter
$E$	modulus of elasticity		
$G$	shear modulus		
$G_F$	Concrete fracture energy		
$G_{t_f}$	CDF of $t_f$		
$G_{t_{ini}}$	CDF of $t_{ini}$		
$G_{\Delta\bar{\sigma}}$	CDF of maximum $\Delta\bar{\sigma}$ value per incident		
$H_B$	Brinell hardness	RC	Reinforced Concrete
$H_V$	Vickers hardness	SRM	Structural Response Monitoring
$K$	Ramberg-Osgood coefficient	CAFL	Constant Amplitude Fatigue Limit
$\Delta K$	stress intensity factor range	CDF	Cumulative Distribution Function
		PDF	Probability Density Function

## 4.1. Introduction

Among the various deterioration phenomena affecting reinforced concrete (RC) elements (corrosion of the reinforcement, alkali-silica reaction etc.), fatigue develops in general with the slowest rate – it has for this reason the smallest probability of becoming critical for structural safety. Indeed, RC element failures involving fatigue are rare and, even in these cases, fatigue is seldom the predominant failure factor [1]. The above probably explain why in the past RC fatigue had received relatively little attention from the engineering community. Current design practice in Europe is largely based on the state of the art report issued by CEB in 1988 [1]. In the last decade, however, the question of fatigue examination of the existing RC railway infrastructure arises with increasing frequency, partly because of the increased railway traffic volumes observed in most industrialized countries.

A rational engineering framework for approaching this question has been developed by Herwig [2] who emphasizes that accurate determination of the stress levels in the reinforcement under service conditions and realistic modeling of the reinforcement fatigue resistance are crucial for an efficient and sustainable fatigue examination procedure. Indeed, as a number of research works have shown [3, 4], steel reinforcement is practically always the critical component of a RC element with respect to fatigue failure. In line with the above approach a number of refinements in the state of the art on fatigue safety verification of steel reinforcement bars embedded in RC elements is proposed in this work.

In particular, the following questions are addressed in the four following sections of this chapter:

- Construction of case specific S-N curves for the reinforcement bars in existing structures by taking into account their surface hardness and the geometry of the ribs formed on their surface in order to ensure proper bond between the bars and the surrounding concrete.
- Formulation of the relation between damage factor and reliability taking into account the probabilistic size effect for the case of bars embedded in concrete.
- For the case of a short span RC slab subject to railway traffic, investigation of the load sequence effect on the average annual damage increase rate and evaluation of the effectiveness of Palmgren-Miner rule by using an advanced damage accumulation method based on statistical microplasticity and loading histories obtained from Structural Response Monitoring (SRM).
- Probabilistic calculation of the safe service life by combined consideration of both the damage factor increase rate and the Constant Amplitude Fatigue Limit (CAFL).

## 4.2. Construction of case specific S-N curves for ribbed steel reinforcement bars

In most design codes, the fatigue properties of steel reinforcement bars are specified uniformly for all types of bars in the form of one or two S-N curves (differentiation is usually made only between bars of small and large diameter and reduction factors are prescribed for the case of bends). Much of the conservatism inherent in the above approach can be avoided by using case specific S-N curves adapted to the characteristics of the bars under examination.

The fatigue behavior of reinforcement bars depends primarily on: (a) the fatigue properties of the material at the surface of the bars – in the case of quenched and tempered bars these properties differ substantially from those of the core material; (b) the geometry of the ribs that induce stress concentrations in the regions of the rib roots where cracks most probably initiate. Accordingly, an engineering method for constructing case specific S-N curves should be based on few measurable parameters that describe as efficiently as possible the above characteristics.

### 4.2.1. Characterization of the fatigue properties of the material at the surface of the bar using hardness

Several researchers have pointed out that in metals hardness correlates quite well with several of the parameters involved in the various fatigue-life models [5, 6]. In addition, hardness can be measured in situ with portable measurement devices and minimal intervention on the element which mainly consists in the local removal of the concrete cover. It is, therefore, investigated in this section whether it is possible to construct useful S-N curves, in acceptable agreement with experimental observation, by assuming hardness as the sole available material parameter (besides the information that the material is steel) and using empirical correlations (already presented in the literature).

As a first step, a fatigue-life model has to be adopted. Although the nominal stress in the reinforcement bars remains well below its elastic limit for all practical applications, the stress in the vicinity of the stress concentration at the root of a rib may regularly enter the plastic domain. In this case, the Basquin-Coffin-Manson model can be used for modeling the fatigue resistance of the base material at the root of the rib. This model refers to constant amplitude strain controlled loading and relates the total (elastic+plastic) strain range  $\Delta\varepsilon$  to the number of loading variations to crack initiation  $2N_{ini}$

$$\Delta\varepsilon = \Delta\varepsilon_e + \Delta\varepsilon_p = 2\{(\sigma_f/E)(2N_{ini})^b + \varepsilon_f(2N_{ini})^c\} \quad (4.1)$$

where  $\sigma_f$  and  $\varepsilon_f$  are the fatigue strength and ductility coefficients respectively and  $b$  and  $c$  are the fatigue stress and strain exponents respectively. According to [7] for the case of ferrite steels the most efficient correlation is achieved by means of the so called hardness method developed by Roessle and Fatemi [8],

$$\begin{aligned} \sigma_f &= 4.25H_B + 225 \\ \varepsilon_f &= 0.32(H_B)^2 - 487H_B + 191 \\ b &= -0.09 \\ c &= 0.56 \end{aligned} \quad (4.2)$$

where  $\sigma_f$  and  $H_B$  should be introduced in N/mm<sup>2</sup>. While, for tempered martensitic steels the best results are achieved by the so called universal material law of Baumel and Seeger [9].

$$\begin{aligned} \sigma_f &= 1.5 \sigma_u \\ \varepsilon_f &= \min[0.812 - 74(\sigma_u/E), 0.59] \\ b &= -0.087 \\ c &= -0.58 \end{aligned} \quad (4.3)$$

These two methods have similar structure and admit constant values for  $b$  and  $c$ . The Baumel and Seeger method is formulated in terms of ultimate stress  $\sigma_u$  which however correlates very well with hardness. For martensitic steel Pavlina [10] proposes the following relation.

$$\sigma_u = -273.6 + 4.279H_V \quad (4.4)$$

The Coffin-Manson parameters for the reinforcement bars of a specific structural element under examination can therefore be calculated from Eq. (4.2-4.4) given the hardness and the information whether the bars are have received a QT treatment or not.

#### 4.2.2. Characterization of the loading conditions in the vicinity of the rib root

**Fig. 4.1** illustrates the stress field in the vicinity of the rib root of a typical rebar as obtained from an axisymmetric finite element calculation. It is interesting to observe that the stress conditions near the hot-spot are essentially uniaxial with very little shear stress being present. This fact simplifies substantially the calculations that follow.

Contrary to the assumption of strain controlled loading inherent in the Coffin-Manson model, the loading conditions in the vicinity of the rib root are neither strain nor stress controlled. In fact, due to the limited plastification of a small volume of material within a much larger volume which remains elastic, Glinka's principle of equivalent elastic strain energy applies [11]. This principle states that in any point in the region of a stress concentration the local energy density rate (or power density) remains proportional to the nominal power applied to the component with a proportionality constant equal to the square of the elastic stress concentration factor for that point. This is expressed as

$$\Delta\sigma\Delta\varepsilon = k^2\Delta\tilde{\sigma}\Delta\tilde{\varepsilon} \quad (4.5)$$



where  $\tilde{\sigma}$  and  $\tilde{\varepsilon}$  are the nominal (remote) stress and strain in the bar,  $\sigma$  and  $\varepsilon$  are the local stress and strain at a given point in the vicinity of a stress concentration and  $k$  is the stress concentration factor for the same point.

Because the nominal stress strain relationship is required to remain elastic in service conditions the relation can be equivalently written as

$$\Delta\sigma\Delta\varepsilon = k^2(\Delta\tilde{\sigma})^2/E = k^2(\Delta\tilde{\varepsilon})^2E \quad (4.6)$$

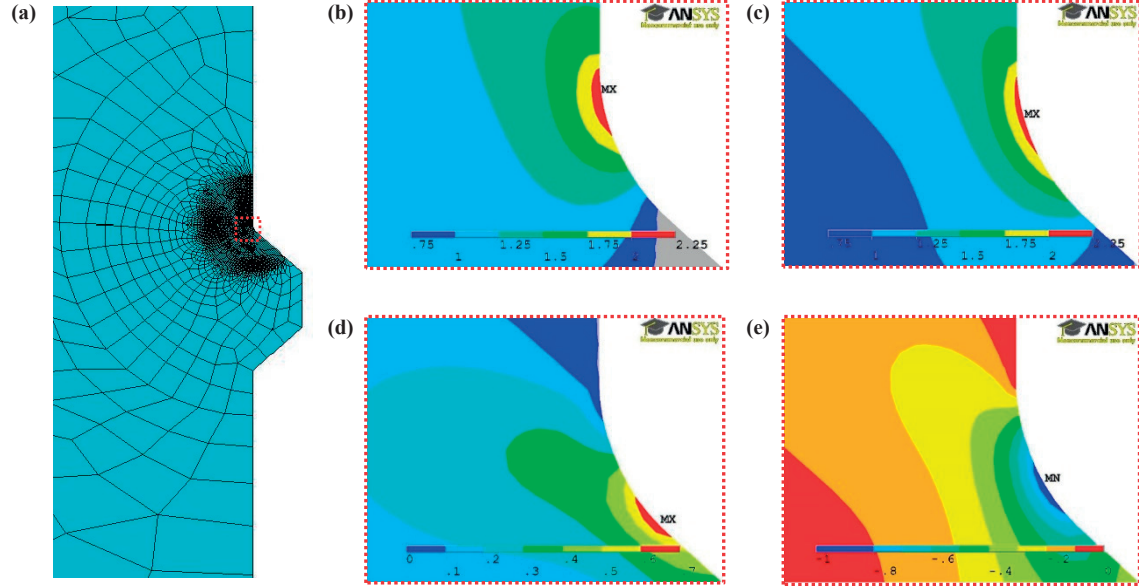


**Fig. 4.1:** (a) Axisymmetric FE model used for the calculations of stress distribution at the root of the rib. (b) Axial stress in the direction of the axis of the bar (vertical direction on the figure). (c) Von Mises equivalent stress. (d) Axial stress in the direction of the radius of the bar (horizontal direction on the figure). (e) Shear stress.

Hence, by virtue of the above principle, the local loading conditions are power controlled independently whether the global loading is stress or strain controlled.

Furthermore, according to the finite volume theory of Taylor [12] (later extended for multiaxial fatigue situations by Susmel and Taylor [13] and Susmel [14]) the elastic stress concentration factor that has to be used for fatigue calculations is not the factor that corresponds to the point of the maximum elastic stress on the surface of the element (generally referred as theoretical stress concentration factor  $k_t$ ) but an “average” value of this factor over a characteristic volume around the point of maximum elastic stress. This representative factor is generally referred as fatigue stress concentration factor  $k_f$ . Taylor proposes various methods for defining  $k_f$  among which the simplest, still quite efficient, consists in taking it equal to the stress concentration factor at the center of this characteristic volume. (Another finite-volume-energy based approach has been proposed by Lazzarin and Zambardi [15] and applied to welded structure by Berto and Lazzarin [16]). The size of this volume is considered as a material property which in general can be thought as a measure of the microstructural inhomogeneity of the material. The classical definition of this characteristic size is given by El Hadad [17] as

$$l_m = \frac{1}{\pi} \left( \frac{\Delta K_{th}}{\Delta\sigma_0} \right)^2 \quad (4.7)$$

where  $\Delta K_{th}$  is the threshold value of the stress intensity factor cracks do not propagate and  $\Delta\sigma_0$  is the fatigue limit of the material. However, since the notion of fatigue limit is sometimes questionable, fatigue limit is

substituted in the above relation with the tensile strength of the material  $\sigma_u$  divided by two<sup>1</sup>. The tensile strength is a very well defined property which also, as already mentioned, correlates very well with hardness.

$$l_m = \frac{4}{\pi} \left( \frac{\Delta K_{th}}{\sigma_u} \right)^2 \quad (4.8)$$

On the other hand the threshold value of the stress intensity factor is a fracture mechanics experimentally measured property whose value is highly influenced by the phenomenon of crack closure. Hertzberg [18], however, pointed out that when the influence of crack closure is excluded the threshold value can be theoretically calculated for a material as

$$\Delta K_{th} = E\sqrt{b} \quad (4.9)$$

where  $b$  is the length of the burgers vector of the material. This theoretical calculation is in very good agreement with results from tests performed at high stress ratios where crack closure does not occur. For steel the above relation results in a constant value of  $100\text{Nmm}^{-3/2}$  independently of the particular type of steel. Hence, the characteristic material size can also be expressed as a function of hardness solely.

The fact that it is an averaged value of stress (over the characteristic volume) and not the maximum stress that has to be taken into account for fatigue calculations, implies that the form of the elastic stress distribution needs also to be known, apart from its maximum value, in order to characterize the loading conditions in the crack initiation region. A number of researchers [19, 20] have shown that as long as the size of the characteristic volume  $l_m$  remains lower than  $1/2$  to  $1/4$  of the radius at the tip of a notch (see **Fig. 4.2(b)**), then, the elastic stress distribution  $\sigma(x)$  ( $x$  axis is in the direction perpendicular to the surface), normalized to the maximum stress on the surface  $\sigma_t$ , depends primarily on the ratio  $x/r$  (for  $x < l_m$ ). Hence, according to Taylor [13]

$$\frac{k_f}{k_t} = \frac{\sigma(l_m/2)}{\sigma_t} = f(l_m/r) \quad (4.10)$$

For notches with opening angle smaller than  $\pi/2$  Lazzarin et al [21] arrive at the following relation

$$k_f = k_t(1 + 4 l_m/r)^{-1/2} \quad (4.11)$$

Remember that for practical purposes the characteristic size is a function of hardness only.

For the geometry of ribbed bars this relation does not give satisfactory results since a rib differs substantially, as a stress raiser, from a notch. Using FEM models it is calculated in this work that for practically any rib geometry the stress distribution close to the surface can be approximate with good accuracy by

$$\frac{\sigma(x)}{\sigma_t} = \frac{k(x)}{k_t} = \left( 1 + 14 \frac{x}{r} \right)^{-1/5} \quad (4.12)$$

$$k_f = k_t(1 + 7l_m/r)^{-1/5} \quad (4.13)$$

In **Fig. 4.2(a)** Eq. (11) is plotted over the normalized distributions calculated by FE models for a set of bars with different rib geometry reported by Zheng and Abel [24].

It is noted that by calculating the stress state at the middle of the characteristic volume behind the root of the rib, the deterministic fracture mechanics related size effect on fatigue resistance is automatically taken into account.

---

<sup>1</sup> This is merely a heuristic alternative definition of  $l_m$ . Its pertinence which can be shown as following: By taking the elastic part of Eq. (4.1) and substituting  $\sigma_f$  from Eq. (4.3) one obtains  $\Delta\sigma = 3\sigma_u(2N_{mi})^b$ . By defining arbitrarily the fatigue limit at 5E6 cycles and taking  $b$  from Eq. (4.3) the fatigue limit for fully reversed stress is obtained as  $\Delta\sigma_{or} = 3\sigma_u 10^{-7+0.087}$ . Since the  $\Delta K_{th}$  calculated by Eq. (4.9) refers to stress variations in tensile domain only, the fatigue limit for R=0 is calculated using the Smith-Watson-Topper model as  $\Delta\sigma_0 = (\sqrt{1-R}/2)3\sigma_u 10^{-7+0.087}$  which gives  $\Delta\sigma_0 = 0.52\sigma_u$ . Hence the proposed definition is in agreement with the universal material law [9]

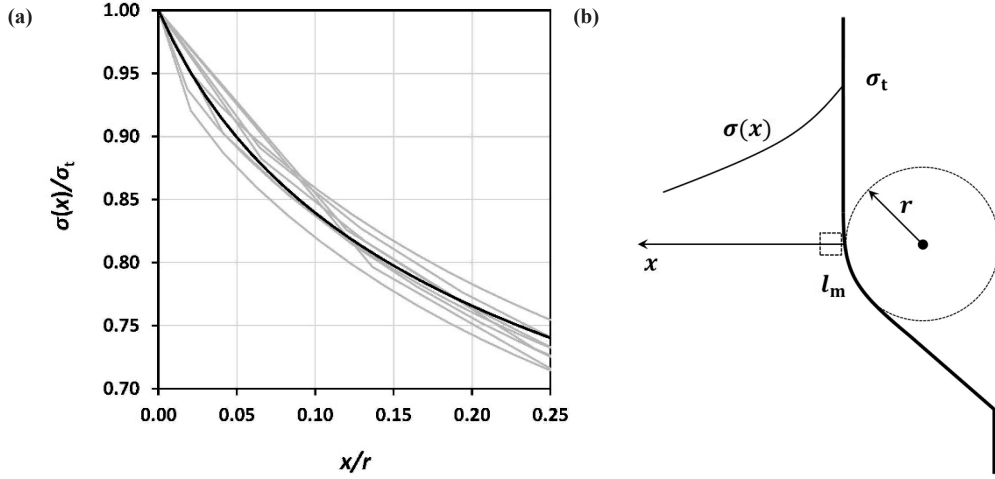


**Fig. 4.2 :** (a) Normalized stress distributions behind the root of a rib as calculated by FE models for various rib geometries (gray lines) and according to the approximation of Eq. (4.13) (black line). (b) Illustration of the distribution of stress behind the root of a rib.

We return now to the observation that the loading in the region of the rib root is power controlled. This suggests that the use of the energy based and very often used Smith-Watson-Topper model might be more appropriate. This model is usually formulated as

$$\Delta\sigma\Delta\varepsilon = 2(1-R)\{(\sigma_f^2/E)(N_f)^{2b} + \sigma_f\varepsilon_f(N_f)^{b+c}\} \quad (4.14)$$

where  $R = \sigma_{\min}/\sigma_{\max}$  and  $\sigma_f$ ,  $\varepsilon_f$ ,  $b$ ,  $c$  are the parameters of the Basquin-Coffin-Manson model. Note that the stress and strain quantities involved in the above equation are the local ones. By substituting Eq. (4.6) in Eq. (4.14) one obtains

$$(\Delta\tilde{\sigma})^2 = \frac{2(1-R)}{k^2}\{\sigma_f^2(2N_{\text{ini}})^{2b} + E\sigma_f\varepsilon_f(2N_{\text{ini}})^{b+c}\} \quad (4.15)$$

In Eq. (4.15),  $R$  still refers to the local loading conditions. In order to calculate the local  $R$  from the nominal  $\bar{R} = \tilde{\sigma}_{\min}/\tilde{\sigma}_{\max}$ , a cyclic stress-strain relation must be introduced. The Ramberg-Osgood model is adopted with parameters  $n$  and  $K$  referring to cyclic loading.

$$\varepsilon = \frac{\sigma}{E} + K\left(\frac{\sigma}{E}\right)^n \quad (4.16)$$

For the evaluation of  $n$  the following compatibility equation, proposed by Nieslony et al. [22], is used

$$n = b/c \quad (4.17)$$

For  $K$  the semi-empirical correlation with hardness, proposed by Cahonn [23] is used

$$K = \frac{H_V}{0.29(0.08)^n} \quad (4.18)$$

After the evaluation of the Ramberg-Osgood parameters the local stress range  $\Delta\sigma$ , maximum stress  $\sigma_{\max}$  and stress ratio  $R$  can be calculated for a given  $\Delta\tilde{\sigma}$  and  $\bar{R}$  by solving the equations

$$k^2(\Delta\tilde{\sigma})^2 = (\Delta\sigma)^2 + 2\Delta\sigma E \left(\frac{\Delta\sigma}{2K}\right)^{1/n} \quad (4.19)$$

$$k^2(\tilde{\sigma}_{\max})^2 = (\sigma_{\max})^2 + \sigma_{\max} E \left(\frac{\sigma_{\max}}{K}\right)^{1/n} \quad (4.20)$$

$$\tilde{\sigma}_{\max} = \Delta\tilde{\sigma}/(1 - \bar{R}) \quad (4.21)$$

$$\sigma_{\max} = \Delta\sigma/(1 - R) \quad (4.22)$$

However since in Eq. (4.15)  $\Delta\bar{\sigma}$  depends on  $R$ , Eq. (4.13, 4.19-4.22) constitute a system of five nonlinear equations with five unknown variables ( $\Delta\bar{\sigma}$ ,  $\bar{\sigma}_{\max}$ ,  $\Delta\sigma$ ,  $\sigma_{\max}$ ,  $R$ ). This system has to be solved by iterative approximations for various values of  $N_{\text{ini}}$  and probably for various nominal stress ratios  $\bar{R}$  in order to construct a set of crack initiation S-N curves representative of the fatigue resistance of the bar.

For the construction of initiation S-N curves intended for practical applications the calculations of three points on each curve corresponding to  $10^5$ ,  $10^6$  and  $10^7$  cycle is sufficient. This leads to a bilinear approximation of the curve as it is also usually done by standards.

The above initiation S-N curves have been constructed using only the hardness, the elastic stress concentration factor and the radius at the root of the rib. These three parameters can be practically obtained for most existing structural elements using minimally invasive methods. The elastic stress concentration factor at the root of the rib is calculated, for various commonly encountered rib geometries, by Zheng and Abel [24] using 2D finite elements and recently by Rocha [24]. using 3D finite elements. Zheng and Abel propose also a series of simplified polynomial relations which are in a good agreement with the more accurate results of the 3D calculation.

The above presented procedure for the construction of a case specific initiation S-N curve can be summarized in the following steps:

- Accept a modulus of elasticity equal to  $2E+11$  Pa and Berger's vector measure of  $2.5E-10$  m for all types of steel and calculate the crack propagation threshold of the stress intensity factor range  $\Delta K_{\text{th}}$  from Eq. (4.9)
- Measure surface hardness  $H_B$  of the bar.
- Calculate the ultimate stress  $\sigma_u$  of the surface material using Eq. (4.4).
- Calculate the characteristic size of the surface material from Eq. (4.8)
- Calculate the fatigue stress concentration factor from Eq. (4.13)
- Using the measured value of surface hardness and other potentially available information conclude whether the surface material is ferrite steel or tempered martensitic steel.
- Calculate the parameters of the Basquin-Coffin-Manson model from Eq. (4.2) or Eq. (4.3) for ferrite steel or tempered martensitic steel respectively.
- Calculate the parameters of the Ramberg-Osgood model from Eq. (4.17, 4.18)
- Solve by iterative approximations the system of nonlinear Eq. (4.15, 4.19-4.22) for a range of values of cycles to crack initiation  $N_{\text{ini}}$  and nominal stress ratio  $\bar{R}$ .

#### 4.2.3. Validation of the crack initiation S-N curve prediction method

The above procedure is applied for the set of reinforcement bars tested by Zheng and Abel [25, 26]. It is a set of 7 bars with diameter 12, 16, 20, 24, 28, 32 and 36 mm (Australian made TEMPCOR 400Y). The data for these bars taken from [26] are summarized in **Table 4.1** (white columns) for the reader's convenience along with the intermediate results of the calculations. Although already calculated in [25] the elastic stress concentration factors  $k_t$  at the root of the rib are recalculate in this work using an axisymmetric FE model. In the present work the obtained values of  $k_t$  are 5%-10% higher than those calculated in [25]. The obtained S-N curves for  $\bar{R} = 0$  are compared to the experimental data in **Fig. 4.3**.

**Table 4.1:** Rebar data [25] and intermediate calculation results.

$\varnothing$ [mm]	$r$ [mm]	$\theta$ [°]	$h$ [mm]	$w$ [mm]	$Y$	$k_t$	$H_V$ [N/mm <sup>2</sup> ]	$\sigma_u$ [N/mm <sup>2</sup> ]	$\sigma_f$ [N/mm <sup>2</sup> ]	$\varepsilon_f$	$b$	$c$	$n$	$K$ [N/mm <sup>2</sup> ]	$l_m$ [mm]	$k_f$	$\Delta\bar{\sigma}_0$ [N/mm <sup>2</sup> ]
12	0.76	35.6	0.78	3.09	0.76	1.777	225	689	1034	0.557				1133	0.027	1.60	279
16	1.10	40.8	1.02	4.28	1.10	1.789	230	711	1066	0.549				1158	0.025	1.60	295
20	1.19	44.3	1.23	5.01	1.19	1.830	243	766	1149	0.529				1224	0.022	1.65	303
24	0.40	46.7	2.73	7.62	0.40	2.798	256	822	1233	0.508	-0.087	-0.58	0.15	1289	0.019	2.37	231
28	1.11	41.2	2.29	7.81	1.11	2.107	266	865	1297	0.492				1340	0.017	1.87	303
32	0.78	37.5	2.52	9.19	0.78	2.359	232	719	1079	0.546				1168	0.025	2.06	232
36	0.91	39.4	3.00	11.1	0.91	2.374	255	818	1226	0.510				1284	0.019	2.13	259

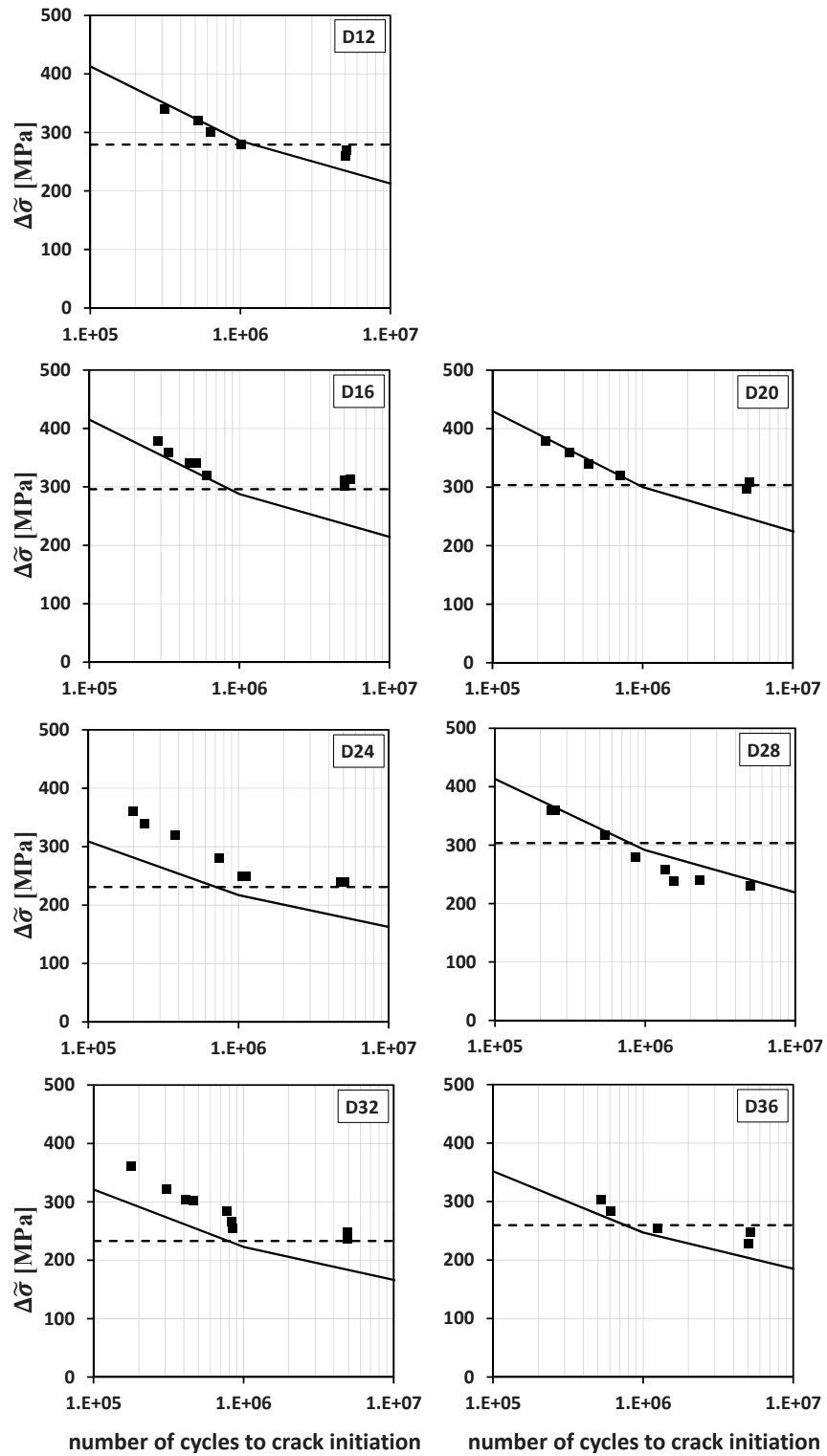


**Fig. 4.3** : Predicted median (0.5 fractile) crack initiation S-N curves (continuous lines) and constant amplitude fatigue limits (dashed lines) compared to the experimental results of Zheng and Abel [26] for a set of 7 reinforcement bars of different diameter (Australian made TEMPCOR 400Y).

It has to be noted that the experimental results presented in **Fig. 4.3** refer to the total number of cycles to failure and not just to crack initiation. Consequently, the comparison is meaningful only if it is assumed that the number of cycles during which the initially shaped crack propagates until failure is only a small fraction of the total number of cycles sustained by the bar. This assumption is discussed in Section 4.2.4.

Under the above assumption, it can be said that in general the proposed method gives predictions which are in good agreement with the experimental observations (i.e. within 15%, in terms of  $\Delta\bar{\sigma}_0$ ). The relatively limited discrepancies may be attributed to a number of factors which are not taken into account in the above method. The most important of them are the presence of residual stress near the surface of the bar which are induced during the fabrication process and the surface roughness which is also related to fabrication.

Both these factors have an effect on the stress distribution in the vicinity of the root of the ribs but their measurement (particularly the measurement of residual stress) presents several practical difficulties and is subject to large uncertainty [24]. Discrepancies may also be due to error in the measurement of surface hardness and geometrical characteristics. Despite the above discrepancies the predicted S-N curves, which are assumed to correspond to the median (50%-fractile) of the number of cycles to crack initiation, either coincide with the experimental data point or fall slightly below them with the exception of the bar with 28mm diameter. In the context of an examination procedure these possible discrepancies, which cannot be known, should be taken into account by means of a heuristic ignorance factor.

The proposed method fails to predict the existence of a constant amplitude fatigue limit which is suggested by the experimental observations. In order to do that the possibility or non-possibility of crack propagation has to be considered. This issue is discussed in the following section.

#### 4.2.4. Crack propagation phase – Constant amplitude limit of fatigue

The crack initiation phase ends with the formation of an initial crack. From this point the phenomenon should be described using fracture mechanics.

Staying for the moment in the case of constant amplitude loading it can be said that if after the formation of the initial crack the stress intensity factor range is higher than the threshold stress intensity factor range, then propagation of the initial crack will occur. The total life time of the bar is the sum of the time until crack initiation plus the time of crack propagation up to final failure of the bar. However, as it has been shown by Rocha [24] for reinforcement bars and by Pereira et al. [27] for notched components, the number of propagation cycles is small compared to the number of initiation time so that for practical applications crack initiation can be considered equivalent to failure.

On the contrary, if after the formation of the crack the stress intensity factor remains below the threshold value the crack will propagate no further and this results in an infinite fatigue life of the bar. The fatigue limit of the bar can be calculated by the condition [17]

$$\Delta K \leq \Delta K_{th} \quad (4.23)$$

The initial size of the formed crack  $a_0$  is assumed equal to the characteristic size of the material  $l_m$ . In order to take into account the size effect related to small cracks the stress intensity factor is calculated according to the modified formula of Tanaka, Nakai and Yamashita [28]

$$\Delta K = Y\Delta\bar{\sigma}\sqrt{\pi a_0 \frac{a_0}{a_0+l_m}} = Y\Delta\bar{\sigma}\sqrt{\pi \frac{l_m}{2}} \quad (4.24)$$

were  $Y$  is a correction factor which in general depends on the crack size. Substituting Eq. (4.8) in Eq. (4.24) and using Eq. (4.23) as an equality the fatigue limit is calculated as

$$\frac{\sigma_u}{Y\sqrt{2}} = \Delta\bar{\sigma}_0 \quad (4.25)$$

$Y$  has to be calculated for a crack at the root of the rib taking into account the particular geometry of the bar and its ribs. This can be done by means of a finite element model. In this work an axisymmetric model has been used. Since an axisymmetric model models essentially the two-dimensional case the following correction has been applied to the calculated factors [29]

$$Y_{3D} = Y_{2D} \frac{1+0.12\left(1-0.75\frac{a}{c}\right)}{1.12} \quad (4.26)$$

In the above the ratio  $a/c$  has been taken equal to 0.5.

The results of the calculations for the set of bars tested by Zheng and Abel are summarized in **Table 4.1** while in **Fig. 4.4** the predicted and experimentally observed fatigue limits are compared. The predicted fatigue limits are also indicated in **Fig. 4.3**. Again, with the exception of the Ø28 bar which seems to be an outlier, the above method gives good predictions. The reasons why the experimentally observed fatigue limit for this bar falls that lower than then predicted one is unclear. It is possible however that an error has interfered to the measurement of the rib geometry or that the presence of a defect on the bar has been ignored.

In the case of variable amplitude loading the notion of fatigue limit has some meaning if all the loading transitions after crack initiation remain below this limit. If however the loading transitions exceed even occasionally the threshold stress intensity factor range, then the crack size will increase and the load intensity required for a further propagation of the crack decreases. In that case a fracture mechanics time domain analysis is required to predict the number of propagation cycles [2, 30].

However for practical problems and on the base of the above discussion, the simplifying assumption of D'Angelo and Nussbaumer [31], which is stated here in slightly different way, can be adopted: The appearance of the initial crack marks the end of the damage accumulation process, however the crack propagation process, which eventually leads to failure, does not begin until the fatigue limit is exceeded for the first time *after* the formation of the initial crack; the beginning of crack propagation – rather than the mere event of the initial crack formation – is considered as practically equivalent to failure. Following the paradigm of D'Angelo and Nussbaumer [31] this assumption is used in Section 4.4 for calculating the reliability of a single rebar taking into account the existence of a constant amplitude fatigue limit.

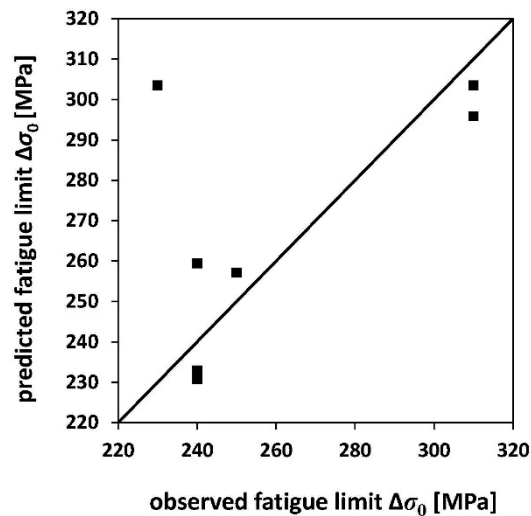


**Fig. 4.4** : Comparison between predicted and experimentally observed fatigue limit for a set of 8 reinforcement bars of different diameter.

### 4.3. Probabilistic size effect in fatigue crack initiation life

#### 4.3.1. Fundamental relation between damage factor and reliability

There is no unique way to define damage as a physical quantity and any possible definition is characterized by either a certain degree of ambiguity or a number of restrictions that limit the domain of validity of the definition. Because of these drawbacks, damage is often introduced in the dimensionless form of a damage factor which is obtained by normalizing damage with its value just before ultimate failure<sup>2</sup>; this value is

<sup>2</sup> Failure here refers to failure of a Representative volume Element (RVE) which defines the formation of an initial crack

always considered as a deterministic and known material property. The above limitations being stated, the analysis of Section 1.2.4.2 is reminded at this point according to which damage (and damage factor respectively) can be defined either by the actual, but in principle unobservable, value of a certain physical quantity or by the observable (calculated) value of the above quantity which can be assumed equal to the expectation of the actual variable. In the former case, actual damage is a random variable, although knowledge of its evolution, if it were possible, would lead to a deterministic prediction of the remaining life time. In the latter case, calculated damage is a deterministic variable and knowledge of its evolution is in principle possible although it can only lead to a probabilistic prediction of the remaining life time i.e. to a probability of failure within a certain period of time. Obviously, only the second type of definition lends itself to calculating of damage evolution—the calculation of the actual value of a random variable not being possible. Hence, calculated damage and damage factor<sup>3</sup> are in general viewed as variables which, at a given moment, completely characterize the *reliability* of an element – here a RVE – with respect to its *ultimate* failure and are calculated as functions<sup>4</sup> of the loading history of the element up to that moment.

In Section 1.2.4.2 a deterministic damage factor  $D$  is defined as the ratio of the *expected* value of the microstructurally blocked free energy  $\langle a_b \rangle$  over the ultimate value of the free energy density  $\alpha_u$  that can be sustained by the material

$$D = \langle a_b \rangle / \alpha_u \quad (4.27)$$

Using the *principle of maximum entropy*, the *a priori* probability that an observable flaw (crack) will have initiated by the time the calculated damage attains a value  $D$ —in other words the probability that at the instant of ultimate failure, the value of damage  $D_{\text{ini}}$  will be less than  $D$ —is calculated as

$$G_{D_{\text{ini}}} = P(D_{\text{ini}} < D) = e^{-1/D} \quad (4.28)$$

Hence, the value of damage factor at the moment of crack initiation  $D_{\text{ini}}$  is a random variable that follows a Fréchet distribution with shape parameter equal to 1 and location and scale parameters equal to 0 and 1 respectively. The CDF of this distribution is given of course by Eq. (4.28) while its PDF is given by

$$g_{D_{\text{ini}}} = \frac{dP(D_{\text{ini}} < D)}{dD} = \frac{1}{D^2} e^{-1/D} \quad (4.29)$$

The CDF and the PDF of the above distribution are plotted in **Fig. 4.5(a, b)**. It has to be noted that neither the expectation nor the variance nor any higher moment of the above distribution has a finite value. Note also that neither the damage factor  $D$  nor of course its particular value at the instant of initiation  $D_{\text{ini}}$  are physically bounded at 1.

In the case where multiple potential crack initiation locations exist and have the same evolution of damage factor, the probability that the value of damage factor at the moment of formation of the first crack is less than  $D$  (i.e.  $D_{\text{ini}}^{\text{min}} = \min(D_{\text{ini},i}) < D$  where  $i = 1 \dots M$  counts the potential crack initiation locations) is given by

$$G_{D_{\text{ini}}^{\text{min}}} = P(D_{\text{ini}}^{\text{min}} < D) = 1 - (1 - e^{-1/D})^M \quad (4.30)$$

#### 4.3.2. Effect of the number of potential crack initiation locations – probabilistic size effect

In the following we will omit the superscript min and by  $D_{\text{ini}}$  we will refer to the value of damage factor at initial formation of the first crack in a component. The PDFs of  $D_{\text{ini}}$  for various values of  $M$  are plotted in **Fig. 4.5(a)** and are given by

$$g_{D_{\text{ini}}} = \frac{dP(D_{\text{ini}} < D)}{dD} = \frac{M}{D^2} (1 - e^{-1/D})^{M-1} e^{-1/D} \quad (4.31)$$

<sup>3</sup>Referred in the following simply as damage (damage factor).

<sup>4</sup> More precisely functionals, i.e. functions defined in a vector or function space; in other words function of histories expressed as vectors or functions.



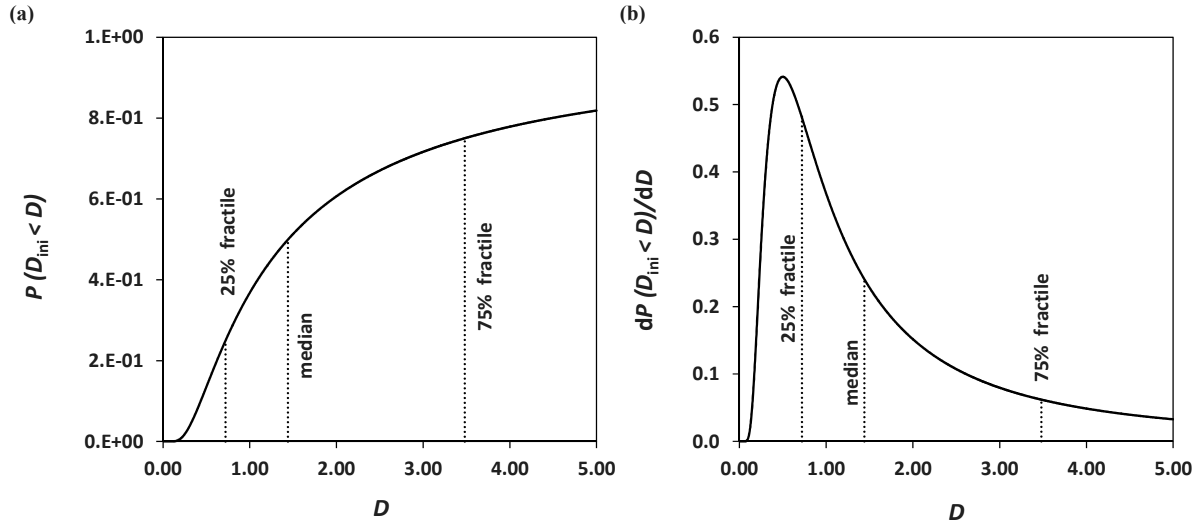


Fig. 4.5 : (a) CDF and (b) PDF of damage factor at formation of the initial crack – a standard Fréchet distribution.

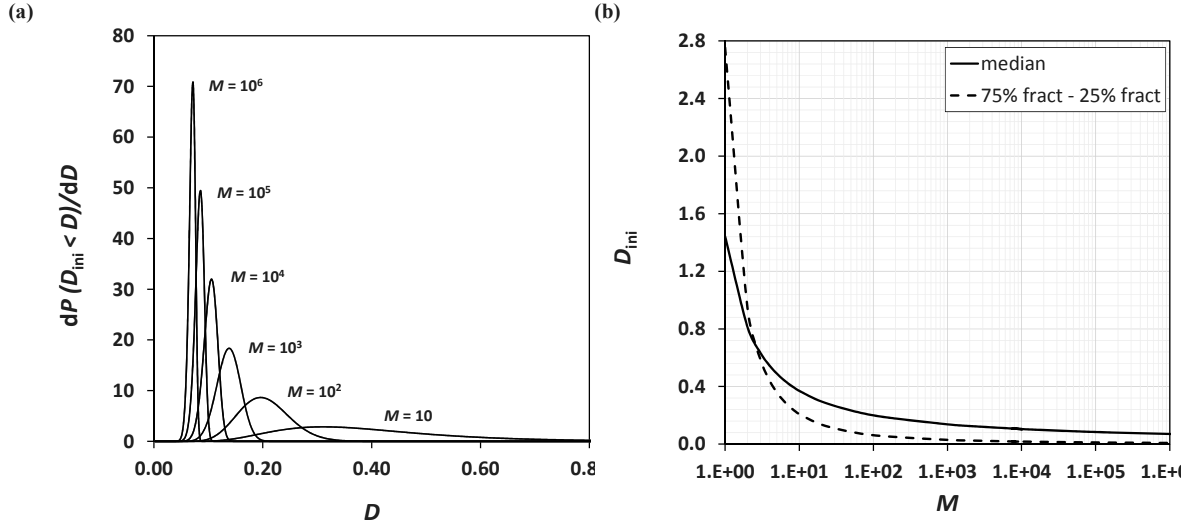


Fig. 4.6 : (a) PDFs of the damage factor at the first initial crack formation for various value of the number of potential crack initiation locations  $M$ . (b) Median and “dispersion” (75% fractile – 25% fractile) of the above distributions as functions of  $M$ .

It can be observed that the median and the dispersion of the distribution decrease with increasing  $M$ . The value  $D_{ini,c}$  of a particular fractile  $c$  of the distribution is calculated by setting  $P(D_{ini} < D) = c$  in Eq. (4.31) and solving for  $D$

$$D_{ini,c} = -(\ln(1 - (1 - c)^{1/M}))^{-1} \quad (4.32)$$

The median (0.5 fractile) and the difference between the 0.75 and the 0.25 fractile (which provides an indication of the dispersion of the distribution) are plotted as functions of  $M$  in Fig. 4.6(b). If the “size” of a component is expressed as the number of its potential locations of crack initiation, then it can be said that the curves of Fig. 4.6(b) describe a probabilistic size effect on fatigue life. This is distinct from the fracture mechanics related size effect which has been considered in Section 4.2.2 by using an averaged value of stress over the characteristic material volume instead of the theoretical maximum value according to analytical continuum mechanics.

#### 4.3.3. Size effect transform of the constant amplitude fatigue crack initiation life

For a prescribed S-N curve derived from experiments, the “size” of the test specimens in terms of the number of potential crack initiation locations should also be given. Then, for a particular structural component with a different “size”, the constant amplitude fatigue crack initiation life can be calculated by formulating Eq. (4.31) for both the experimental specimens and the structural components as follows

$$D_{ini,c_0}^{exp} = D' N_{ini,c_0}^{exp} = -(\ln(1 - (1 - c_0)^{1/M_{exp}}))^{-1} \quad (4.33a)$$

$$D_{ini,c}^{str} = D' N_{ini,c}^{str} = -(\ln(1 - (1 - c)^{1/M_{str}}))^{-1} \quad (4.33b)$$

In the above equation  $c_0$  is the fractile for which the experimental fatigue life is given and  $c$  is the fractile for which the fatigue life of the structural component is calculated. It should be noted here that  $c_0$  refers to the distribution of fatigue life due to the inherent randomness for a given type of component and not to the statistical variability that can be observed when S-N curves are derived from samples including different types of components.  $D'$  is the calculated damage factor increase per cycle which is independent of the number of probable crack initiation locations and of course from the considered fractile of fatigue life. Combination of Eq.(4.33a,b) leads to the following analogy

$$N_{ini}^{str} = N_{ini}^{exp} \frac{\ln(1 - (1 - c_0)^{1/M_{exp}})}{\ln(1 - (1 - c)^{1/M_{str}})} \quad (4.34)$$

#### 4.3.4. Number of potential crack initiation locations for test specimens and structural components

It is not always easy to determine the number of potential crack initiation locations for a given component. In the following however an approximation is attempted for three cases of particular interest for the present investigation.

For the prismatic axially loaded smooth specimens that are often used for determining material fatigue properties, the number of potential crack initiation locations can be calculated as the ratio of the gauge surface over the square of the material characteristic length. These specimens are often cylindrical with diameter and gauge length in the range of 5-10 mm and 10-20 mm respectively (the lower values being preferred). Assuming a gauge diameter of 6 mm, a gauge length of 12 mm and a characteristic material length of 0.02 mm results in a number of potential initiation locations  $M = 11310$ . Since the empirical correlations used in Section 4.2.1 for the construction of case specific S-N curves are based on results of tests conducted on similar specimens, a value of  $M$  close to that calculated above can be assigned to those constructed S-N curves.

For a steel reinforcement bar specimen the potential crack initiation locations lay on the lines defined by the roots of its ribs; also the rib height usually increases towards the middle of the rib so that that stress concentration obtains its maximum value over a small segment of the above root-line near the center of the rib. Hence, for a typical specimen containing around 30 ribs with an assumed maximum stress length of 5 mm on the root of each rib and for a characteristic material length of 0.02 mm, the number of potential crack initiation locations is calculated as  $M = 7500$ . This value can be considered typical for the experimental data to which the constructed S-N curves are compared in Section 4.2.3. It can be verified from **Fig. 4.6(b)** that the two values of  $M$  ( $M = 11310$  in the previous paragraph for constructed S-N curves and  $M = 7500$  in this paragraph for experimental S-N data from reinforcement bar specimens) result in practically the same value for the median of  $D_{ini}$ . This observation confirms that the comparison of Section 4.2.3 is indeed meaningful.

Finally, in the case of a single bar belonging to the principal bending reinforcement of a simply supported RC slab it is reasonable to assume that the potential crack initiation locations will be limited within a segment of the bar near the middle of the span where bending moment obtains its maximum value and presents small gradient; moreover crack initiation will occur at the ribs of the bar that are located very close to the concrete cracks that cross the above segment, since it is at the locations of concrete cracks where the nominal stress in the bar obtains its maximum value. Assuming 4 concrete cracks within the near-constant-moment central segment of the slab and 2 exposed ribs per concrete crack and bar, the number of potential initiation locations

per bar results in  $M = 2000$  (with the same assumptions as in the previous paragraph for the stress distribution on the rib root line and the material characteristic length)

For the calculations that follow, a value  $M_{\text{exp}} = 10000$  is assumed for both experimentally derived and constructed S-N curves for free steel reinforcement bars, while  $M_{\text{str}} = 2000$  is assumed for bars embedded in a bending RC slab. According to Eq. (4.34), this assumption results in a median of the constant amplitude fatigue crack initiation life which is approximately 20% higher for embedded bars in bending than for free bars under the same nominal stress amplitude and is in agreement with experimental observations [1].

#### 4.4. Damage factor increase rate

In the current engineering practice [32], damage accumulation in structural elements of railway infrastructure is calculated using two main simplifications:

- Loading sequence effects are empirically taken into account within the framework of Palmgren-Miner rule by applying the rainflow cycle counting method which in general gives counts that correspond to the energy dissipation loops of the plastic behavior of metals.
- Stress histories at the element level are obtained by means of structural analysis and standard train axle models, while dynamic effects are taken into account by applying a prescribed amplification factor on the entire history. This results in that the statistical characteristics of the calculated stress histories differ substantially from those of the stress history actually experience by the element under service conditions.

The objective of this section is to investigate the influence of each of these two simplifications on the calculated damage accumulation rate. To this goal calculations are performed using:

- two different damage accumulation theories:
  - Palmgren-Miner rule combined with rainflow cycle counting and
  - an advanced theory recently proposed by the authors [33]; and
- two different methods of acquisition of the input stress histories:
  - structural analysis with prescribed traffic action models and
  - Structural Response Monitoring (SRM).

The investigation is performed for the case of a short single span bridge on which a monitoring campaign has recently been completed by the authors. The fatigue properties of the reinforcement bars are described by artificial S-N curves constructed according to Section 4.2 on the basis of assumed values for surface hardness and rib geometry.

##### 4.4.1. Calculation of damage factor increase

Returning now to the definition of damage factor of Eq. (4.27), the expected value  $\langle a_b \rangle$  is assumed equal to the *apparent* value of blocked free energy accumulated in the material during its loading history and is calculated as the integral of the intrinsic dissipation rate  $\dot{\phi}$  over time. If the process of intrinsic dissipation is practically independent of the loading rate, the calculation of the evolution of damage factor takes the following form

$$D_n = \frac{\langle a_b \rangle_n}{a_u} = \sum_{i=1}^n \Delta\phi_i \quad (4.35)$$

where  $i$  counts the stress variations between two successive local extremes of the loading history (stress reversal points) and  $\Delta\phi_i$  is the intrinsic dissipation during load variation  $i$  while  $D_n$  and  $\langle a_b \rangle_n$  are the damage factor and the expectation of blocked free energy at the end of the  $n^{\text{th}}$  transition.

Each of these variations is, in turn, described by the loading range, the direction of loading (sign of the loading range), and the loading ratio (minimum over maximum load). Each loading variation induces a non-negative increase of damage. In general the amount of damage increment in the current load step does not depend only on that step but also on the sequence of the preceding steps. Besides the empirical Palmgren-Miner rule combined with rainflow cycle counting, a number of advanced physically meaningful methods have been developed in order to take into account this history.

#### 4.4.1.1 Palmgren-Miner rule

Palmgren-Miner rule has been presented in the introduction of the thesis (Section 0.3). It consists in calculating a hypothesis consists in calculating a damage factor

$$D_M = \sum_{j=1}^n 1/N_{ini,j} \quad (4.36)$$

where,  $N_{ini,j}$  is the number of cycles to first initial crack formation, obtained from a given S-N curve, under constant amplitude loading at the load range of the  $j^{th}$  cycle counted by the rainflow method. Here it will only be mentioned in addition that because of the probabilistic size effect described above and the fact that an S-N curve can be defined for different fractiles of the fatigue life, the Miner's damage factor  $D_M$  is not generally equivalent to the absolute damage factor  $D$  of Eq. (4.27). It will be shown in Section 4.4.1.4 that the two damage factors are actually proportional with the proportionality factor depending on the "size" of the specimens from which the S-N curve has been derived and its corresponding fractile.

#### 4.4.1.2. Advanced theories for accounting for load sequence effects

From a physical point of view, the history dependence of damage accumulation rate is mainly due to the manifestation of two irreversible processes:

- plastic flow and
- damage accumulation, i.e damage increase rate depends on the actual value of damage.

The effect of accumulated damage is more important for low cycle fatigue, while as the number of cycles increases plasticity effects become dominant.

A number of theories have been developed in which only the effect of already accumulated damage is taken into account while the plasticity is ignored (Cheng and Plumtree [34], Sun et al. [35], Mesmacque et al [36]). According to these theories, which are often referred as non-linear damage accumulation rules, the effect of past loading history is adequately represented by the value of damage at present.

Lynn and DuQuesnay [37] take into account loading sequence effects due to plastic behavior of material by applying rain-flow cycle-counting enhanced by the consideration of a micro-crack opening strain and an intrinsic fatigue limit.

Lemaitre et al. [38] and Desmorat et al. [40] propose a theory in the context of continuum damage mechanics, in which both plasticity and accumulated damage are taken into account.

#### 4.4.1.3. Proposed microplasticity theory

The authors propose in [33] a statistical micro plasticity model for the sequential calculation (variation by variation) of the sum of Eq. (4.35) for any loading history expressed in terms of successive variations of the local distortional and volumetric elastic strain energy density. This energy formulated model is particularly suitable for the calculation of damage evolution at the locations of geometric stress concentration where, by virtue of the principle of strain energy equivalence, the local loading is in fact controlled by the local elastic power density rather than the local stress or strain.

#### 4.4.1.4. Relation between damage factors as calculated by Miner's theory and the microplasticity theory

We will now derive the relation between the Miner's damage factor  $D_M$  and the absolute damage factor  $D$ . Assume that Miner's damage factor is calculated using an S-N curve corresponding to a fractile  $c$  of number of cycles to crack initiation and that this S-N curves have been obtained by tests on specimens of a certain size  $M_{exp}$ . In fact this relation is directly derived by rearranging Eq. (4.31a) as

$$D' = -(N_{ini,c_0}^{exp})^{-1} (\ln(1 - (1 - c)^{1/M_{str}}))^{-1} \quad (4.37a)$$

And observing that according to Palmgren-Miner rule the rate of Miner's damage factor increase is  $D'_M = (N_{ini})^{-1}$

Solving for  $D'$  we obtain

$$D' = -(\ln(1 - (1 - c_0)^{1/M_{exp}}))^{-1} D'_M \quad (4.37b)$$

and because the relation is linear it is also possible to express it in terms of damage factor as

$$D = -(\ln(1 - (1 - c_0)^{1/M_{\text{exp}}}))^{-1} D_M \quad (4.37c)$$

It is also possible to calculate the CDF of the value of Miner's damage factor at first initial crack formation  $D_{M,\text{ini}}$  by substituting Eq. (4.37c) in Eq. (4.30).

$$G_{D_{M,\text{ini}}} = P(D_{M,\text{ini}} < D_M) = 1 - \left(1 - \left(\frac{1}{1 - (1 - c_0)^{1/M_{\text{exp}}}}\right)^{-\frac{1}{D_M}}\right)^{M_{\text{str}}} \quad (4.38)$$

This is essentially the same equation as Eq. (4.30) with the only difference that Euler's number has been substituted by  $(1 - (1 - c_0)^{1/M_{\text{exp}}})^{-1}$

#### 4.4.2. Material properties

Since Palmgren-Miner rule and the proposed microplasticity theory consider the fatigue behavior of the material in a completely different way it is necessary that the sets of material parameters used with each of the two theories are equivalent between them so that the comparison be indeed meaningful. In order to ensure this equivalence the following approach is followed.

First a rib geometry and a surface hardness are specified. In this work these data are not obtained from measurements on the bars that are actually placed on the monitored structure but are taken from [24] for a typical contemporary quenched and tempered reinforcement bar in Switzerland. Then for this bar S-N curves for various nominal stress ratios are constructed according to the method presented in Section 2. The characteristics of the bar and the results of the calculations for S-N curve construction are summarized in **Table 4.2**. The constructed S-N curves are plotted as continuous lines in **Fig. 4.7** for various values of loading ratio  $\tilde{R}$ . These curves are assumed to give the median (0.5 fractile) of the constant amplitude fatigue crack initiation life and in Section 4.4.4 they are used without modification with Palmgren-Miner theory.

For the evaluation of the material parameters of the microplasticity model, the model is fitted to the above constructed S-N curves. In fact, during the calibration process, the model is iteratively used with varying input parameters in order to calculate the number of cycles required to reach a value of damage factor  $D_{\text{ini},0.5} = 0.104$  calculated from Eq. (4.32) by setting  $c = 0.5$  and  $M = M_{\text{exp}} = 10000$ .

The values of the microplasticity model material parameters as determined by the above calibration process are listed in **Table 4.3** while the S-N curves predicted by the microplasticity model after its calibration are plotted in dashed lines in **Fig. 4.7** against the constructed S-N curves. The good agreement between the corresponding curves suggests that the same material is being considered by the two methods. Hence, any difference in the calculated values of damage accumulation rate shall reflect the inclusion or not of the sequence effects.

**Table 4.2:** Rebar characteristics considered in the present application.

$H_V$ [N/mm <sup>2</sup> ]	$\sigma_u$ [N/mm <sup>2</sup> ]	$l_m$ [mm]	$\sigma_f$ [N/mm <sup>2</sup> ]	$\epsilon_f$	$b$	$c$	$K$ [N/mm <sup>2</sup> ]	$n$	$\phi$ [mm]	$h$ [mm]	$w$ [mm]	$\theta$ [°]	$r$ [mm]	$k_t$	$k_f$
265	860	0.017	1290	0.494	-0.087	-0.58	1334	0.15	16	0.8	3.5	47.5	0.2	2.795	2.543

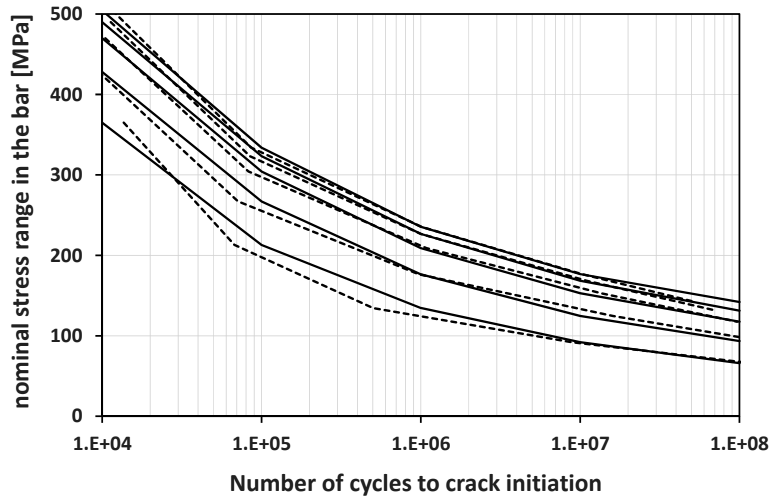


Fig. 4.7: Comparison of the constructed S-N curves (continuous lines) with the S-N curves obtained by the microplasticity model (dashed lines) after its calibration to the constructed S-N curves.

Table 4.3: Microplastic model material parameters obtained by model calibration to the constructed S-N curves.

$\alpha_u$ [GJ/m <sup>3</sup> ]	$\beta$	$\alpha_{my}$ [MJ/m <sup>3</sup> ]	$\gamma_I$	$\zeta_I$	$\eta_{m,I}$	$\lambda_{M,I}$	$\lambda_{C,I}$	$\mu_{M,I}$	$\mu_{C,I}$
104	0.85	1.32	1	1	0.39	1	1	0.65	0.08

#### 4.4.3. Input load history

##### 4.4.3.1. Artificial action effect histories

For the construction of the artificial time history the traffic action models for the train types specified in EN1991-2, Annex D [40] are used. These types are not combined in any of the mixes proposed in the same annex but in a mix that best represents the actual traffic mix passing on the bridge in terms of the number and type of trains. The characteristics of the used mix are summarized in **Table 4.4**. The order of passage of these trains has been chosen so as to reflect in general the actual order that is observed. In order to take into account the average effect of dynamic excitations on the damage accumulation rate, the axle loads of the above models are multiplied by a fatigue damage equivalent dynamic enhancement factor which is calculated according to [40]. For the structure at hand this factor equals to 1.229<sup>5</sup>. The dynamically enhanced traffic action models are sequentially applied to a FE model of the slab, taking into account the distribution of load through rails and ballast, and the one day-block-history of the principal bending moment at mid span is obtained. Finally, the calculated history is reduced to a sequence of moment variations (between local maxima (peaks) and local minima (valleys)) in order to reduce the volume of data.

##### 4.4.3.2. Action effect histories obtained from structural response monitoring

A monitoring campaign has been conducted during which the curvature variations of a 3.44 m short single span railway bridge have been recorded during the train passages for several consecutive months. From the curvature records the history of the principal bending moment at mid span is obtained by multiplying with the elastic sectional stiffness, which can be used in this case since the section is uncracked. These histories which were originally obtained at the monitoring frequency of 600Hz are reduced to sequences of moment variations and finally concatenated in a single block. This block includes the records of the train passages that occurred during a total of 156 days within a period of 7 months. These days are not

<sup>5</sup> According to EN1991-2, Annex D [40]  $K = v/160$  for  $L < 20$  m where  $v$  is the maximum permitted velocity in m/s and  $L$  is the determinant length in m; additionally,  $\varphi' = K/(1 - K + K^4)$ ,  $\varphi'' = 0.56\exp(-L^2/100)$  and  $AF_{fat} = 1 + 0.5(\varphi' + 0.5\varphi'')$ . For  $v = 27.89$  m/s (100 km/h) and  $L = 3.44$  m:  $AF_{fat} = 1.229$

consecutive. In fact the days during which the function of the monitoring was interrupted (so that some of the train passages in those day were not recorded) are omitted in order not to introduce bias in the representation of the traffic mixture.

**Table 4.4:** Traffic mix used in the calculations.

Type <sup>1</sup>	description	Number /day	mass of train [t]
2	Locomotive hauled passenger train	42	530
4	High speed passenger train	4	510
6	Locomotive hauled freight	2	1431
8	Locomotive hauled freight	4	1035
9	Suburban multiple unit train	42	296
12	Locomotive hauled freight	4	1135

<sup>1</sup>According to EN1991-2, Annex D

#### 4.4.3.3. Calculation of nominal stress histories

In a first step, the block history of the nominal stress in the principal tensile reinforcement is calculated from the moment histories obtained in Sections 4.3.3.1 and 4.3.3.2 under the assumption of a fully developed crack pattern (no contribution of concrete to the tensile force in the section) and linear elastic behavior of concrete. The following formula can be used for the above calculation

$$\tilde{\sigma}_{lin} = (1/A_s) \left( (M - N(h/2 - d_1)) / ((1 - \xi/3)d) + N \right) \quad (4.39)$$

$$\xi = \frac{nA_s}{d} \left( \sqrt{1 + \frac{2d}{nA_s}} - 1 \right)$$

$$n = E_s/E_c$$

Where  $M$  and  $N$  are the moment and axial force respectively,  $A_s$  is the reinforcement area per unit width of the slab,  $h$  and  $d$  are the depth and static depth of the cross-section respectively and  $d_1$  is the thickness of the cover of the tensile reinforcement; finally  $E_s$  and  $E_c$  are the moduli of elasticity for steel and concrete respectively. In reality however the relation between applied moment and stress in the reinforcement at the location of the crack is not linear. After the development of the crack pattern the roughness on the crack lips results in that during the unloading segments of the moment history, the lips of the crack begin to interact and transfer compressive stress in the cracked concrete zone at a bending moment higher or equal to the cracking moment. If unloading continues full contact is eventually established between the lips of the crack which means that for the rest of the unloading variation the cracked concrete zone behaves elastically in compression as if it were uncracked. Because the roughness on the crack lips creates a virtual residual deformation of the crack lip material, the elongation of the fibers of the cracked concrete zone when full contact is established is not zero which means that the strain in the tensile steel reinforcement is also higher than zero. After the establishment of full contact the decrease in the applied bending moment is mainly compensated, at the level of the cracked concrete zone, by an increase of the compressive stresses in concrete rather by a decrease of the tensile stress in the reinforcement which remains almost constant for the rest of the unloading variation. This concrete crack closure phenomenon results in that the stress ranges actually experienced by the reinforcement is lower than those calculated by Eq. (4.39). An acceptable simplification would be to ignore the crack lip interaction before full contact establishment and consider a lower bound in the stress of the tensile reinforcement imposed by the residual elongation of the cracked concrete zone fibers. This lower bound can be thought as a light prestress applied in a steel reinforcement segment between two successive mid-crack points by the residual elongation  $w_{res}$  occurring at the single crack that crosses the segment.

If the bond between reinforcement bars and surrounding concrete could be neglected, the strain along this segment of reinforcement would be constant and its residual value (corresponding to the above mentioned prestress) could be calculated by dividing the residual elongation of the fibers at the crack lips by the total length of this segment (since the relative displacement between steel and concrete can be assumed zero at the extremities of the segments A and B). Assuming regular spacing of the cracks, this length is equal to the distance between successive cracks. By assuming a small length  $2c$  around the crack where the reinforcement is completely free, the stabilized value of crack spacing can be calculated as:

$$l_{cs} = 2c + \frac{2}{4 \cdot 1.8} \phi / \rho_{\text{eff}} \quad (4.40)$$

The above formula is based on the model adopted by the *fib* Model Code 2010 [41] where the way to calculate  $\rho_{\text{eff}}$  can also be found. In this formula  $c$  is the thickness of the concrete cover and 1.8 is the ratio of the mean shear strength to mean tensile strength of concrete for stabilized crack stage.

In the above approach the greatest uncertainty lies in the determination of the residual concrete deformation at the lips of the crack. It is proposed that this value be calculated from the fracture properties of the concrete as a fraction of the crack width at the break-point of the softening curve of the concrete. On the basis of the experimental results presented in [42] this fraction is estimated between 1/3 and 2/3. It seems that the value of 1/3 can be used in all cases for calculating a conservative lower bound of the residual stress in the reinforcement

$$w_{\text{res}} = \frac{1}{3} G_{\text{F}} / f_{\text{t}} \quad (4.41)$$

$$\tilde{\sigma}_{\text{cl}} = E(w_{\text{res}} / l_{\text{eq}}) \quad (4.42)$$

The above calculations are summarized in **Table 4.5**. Hence, the nominal stress in the reinforcement is calculated as

$$\tilde{\sigma} = \tilde{\sigma}_{\text{lin}} \quad \text{if} \quad \tilde{\sigma}_{\text{lin}} \geq \tilde{\sigma}_{\text{cl}} \quad (4.43\text{b})$$

$$\tilde{\sigma} = \tilde{\sigma}_{\text{cl}} + \left(1 - \frac{\tilde{\sigma}_{\text{cl}}}{\tilde{\sigma}_{\text{lin}}}\right) \left(n(M/I)(h/2 - d_1) + n\left(\frac{N}{A}\right)\right) \quad \text{if} \quad \tilde{\sigma}_{\text{lin}} < \tilde{\sigma}_{\text{cl}} \quad (4.43\text{c})$$

where  $n$  is the ratio of steel modulus of elasticity to concrete modulus of elasticity.

It has to be noted that this is a rather simplified approach. A more rigorous method for calculating the stress variation in the reinforcement could be based on an advanced tension chord model as the one developed by Marti [46] and extended by Muttoni and Fernandez-Ruiz [47]. This issue is also treated by Koppitz [48].

Finally the above calculated stress is augmented by a factor of 1.20, as suggested by Schläfli [4], in order to take into account the additional bending of the bars which is not taken into account by the elastic section model.

In the case where stress histories are obtained from strain measurements on reinforcement bars themselves and at the location of a crack, then the above procedure including the above factor is obviously not required.

It has to be noted that the assumption of cracked section is not always realistic since very often such RC element remain uncracked under service conditions in which case it is very easy to show that the stress variations in the reinforcement are too small to be of any significance with respect to fatigue. Besides that, the amount of reinforcement ( $\emptyset 22/20 + \emptyset 18/20$ ,  $3171 \text{ mm}^2/\text{m}$ ,  $\rho = 1.057\%$ ) actually placed in the structure at hand is so large that the resulting stress ranges are very low ( $< 70 \text{ MPa}$ ) even if a cracked section is considered. Hence in order to render the application more meaningful, a reduced amount of reinforcement is considered. This amount is calculated, according to the methodology presented in Section 3, as the exact amount of reinforcement that is required for ensuring structural safety at the ULS of fracture or excessive deformation ( $(\emptyset 16/12.5$ ,  $1608 \text{ mm}^2/\text{m}$ ,  $\rho = 0.54\%$ ). Additionally, calculations are performed for the above amount of reinforcement increased by 1/3 ( $2144 \text{ mm}^2/\text{m}$ ,  $\rho = 0.71\%$ )



**Table 4.5:** Concrete crack closure variables

$\rho$	$\rho_{\text{eff}}$	$l_{\text{eq}}$ [mm]	$w_{\text{res}}$ [mm]	$\tilde{\sigma}_{\text{cl}}$ [MPa]
0.54%	2.68%	126	0.02	32
0.71%	3.57%	116	0.02	34

#### 4.4.3.4. Calculation of local work density histories for use with the proposed microplasticity theory

For the application of proposed microplasticity model the nominal stress histories calculated in Section 4.4.3.3 need to be further pre-processed in order to obtain the history of the applied local distortional and volumetric work density. Assuming uniaxial stress conditions these are calculated as

$$\Delta w_i^d = k_f^2 (\tilde{\sigma}_i^2 - \tilde{\sigma}_{i-1}^2) / (6G) \quad (4.44a)$$

$$\Delta w_i^v = k_f^2 (\tilde{\sigma}_i^2 - \tilde{\sigma}_{i-1}^2) / (6B) \quad (4.44b)$$

where  $i$  count the stress variations,  $\tilde{\sigma}_i$  is the nominal stress at the end of variation  $i$ , and  $G$  and  $B$  are the shear and bulk modulus respectively. For each step it is additionally required as input the sign (+1 or -1) of the equivalent local elastic strain energy. This sign is conventionally taken equal to the sign of the local volumetric stress which for the present example coincides with the sign of  $\tilde{\sigma}_i$ . It is easy to verify that the stress conditions are uniaxial by examining the stress plots of **Fig. 4.1**.

#### 4.4.4. Results and discussion

In **Fig. 4.8** the evolution of the damage factor as calculated by the microplasticity theory for both monitoring and artificial nominal stress histories and for both the case where all train types are included in the history and the case where only freight trains are included. Each plot shows the evolution of the damage factor for 10 successive blocks. It is reminded that each block corresponds to one day of traffic for the case of artificial histories and to 156 days for the case of monitoring histories. Also because the horizontal axes count the successive half cycles (load transitions) these axes are not directly comparable between them. It can be seen that the damage increment per block almost stabilizes after the first block. This is because in the calculation method the effect of damage itself in the damage accumulation rate is not taken into account (damage production depends only on plasticity). The fact that the block used in the analysis is necessary limited introduces a certain bias.

In order to compare the results of the calculations the average damage factor increment per day is used. For the monitoring histories this average increment is taken by simply dividing the stabilized damage factor increment per block by the number of traffic days to which this block corresponds; for the artificial histories, it is simply taken as the stabilized damage factor increment per day-block.

For the calculation according to Miner's theory the block histories are transformed to equivalent stress range histograms for which Eq. (4.36) is applied. It has to be noted that the S-N curve, which is used with Palmgren-Miner rule, is derived (according to Section 4.2) for a nominal stress ratio  $\tilde{R} = 0.175$  which corresponds better to the monitoring and artificial stress histories than the standard value of  $\tilde{R} = 0.1$ . Also for these calculations a bilinear approximation of the S-N curve is used with the second branch assumed to extend to infinite number of cycles. It is interesting to note that when the calculations were repeated for using a trilinear approximation with a softer slope after  $10^7$  cycles, almost identical results were obtained. The Miner's damage factor increment per block is transformed to ordinary damage factor increment by using Eq. (4.37c) in order to compare Miner's results with microplasticity results. Again the damage per monitoring block (156 days) is divided by the number of days in order to obtain an equivalent damage factor increment per day. The above average damage factor increment rate results are summarized in **Table 4.6**.

In **Fig. 4.9** the damage factor increase rate, calculated according to the various methods and assumptions of **Table 4.6** but for values of the dynamic enhancement factor (used with the artificial histories) varying between 1.00 and 1.40, is plotted.

**Table 4.6:** Damage factor increment rate according to the various calculations methods and assumptions.

$\dot{D}$ [ $10^{-6}$ day $^{-1}$ ]			all train types				only freight trains			
			microplasticity		Palmgren Miner		microplasticity		Palmgren Miner	
			monitor.	artificial	monitor.	artificial	monitor.	artificial	monitor.	artificial
			1	2	3	4	5	6	7	8
with crack closure effect	$\rho = 0.536\%$	a	0.70	1.57	0.89	2.58	0.67	1.45	0.58	2.28
	$\rho = 0.715\%$	b	0.032	0.034	0.073	0.25	0.033	0.100	0.052	0.231

By examining the above results, the following conclusions can be drawn:

- The use of the microplasticity method with monitoring data shows that the contribution of freight trains alone to damage factor rate amounts to around 90% of the total contribution of all train types (compare columns 1 and 5 of **Table 4.6**). On the other hand, the combination of monitoring histories with the Palmgren-Miner rule gives a freight train damage contribution of just 65%-70% (columns 3 and 7 of **Table 4.6**); this suggests that the contribution of the lighter passenger trains may be in some cases overestimated by Palmgren-Miner rule. Additionally, comparison of columns 5 and 7 shows that in some cases the use of Palmgren-Miner rule with monitoring histories slightly underestimates the contribution of freight trains.
- Despite the above observations, when all train types are taken into account, the results obtained by the Palmgren-Miner rule are always less favorable than those obtained by the microplasticity theory.
- The use of the monitoring history results always in significantly lower damage factor increment rates (27% according to both calculation methods). This conservatism resulting from the use of artificial histories is mainly due to the prescribed value of the average dynamic enhancement factor being slight higher than its actual value for the present case. This is absolutely reasonable since the prescribed value intends to cover the uncertainty related to the dynamic effects in different types of structures. The advantage of using monitoring signals over artificial signal lies mainly in the more accurate representation of dynamic effects in the verification.

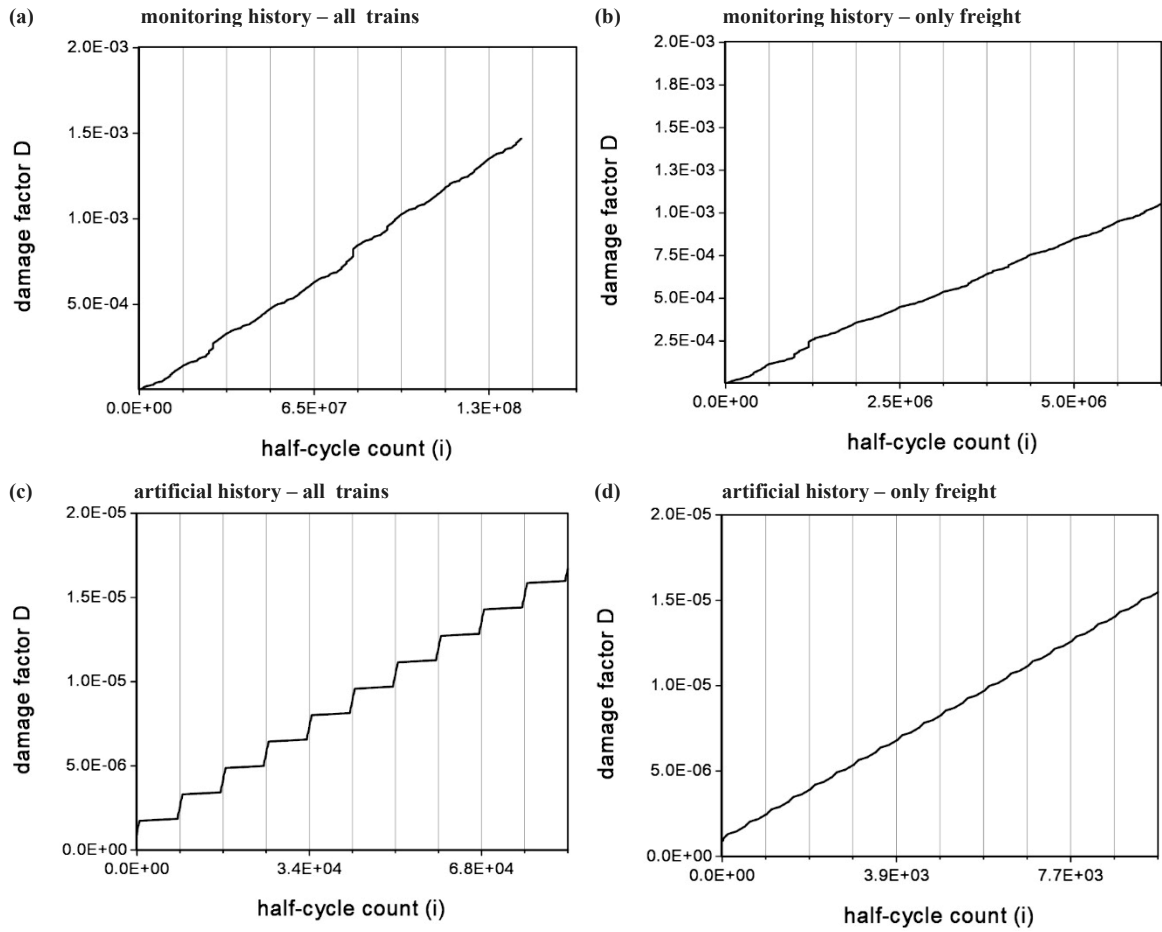


**Fig. 4.8:** Damage factor evolution calculated by the microplasticity theory for 10 successive stress history blocks acquired by different methods and assumptions. Blocks are defined by vertical gridlines. Note that for monitoring histories each block corresponds to the monitoring period of 156 days while for artificial histories each block correspond to 1 day.

## 4.5. Reliability of a single bar

### 4.5.1. Reliability with respect to formation of the first initial crack

From the above it results that if the time scale is taken sufficiently large (multiples of one year) and if the general traffic conditions remain invariable, damage factor increase can be considered linear with time. In that case Eq. (4.30) may be written as

$$G_{t_{ini}} = P(t_{ini} < t) = 1 - (1 - e^{-1/\dot{D}t})^{M_{str}} \quad (4.45)$$

where  $\dot{D}$  is assumed constant. Under the above assumptions Eq. (4.45) represents in fact the CDF of the time to formation of the first initial fatigue crack. In order to ensure adequate safety (with respect to formation of an initial crack) from a socioeconomic point of view, the probability of Eq. (4.45) should be compared to a maximum accepted cumulative probability of failure prescribed for the entire service-life of the structure independently of its actual duration [43].

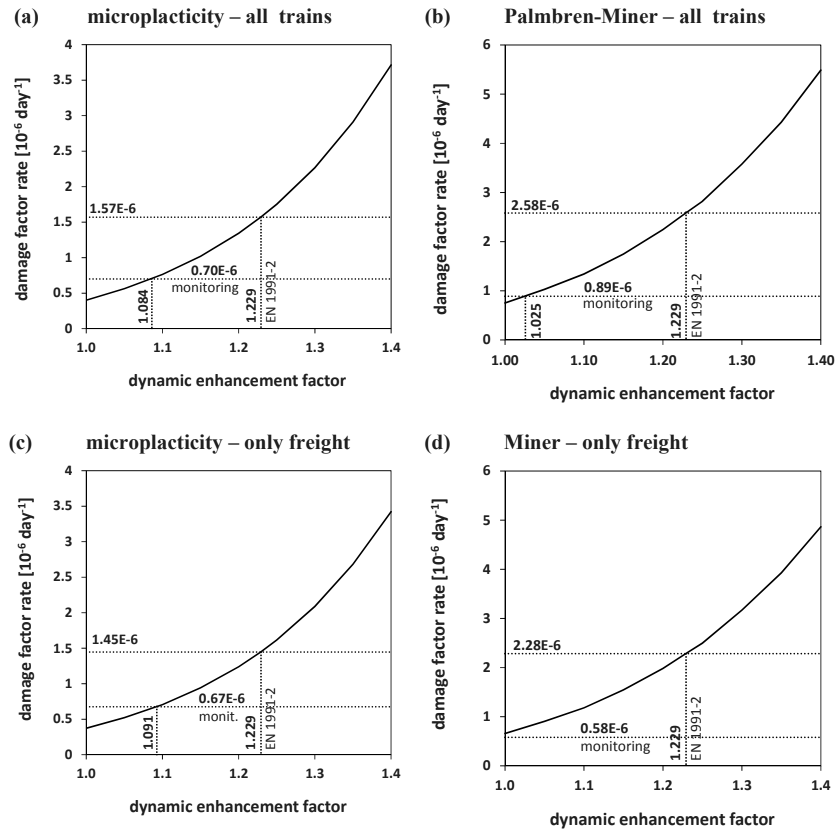


Fig. 4.9 : Damage factor increase rate vs dynamic amplification factor for  $\rho = 0.536\%$  with concrete crack closure effect, predicted after various calculations methods and assumptions.

The comparison determines the maximum period during which the safety requirements are satisfied from a socioeconomic point of view without intermediate verification of the integrity of the bars. Although such a maximum accepted probability of failure is not explicitly specified in most standards, the probability that correspond to the target reliability index of 3.8 mentioned in [44] for a period of 50 years is taken here as a reference<sup>6</sup>. The durations of safe service life that result using the above comparison are listed in **Table 4.7**.

It is also possible to calculate the PDF of the time to formation of an initial crack as

$$g_{t_{ini}}(t) = P(t - dt/2 < t_{ini} < t + dt/2) = \frac{M_{str}}{Dt^2} (1 - e^{-1/\dot{D}t})^{M_{str}-1} e^{-1/\dot{D}t} \quad (4.46)$$

The initial part of these PDFs are plotted in **Fig. 4.10** for some of the same cases of **Table 4.7**.

Again, the probability density of Eq. (4.45) should be compared to a maximum accepted failure probability density (probability “per unit of time”) in order to ensure adequate safety (with respect to formation of an initial crack) from the human individual point of view [43]. Here the probability corresponding to a target reliability index of 4.7 for a period of one year [44] is taken as the maximum accepted failure probability density. The durations of safe service life that result using the above comparison are also listed in **Table 4.7**. It is interesting to note that the human individual safety criterion results in shorter durations of safe-service life than the socioeconomic safety criterion.

The reason for which fatigue safety should be checked using *both* a socioeconomic criterion (defined by a target failure probability for the entire service life) and a personal safety criterion (defined by an annual failure probability) is because, contrary to failures due to extreme action effects, fatigue failures do not have

<sup>6</sup> In general the target reliability index should be calculated after appropriate consideration of the involved risk using for example the method prescribed in the Swiss standard for existing structures [45].

the same annual probability for all the years in the service life of an element. Obviously the a priori probability of fatigue failure in the first year of the life of an element is much lower than the a priori probability of failure in the 50<sup>th</sup> (for example) year of its life. It is also obvious that the personal safety criterion should be satisfied even for the last year of the service life of the element. As a matter of fact, it is not possible to establish a unique relation between an annual target probability of failure and a target probability of failure for the entire service life. This relation varies from case to case and depends on the value of the mean damage factor increase rate.

Finally, if at a certain moment  $t_0$  it is possible to assert that a crack has not yet formed, the probability that a crack will initiate the immediately following period  $\Delta t$  is given as

$$G_{\Delta t_{\text{ini}}}(\Delta t; t_0) = P(\Delta t_{\text{ini}} < \Delta t | \Delta t_{\text{ini}} > 0) = (G_{t_{\text{ini}}}(t_0 + \Delta t) - G_{t_{\text{ini}}}(t_0)) / (1 - G_{t_{\text{ini}}}(t_0)) \quad (4.47)$$

In this way it is in theory possible to take into account the outcome of a detailed intermediate examination. Of course in the cases considered here the usefulness of Eq. (4.47) is very limited because (a) it is usually very difficult to assert that an initial crack has not formed on the reinforcement bars of an existing structure and (b) for small failure probabilities Eq. (4.47) gives practically the same results as Eq. (4.45).

#### 4.5.2. Reliability with respect to failure taking into account the CAFL

As discussed in Section 4.2.4, crack initiation is a necessary but not sufficient condition for failure of a bar. Following the paradigm of D'Angelo and Nussbaumer [31] (in a different formulation more adapted to the present problem), it is assumed that the probability that the bar fails before a given moment  $t$  is given by the integral from 0 to  $t$  of the PDF of the time of formation of the initial crack  $t_{\text{ini}}$  times the probability that *after* crack formation at  $t_{\text{ini}}$  and before  $t$  an exceedance of the CAFL takes place. It should be noted here that a CALF exceedance within a certain stress history of finite duration is defined as the fact that the difference between the maximum and the minimum stress value within the entire history exceeds the CAFL  $\Delta\tilde{\sigma}_0$ . However, if a sufficiently large time scale is used, the minimum value  $\tilde{\sigma}_{\text{min}}$  in a nominal stress history tends to be deterministic and independent from the duration of the history contrary to the maximum value which is random and depends on history duration. Hence the CDF of the time to bar failure  $t_f$  is given by

$$G_{t_f} = P(t_f < t) = \int_0^t g_{t_{\text{ini}}}(\tau) \left(1 - (G_{\tilde{\sigma}}(\Delta\tilde{\sigma}_0 - \tilde{\sigma}_{\text{min}}))^{\hat{N}_{t1}(t-\tau)}\right) d\tau \quad (4.48)$$

where, following the concepts presented in Section 3.5,  $G_{\tilde{\sigma}}$  is the CDF of the maximum value of nominal stress  $\tilde{\sigma}$  per freight train passage (type-1 incident),  $\hat{N}_{t1}$  is the rate of occurrence of type-1 incidents and  $\tau$  is the symbol used for the integration variable. If one wishes to consider also the uncertainty in the actual value of the fatigue limit, he may consider a probability distribution for  $\Delta\tilde{\sigma}_0$  characterized by a PDF  $f_{\Delta\tilde{\sigma}_0}$ . In that case Eq. (4.48) becomes

$$G_{t_f} = P(t_f < t) = \int_0^t g_{t_{\text{ini}}}(\tau) \left(1 - \int_{-\infty}^{\infty} g_{\Delta\tilde{\sigma}_0}(s) (G_{\tilde{\sigma}}(s - \tilde{\sigma}_{\text{min}}))^{\hat{N}_{t1}(t-\tau)} ds\right) d\tau \quad (4.49)$$

For the monitoring data of the present application  $G_{\tilde{\sigma}}(s - \tilde{\sigma}_{\text{min}})$  has already been derived in Sections 3.5 and 3.6, as the CDF of the maximum value of force in the tensile reinforcement per type-1 incident. More precisely,  $G_{\tilde{\sigma}}$  can be calculated by Eq. (3.26) using  $1 - G_{\tilde{\sigma}}$  instead of  $p^*$  and  $(s - \tilde{\sigma}_{\text{min}})A_s$  instead of  $F_{Q1,e}$  and solving for  $G_{\tilde{\sigma}}$ . This gives

$$G_{\tilde{\sigma}}(s - \tilde{\sigma}_{\text{min}}) = 1 - \hat{\zeta}_{t1} \exp \left[ - \frac{\frac{(s - \tilde{\sigma}_{\text{min}})A_s}{\gamma_{\text{IGN}}} \lambda}{\hat{\tau} (1 + \kappa_a / \sqrt{n_{\text{th}}})} \right] \quad (4.50)$$

All the parameters in the above equation have been calculated or specified in **Tables 3.2** and **3.4**.

The probability distribution of the fatigue limit is taken here as a normal distribution. The mean value of the distribution is calculated by the method presented in Section 4.2.4, while the standard deviation needs to be determined on the base of experimental results. For the present application it is assumed that the standard

deviation is independent of the mean value and it will be roughly approximated as the sample standard deviation of the difference between predicted and experimental value for the experimental results of Zheng and Abel [25] also presented in Section 4.2.4. On the bases of this approximation a value of 15MPa is accepted.

The integrals of Eq. (4.49) are calculated numerically using a Fortran routine for discrete values of time from 1 to 1000 years. The resulting CDF of the time to failure is subsequently differentiated numerically in order to calculate the PDF. In Fig. 4.10 the PDFs calculated taking into account the probability of CALF exceedance is compared to the PDFs calculated above. The comparison shows that considering the probability of failure instead of the probability of initial crack formation allows the extension of the safe service life by up to 150%.

It has to be noted that in the above calculations, we are exploiting the fact that CAFL exceedances are rather rare events in this type of loading. So probably there will be a considerable time laps between the formation of the initial crack and the first CAFL exceedance after its formation. It is exactly this time laps that we are taking advantage of. After the first CAFL exceedance we assume that the crack starts to propagate with increasing rate and we consider this point in time as the conventional bar failure time. This is not the case in constant amplitude loading under which an initial crack after its formation either propagates very quickly until final failure or it does not propagate at all depending on whether the stress range (which is repeated in each cycle) exceeds the CAFL or not.

**Table 4.7:** Safe service life for  $\rho = 0.536\%$  predicted after various calculations methods and assumptions.

safe service life [years]		all train types				only freight trains				
		microplasticity		Palmgren Miner		microplasticity		Palmgren Miner		
		monitor.	artificial	monitor.	artificial	monitor.	artificial	monitor.	artificial	
with crack closure effect	NO	social criter.	228	101	179	61	236	110	275	69
	CAFL	personal criter.	209	89	162	53	217	97	255	61
	CAFL	social criter.	348	155	274	95	361	168	518	107
		personal criter.	328	136	253	80	341	147	509	91

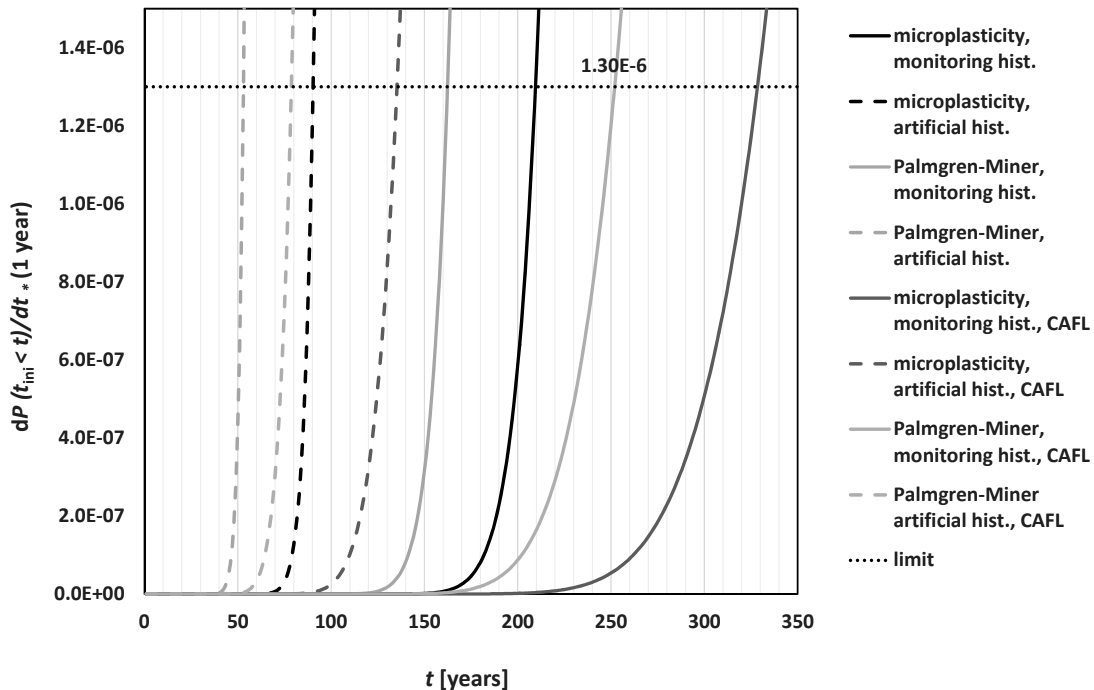


**Fig. 4.10:** PDF of the time to formation of the initial crack for  $\rho = 0.536\%$  with concrete crack closure effect and with all trains included in the history.

#### 4.6. Conclusions

A number of advancements in the current state of the art in fatigue safety verification of existing RC elements has been developed and applied in the case of short span RC slab subject railway traffic. These advancements combined constitute an integrated novel and theoretically consistent approach to this problem.

In particular:

- By means of the theory of fatigue of notched components it is possible to construct (calculate) case specific S-N curves and CAFLs in good agreement with experimental results. Further development and validation of the method may however be needed before its practical application.
- Consideration of a probabilistic size effect results in an increase by approximately 20% of the median fatigue resistance of reinforcement bars embedded in concrete compared to those teste in air.

Additionally for the present case it has been found that:

- The use of nominal stress histories obtained from monitoring data, instead of artificial stress histories calculated from standard load models, results in an increase of the predicted safe service life by up to 230%.
- The use of the advanced statistical microplasticity model results also in an increase of the predicted safe service life by up to 130%.

#### 4.7. References

- [1] CEB, Comité euro-international du béton. Fatigue of concrete structures - state of the art report, bulletin d'information No 188. Lausanne; 1988.
- [2] Herwig A. Reinforced concrete bridges under increased railway traffic loads – fatigue behavior and safety measures [dissertation]. Lausanne: Ecole Polytechnique Fédérale de Lausanne; 2008.
- [3] Salah el din AS, Lovegrove JM. Fatigue of cold worked ribbed reinforcing bar—a fracture mechanics approach. *Int J Fatigue*. 1982;4(1):15-26.
- [4] Schläfli M, Brühwiler E. Fatigue of existing reinforced concrete bridge deck slabs. *Engng Structures*. 1998;20(11):991-998.
- [5] Meggiolaro MA, Castro JTP. Statistical evaluation of strain-life fatigue crack initiation predictions. *Int J Fatigue*. 2004;26(5):463-476.
- [6] Troshchenko VT, Khamaza LA. Strain–life curves of steels and methods for determining the curve parameters. Part 1. Conventional methods. *Strength Mater*. 2010;42(6):647-659.
- [7] Hartman D. Robust model for fatigue life estimation from monotonic properties data for steels [dissertation]. Waterloo: University of Waterloo; 2013.
- [8] Roessle ML, Fatemi A. Strain-controlled fatigue properties of steels and some simple approximations. *Int J Fatigue*. 2000;22(6):495-511.
- [9] Baumel Jr A, Seeger T. Materials data for cyclic loading. Supplement 1. Amsterdam: Elsevier Science; 1990.
- [10] Pavlina EJ, Van Tyne CJ. Correlation of Yield Strength and Tensile Strength with Hardness for Steels. *J Mater Engng Perform*. 2008;17(6):888-893.
- [11] Glinka G. Calculation of inelastic notch-tip strain-stress histories under cyclic loading. *Eng Fract Mech*. 1985;22(5):839-854.
- [12] Taylor D. Geometrical effects in fatigue: a unifying theoretical model. *Int J Fatigue*. 1999;21(5):413-420.
- [13] Susmel L, Taylor D. Two methods for predicting the multiaxial fatigue limits of sharp notches. *Fatigue Fract Eng M*. 2003;26(9):821-833.
- [14] Susmel L. A unifying approach to estimate the high-cycle fatigue strength of notched components subjected to both uniaxial and multiaxial cyclic loadings. *Fatigue Fract Eng M*. 2004;27(5):391-411.
- [15] Lazzarin P, Zambardi R. A finite-volume-energy based approach to predict the static and fatigue behavior of components with sharp V-shaped notches. *Int J Fracture*. 2001;112(3):275-298.
- [16] Berto F, Lazzarin P. A review of the volume-based strain energy density approach applied to V-notches and welded structures. *Theor Applied Fract Mec*. 2009;52(3):183-194.
- [17] El Haddad MH, Smith KN, Topper TH. Fatigue Crack Propagation of Short Cracks. *J Eng Mater-T ASME*, 1979;101(1):42-46.
- [18] Hertzberg R. A simple calculation of DA/DN-ΔK data in the near threshold regime and above. *Int J Fracture*. 1993;64(3):R53-R58.
- [19] Glinka G, Newport A. Universal features of elastic notch-tip stress fields. *Int J Fatigue*. 1987;9(3):143-150.
- [20] Filippi S, Lazzarin P, Tovo R. Developments of some explicit formulas useful to describe elastic stress fields ahead of notches in plates. *Int J of Solids Struct*. 2002;39(17):4543-4565.
- [21] Lazzarin P, Tovo R, Meneghetti G. Fatigue crack initiation and propagation phases near notches in metals with low notch sensitivity. *Int J of Fatigue*. 1997;19(8–9):647-657.
- [22] Nieslony A, Dsoki C, Kaufmann H, Krug P. New method for evaluation of the Manson–Coffin–Basquin and Ramberg–Osgood equations with respect to compatibility. *Int J Fatigue*. 2008;30(10–11):1967-1977.
- [23] Cahoon JR, Broughton WH, Kutzak AR. The determination of yield strength from hardness measurements. *Metall Trans*. 1971;2(7):1979-1983.
- [24] Zheng H, Abel A. Stress concentration and fatigue of profiled reinforcing steels. *Int J Fatigue*. 1998;20(10):767-773.
- [25] Zheng H, Abel A. Fatigue Properties of Reinforcing Steel Produced by TEMPCORE Process. *J Mater Civil Eng*. 1999;11(2):158-165.

- [26] Rocha M. Fatigue Behaviour of Steel Reinforcement Bars at Very High Number of Cycles [dissertation]. Lausanne: Ecole Polytechnique Fédérale de Lausanne; 2014.
- [27] Pereira HFSG, De Jesus AMP, Ribeiro AS, Fernandes AA. Fatigue Damage Behavior of a Structural Component Made of P355NL1 Steel Under Block Loading. *J Press Vess-T ASME*. 2009;131(2):021407-021407.
- [28] Tanaka K, Nakai Y, Yamashita M. Fatigue growth threshold of small cracks. *Int J Fracture*. 1981;17(5):519-533.
- [29] Hirt MA, Bez R, Nussbaumer A. Construction métallique, Notions fondamentales et méthodes de dimensionnement, *Traité de Génie Civil* vol. 10. Lausanne: Presses polytechniques et universitaires romandes; 2006. p. 442-460
- [30] Pecker E. Extended numerical modeling of fatigue behavior [dissertation]. Lausanne: Ecole Polytechnique Fédérale de Lausanne; 1997.
- [31] D'Angelo L, Nussbaumer A. Reliability based fatigue assessment of existing motorway bridge. *Struct Saf*. 2015;57:35-42.
- [32] Kühn B, Lukić M, Nussbaumer A, Günther HP, Helmerich R, Herion S, Kolstein MH, Walbridge S, Androic B, Dijkstra O, Bucak Ö. Assessment of Existing Steel Structures: Recommendations for Estimation of Remaining Fatigue Life. Joint report EUR 23252 EN – 2008 JRC European Commission.
- [33] Grigoriou V, Brühwiler E. Probability of observable flaw initiation at high cycle fatigue. *Eng Fract Mech*. 2015; in press, accepted manuscript, available online 27 May 2015.
- [34] Cheng G, Plumtree A. A fatigue damage accumulation model based on continuum damage mechanics and ductility exhaustion. *Int J Fatigue*. 1998;20(7):495-501.
- [35] Sun B, Yang L, Guo Y. A high-cycle fatigue accumulation model based on electrical resistance for structural steels. *Fatigue Fract Eng M*. 2007;30(11):1052-1062.
- [36] Mesmacque G, Garcia S, Amrouche A, Rubio-Gonzalez C. Sequential law in multiaxial fatigue, a new damage indicator. *Int J Fatigue*. 2005;27(4):461-467.
- [37] Lynn AK, DuQuesnay DL. Computer simulation of variable amplitude fatigue crack initiation behaviour using a new strain-based cumulative damage model. *Int J Fatigue*. 2002;24(9):977-986.
- [38] Lemaitre J, Sermage JP, Desmorat R. A two scale damage concept applied to fatigue. *Int J Fracture*. 1999;97(1-4):67-81.
- [39] Desmorat R, Kane A, Seyedi M, Sermage JP. Two scale damage model and related numerical issues for thermo-mechanical High Cycle Fatigue. *Eur J Mech A-Solid*. 2007;26(6):909-935.
- [40] CEN. Annex D: Basis for the fatigue assessment of railway structures in EN 1991-2:2003: Eurocode 1: Actions on structures - Part 2: Traffic loads on bridges,. Brussels: European Committee of Standardisation; 2003.
- [41] *fib. fib* Model code for concrete structures 2010 – 7 Design: Berlin: Ernst & Sohn; 2010.
- [42] Reinhart HW, Cornelissen HAW, Hordijk DA. Tensile tests and failure analysis of concrete. *J Struct Eng*. 1986;112(11):p.2462-2477.
- [43] Steenbergen RDJM, Vrouwenvelder ACWM. Safety philosophy for existing structures and partial factors for traffic loads on bridges. *HERON*. 2010;55(2):123-139.
- [44] CEN. EN 1990:2002: Eurocode – Basis of structural design. Brussels: European Committee of Standardisation; 2002.
- [45] SIA. SN 505 269: Existing structures –Bases. Zurich: Swiss Society of Engineers and Architects; 2011.
- [46] Marti P, Alvarez M, Kaufmann W, Sigrist V. Tension Chord Model for Structural Concrete. *Struct Eng Int*. 1998;8(4):287-298.
- [47] Muttoni A, Fernandez Ruiz M. Concrete Cracking in Tension Members and Application to Deck Slabs of Bridges. *J Bridge Eng*. 2007;12(5):646-653.
- [48] Koppitz R. Effect of Deformation History on Punching Resistance of Reinforced Concrete Slabs [dissertation]. Lausanne: Ecole Polytechnique Fédérale de Lausanne; 2015.



## **Conclusions and outlook**



## 5.1. Main contributions and findings

With respect to the objectives set in the introduction of this document (Section 0.4), the following contributions and findings have resulted from this research work.

### 5.1.1. Resistance side

1. *Energy based definition of damage.* During the crack initiation phase fatigue evolution is macroscopically described (at the RVE level) by the observable value of the internally blocked strain energy density. This quantity can be considered as the definition of the observable damage variable. It has been shown why this observable value should not be interpreted as the actual value but merely as the mathematical expectation of the actual but unobservable value of internally blocked strain energy density on which the stability of the RVE (with respect to fracture) depends. The observable value of the damage factor is defined as the ratio of the observable value of the internally blocked strain energy density over the (deterministic) ultimate value of this energy density that corresponds to fracture of the RVE.

2. *Damage and reliability.* The fundamental relation between the observable (calculated) value of damage factor and the reliability at the level of a RVE has been derived from the principle of maximum entropy. It has been shown that this relation can be expressed as a standard Fréchet distribution.

3. *Statistical microplasticity model.* The observable value of internally blocked strain energy density increase rate is assumed a constant fraction of the inelastic work-per-volume rate whose evolution is calculated by means of a statistical microplasticity model is developed. The model is formulated entirely in terms of energy density and is based on the statistical simulation of the behavior of a hierarchically organized population of elastic – perfectly plastic microsystems. Adopting the principle of strain energy equivalence, the power density applied at the RVE is assumed distributed over the classes of the population according to their characteristic power concentration factor. The frequency of microsystems as a function of their power concentration factor is modeled by a gamma distribution at each level of hierarchy. The above features make this model particular suitable for damage evolution calculation in the case of components with geometrical stress raisers (notches, ribs etc.) working mainly in their quasi-linear-elastic domain.

4. *Calculation of case specific S-N curves.* By means of the theory of fatigue of notched components, which has been enriched and adapted for the case of ribbed bars, and using as input only the surface hardness of the reinforcement bars and the geometry of their ribs, it is possible to construct (calculate) case specific S-N curves and CAFLs in good agreement with experimental results. In the case of examination of existing structures the above case specific S-N curves and CAFLs can be used instead of the generic ones prescribed by design codes, eliminating in this way the conservatism originating from the fact that code prescription are based on samples of bars with highly varying material properties and geometric characteristics. These curves can also be used for calibration of the above presented energy model which can subsequently be used with any general action effect history.

5. *“Size” effect.* The proposed method for case specific S-N curve and CAFL calculation takes fully account of both the fracture mechanics and the probabilistic “size” effect on fatigue resistance of steel reinforcement bars embedded in concrete. Both these effects have a favorable influence on calculated reliability. The fracture mechanics “size” effect is taken into account in the framework of the theory of fatigue of notched components by considering a material characteristic volume (or length), while the probabilistic “size” effect is taken into account by considering the number of potential locations of first crack formation and using the fundamental relation between observable damage factor and reliability expressed previously as a Fréchet distribution.

### 5.1.2. Action effect side

6. *Curvature variation monitoring.* A novel monitoring scheme base on the monitoring of curvature variations and oriented towards RC slabs is developed. Compared to direct measurement of strain variation on the reinforcement bars, this scheme results in a more complete representation of the strain profile at the section level and to an easier interpretation of the results in the context of safety verifications at the ULS

of fracture. The proposed monitoring scheme gives results of acceptable accuracy and precision but the device itself needs some improvement in order to further reduce its free vibrations and eliminate electromagnetic interference so as to achieve more clear signals and be able to have accurate data even in high frequencies. The monitoring results show that even for the simple case of a simply supported slab subject to very well defined loads, detailed structural analysis fails to represent accurately the behavior of the slab. This observation demonstrates the importance of structural response monitoring for a realistic determination of structural demand at an element level, especially in the cases where there is considerable interaction between structural and non-structural elements.

7. *Monitoring based safety verification.* A semi-probabilistic format for safety verification at the ULS of fracture using exclusively SRM data has been developed and applied in the above case. This format can be used directly for determining action effect examination values. For the probabilistic modeling the action effect maxima per incident (train passage) are considered while the determinant population of incidents is identified semi-heuristically. The random statistical error due to the finite duration of the monitoring period (finite number of recorded determinant incidents) is formally taken into account into the examination value of the action effect by means of a confidence upper bound. On the other hand, monitoring should be preferably applied for a minimum duration of 1 year (independently of the number of recorded determinant incidents) so as to avoid bias originating from indirect seasonal temperature effects, while a heuristic ignorance factor should be included for the random statistical error due to these seasonal variations. In this application the distribution of the determinant action incident effect instances can be modeled excellently by a shifted exponential distribution.

### 5.1.3. Reliability calculation

8. *Reliability consequences of load sequence effects.* By a practical application in the case of a short span RC slab railway bridge on which a monitoring campaign has been performed, it has been shown that: (a) The use of nominal stress histories obtained from monitoring data, instead of artificial stress histories calculated from standard load models, results in an increase of the predicted safe service life by up to 230%. (b) The use of the advanced statistical microplasticity model results also in an increase of the predicted safe service life by up to 130%. (c) In the application of Palmgren-Miner rule the use of S-N curves for load ratios  $\tilde{R}$  representative of the actual loading history is essential. (d) Fatigue safety verification should be based on a specified maximum accepted value of failure probability density (i.e. probability per unit of time) instead of a failure probability over the entire service life, since the former criterion gives slightly less favorable safe service life predictions than the later.

9. *Damage accumulation and CAFL.* The evolution of reliability at the level of a single reinforcement bar is calculated taking into account the existence of a CAFL. The key concept in this calculation is that, in the case of ribbed reinforcement bars, the existence of a CAFL originates from the fact that *once* a macroscopic crack has been formed this crack will not start to propagate until at least one CAFL exceedance occurs. In fact according to the proposed approach, the CAFL does not affect in any way the damage accumulation process before the formation of an initial crack (since the CAFL itself refers to the non-propagation of an existing crack), while after the initial crack formation the damage accumulation process, in the way defined in this work, ceases to exist. The combined consideration of damage accumulation and CAFL results in an increase of the predicted safe service life by up to 160%.

## 5.2. Outlook

This work proposes a more insightful and more precise approach to fatigue safety verification of steel reinforcement in existing RC structural elements. The primer concern in the development of this approach has been the rational and systematic treatment of the various kinds of uncertainty interfering in both the action effect and the resistance aspect of the problem. Hence, in order to reduce, on the one hand, the uncertainty that can possibly be reduced (epistemic uncertainty), a series of examination methods has been developed for extracting, from the structural element itself, as much information as possible and incorporating it into the verification procedure. On the other hand, the uncertainty that cannot be reduced – the inherent randomness of the phenomenon – is taken into account in a theoretically consistent way. From the

author's point of view, clear physical origin and theoretical consistency of the used probability distributions is of paramount importance in the calculation of structural reliability and should be prioritized over fitness of the distributions to experimental data, especially when the reliability requirements involve extremely small, quasi-nominal, failure probabilities as it is the case in structural safety verifications.

In general, the findings of this work provide scientific support to the empirical conclusion that fatigue deterioration of railway bridge RC elements might raise safety issue only in cases where large freight traffic volumes are combined with low reinforcement ratios which ensure barely sufficient safety against fracture ULS.

### 5.3. Further work

It is in the experimental direction that the author sees possible improvements and advancements of the work presented in this thesis. In the framework of a future research program, work motivated by the conclusions of this thesis could be undertaken in the following domains.

1. *Experimental investigation of the stress variations in the reinforcement embedded in cracked elements under service load conditions.* The phenomenon of concrete crack closure affects significantly the nominal stress history in the reinforcement and deserves further investigation. Such investigation can be performed by monitoring of existing RC elements that present a developed pattern of bending cracks under real service conditions. Strain variations should be measured directly on the bars at the location of active cracks and with particular care in removing the concrete cover over the minimum possible area. Alternatively, experiments could be carried out in the laboratory using pre-cracked RC elements and loading protocols constructed on the basis of action effect histories recorded on existing structures. In this case sensors can be installed along the reinforcement bars before casting of the concrete so that distortion induced by the concrete cover removal will be avoided.

2. *Very long term monitoring for revealing the statistical characteristics of the indirect seasonal effect on traffic action effect.* Although a detailed investigation of seasonal effects has not been performed in this work, the examination of the monitoring data supports the conclusion of other researchers that indirect seasonal effects have a small but significant impact on predicted reliability for both the ULS of fracture and fatigue. Results from very long term monitoring (several years) will certainly improve the quality of the predictions. For such applications several technological issues mainly related to the durability of sensors and the management of very large volumes of monitoring data need to be addressed.

3. *Concerning the microplasticity model, a more systematic method for determining the required material properties needs to be developed.* The development of such method should probably include both a theoretical consideration of microstructural mechanisms and experimental investigation on structural components with geometric stress raisers.

Despite the large room for improvement that still remains in the domain of fatigue safety verification of RC structures, the fact that the number of such structures that really have fatigue safety issues is relatively small, poses the question whether the limited research resources should be preferably directed in further refinement of examination methods or in the development of innovative technological methods for economical and sustainable amelioration of those few problematic structures which can be efficiently identified by a meticulous and insightful application of the current state of the art provided that engineers properly educated and willing to perform this task exist.



## Epilogue<sup>1</sup>

With the exception of purely mathematical problems, every scientific problem can ultimately be stated in this form: *Given* a certain system, its state in a certain region of space and time and the evolution of stimulus during its history, *to calculate* the state of the system at another region of space and time. This is *a priori* a feasible task since the notion of state is only defined for systems which are in some kind of internal equilibrium and “internal equilibrium” is in fact synonymous to “predictability”.

Hence, science is all about certainty and calculations provided that what needs to be given *is* given. However, the world can only be described in terms of the *apparent state* of its observation elements. One can only have a *belief* – more or less substantiated by experience but in essence always subjective – that the apparent state of an observation element says something meaningful about the element itself. What is this “something” depends on how one *imagines* the “*internal*” of the observation element; or in other words on his *imaginary picture of the unobservable*.

Hence, although the statement of scientific problems starts with “given...”, the state of a system, in reality, can never be entirely given, nor can the system itself be given (for any system is defined by the totality of its possible states), nor the stimulus can be given (for it depends on the state of the rest of the systems considered as environment).

Of what needs to be given there will always remain a part to be *imagined*. This explains the presence in the world of *the unpredictable* (which in some cases is called free will). It is not possible to say something by mathematics about that which is to be imagined; it might be possible to show something about it by *praxis*. This is the practicing of art.

The truly important problems in life are problems of art: The art of building which is found in engineering, the art of curing illness which is found in medicine, the art of setting laws which is found in politics, the art of living which is found in ethics. Experience indeed suggests that knowledge obtained by science may be useful but it is not strictly necessary and by no means sufficient for a virtuous engineer, physician, politician, human.

Perfection in art can only be achieved through conscious and persistent exercise, for problems of art have neither definite formulation neither definite answer; they can only be *instantly* experienced and resolved in praxis.

Indulging in science is indulging to the cozy and revitalizing feeling of certainty. Humans however fulfil their potential and achieve happiness walking on the tightrope of imagination over the chaos of uncertainty.

---

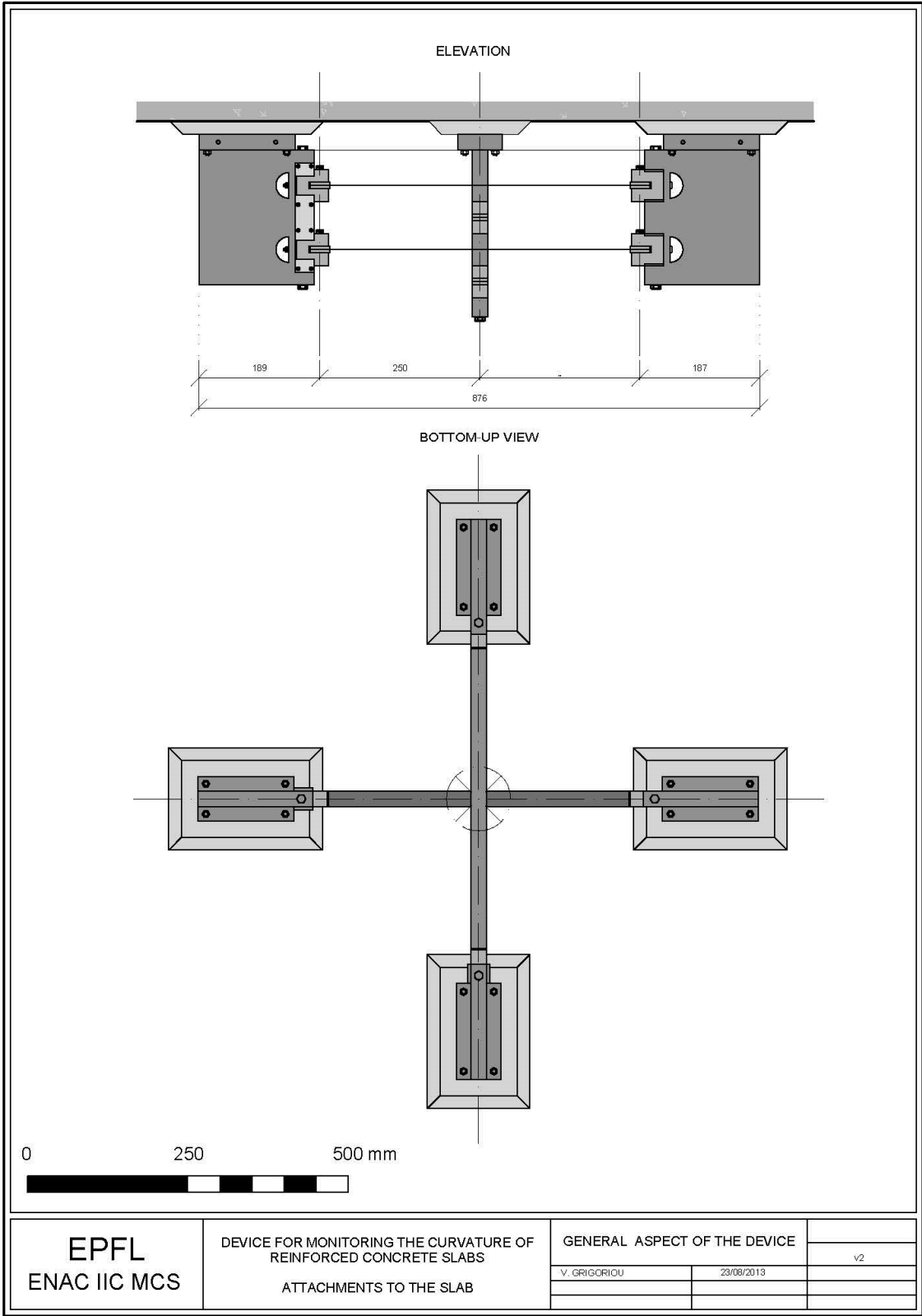
<sup>1</sup> My personal point of view on science, art and their relation within life at the end of my doctoral studies. A view developed through my effort to grasp some fundamental notions that I had to use in this work and strongly influenced by: Aristoteles’ “Nicomachean Ethics”, L. Wittgenstein’s “Tractatus Logico-Philosophicus” and C. Castoriadis’ “L’institution imaginaire de la société”.



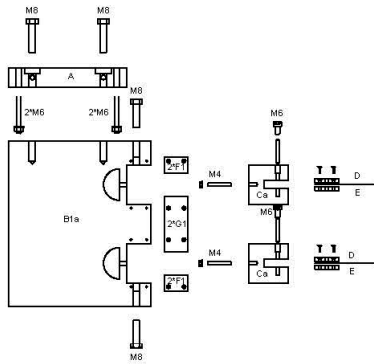


## **Annex: Drawings of the monitoring device.**

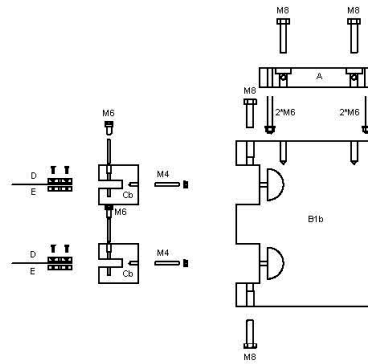




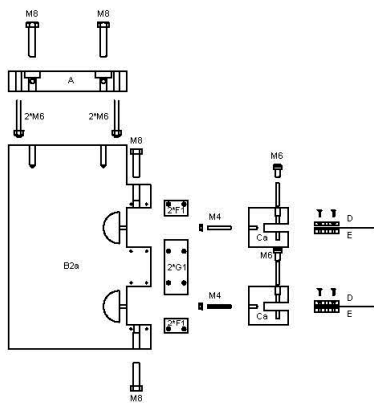
1a



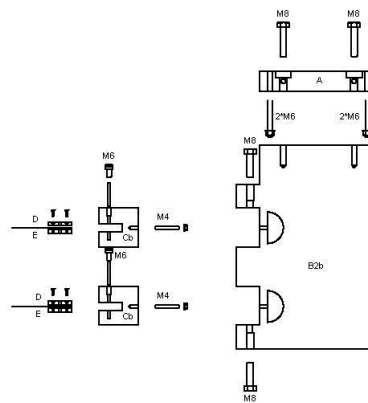
1b



2a



2b



EPFL  
ENAC IIC MCS

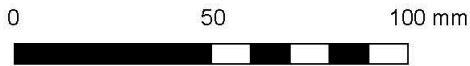
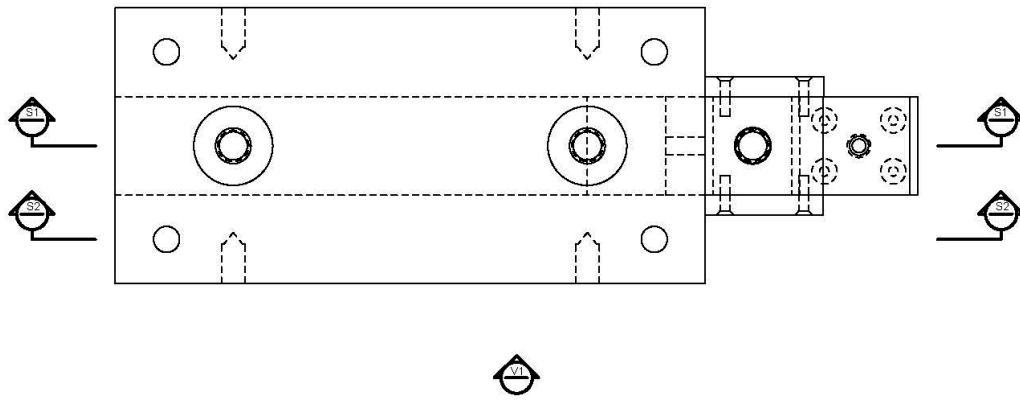
DEVICE FOR MONITORING THE CURVATURE OF  
REINFORCED CONCRETE SLABS  
ATTACHMENTS TO THE SLAB

KAY PLAN  
ELEMENT NAMES

V. GRIGORIOU 23/08/2013

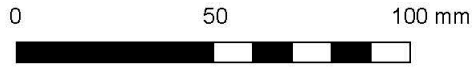
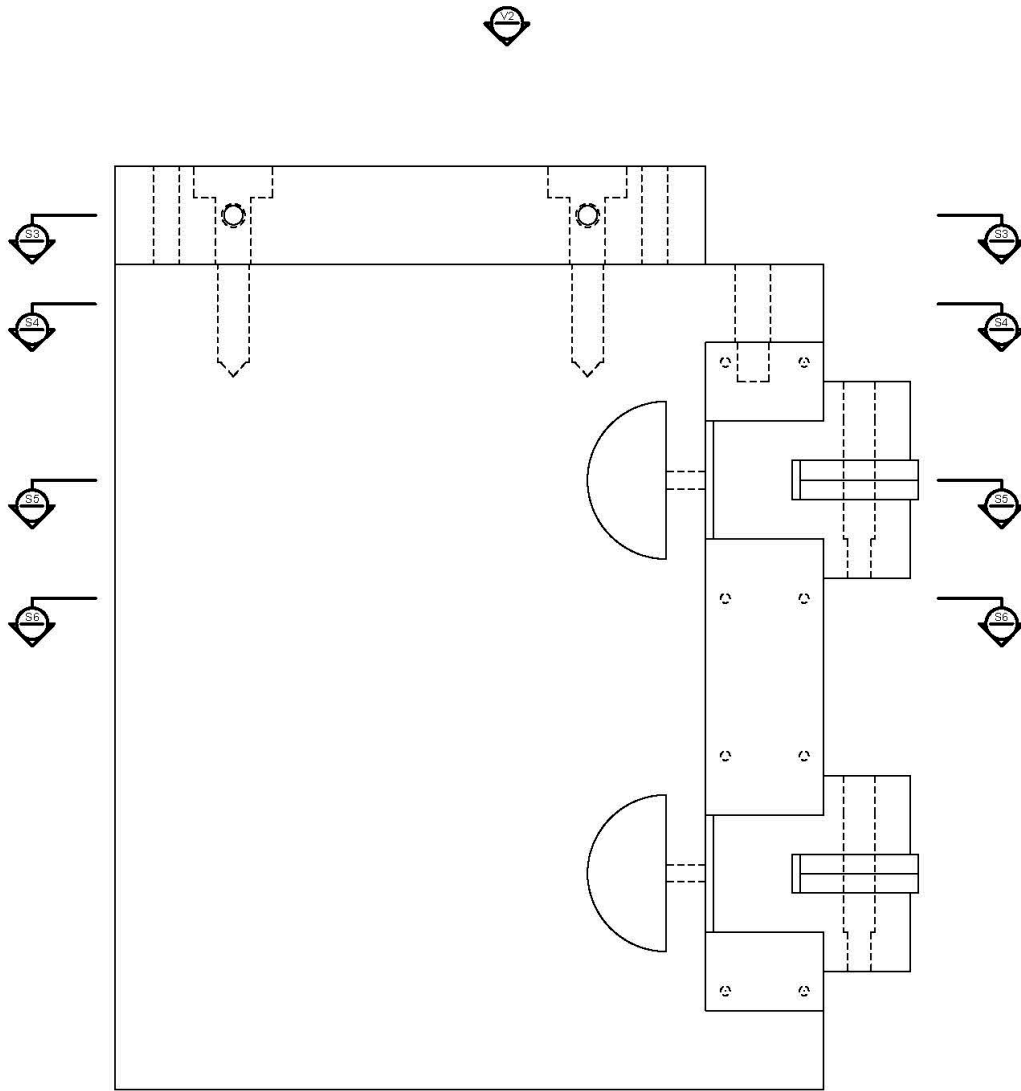
v2

TOP VIEW  
(screws and bolts not shown)



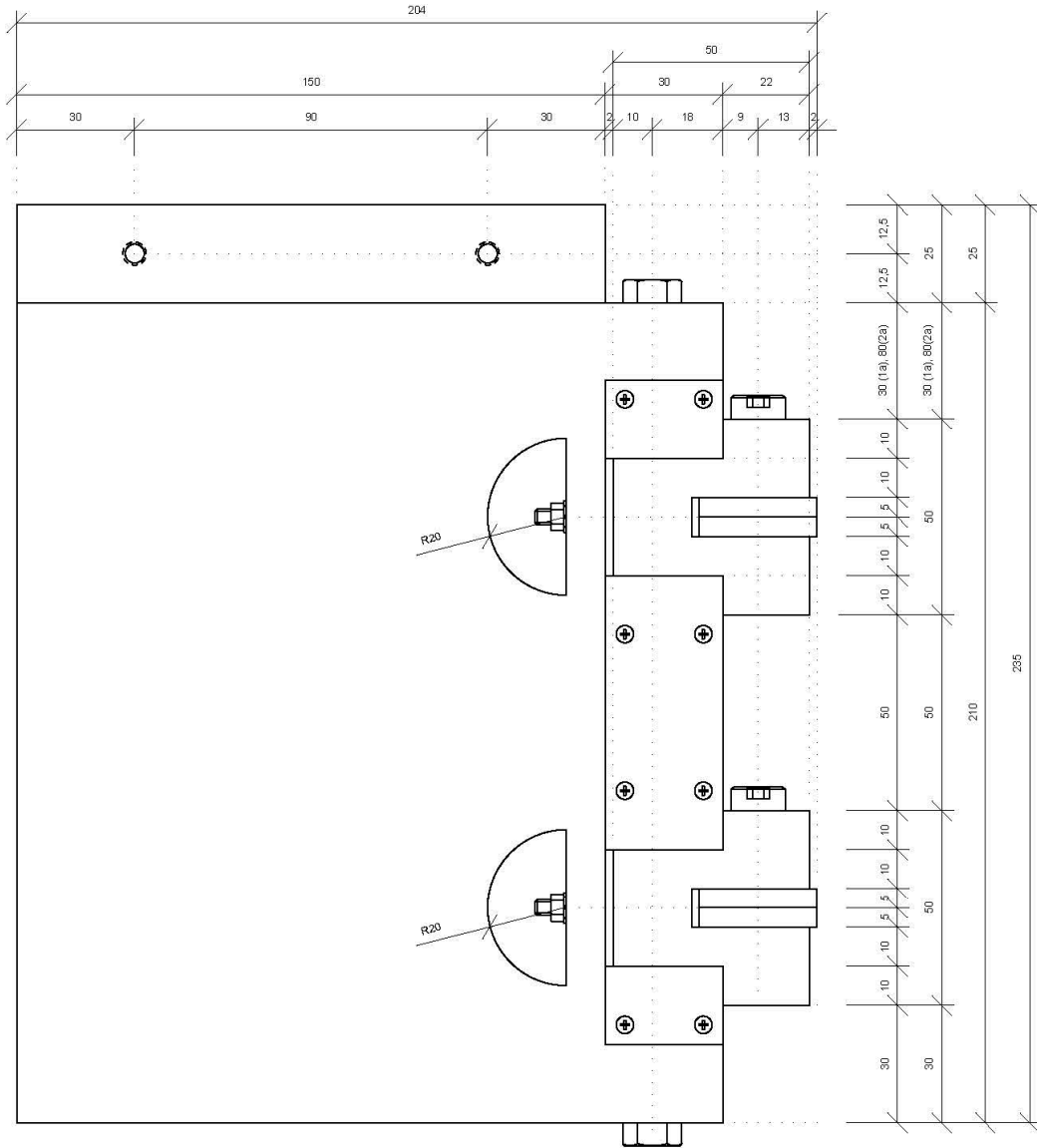
EPFL ENAC IIC MCS	DEVICE FOR MONITORING THE CURVATURE OF REINFORCED CONCRETE SLABS ATTACHMENTS TO THE SLAB	ELEMENTS 1a & 2a INDICATION OF SECTION LEVELS I		
		V. GRIGORIDU	23/08/2013	v2

SIDE VIEW (1a)  
(screws and bolts not shown)



<p><b>EPFL</b> ENAC IIC MCS</p>	<p>DEVICE FOR MONITORING THE CURVATURE OF REINFORCED CONCRETE SLABS ATTACHMENTS TO THE SLAB</p>	<p>ELEMENTS 1a &amp; 2a INDICATION OF SECTION LEVELS II</p>		
		<p>V. GRIGORIU</p>	<p>23/08/2013</p>	<p>v2</p>

VIEW 1  
(screws and bolts included)



EPFL  
ENAC IIC MCS

DEVICE FOR MONITORING THE CURVATURE  
OF REINFORCED CONCRETE SLABS  
ATTACHMENTS TO THE SLAB

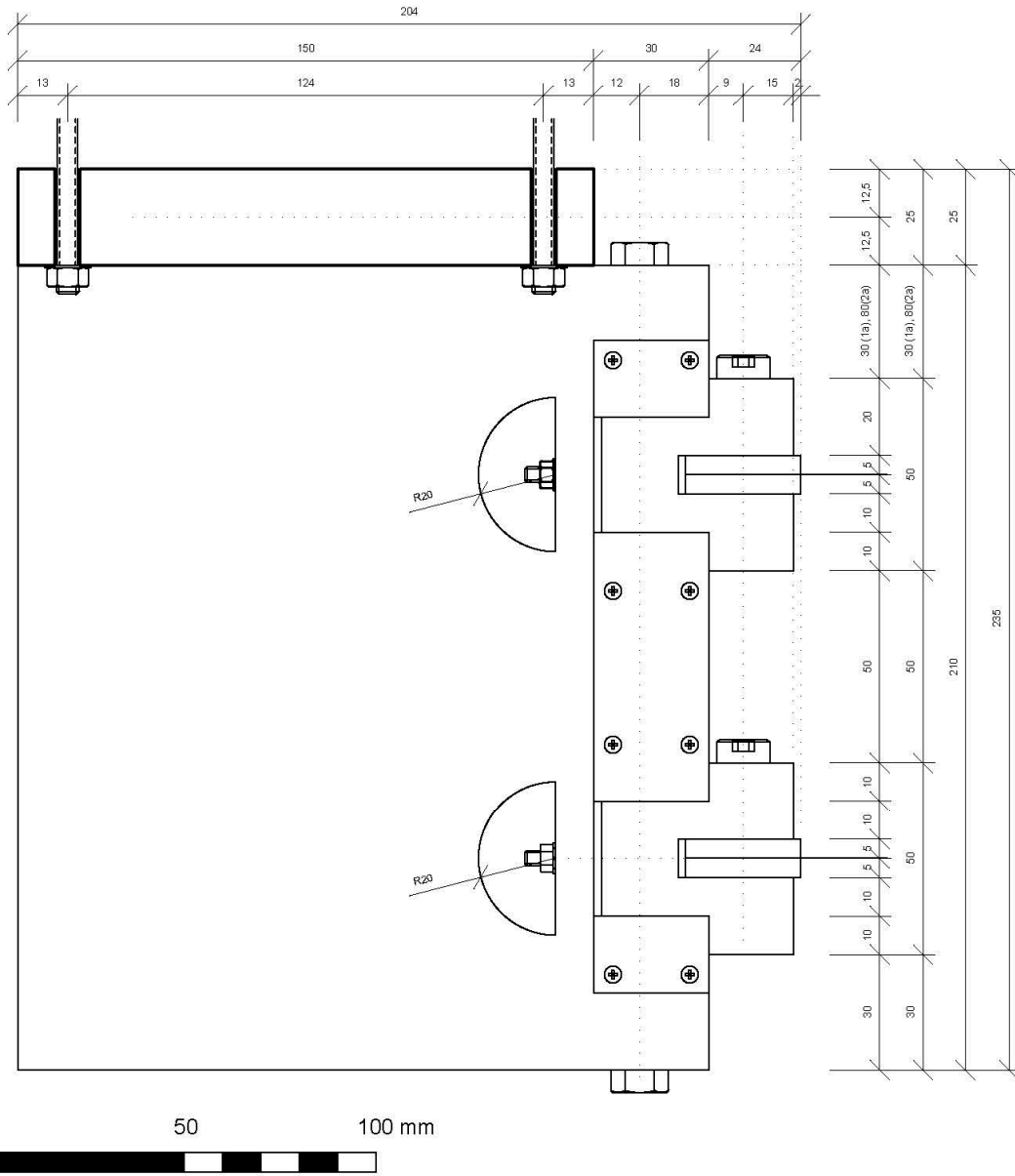
ASSEMBLED ELEMENTS 1a & 2a, I

V. GRIGORIOU

23/08/2013

v2

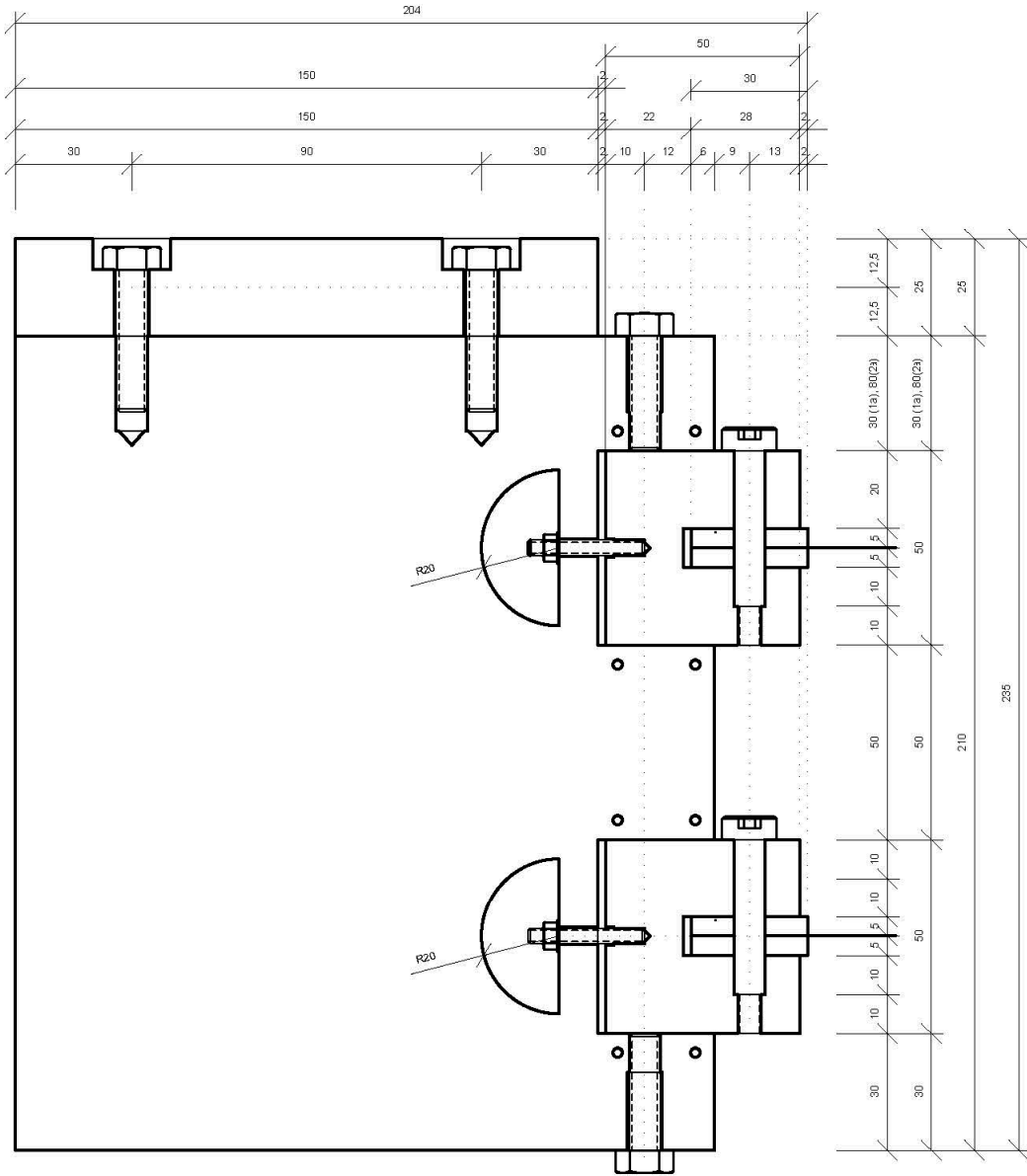
SECTION 1  
(screws and bolts included)



<p><b>EPFL</b> ENAC IIC MCS</p>	<p>DEVICE FOR MONITORING THE CURVATURE OF REINFORCED CONCRETE SLABS ATTACHMENTS TO THE SLAB</p>	<p>ASSEMBLED ELEMENTS 1a &amp; 2a, II</p>		<p>v2</p>
		<p>V. GRIGORIOU</p>	<p>23/08/2013</p>	



SECTION 2  
(screws and bolts included)



EPFL  
ENAC IIC MCS

DEVICE FOR MONITORING THE CURVATURE  
OF REINFORCED CONCRETE SLABS  
ATTACHMENTS TO THE SLAB

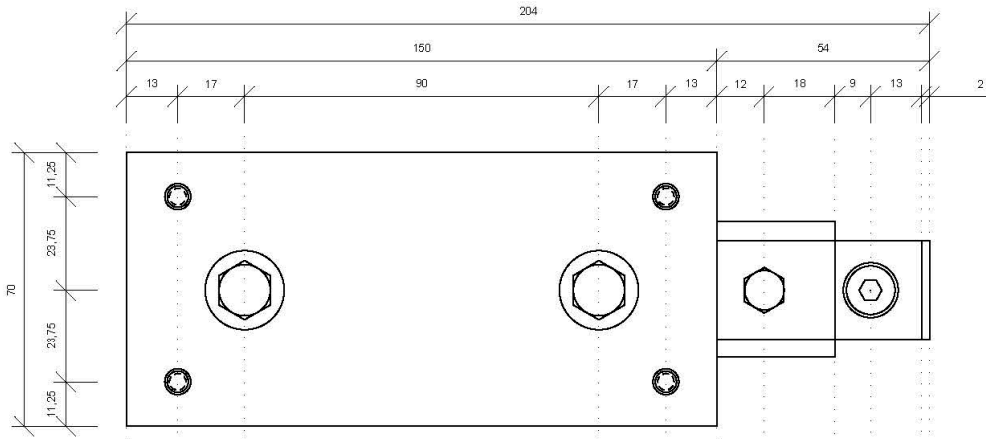
ASSEMBLED ELEMENTS 1a & 2a, III

V. GRIGORIOU

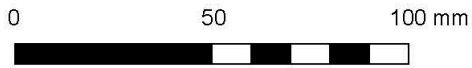
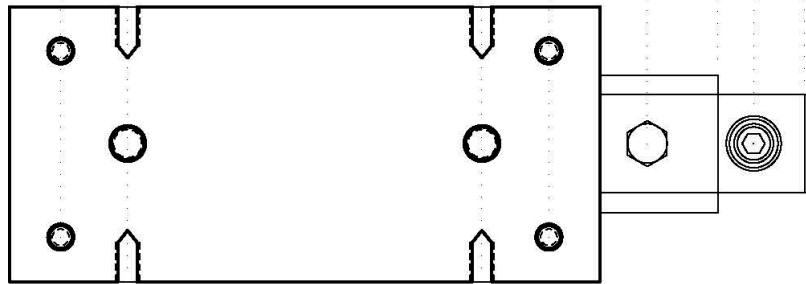
23/08/2013

v2

VIEW 2  
(screws and bolts included)

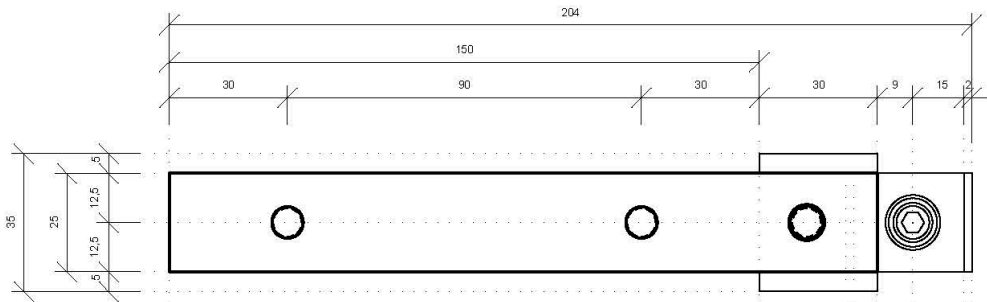


SECTION 3  
(screws and bolts at the final stage included)

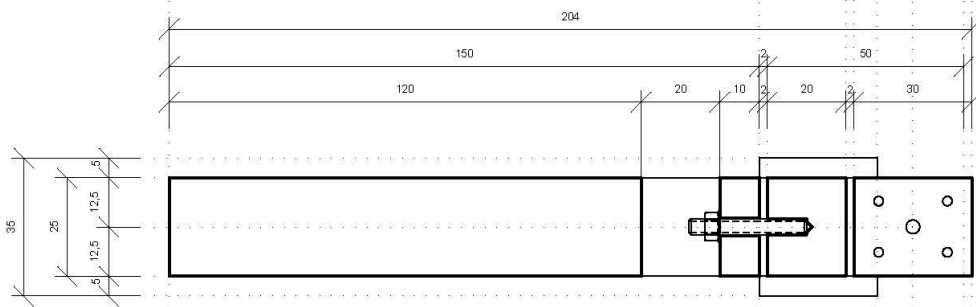


<p><b>EPFL</b> ENAC IIC MCS</p>	<p>DEVICE FOR MONITORING THE CURVATURE OF REINFORCED CONCRETE SLABS ATTACHMENTS TO THE SLAB</p>	<p>ASSEMBLED ELEMENTS 1a &amp; 2a, IV</p>		<p>v2</p>
		<p>V. GRIGORIQU</p>	<p>23/08/2013</p>	

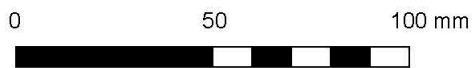
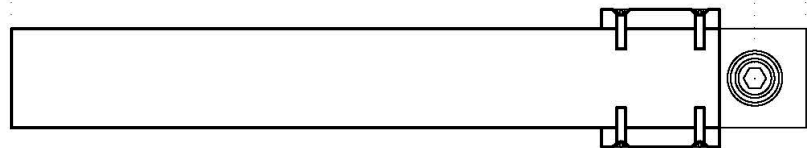
SECTION 4  
(screws and bolts included)



SECTION 5  
(screws and bolts included)

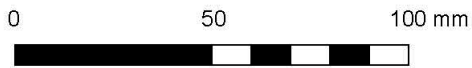
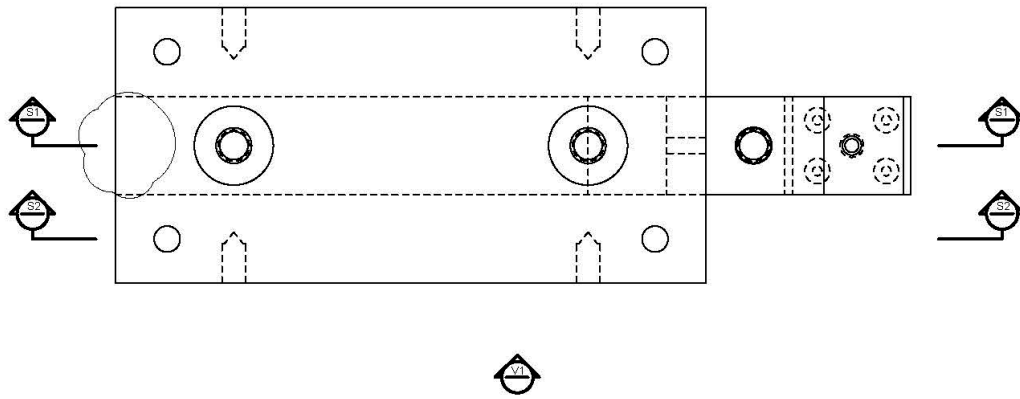


SECTION 6  
(screws and bolts included)



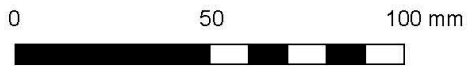
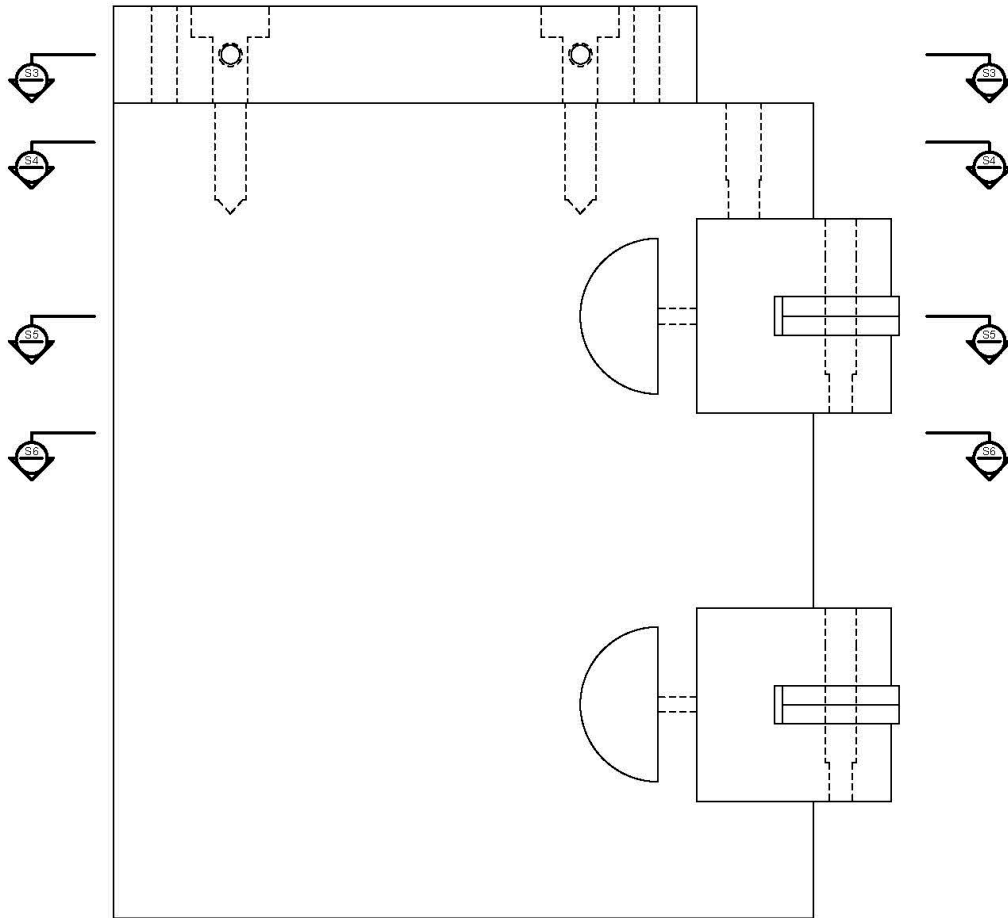
EPFL ENAC IIC MCS	DEVICE FOR MONITORING THE CURVATURE OF REINFORCED CONCRETE SLABS ATTACHMENTS TO THE SLAB	ASSEMBLED ELEMENTS 1a & 2a, V		
		V. GRIGORIOU	23/08/2013	v2

TOP VIEW  
(screws and bolts not shown)



<p><b>EPFL</b> ENAC IIC MCS</p>	<p>DEVICE FOR MONITORING THE CURVATURE OF REINFORCED CONCRETE SLABS ATTACHMENTS TO THE SLAB</p>	<p>ELEMENTS 1b &amp; 2b INDICATION OF SECTION LEVELS I</p>		
		V. GRIGORIDU	23/08/2013	v2

SIDE VIEW (1a)  
(screws and bolts not shown)



EPFL  
ENAC IIC MCS

DEVICE FOR MONITORING THE CURVATURE  
OF REINFORCED CONCRETE SLABS  
ATTACHMENTS TO THE SLAB

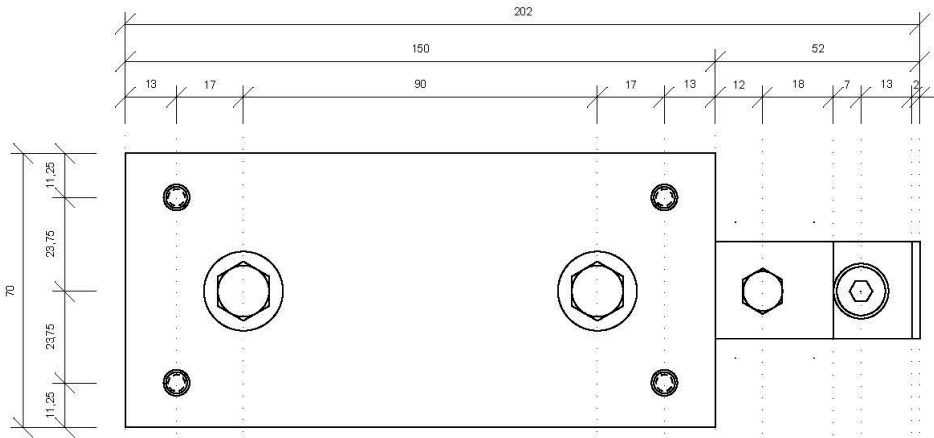
ELEMENTS 1b & 2b  
INDICATION OF SECTION LEVELS II

V. GRIGORIOU

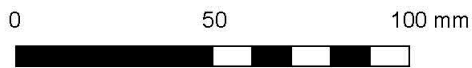
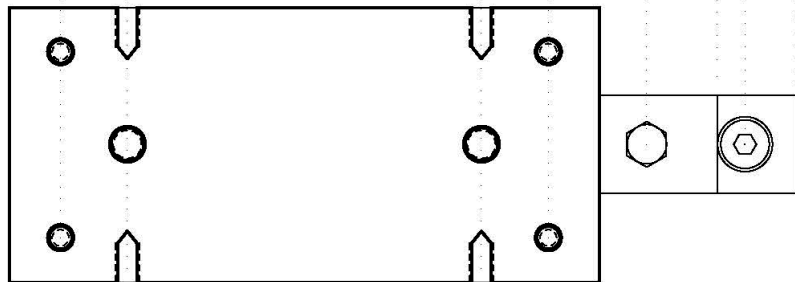
23/08/2013

v2

VIEW 2  
(screws and bolts included)



SECTION 3  
(screws and bolts at the final stage included)



EPFL  
ENAC IIC MCS

DEVICE FOR MONITORING THE CURVATURE  
OF REINFORCED CONCRETE SLABS  
ATTACHMENTS TO THE SLAB

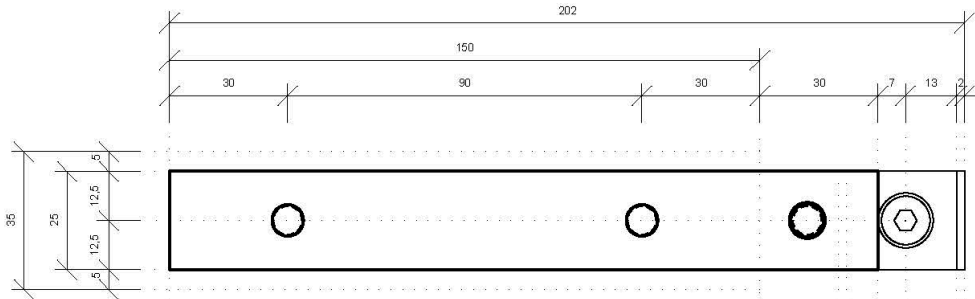
ASSEMBLED ELEMENTS 1b & 2b, I

V. GRIGORIOU

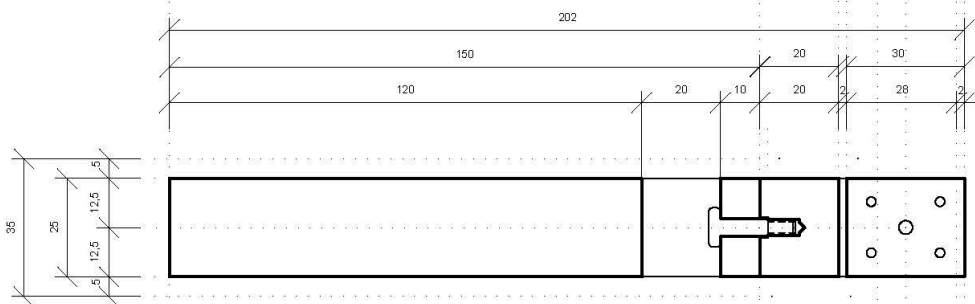
23/06/2013

v2

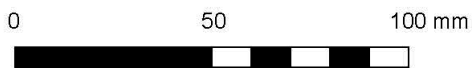
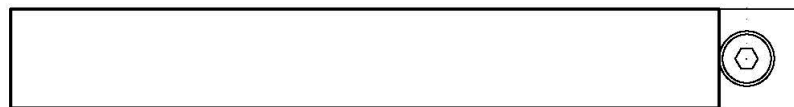
SECTION 4  
(screws and bolts included)



SECTION 5  
(screws and bolts included)



SECTION 6  
(screws and bolts included)



EPFL  
ENAC IIC MCS

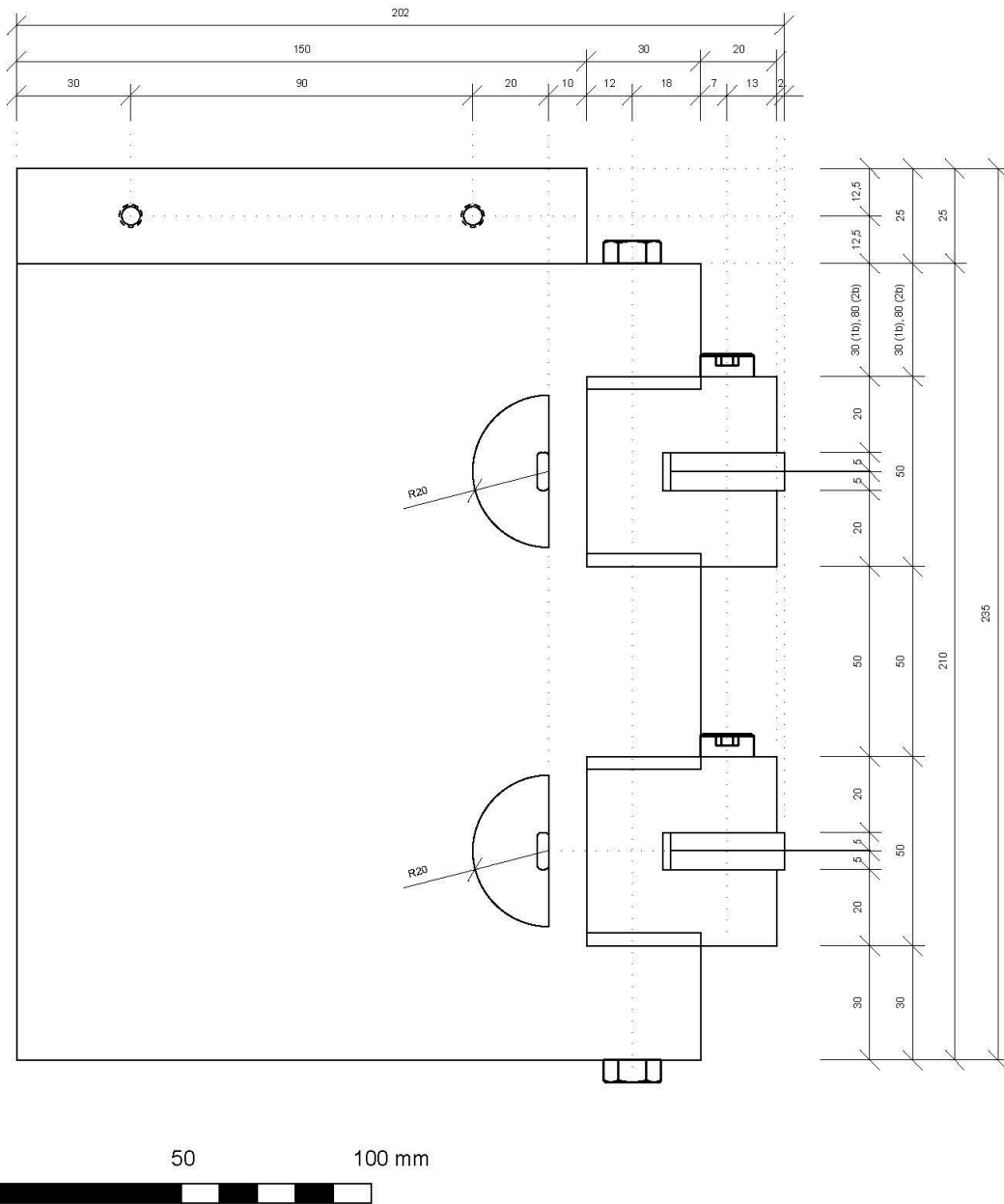
DEVICE FOR MONITORING THE CURVATURE  
OF REINFORCED CONCRETE SLABS  
ATTACHMENTS TO THE SLAB

ASSEMBLED ELEMENTS 1b & 2b, II

V. GRIGORIOU	23/08/2013
--------------	------------

v2

VIEW 1  
(screws and bolts included)



EPFL  
ENAC IIC MCS

DEVICE FOR MONITORING THE CURVATURE  
OF REINFORCED CONCRETE SLABS  
ATTACHMENTS TO THE SLAB

ASSEMBLED ELEMENTS 1b & 2b, III

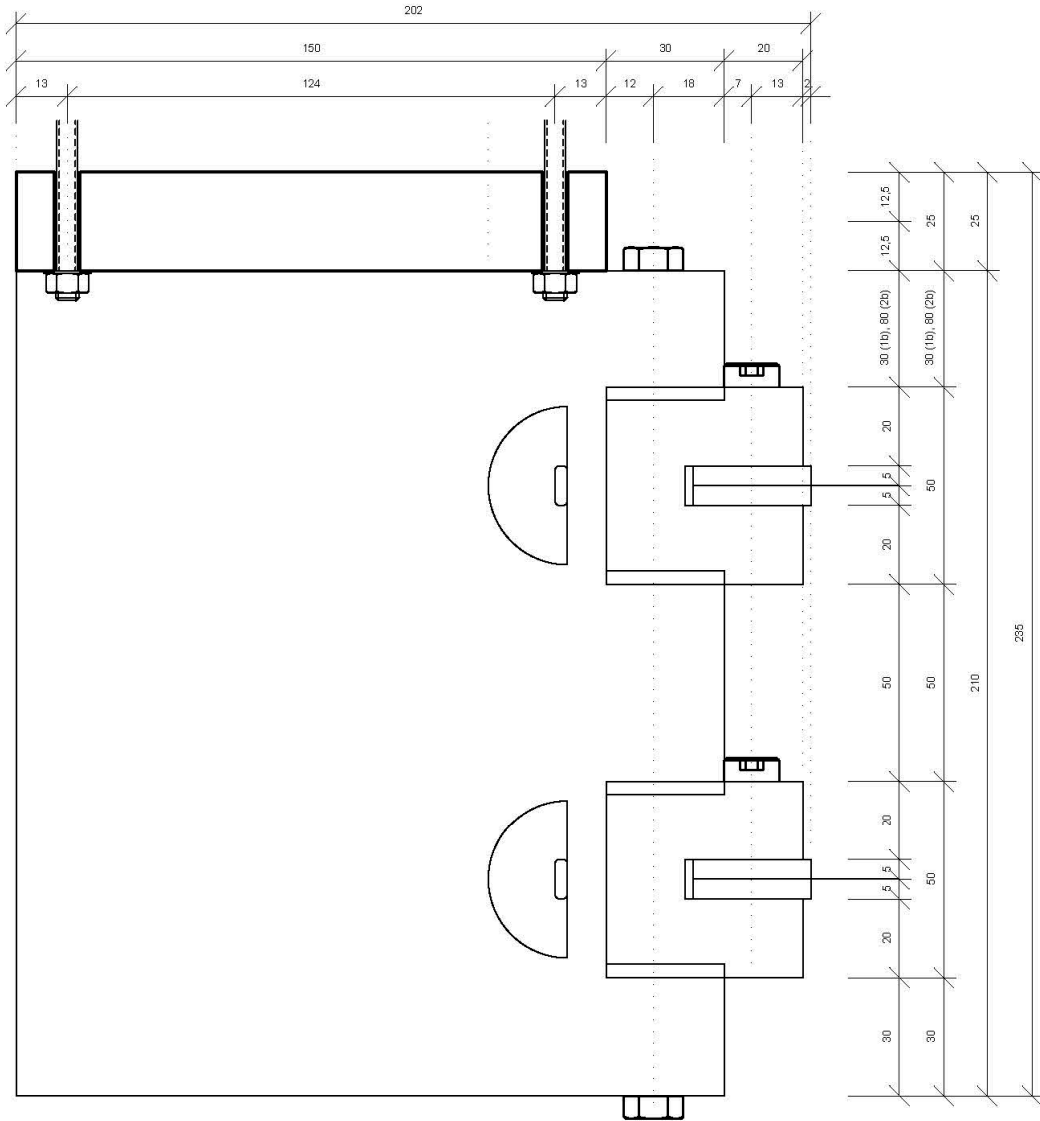
V. GRIGORIU

23/08/2013

v2

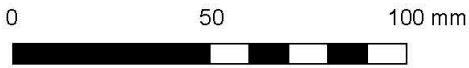
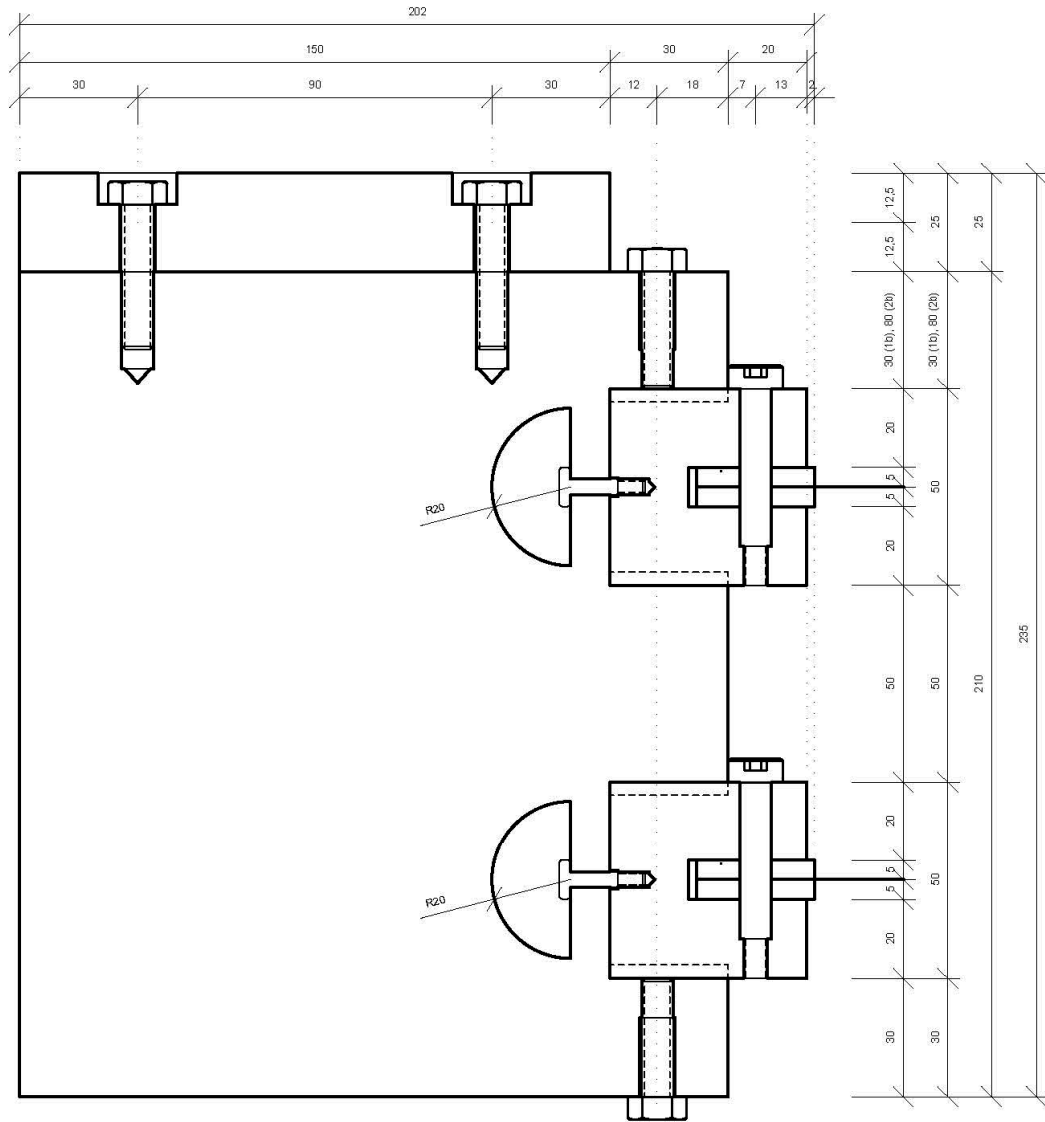


SECTION 1  
(screws and bolts included)



<p><b>EPFL</b> ENAC IIC MCS</p>	<p>DEVICE FOR MONITORING THE CURVATURE OF REINFORCED CONCRETE SLABS ATTACHMENTS TO THE SLAB</p>	<p>ASSEMBLED ELEMENTS 1b &amp; 2b, IV</p>		<p>v2</p>	
		<p>V. GRIGORIOU</p>	<p>23/08/2013</p>		

SECTION 2  
(screws and bolts included)



EPFL  
ENAC IIC MCS

DEVICE FOR MONITORING THE CURVATURE  
OF REINFORCED CONCRETE SLABS  
ATTACHMENTS TO THE SLAB

ASSEMBLED ELEMENTS 1b & 2b, V

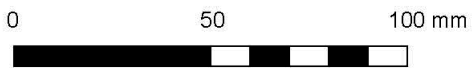
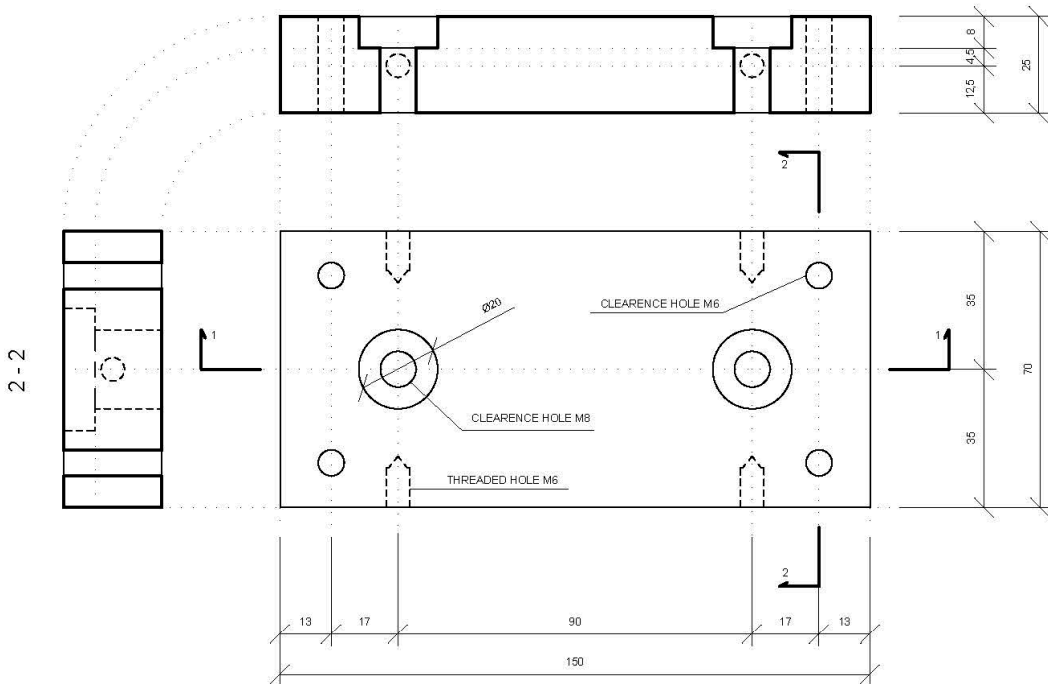
V. GRIGORIOU

23/08/2013

v2

4 SIMILAR

1 - 1



EPFL  
ENAC IIC MCS

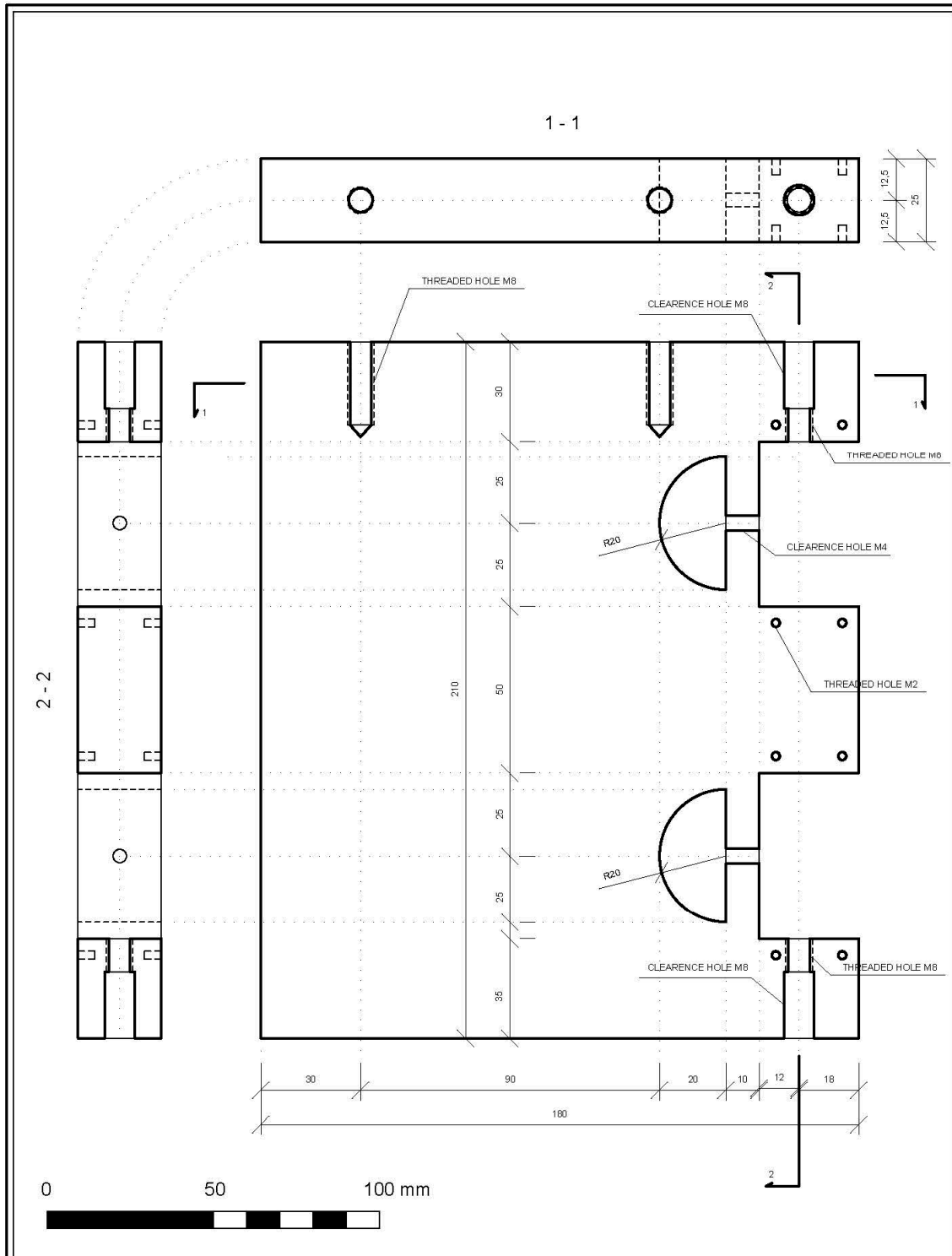
DEVICE FOR MONITORING THE CURVATURE  
OF REINFORCED CONCRETE SLABS  
ATTACHMENTS TO THE SLAB

PIECE A

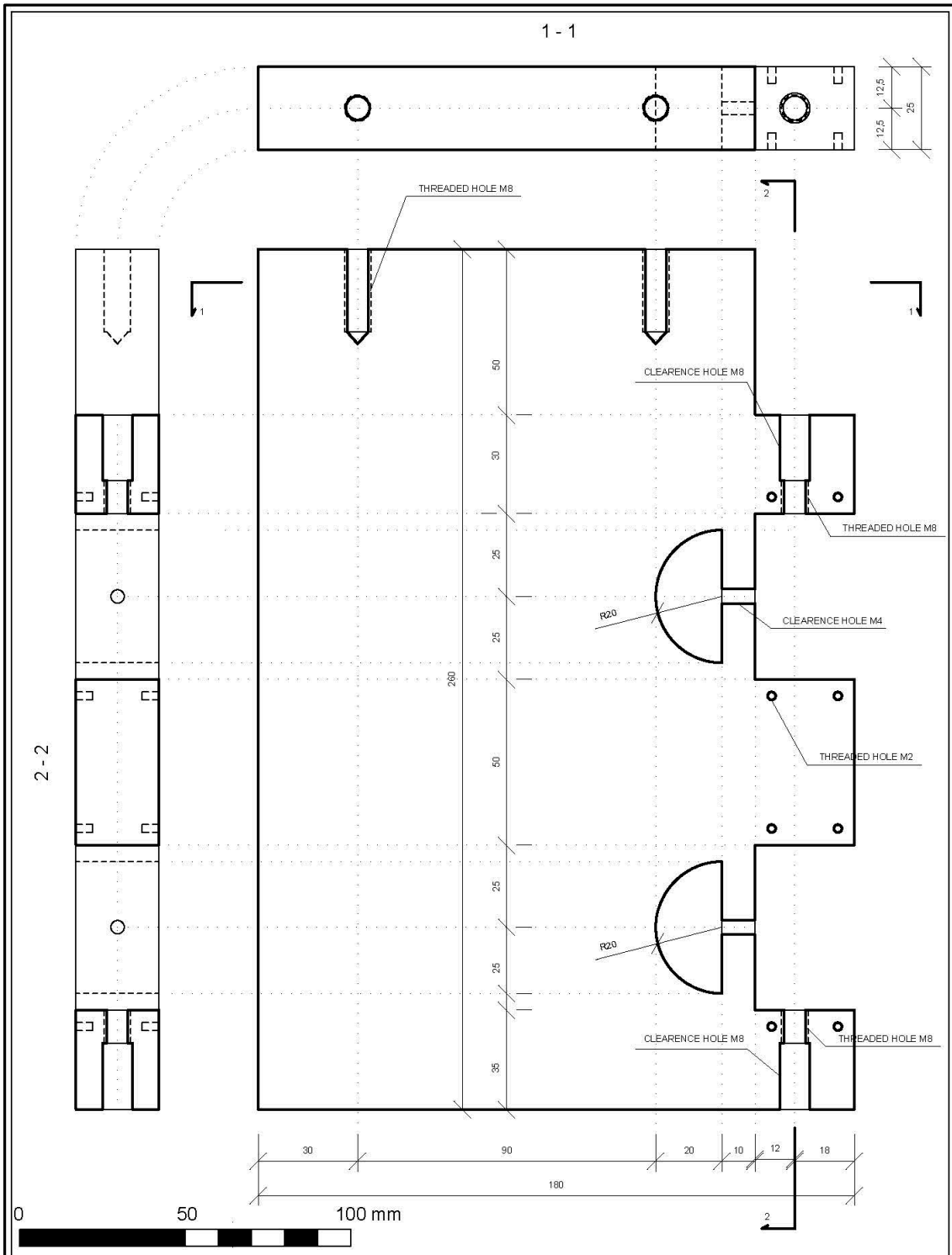
V. GRIGORIU

23/08/2013

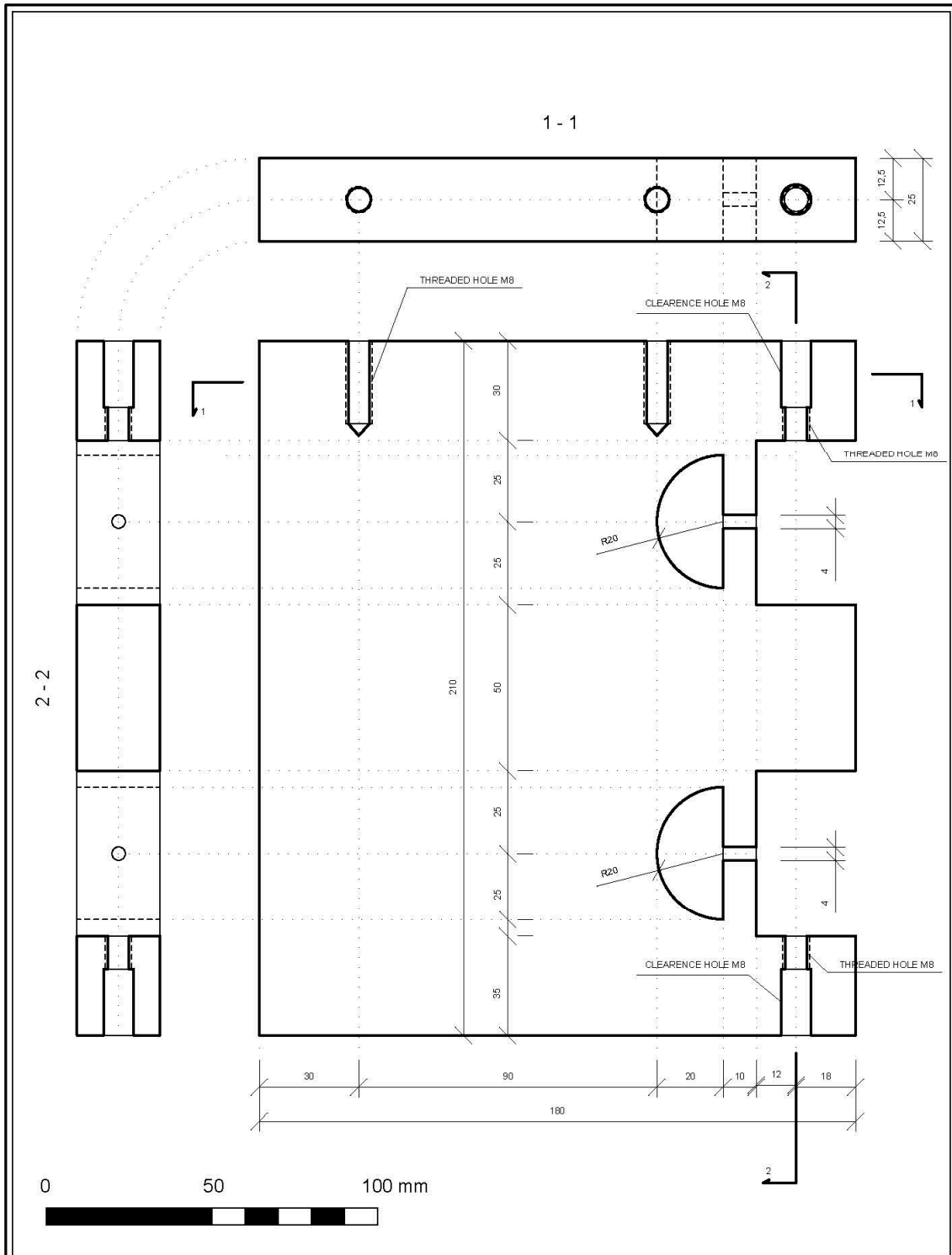
v2



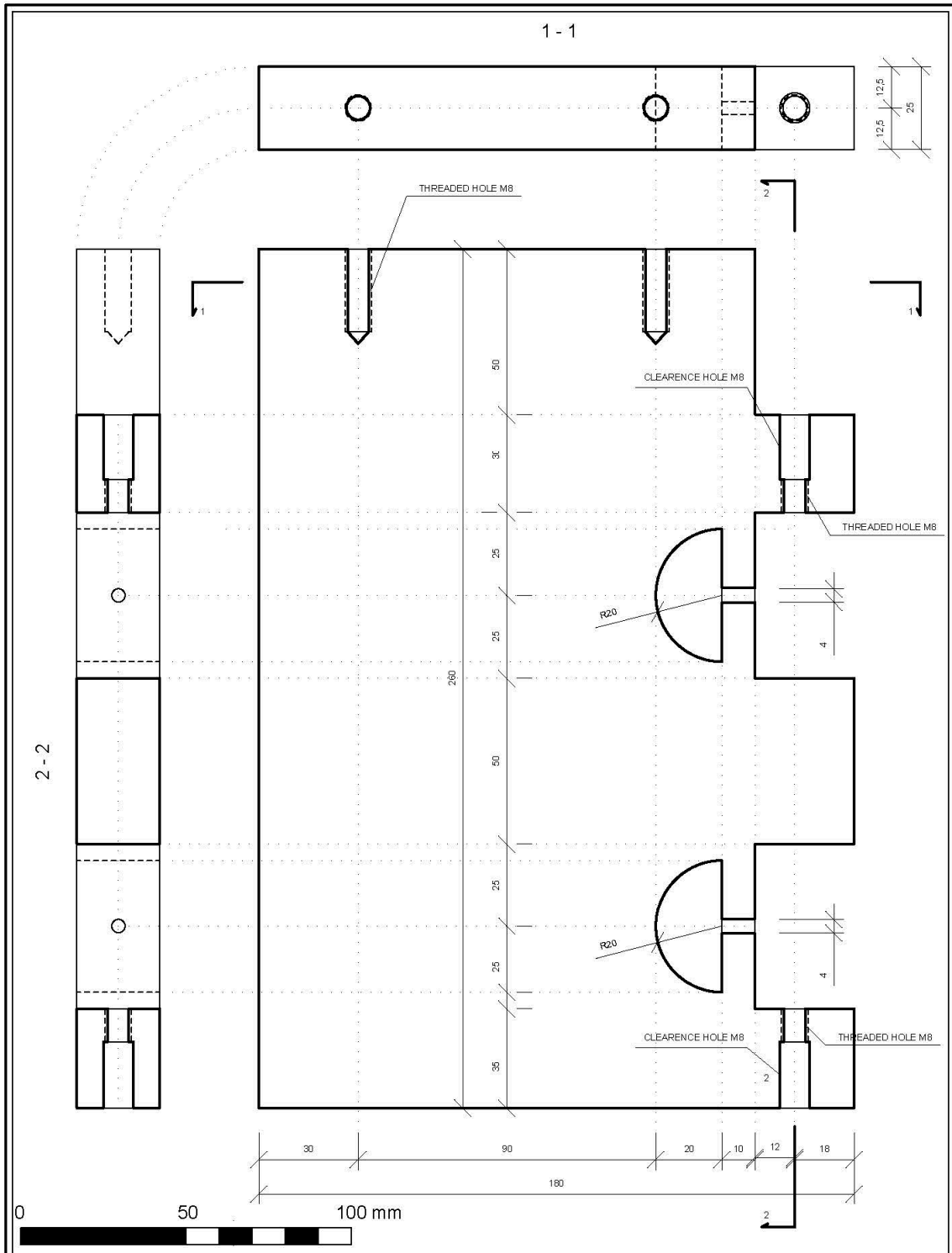
<b>EPFL</b> <b>ENAC IIC MCS</b>	DEVICE FOR MONITORING THE CURVATURE OF REINFORCED CONCRETE SLABS ATTACHMENTS TO THE SLAB	<b>PIECE B1a</b>		v2
		V. GRIGORIOU	23/08/2013	



<b>EPFL</b> <b>ENAC IIC MCS</b>	DEVICE FOR MONITORING THE CURVATURE OF REINFORCED CONCRETE SLABS ATTACHMENTS TO THE SLAB	<b>PIECE B2a</b>		v2
		V. GRIGORIOU	23/08/2013	



<p><b>EPFL</b> ENAC IIC MCS</p>	<p>DEVICE FOR MONITORING THE CURVATURE OF REINFORCED CONCRETE SLABS</p> <p>ATTACHMENTS TO THE SLAB</p>	<p>PIECE B1b</p>		<p>v2</p>
		<p>V. GRIGORIOU</p>	<p>23/08/2013</p>	



EPFL  
ENAC IIC MCS

DEVICE FOR MONITORING THE CURVATURE  
OF REINFORCED CONCRETE SLABS  
ATTACHMENTS TO THE SLAB

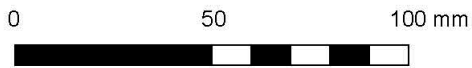
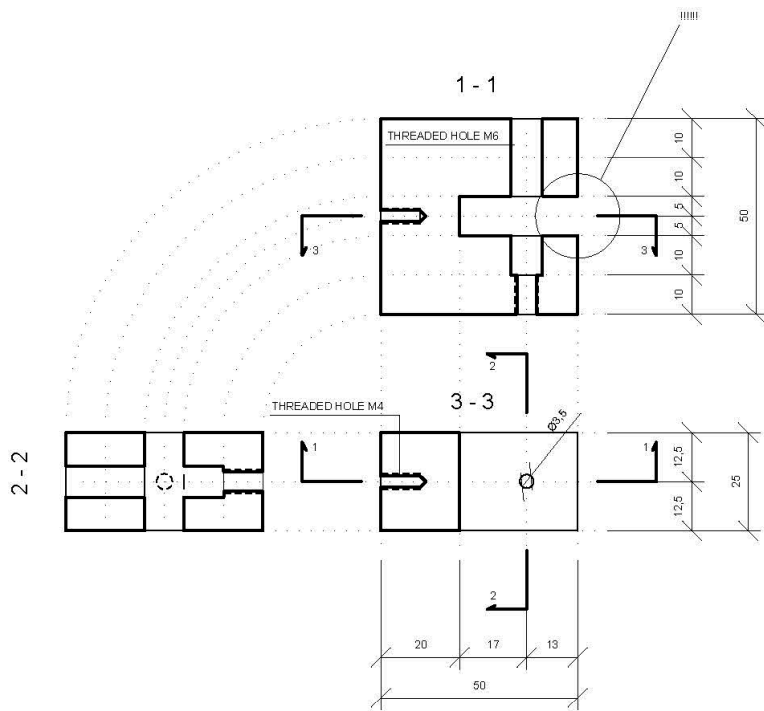
PIECE B2b

V. GRIGORIOU

23/08/2013

v2

4 SIMILAR



EPFL  
ENAC IIC MCS

DEVICE FOR MONITORING THE CURVATURE  
OF REINFORCED CONCRETE SLABS  
ATTACHMENTS TO THE SLAB

PIECE Ca

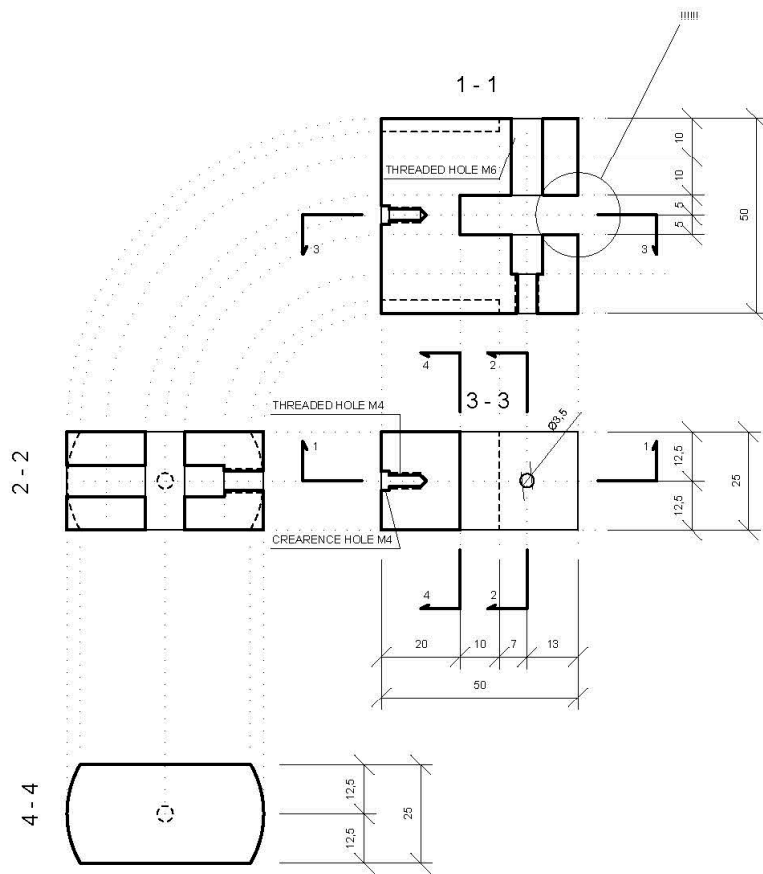
V. GRIGORIU

23/08/2013

v2



4 SIMILAR



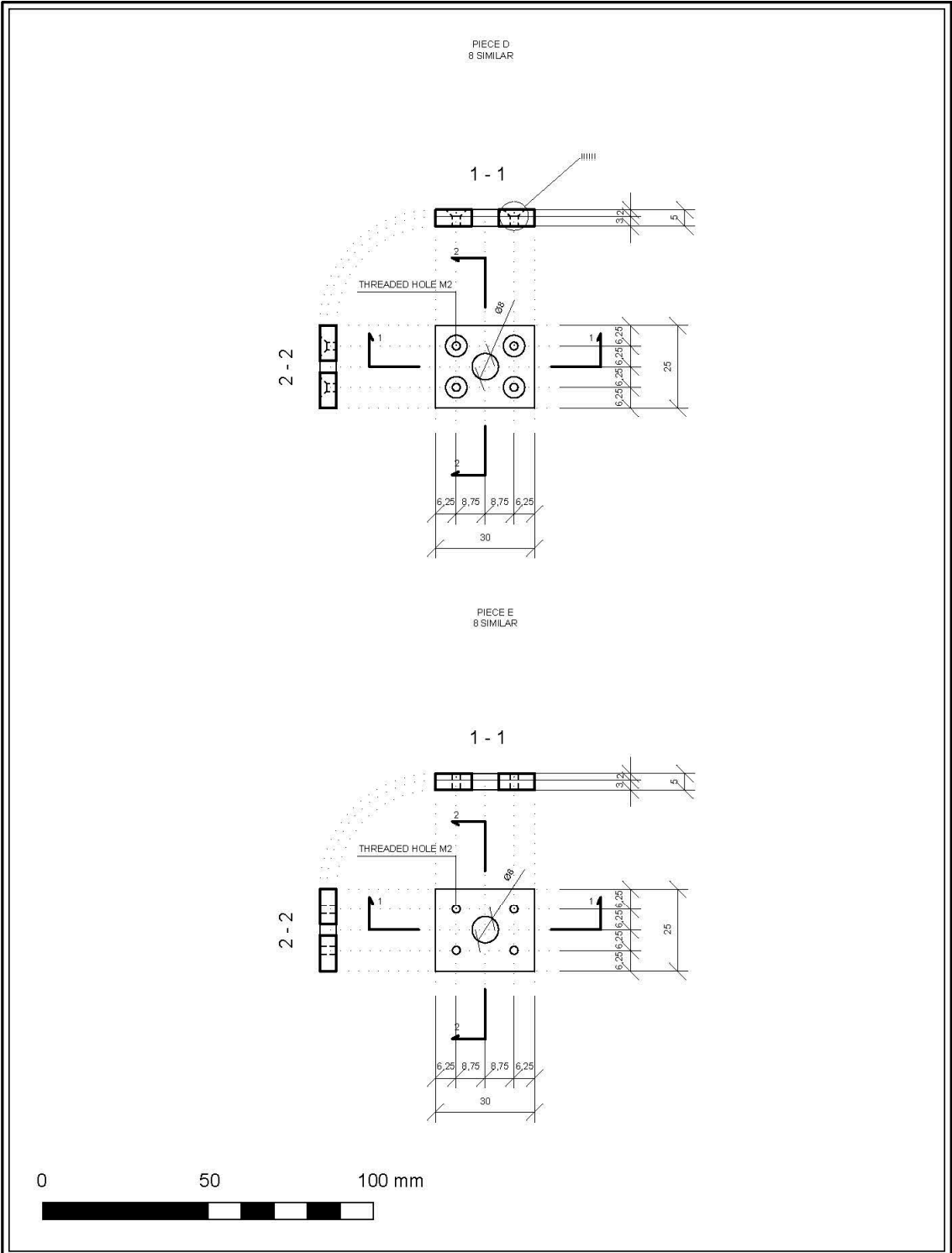
EPFL  
ENAC IIC MCS

DEVICE FOR MONITORING THE CURVATURE  
OF REINFORCED CONCRETE SLABS  
ATTACHMENTS TO THE SLAB

PIECE Cb

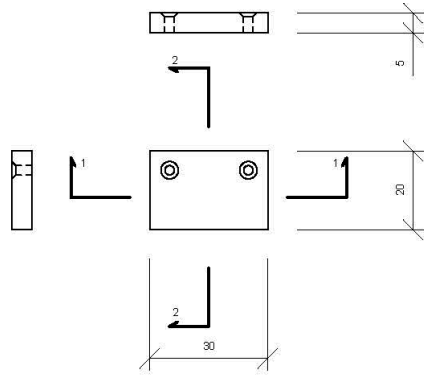
V. GRIGORIOU 23/08/2013

v2

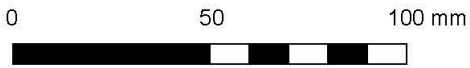
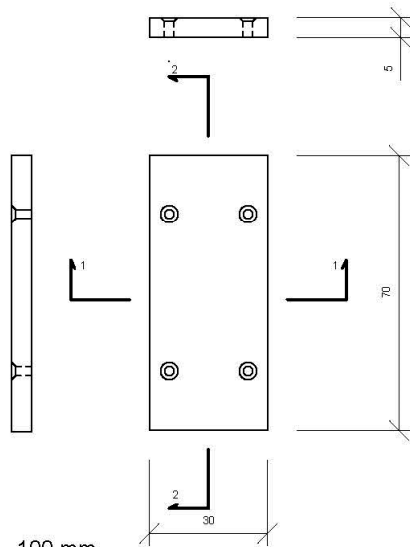


<p><b>EPFL</b> ENAC IIC MCS</p>	<p>DEVICE FOR MONITORING THE CURVATURE OF REINFORCED CONCRETE SLABS</p> <p>ATTACHMENTS TO THE SLAB</p>	<p>PIECES D &amp; E</p>		<p>v2</p>
		<p>Y. GRIGORIOU</p>	<p>23/08/2013</p>	

PIECE F  
8 SIMILAR



PIECE G  
4 SIMILAR



<p><b>EPFL</b> ENAC IIC MCS</p>	<p>DEVICE FOR MONITORING THE CURVATURE OF REINFORCED CONCRETE SLABS</p> <p>ATTACHMENTS TO THE SLAB</p>	<p>PIECES F &amp; G</p>		
		<p>V. GRIGORIOU</p>	<p>23/08/2013</p>	<p>v2</p>



**Vasileios GRIGORIOU**

**Nationality:** Hellenic. **1980**, Born in Athens, GR. **1986–1998:** Lycée Leonin de Nea Smyrni, Athens, GR, *primary and secondary education*. **1998–2005:** University of Patras, GR, *civil engineering studies and postgraduate specialization in analysis and design of civil infrastructure*. **Nov 2004–Apr 2005:** PRINCIPIA consulting engineers, Madrid, ES, *trainee*. **Aug 2005–Aug 2006:** Greek army, *national service as sergeant sapper*. **2006–2011:** TTA structural engineers, Athens, GR, *structural engineer*. **2011–2005:** Swiss federal institute of technology in Lausanne, CH, *doctoral studies in civil engineering*. **Languages:** EL (native), EN (proficient), FR (proficient), ES (basic).